This is the Green Open Access version of: Georgiev, S., von Quadt, A., Heinrich, C. A., Peytcheva, I., Marchev, P., 2012. Time evolution of a rifted continental arc: integrated ID-TIMS and LA-ICPMS study of magmatic zircons from the Eastern Srednogorie, Bulgaria. Lithos, vol. 154, pp. 53-67.
https://doi.org/10.1016/j.lithos.2012.06.020

Time evolution of a rifted continental arc: integrated ID-TIMS and LA-ICPMS study of magmatic zircons from the Eastern Srednogorie, Bulgaria

S. Georgiev[1*], A. von Quadt[1], C. A. Heinrich[1,2], I. Peytcheva[1,3], P. Marchev[3]

[1]Institute of Geochemistry and Petrology, ETH Zurich, Clausiusstrasse 25, CH-8092 Zurich, Switzerland
[2]Faculty of Mathematics and Natural Sciences, University of Zurich, Switzerland
[3]Geological Institute, Bulgarian Academy of Sciences, Acad. G. Bonchev St., 1113 Sofia, Bulgaria

[*] Corresponding author. Present address: Geological Survey of Norway, Trondheim and AIRIE Program, Department of Geosciences, Colorado State University, Fort Collins CO, USA
Telephone: ++1 970 491 3816. Fax: +41 44 632 11 79. E-mail: georgiev@colostate.edu.

Abstract

Eastern Srednogorie in Bulgaria is the widest segment of an extensive magmatic arc that formed by convergence of Africa and Europe during Mesozoic to Tertiary times. Northward subduction of the Tethys ocean beneath Europe in the Late Cretaceous gave rise to a broad range of basaltic to more evolved magmas with locally associated Cu-Au mineralization along this arc. We used U-Pb geochronology of single zircons to constrain the temporal evolution of the Upper Cretaceous magmatism and the age of basement rocks through which the magmas were emplaced in this arc segment. High precision isotope dilution - thermal ionization mass spectrometry (ID-TIMS) was combined with laser ablation - inductively coupled plasma mass spectrometry (LA-ICPMS) for spatial resolution within single zircon grains.

Three tectono-magmatic regions are distinguished from north to south within Eastern Srednogorie: East Balkan, Yambol-Burgas and Strandzha. Late Cretaceous magmatic activity started at ~90 Ma in the northernmost East Balkan region, based on stratigraphic evidence and limited geochronology, with the emplacement of minor shallow intrusions and volcanic rocks onto pre-Cretaceous basement. In the southernmost Strandzha region, magmatism was initiated at ~86 Ma with emplacement of gabbroic to dioritic intrusions and related dikes into metamorphic basement rocks that have previously been overprinted by Jurassic-Lower Cretaceous metamorphism. The Yambol-Burgas region is an extensional basin between the East Balkan and the Strandzha regions, which broadens and deepens toward the Black Sea further east and is filled with a thick pile of marine sediments and submarine extrusive volcanic rocks accompanied by coeval intrusions. This dominantly mafic magmatism in the intermediate Yambol-Burgas region commenced at ~81 Ma and produced large volumes of potassium-rich magma until ~78 Ma. These shoshonitic to ultrapotassic basaltic to intermediate magmas formed by differentiation of ankaramitic (high Ca) parental melts, produced from partial remelting

of amphibole clinopyroxenites upon interaction with subduction-modified mantle wedge melts, according to earlier petrological studies. This peak of dominantly extrusive activity in the Yambol-Burgas region extended into the Strandzha region further south, in the form of numerous tholeiitic, calc-alkaline and high-K intrusions emplaced in the same time period between 81 and 78 Ma.
Granitic rocks from exposed basement of Eastern Srednogorie zone are dated as Permian/Carboniferous (~275–300 Ma). Zircons with similar ages occur in Upper Cretaceous rocks from the East Balkan and Strandzha regions, indicating local incorporation as xenocrysts. In contrast, magmatic rocks from the intermediate Yambol-Burgas region contain mostly Ordovician (~460 Ma) or older inherited zircons, suggesting a either a different basement history or, more likely, a different level of magma storage and crustal assimilation.
Integrating these geochronological results with a synthesis of the regional geology, we propose a two-stage geodynamic evolution for the Eastern Srednogorie segment of the Tethyan arc. The earlier stage of normal arc magmatism was driven by a southward-retreating, which formed the ~ 90 Ma calc-alkaline to high-K shallow intrusions and volcanics in the north (East Balkan), 87-86 Ma old tholeiitic and calc-alkaline intrusions in the south (Strandzha), and the voluminous 81-78 Ma old gabbroic to granitic intrusions with predominantly calc-alkaline to high-K composition throughout the Strandzha region. This stage continued westward into the Central Srednogorie zone, where the southward younging of calc-alkaline magmatism correlates well with an increased input of primitive mantle melts, indicating astenospheric incursion into a widening mantle wedge as a result of slab roll-back. The second stage proceeded in the Eastern Srednogorie zone only, where more extreme extension associated with the opening of the Black Sea back-arc basin led to the formation of an intra-arc rift in the Yambol-Burgas region, which now separates the East Balkan region from the Strandzha region. In this extensional environment, crustal thinning lead to decompression and increased heat flow, facilitating large-scale melting of lower crustal rocks and the formation of 81-78 Ma magmas. The unusual calcic composition of the parent magmas, their isotopic character and distinct xenocrystic population are consistent with a component of re-melting of hydrous lower-crustal cumulates, which probably formed in part during the first stage of the evolving arc.

Keywords: U-Pb zircon ages, ID-TIMS, LA ICPMS, Eastern Srednogorie arc, geodynamic evolution

1. Introduction

The Alpine orogeny in Europe formed from the long-term convergence between Africa and Europe and the associated consumption of Mesozoic oceanic basins through northward subduction of oceanic lithosphere beneath the European continent (Jankovic, 1997; Neubauer, 2002; Schmid et al., 2008; Burg, 2011). The Carpathian-Balkan segment of the Alpine orogen preserves geochemical evidence for these large-scale processes. The Apuseni-Banat-Timok-Srednogorie (ABTS) belt (Popov et al., 2002) is a more than 1000 km long belt of Upper Cretaceous calc-alkaline magmatic rocks with subduction-like geochemical signature. Presently, the ABTS belt extends from south Romania through east Serbia and across Bulgaria (Fig. 1) and hosts Europe's major Cu–porphyry deposits (Mitchell, 1996; Berza et al., 1998; Heinrich and Neubauer, 2002).
Since the first plate-tectonic interpretations, the formation of the ABTS belt and the Srednogorie zone is attributed to the northward subduction of the Vardar oceanic branch of the Tethys Ocean beneath the Serbo-Macedonian-Rhodope massif and the Moesian promontory of the European continent (Dewey et al., 1973; Boccaletti et al., 1974; Aiello et al., 1977; Hsü et al., 1977; Dabovski et al., 1991; Jankovic, 1997; Ricou et al., 1998; Stampfli and Borel, 2004). Other models had considered the ABTS belt as an extensional structure in an epicontinental rift environment that formed as a result of post-collisional

collapse and related astenospheric diapirism (Antonijevic et al., 1974; Popov, 1981; Popov, 1987). Neubauer (2002) suggested that some characteristics of the ABTS belt can be explained by progressive east to west tear-off of the subducted oceanic slab in a syn-collisional regime.

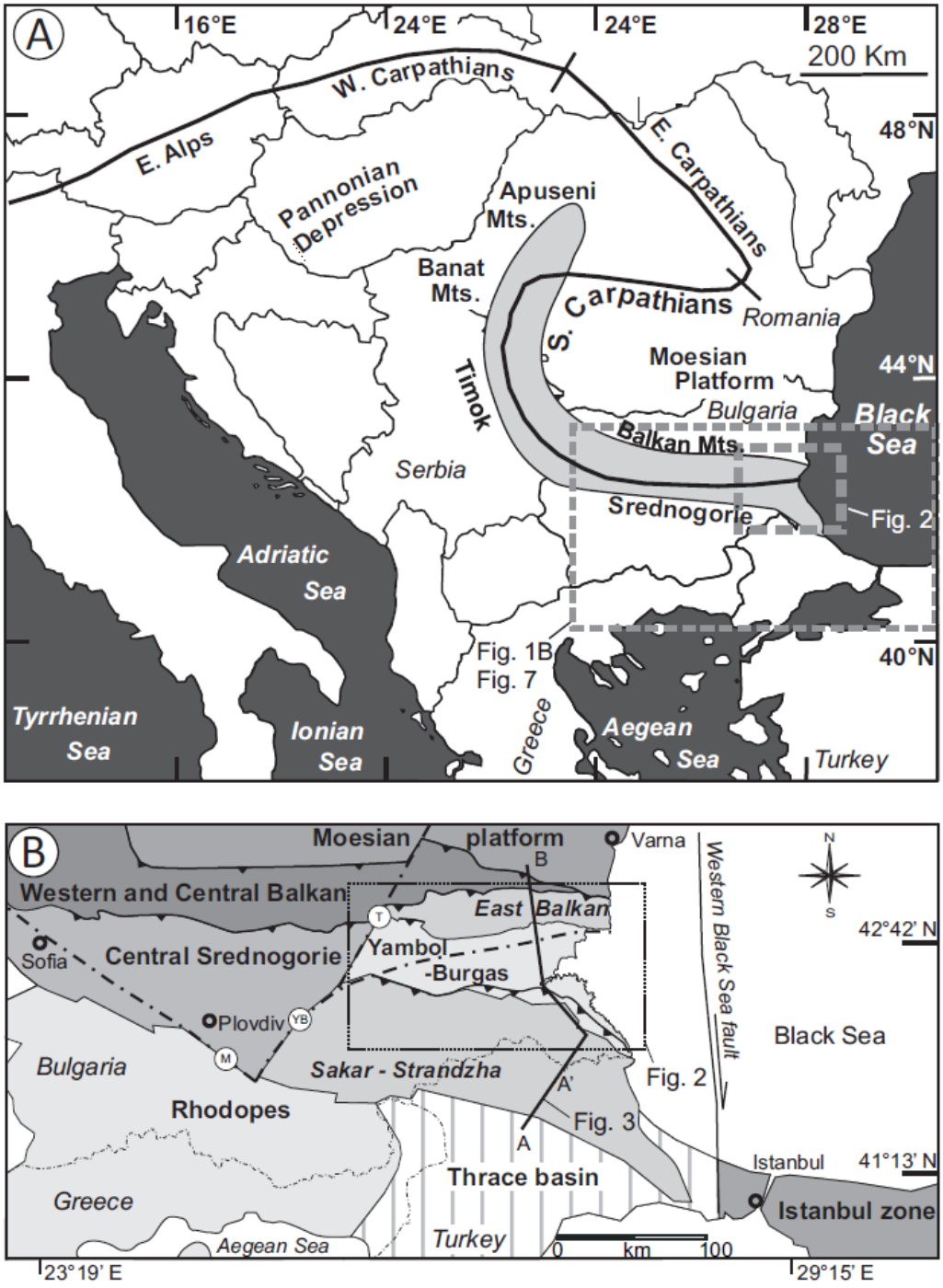

Figure 1. A) Sketch map of south-eastern Europe showing the location of Apuseni-Banat-Timok-Srednogorie Upper Cretaceous magmatic belt (gray field). Solid black line is the main front of the Alpine-Carpathian-Balkan orogeny. Eastern Srednogorie zone occupies the easternmost parts of ABTS belt (grey dashed square). Modified after Ciobanu et al. (2002). **B**) Simplified tectonic map of Eastern Srednogorie zone (dotted rectangle) and adjacent units. Modified after Banks (1997), Dabovski et al. (2009-a), Ivanov (in press), Kamenov et al. (2003) and Okay et al. (2001). Location of Western Black Sea fault after Okay et al. (1994). Thick dash-dot-dash lines are major deep seated faults: YB- Yambol-Burgas fault (Dachev, 1988); M- Maritsa fault; T- Tvarditsa fault (Bončev, 1971). Additional details are shown in Fig. 7.

Intense post-emplacement tectonics and erosion during the Alpine orogeny, combined with poor outcrops due to the low relief and young sediment infills, hinder a detailed geodynamic reconstruction of this area. High-precision geochronological dating provides a key tool to decipher the sequence of magmatic events in such terranes with complex post-emplacement history and poor preservation. High-precision U-Pb ID-TIMS zircon ages were reported for Late Cretaceous rocks from the Central Srednogorie zone (von Quadt et al., 2005). In the Panagyurishte transect, a Cu-Au-mineralized trend oriented obliquely to the main strike of the ABTS belt, magmatic ages gradually decrease from ~ 92 Ma in the north to ~ 78 Ma in the south. Re-Os molybdenite ages confirm the age progression of porphyry and epithermal Cu-Au mineralization in this transect (Zimmerman et al., 2008). This trend is accompanied by changing igneous geochemistry, showing increasing mantle input from north to south (von Quadt et al., 2005; Kamenov et al., 2007). The combination of age and geochemical progressions is explained by a geodynamic model involving north-dipping subduction of Vardar oceanic lithosphere that experienced a progressive southward roll back of the subducting slab (von Quadt et al., 2005). In this model, steepening of the slab during rollback leads to an increased corner flow of upper lithospheric mantle and asthenospheric material, combined with extension of the upper plate.

The Eastern Srednogorie zone is the easternmost part of the ABTS belt, situated between the Central Srednogorie zone and the Black Sea (Figs. 1, 2). It is characterized by a presently thinner crust (28-30 km) compared to the rest of the Balkan Peninsula (e.g. crustal thickness in the adjacent Central Srednogorie zone is ~ 40 km; Dachev, 1988). Compared to the remaining ABTS belt, this zone hosts voluminous, mostly extrusive magmatism with unusually mafic and alkaline composition and a clear across-arc geochemical zonation (Georgiev et al., 2009 and references therein). The large volume and geochemical diversity of Eastern Srednogorie magmatism provides an excellent opportunity for detailed geochronological and geochemical studies to aid deciphering the evolution of the whole ABTS belt and the Balkan region. The position of Eastern Srednogorie zone next to the Central Srednogorie zone allows direct age and geochemical correlations within the Upper Cretaceous belt. Eastern Srednogorie zone is also the potential link of the ABTS belt with the Upper Cretaceous Pontide belt in Turkey to the southeast (Jankovic, 1997), and with the Black Sea basin to the east. The Black Sea is an extensional back-arc basin (Zonenshain and Le Pichon, 1986) that formed during an Aptian-Albian (~125Ma to 100 Ma) main rifting phase, followed by intensive oceanic crust formation in spreading centers (Görür, 1988; Kaz'min and Tikhonova, 2006; Nikishin et al., 2001; Starostenko et al., 2004).

In this paper we aim to constrain the time evolution of the Late Cretaceous magmatism in the Eastern Srednogorie zone. We address the following main questions: 1) what is the precise age of magmatic rocks? 2) is there any along- or across strike age zonation within Eastern Srednogorie zone or correlations between ages and geochemistry of the magmatic rocks? 3) what is the age of the exposed basement intrusive rocks and is there any evidence for assimilation of basement rocks by the Upper Cretaceous magmas? 4) what is the geodynamic significance of the age data? To address these issues, we present and discuss an extensive dataset of U-Pb zircon ages from Eastern Srednogorie zone.

2. Regional geology

2.1. Geology of Eastern Srednogorie zone

. The basement of Eastern Srednogorie zone begins with Precambrian (?) high-grade metamorphic rocks, Paleozoic granites and greenschist facies rocks, followed by Permian clastics, Triassic carbonates and Lower-Middle Jurassic marine clastics and shales exposed in the present-day Strandzha Mountains (Figs. 2 and 3) (Chatalov, 1990; Dabovski et al., 2002; Gerdjikov, 2005). In the southeastern part of Strandzha these rocks are tectonically overlain by allochthonous Paleozoic and Triassic metasediments. In the East Balkan region, basement rocks are exposed in a narrow strip of Triassic carbonates

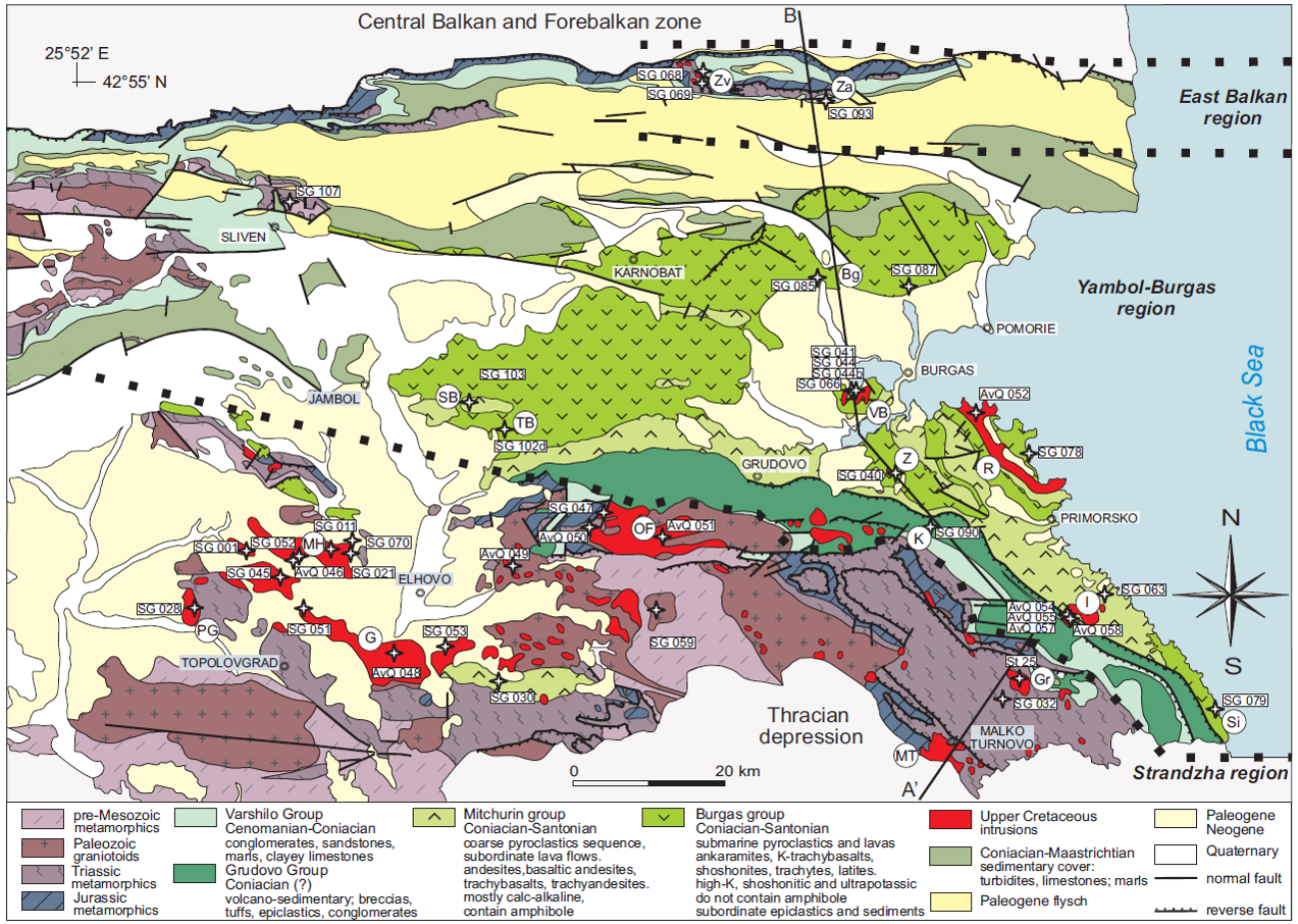

Figure 2. Geological map of Eastern Srednogorie zone, modified after Cheshitev and Kanchev (1989), showing U-Pb zircon ages of magmatic rocks (SG-and AvQ- numbered samples). Bold letters indicate confidently determined ages and italic letters are for tentative ages. Ages preceded with * are obtained by LA-ICPMS. The A'-B line marks the approximate location of a summary cross-section, presented on Fig. 3. Thick dotted lines mark the three magmatic regions within Eastern Srednogorie. White labeled circles are major magmatic centers as follows: in Strandzha region - PG – Polski Gradetz; MH – Monastery Heights; G – Granitovo; OF – Oman-Fakya; MT – Malko Turnovo; Gr – Gramatikovo; in Yambol-Burgas region - Si – Silistar; I – Izgrev; K – Krushevetz; R – Rossen; Z – Zidarovo; VB – Vurli Brjag; TB – Tamarino Bakadzhik; SB – Sveti Spaski Bakadzhik; Bg – Bulgarovo; in East Balkan region – Za – Zaimchevo; Zv – Zvezda.

and flysch-like sediments, and Jurassic shales (e.g. Dabovski et al., 2002). The Upper Cretaceous succession begins with Cenomanian continental and shallow marine clastic sediments preserved along the border between the Strandzha Mountains and the Yambol-Burgas depression, and also in the East Balkan Mountains. During the Turonian, deeper marine shales and argillaceous carbonates were deposited in a deepening basin. In the Coniacian-Campanian the Yambol-Burgas depression was filled with a 5-6 km thick volcano-sedimentary succession (Nachev and Dimitrova, 1995a; Nachev and Dimitrova, 1995b). The East Balkan basin also records a thick Coniacian-Campanian deep marine sequence but lacks voluminous volcanic products. The Upper Cretaceous volcano-sedimentary sequence is unconformably overlain by shallow-marine Maastrichtian carbonates in the Yambol-Burgas depression and by Paleogene and Neogene continental to shallow marine clastics and carbonate rocks in the East Balkan. Additional description of the geology of Eastern Srednogorie zone is given in Dabovski (1991), Dabovski et al. (2002), Georgiev et al. (2001) and Georgiev (2008).

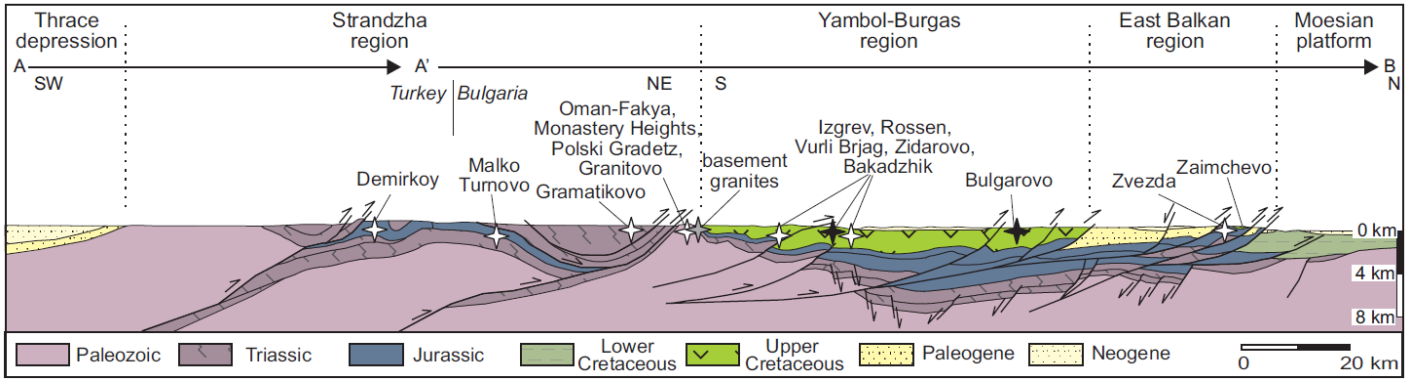

Figure 3. Schematic cross-section of Eastern Srednogorie zone along the A'-A-B line shown on Fig. 1b and Fig. 2, with approximate north-south location of dated Upper Cretaceous intrusions (white stars), Late Cretaceous lavas (black stars), and basement granitoids (gray stars). Cross-section based on tectonic interpretations and geophysical data from Georgiev et al. (2001) and Banks (1997).

2.2. Magmatism

More than 90 intrusions and volcanic centers are described in the Eastern Srednogorie zone (Popov, 1981; Nachev and Nachev, 2003), comprising more than 60 area percent of the exposed magmatic rocks of Cretaceous age in the whole Srednogorie zone (Stanisheva-Vassileva, 1989). In contrast to most of the ABTS magmatic belt, where calc-alkaline rocks of intermediate composition prevail, the Eastern Srednogorie zone is characterized by a large geochemical variability and a predominance of mafic to intermediate over felsic magmas. Primitive nepheline-normative ankaramites have been reported among the mafic lavas (Georgiev et al., 2009; Marchev et al., 2009). Abundant major element geochemical data show that the mafic and intermediate magmatism in Eastern Srednogorie zone covers the entire spectrum of chemical series observed in volcanic arcs: from tholeiitic through calc-alkaline to alkaline (shoshonitic) compositions (Stanisheva-Vassileva, 1980; Popov, 1981; Stanisheva-Vassileva, 1989; Georgiev et al., 2009). An increase of the K_2O content of the rocks from south to north has been interpreted as evidence for the progressive deepening of the melt-generation regions, consistent with a northward subduction of the Vardar Ocean plate below the European platform (Stanisheva-Vassileva, 1980; Stanisheva-Vassileva, 1989; Dabovski et al., 1991). However, new geochemical data from the northernmost magmatic products in Eastern Srednogorie zone reveals a complex zonation with more evolved calc-alkaline magmas to the south and north and more mafic shoshonitic to ultra-potassic magmas in the center (Georgiev et al., 2006; Georgiev, 2008; Georgiev et al., 2009). Four magmatic regions are traditionally distinguished within Eastern Srednogorie zone: Strandzha, Yambol-Burgas, North Burgas and East Balkan from south to north. The North Burgas region, which has been considered a back-arc rift (Dabovski et al., 1991; Georgiev et al., 2001), shows similar

major and trace element characteristics and isotopic fingerprints as the Yambol-Burgas region (Marchev et al., 2009; Georgiev et al., 2009). Based on these similarities, Georgiev et al., (2009) proposed a common origin for the magmatic rocks from the Yambol-Burgas and the North Burgas regions. Here, we adopt this view and merge the two regions into one extended region named Yambol-Burgas region (Figs. 2 and 3).

The Yambol-Burgas and Strandzha regions host most of the Upper Cretaceous magmatic products in the Eastern Srednogorie zone, whereas only few small outcrops are known in the East Balkan region (Georgiev et al., 2009). Magmatic rocks from the Strandzha and East Balkan regions are mostly calc-alkaline to high-K intrusions containing hydrous phases, whereas in the central Yambol-Burgas region they are dominantly basic to intermediate submarine shoshonitic volcanic rocks that rarely contain hydrous minerals (Georgiev et al., 2009). Stratigraphic relations constrain the magmatism in Eastern Srednogorie zone as broadly Turonian–Campanian (from ~ 94 to ~70 Ma) and the peak of the magmatic activity is considered as Coniacian-Campanian, from ~ 90 to ~70 Ma (e.g. Dabovski et al., 1991; Georgiev et al., 2001). Prior to this study, available radiometric data consisted exclusively of K-Ar ages of whole-rocks or mineral separates varying between 130 and 50 Ma (summarized in von Quadt et al., 2005). The exposed basement rocks in this zone were not dated radiometrically.

2.3. Metallogeny

The ABTS belt is the most important metallogenic belt in the Alpine-Balkanide-Carpathian-Dinaride region (Heinrich and Neubauer, 2002), hosting major porphyry style and high-sulphidation Cu ± Au polymetallic and carbonate-replacement deposits. In contrast to the Central Srednogorie and Timok parts of the ABTS belt that host the economically most important deposits, magmatism and associated hydrothermal activity in the Eastern Srednogorie zone produced mostly Fe ± Cu skarn deposits and mesothermal- to epithermal Cu-Au polymetallic vein deposits with smaller size. The different chemical composition and depth of magma emplacement predetermined the contrasting mineralization style between the Strandzha and Yambol-Burgas regions of Eastern Srednogorie zone. In the Strandzha region, emplacement of tholeiitic to calc-alkaline gabbro-dioritic intrusions in Triassic carbonates formed the Fe-skarn magnetite-rich deposit of Krumovo in the Monastery Heights and the Cu-skarn deposits near Malko Turnovo (Fig. 2), as well as numerous smaller occurrences and showings, including orthomagmatic Fe-Ti mineralizations. In the Yambol-Burgas region, ore deposits of mesothermal to epithermal Cu-polymetallic vein type are related to volcano-plutonic systems with shoshonitic and high-K magmatism (Popov, 1996), including the Zidarovo, Vurli Brjag, Rossen and Tamarino Bakadzhik ore fields (Fig. 2) that formed at shallower crustal depth compared to the skarn deposits in the Strandzha region.

3. Sample selection and analytical techniques

We sampled fresh to minimally altered intrusive and extrusive rocks, selecting samples where field relations indicated clear temporal succession of emplacement. Samples were crushed and ground, and mineral concentrates were purified by magnetic and density separation (Wilfley table and heavy liquids) techniques. Individual zircons were further selected using a binocular microscope.

3.1. Conventional high-precision TIMS single-grain dating

Prior to analyses, most single zircon crystals were pre-treated to remove zircon domains prone to post-crystallization Pb loss. The majority of the analyzed zircons (~60%) were air-abraded for several hours in the presence of pyrite grains following the method of Krogh (1982). The chemical abrasion technique of Mattinson (2005) was tested on ~20% of the grains, and the remaining 20% of zircon grains were analyzed without any pre-treatment (unabraded). All zircon grains were separately cleaned, spiked with a ^{205}Pb-^{235}U tracer and digested following procedures in Krogh (1973). After anion exchange column chemistry, both Pb and U were loaded on an outgassed Re filament. Isotope ratios

were determined in ETH-Zurich on a Finnigan MAT 262 mass-spectrometer, using electron multiplier for most samples. Further details are given by Georgiev (2008) and von Quadt et al. (2011). The Pb MacDat Excel spreadsheet (Coleman, unpublished), which incorporates error propagation equations of Ludwig (1980), was used for data reduction. We used a mass fractionation of 0.11±4.6 %/AMU for Pb measured with Faraday cups, and 0.13±4.0 %/AMU for Pb measured with the electron multiplier, determined from multiple analyses of the NBS982 Pb standard. Total procedural blank was on average 0.8 pg Pb and 0.01 pg U with a Pb isotopic composition of $^{206}Pb/^{204}Pb$ = 17.8±0.29, $^{207}Pb/^{204}Pb$ = 15.47±0.30, $^{208}Pb/^{204}Pb$ = 37.35±0.80. Concordia plots, weighted averages, and probability density plots were constructed with the Isoplot 3.00 software (Ludwig, 1991; Ludwig, 2003).

3.2. Zircon imaging and LA-ICPMS single grain dating

The largest and inclusion free grains were handpicked, mounted in epoxy resin and polished to expose grain cores. Chips were then carbon-coated for electron-microscope imaging. Backscattered electron (BSE) and cathode-luminescence (CL) images were acquired at ETH Zurich using a CamScan CS44LB scanning electron microscope. After imaging, chips were re-polished to remove coating and cleaned. Laser dating was performed at ETH Zurich using a 193nm ArF excimer laser (Lambda Physik) coupled to an Elan 6100 DRC ICP-MS instrument (Perkin Elmer). More detailed description of the instrumentation is given in Günther et al. (1998) and Heinrich et al. *(*2003). Ablation spots were chosen based on CL and BSE images and transmitted-light petrography. Energy densities of 20 to 25 J/cm^2 and laser pulse frequency of 10 Hz were used. A typical analytical block consisted of 20 measurements (3 NIST 610 standards at the beginning, 14 zircons, and 3 standards at the end). Additional details are given in Georgiev (2008).
The reported ages and errors were calculated using an in-house Excel-based spreadsheet (Georgiev, 2008). Data were corrected for laser-induced elemental fractionation using the intercept of the linear regression through the raw ratios as described in Chang et al. (2006). Mass discrimination was controlled and corrected by applying an external correction method. First, we measured NIST 610 as an unknown, corrected the raw data for laser induced fractionation, and used numerous point analyses of the zircon standards Plesovice (Slama et al., 2008) and 91500 (Wiedenbeck et al., 1995) for external mass-bias correction. The resulting NIST 610 values of $^{206}Pb/^{238}U$= 0.21938, $^{207}Pb/^{235}U$ = 89.53417 and $^{208}Pb/^{232}Th$ = 0.44836 were reproducible and independent of crater diameters between 20 to 70 microns provided that crater depth stayed smaller than the crater radius. These calculated NIST 610 values thus include a correction for any matrix dependence between zircon and silicate glass, and were subsequently used for external calibration of unknown zircon samples. This calibration procedure has the advantage of better counting-statistical reproducibility of the comparatively Pb-rich (426 ppm Pb) NIST 610. The calculated U-Th-Pb isotope ratios differ from published TIMS values for NIST 610 (Stern and Amelin, 2003), but are close to the U-Th-Pb isotope ratios derived from concentrations and isotope abundances in NIST 610 (data from Rocholl et al., 2000). The amount of common Pb was calculated from ^{204}Hg-corrected ^{204}Pb intensities. ^{201}Hg or ^{202}Hg masses were monitored and used to calculate ^{204}Hg counts, which were subtracted from the ^{204}Pb counts. Following Hg-correction, the $^{206}Pb/^{238}U$ age calculated from background and mass-bias corrected $^{206}Pb/^{238}U$ ratio was used to estimate the initial common Pb composition from the Stacey and Kramers (1975) model for Pb isotopic evolution through time. Using this composition, the fraction of ^{206}Pb, ^{207}Pb, ^{208}Pb proportional to the measured Hg-corrected ^{204}Pb was subtracted from the calculated $^{206}Pb/^{238}U$, $^{207}Pb/^{235}U$ and $^{208}Pb/^{232}Th$ ratios.

3.2.1. Error propagation, precision and accuracy

The reported error of individual laser dates includes two components. In addition to the counting error on the intercept regression, we included the 2σ errors from the first three and the last three standard measurements by standard error propagation. The accuracy

of our LA-ICPMS U-Pb method was estimated continually by analyzing zircon standards Plesovice and 91500 as unknowns, bracketed by NIST 610 silicate glass standard and using the calibrated NIST values for mass bias correction. The long-term average for Plesovice zircon over several sessions gives an age of 338.3±2.5 Ma (weighted average $^{206}Pb/^{238}U$, n = 13, MSWD = 2.9), which is in agreement with the ID-TIMS age of 337.13±0.37 (Slama et al., 2008). Our $^{206}Pb/^{238}U$ LA-ICPMS age for the 91500 standard is 1058.4±9.4 Ma (n = 15, MSWD = 2.5), which overlaps within errors the 91500 ID-TIMS age of 1065±0.4 Ma (Wiedenbeck et al., 1995).

4. Results

Zircon grains from 43 samples were analyzed in this study, 39 from Cretaceous magmatic rocks and 4 from the exposed pre-Cretaceous basement. Results from single-grain U-Pb ID-TIMS dating are presented in Appendix 1; LA-ICPMS U-Pb data are given in Appendix 2. The North-Burgas area is presented as a separate region in the electronic supplement for easier comparison with some published literature. However, this area is considered as part of the Yambol-Burgas region in the discussion, as noted earlier. To better constrain the crystallization age of a rock and minimize subjectivity, we followed several criteria for age calculations. We gave preference to ID-TIMS ages over LA-ICPMS data, where sufficient numbers of zircon grains were analyzed by both methods. Depending on sample population and number of studied grains, concordia ages were preferred rather than upper - or lower intercept ages or weighted averages of $^{206}Pb/^{238}U$ ages. Intercept ages and weighted $^{206}Pb/^{238}U$ ages were filtered based on the number of grains and MSWD values that indicate the overlap and scatter of data points. Although these general rules were taken into account, every sample has its own specifics. The dated samples are subdivided into two categories based on our confidence in the calculated crystallization age: a) samples with high-confidence crystallization ages; b) samples with tentative ages. The tentative ages reflect either the small number of analyzed grains or the large uncertainty, but these are geologically meaningful ages; additional analyses are likely to better constrain the age. In some rocks, however, the number of studied grains and/or the complex U-Pb systematic did not allow calculations of reliable U-Pb crystallization ages. Discussion of U-Pb zircon age data for individual rock samples is given in Appendix 3 and summarized below. BSE and CL zircon images are given together with the location of the LA-ICPMS dating in Appendix 4.

4.1. Age of Upper Cretaceous magmatic rocks

4.1.1. U-Pb crystallization ages

High-confidence crystallization ages were obtained for 14 Upper Cretaceous rocks (Table 1). From these, ten are from the Strandzha region and four from the Yambol-Burgas region. Most high-confidence ages are for intrusive rocks, with the exception of samples SG 021 (dike) and SG 103 (lava flow). For nine samples the calculated crystallization ages are tentative. The U-Pb ages range from ~87 Ma to ~ 78 Ma, constraining the duration of the Late Cretaceous magmatic activity to ca. 9 Ma (Fig.2, Fig. 4). Most rocks from all regions crystallized between 81.23 and 78.00 Ma. A second, clearly visible age group comprises intrusive and dike rocks from Strandzha region (from Monastery Heights and Gramatikovo plutons) with ages ranging from 87.1 to 86.2 Ma. Additionally, a dioritic intrusion from Silistar has a slightly younger age near 76 Ma, but the age errors are large and overlap the 78 Ma event.

The ages within a given magmatic center vary within a narrow range and generally overlap within their errors (e.g. Izgrev pluton; Granitovo pluton). The only notable exception is the Monastery Heights pluton in the Strandzha region, where two distinct magmatic events with high-confidence ages of 86 (diorite) and 81-79 Ma (gabbro, basalt and granite) are detected. This age spread is too large to be explained with the presence of a long-lived magma chamber and indicate that the Monastery Heights intrusion was

Table 1. Calculated crystallization ages for Late Cretaceous rocks from Eastern Srednogorie zone.

Sample	Region	Center	Type	Method	N	N*	Age, Ma	Error, Ma	Age type	MSWD	Type of error	Category
SG 085	Yambol-Burgas	Bulgarovo	v	ID-TIMS	3	1	79.90	3.20	C		95% conf.	tentative
SG 103	Yambol-Burgas	Bakadzhik	v	ID-TIMS	1	1	80.08	3.10	C		95% conf.	tentative
SG 102d	Yambol-Burgas	Bakadzhik	v	ID-TIMS	3	1	79.59	3.00	C		95% conf.	tentative
SG 044	Yambol-Burgas	Vurli Brjag	i	ID-TIMS	7	4	78.98	0.31	LI	1.5	95% conf.	confident
SG 044b	Yambol-Burgas	Vurli Brjag	v	ID-TIMS	4	1	79.46	0.60	C		2 sigma	tentative
SG 040	Yambol-Burgas	Zidarovo	i	LA-ICPMS	9	4	78.00	2.80	WTD	1.3	95% conf.	tentative
AvQ 052	Yambol-Burgas	Rossen	i	ID-TIMS	2	2	79.62	0.47	C		95% conf.	confident
AvQ 057	Yambol-Burgas	Izgrev	i	ID-TIMS	13	2	79.93	0.22	C		2 sigma	confident
AvQ 054	Yambol-Burgas	Izgrev	i	ID-TIMS	5	4	81.23	0.17	C		2 sigma	confident
SG 079	Yambol-Burgas	Silistar	i	LA-ICPMS	5	4	76.20	1.60	WTD	0.71	95% conf.	tentative
SG 028	Strandzha	Polski Gradetz	i	ID-TIMS	7	1	78.27	0.18	C		2 sigma	confident
SG 001	Strandzha	Monastery Heights	i	LA-ICPMS	5	3	80.60	1.10	C		2 sigma	confident
AvQ 046	Strandzha	Monastery Heights	i	ID-TIMS	4	1	79.10	0.17	C		2 sigma	tentative
SG 052	Strandzha	Monastery Heights	d	ID-TIMS	5	2	78.83	0.17	C		2 sigma	confident
SG 011	Strandzha	Monastery Heights	i	ID-TIMS	5	3	86.36	0.14	C		2 sigma	confident
SG 021	Strandzha	Monastery Heights	d	ID-TIMS	4	3	78.95	0.30	C		95% conf.	confident
SG 053	Strandzha	Chernozem-Razdel	i	LA-ICPMS	8	3	79.91	2.00	tuffzirc		75% conf.	tentative
SG 045	Strandzha	Granitovo	i	ID-TIMS	4	1	79.66	0.14	C		2 sigma	confident
AvQ 048	Strandzha	Granitovo	i	ID-TIMS	15	6	79.94	0.14	WTD	2.2	95% conf.	confident
AvQ 050	Strandzha	Oman-Fakya	i	ID-TIMS	3	3	80.98	0.32	C		95% conf.	confident
AvQ 051	Strandzha	Oman-Fakya	i	ID-TIMS	6	3	79.77	0.30	C		95% conf.	confident
SG 032	Strandzha	Gramatikovo?	d	ID-TIMS	3	1	85.23	3.60	C		95% conf.	tentative
ST 25	Strandzha	Gramatikovo	i	ID-TIMS	4	4	86.84	0.29	C		95% conf.	confident

Abbreviations: v - volcanic; d - dike; I - intrusive; N - number of grains analyzed from the sample with the reported method; N - the number of grains, used for the calculation of the crystallization age; C – concordia; WTD - weighted average $^{206}Pb/^{238}U$ age; LI - lower intercept; tuffzirc - age, calculated with the zircon age extraction algorithm of ISOPLOT.*

generated in at least two separate magmatic pulses. The two pulses, however, have similar Sr and Pb whole-rock isotopes (Georgiev et al., 2009).

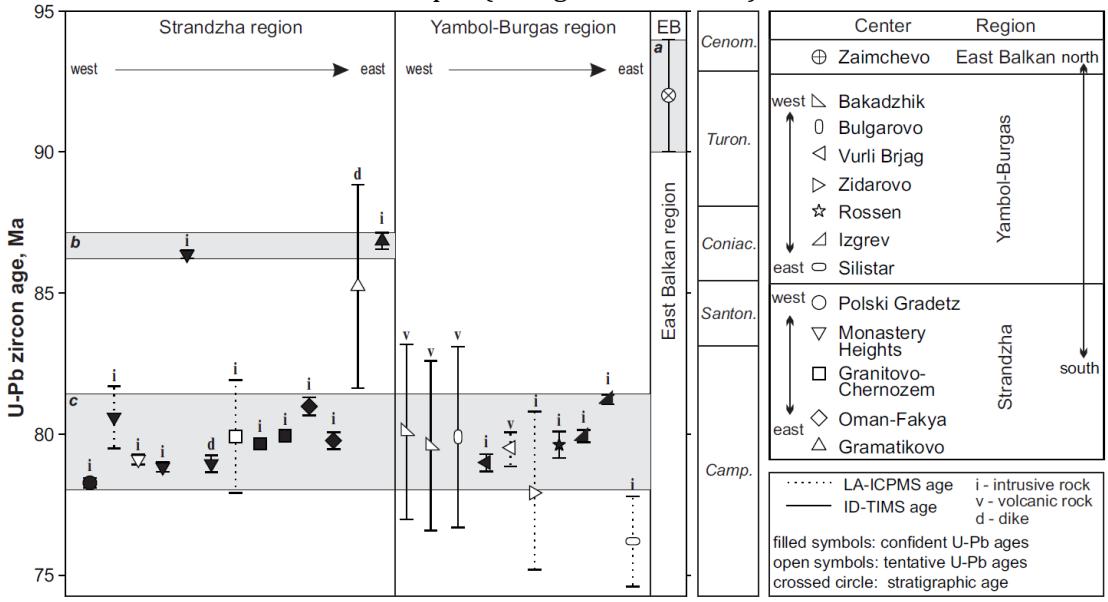

Figure 4. High-confidence and tentative U-Pb crystallization ages of Upper Cretaceous magmatic rocks from Eastern Srednogorie zone and corresponding 2 sigma errors. Stratigraphic constraints for a Late Cenomanian-Early Turonian age (Kunchev, 1966; Dabovski et al., 2009b) are used to plot the East Balkan magmatism at 92±2 Ma. Ages for the Upper Cretaceous stage boundaries taken from Ogg et al. (2008). Gray fields delineate the three major magmatic events discussed: (*a*) the ~92 Ma event observed only in the East Balkan, ages are based on biostratigraphy; (*b*) the 87.1-86.2 Ma event based on high-confidence U-Pb ID-TIMS zircon ages, observed only in the Strandzha region; and (*c*) the 81.4-78.0 Ma event based on high-confidence U-Pb ID-TIMS zircon ages, observed in the Strandzha and Yambol-Burgas regions.

4.1.2. Distribution of U-Pb single zircon ages

Histograms of individual $^{206}Pb/^{238}U$ zircon ages show a prominent peak at 80 - 79 Ma (Fig. 5a), especially if the data of high confidence (TIMS data and concordant LA-ICPMS ages) are considered. This 80-79 Ma peak is particularly pronounced in the Strandzha region, where the number of dated grains is largest. Even though LA-ICPMS ages in Strandzha are generally more dispersed, their distribution matches ID-TIMS ages with a peak between 82 and 77 Ma. A second notable age peak at 87-85 Ma is defined by both ID-TIMS and LA-ICPMS data.

Similar to the Strandzha region, the most prominent peak in the Yambol-Burgas region is also at 80-79 Ma, with most of the zircons ranging from 82 to 77 Ma. However, the 87-85 Ma peak is not observed in the Yambol-Burgas region. Additionally, there is an indication of a 71 Ma event in the Yambol-Burgas region, defined by LA-ICPMS data, but this peak is not confirmed by ID-TIMS data. These younger ages may reflect Pb loss from zircons, undetected with the lower precision of LA data (larger error ellipses do not allow unambiguous distinction between concordant and slightly discordant grains). Few even younger LA-ICPMS zircon ages in the Strandzha and Yambol-Burgas regions are also attributed to Pb loss. The few grains showing ages older than 86 Ma from both Strandzha and Yambol-Burgas regions are not sufficient indication for an older magmatic event and probably reflect the presence of minor inherited components.

The number of studied rocks and/or analyzed zircons from the East Balkan region is insufficient for a detailed interpretation. Three rocks have zircons with $^{206}Pb/^{238}U$ ages ranging from 45 to 98 Ma, with no overlap within single samples.

In summary, zircon U-Pb age data unequivocally shows that the peak of the Late Cretaceous magmatic activity in the Eastern Srednogorie zone was from 82 until 77 Ma. Abundant magmatism within this time interval is observed in the southernmost Strandzha and the intermediate Yambol-Burgas regions. Few rocks from the Strandzha region are older (87-85 Ma). The radiometric age of the magmatism in East Balkan region

remains undetermined. However, stratigraphic relations constrain the age of East Balkan magmatism to ca. 90 Ma (see below).

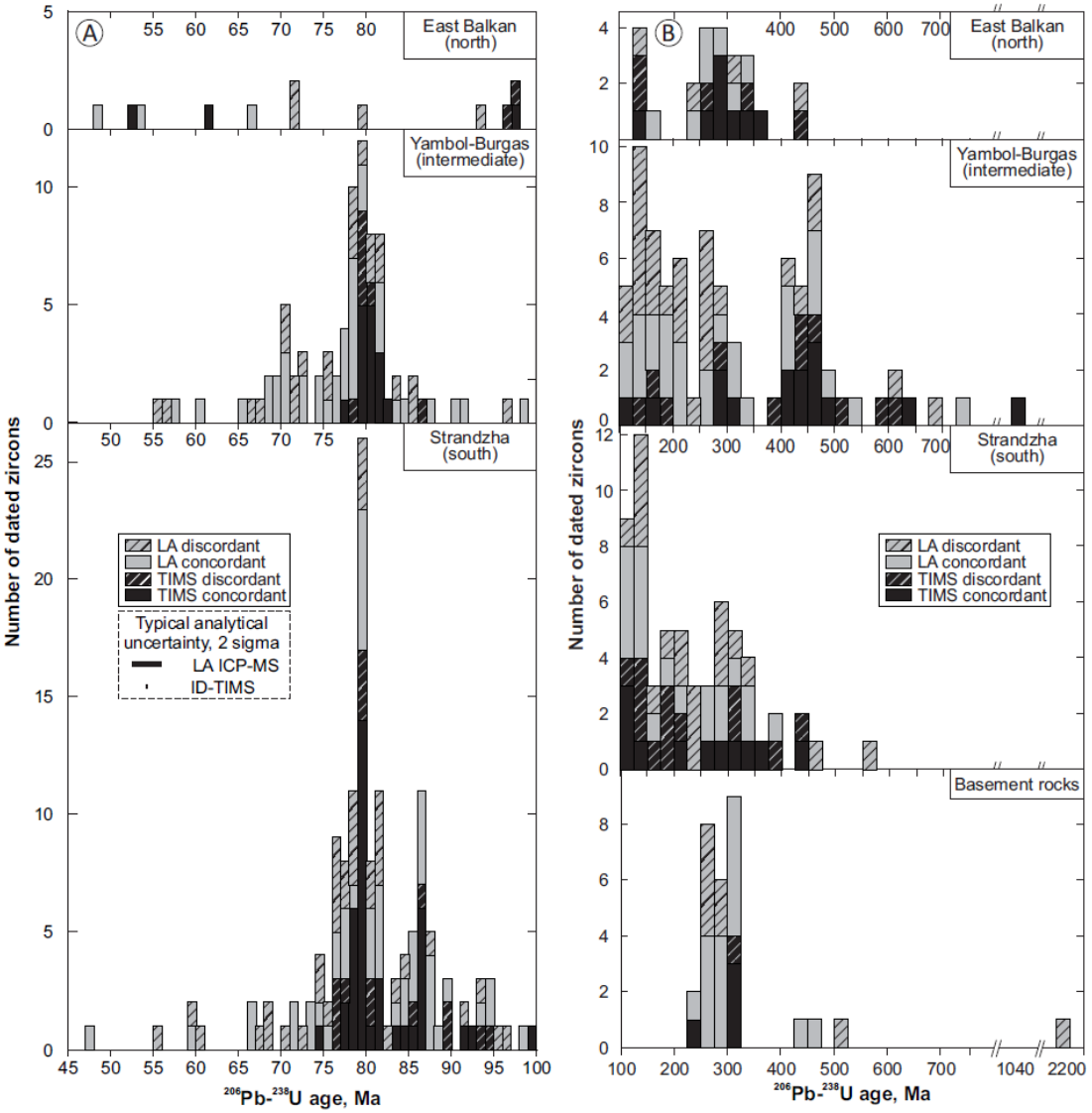

Figure 5. Histograms of single grain 206Pb/238U ages of all studied zircons. **A**) zircons younger than 100 Ma. Bin width is 1Ma; **B**) zircons older than 100 Ma. Bin width is 25 Ma. For plotting purposes, analyses that overlap the Concordia curve are classified and plotted as concordant. This approach avoids subjective decisions on the concordance of the grains, but it does not take into account the size of the error ellipse, or sometimes the unproportionally large error of the 207Pb/235U age compared to the 206Pb/238U age.

4.2. Age of basement rocks

U-Pb crystallization ages of three basement rocks from the Eastern Srednogorie zone range from 301 to 274 Ma (Table 2). These ages are similar to published zircon evaporation Pb ages for basement granites from the Turkish part of Strandzha: 271±2 Ma for Kirklareli metagranite, 271±11 Ma for Kula metagranite and 309±24 Ma for Uskup metagranite (Okay et al., 2001).

4.3. Age of inherited zircons

The studied rocks contain variable amounts of inherited older zircons in the form of xenocrysts and/or xenocrystic cores overgrown by Late Cretaceous rims (Appendix 3, Appendix 4). The distribution of single-grain $^{206}Pb/^{238}U$ ages of inherited zircons is shown on Fig. 5b. Zircons with 120-170 Ma ages are detected in all regions. All regions also contain a peak at ~300 Ma, but only the central Yambol-Burgas region has a prominent peak at ~460 Ma. Rare older zircon ages (550-1050 Ma) are detected only in this central region, whereas concordant Upper Cretaceous inherited zircons (80-92 Ma and

discernibly older than the host rock) are found only in Granitovo and Monastery Height intrusions in the Strandzha region. Geographically, most samples with inherited zircons are from the western and central parts of the Strandzha region and from the southeastern part of the Yambol-Burgas region (Fig. 6). This could represent local variations in the basement, but may also result from the unevenly distributed sampling and the different number of studied grains from different samples.

Table 2. Calculated crystallization ages of exposed basement rocks from Eastern Srednogorie zone.

Sample	Region	Center	Type	Method	N	N*	Age, Ma	Error, Ma		Type of error	category
SG 047	Strandzha	Oman-Fakya	i	LA-ICPMS	10	5	293.80	7.60	C	95% conf.	confident
SG 059	Strandzha	Zheljazkovo	i	ID-TIMS	4	3	301.26	0.97	C	2 sigma	confident
SG 070	Strandzha	Monastery Heights	i	LA-ICPMS	11	5	274.10	4.50	C	2 sigma	confident

Abbreviations: v – volcanic; i - intrusive; N - number of grains analyzed from the sample with the reported method; N - the number of grains, used for the calculation of the crystallization age; C – concordia*

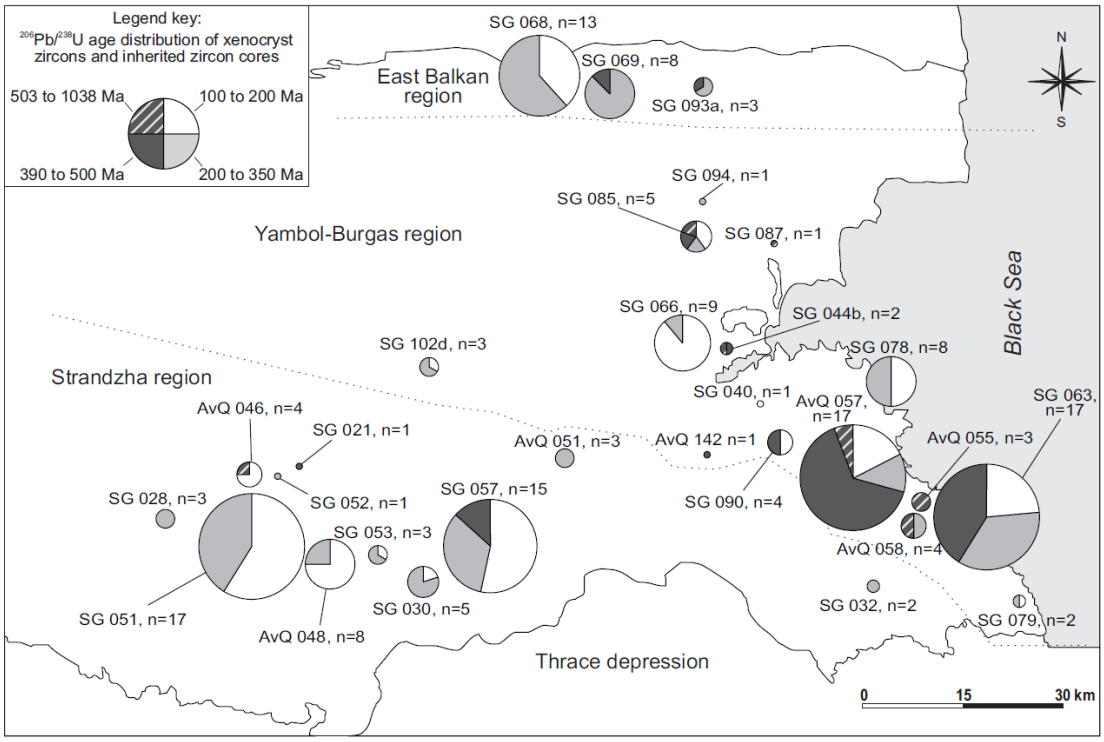

Figure 6. Sketch map showing the $^{206}Pb/^{238}U$ age distribution of inherited zircon cores and xenocryst zircons detected in Upper Cretaceous magmatic rocks (ID-TIMS and LA-ICPMS data). Some ID-TIMS $^{206}Pb/^{238}U$ zircon ages may represent mixtures of inherited cores and younger, Late Cretaceous rims. Sample location is approximate. The size of each circle is proportional to the number of inherited cores and xenocryst zircons (n) detected in the sample.

Calculated ages from ID-TIMS analyzed inherited grains are presented in Table 3. As with the single-grain $^{206}Pb/^{238}U$ ages, in the southernmost and northernmost regions (Strandzha and East Balkan) most inherited ages are 270-350 Ma old, whereas in the central regions the 404-450 Ma inherited ages dominate. Three significantly older ages at 1, 1.4 and 2 Ga are recorded in inherited zircons from the Yambol-Burgas region; such older ages were not found in Upper Cretaceous igneous rocks from the East Balkan and

Strandzha region (Fig. 5b, Table 3). An inherited core in a Variscan basement rock (sample SG 047) also has a similar concordant 2 Ga LA-ICPMS age.
In summary, the Strandzha and East Balkan regions have similar inheritance patterns with most grains clustering at ~300 Ma, while in the Yambol-Burgas region the most prominent peak is at ~460 Ma, with several grains showing considerably older ages.

Table 3. Calculated crystallization ages for unexposed basement rocks from Eastern Srednogorie zone, based on inherited grains entrained in Late Cretaceous igneous rocks.

Sample	Region	Center	Type	N	N*	Age, Ma	Error, Ma	Age type	MSWD	Type of error
SG 093a	East Balkan	Zaimchevo	v	3	1	271	0.7	C		2 sigma
SG 093a	East Balkan	Zaimchevo	v	3	3	577	57.0	UI	0.13	95% conf.
SG 068	East Balkan	Zvezda	i	17	4	109	6.7	LI	0.33	95% conf.
SG 068	East Balkan	Zvezda	i	17	4	139	18.0	UI	2.20	95% conf.
SG 069	East Balkan	Zvezda	d	3	1	281	0.9	C		2 sigma
SG 068	East Balkan	Zvezda	i	17	1	303	0.5	C		2 sigma
SG 068	East Balkan	Zvezda	i	17	1	350	8.8	C		95% conf.
SG 085	Yambol-Burgas	Bulgarovo	v	3	1	631	23.0	C		95% conf.
SG 044b	Yambol-Burgas	Vurli Brjag	v	4	1	442	20.0	C		95% conf.
SG 044b	Yambol-Burgas	Vurli Brjag	v	4	1	1039	4.2	C		2 sigma
AvQ 057	Yambol-Burgas	Izgrev	i	13	1	160	0.6	C		2 sigma
AvQ 057	Yambol-Burgas	Izgrev	i	13	1	280	0.7	C		2 sigma
AvQ 058	Yambol-Burgas	Izgrev	v	4	3	296	3.7	LI	0.60	95% conf.
AvQ 057	Yambol-Burgas	Izgrev	i	13	2	404	0.9	C		2 sigma
AvQ 058	Yambol-Burgas	Izgrev	v	4	1	445	1.6	C		2 sigma
AvQ 057	Yambol-Burgas	Izgrev	i	13	1	462	1.2	C		2 sigma
AvQ 057	Yambol-Burgas	Izgrev	i	13	3	1353	30.0	UI	0.46	95% conf.
AvQ 058	Yambol-Burgas	Izgrev	v	4	3	1948	3.7	UI	0.60	95% conf.
SG 063	Yambol-Burgas	Izgrev?	d	5	3	450	26.0	UI	0.56	95% conf.
SG 063	Yambol-Burgas	Izgrev?	d	5	3	507	9.2	UI	0.30	95% conf.
AvQ 046	Strandzha	Monastery Heights	i	4	1	85	0.3	C		2 sigma
AvQ 046	Strandzha	Monastery Heights	i	4	1	92	0.2	C		2 sigma
AvQ 046	Strandzha	Monastery Heights	i	4	1	104	2.0	C		2 sigma
SG 021	Strandzha	Monastery Heights	d	4	3	541	33.0	UI	0.05	95% conf.
AvQ 048	Strandzha	Granitovo	i	15	1	81	0.3	C		2 sigma
SG 051	Strandzha	Granitovo	i	6	4	268	37.0	UI	1.50	95% conf.
AvQ 048	Strandzha	Granitovo	i	15	6	281	64.0	UI	0.65	95% conf.
AvQ 051	Strandzha	Oman-Fakya	i	6	5	329	27.0	UI	6.10	95% conf.
SG 057	Strandzha	Sharkovo	i	5	3	112	5.2	LI	2.00	95% conf.
SG 057	Strandzha	Sharkovo	i	5	1	138	0.3	C		2 sigma
SG 057	Strandzha	Sharkovo	i	5	1	291	0.6	C		2 sigma
SG 057	Strandzha	Sharkovo	i	5	4	296	14.0	UI	0.28	95% conf.
SG 057	Strandzha	Sharkovo	i	5	3	442	6.1	UI	2.00	95% conf.
SG 030	Strandzha	Voden	v	5	5	162	8.1	LI	1.40	95% conf.
SG 030	Strandzha	Voden	v	5	5	285	35.0	LI	0.40	95% conf.
SG 030	Strandzha	Voden	v	5	5	397	24.0	UI	1.40	95% conf.
SG 032	Strandzha	Gramatikovo?	d	3	3	470	15.0	UI	1.90	95% conf.

Abbreviations: v – volcanic; i - intrusive; N - number of grains analyzed from the sample with the reported method; N - the number of grains, used for the calculation of the crystallization age; C – concordia; LI - lower intercept; UI - upper intercept*

5. Discussion

5.1. Across- arc age zonation of the Late Cretaceous magmatism

Stratigraphic relations with fossil-bearing Upper Cretaceous sediments provide age constraints for the extrusive magmatism in the northernmost East Balkan region (Kunchev, 1966; summary in Dabovski et al., 2009b). These authors assign a Late Cenomanian-Early Turonian age of the magmatism based on abundant ammonite and foraminifera assemblages preserved in marly-calcareous and in flysch-like sediments intercalated with the volcanic products in the East Balkan. These stages correspond to ~95-90 Ma based on numerical ages in Ogg et al. (2008). We were unable to obtain high-confidence ages for East Balkan magmatism, but the indications for ~90 Ma old ages (Fig. 5a) are consistent with the well constrained stratigraphic age of the samples.

Further south, volcanism and sedimentation in the central Yambol-Burgas region are considered Coniacian-Santonian-Campanian (90-70 Ma) based on rare fossils in the successions (Georgiev et al., 2001; Dabovski et al., 2009b), but our data suggest a much narrower time interval between 81 and 78 Ma (Fig. 4). The Izgrev, Vurli Brjag and Rossen plutons, intruded in the volcano-sedimentary Late Cretaceous successions, yield precise and high-confidence TIMS zircon ages at ca. 80-79 Ma (Figs. 3, 4). These ages constrain the minimum age of the intruded volcano-sedimentary sequence. Volcanic rocks have similar, but less precise U-Pb zircon ages (Fig. 4). The geochemistry and Pb and Sr isotopic composition of intrusive and volcanic rocks from a given center (e.g. Izgrev or Rossen, data from Georgiev et al., 2009) suggests that they evolved from chemically similar magmas and are therefore essentially coeval. In this region, zircons concordant within the small uncertainties of the ID-TIMS data form a single population with a clear peak at 82-79 Ma (Fig. 5a), providing additional evidence that volcanism in the Yambol-Burgas region is largely coeval with the dated intrusions. Less precise LA-ICPMS ages indicate that some of the magmatism may be younger than 78 Ma (Figs. 4, 5a), consistent with scarce field observations for post-intrusive emplacement of volcanic rocks (Ivanov, 1979).

High-confidence crystallization ages in the southernmost Strandzha region define two distinct Late Cretaceous magmatic events at ~87-85 Ma and ~ (Fig. 4). Concordant ID-TIMS inherited zircons at ~86 and ~90 Ma (Fig. 5a) suggest incorporation of older Upper Cretaceous rocks by the 81-78 Ma Upper Cretaceous magmas.

5.2. Comparison with Central Srednogorie zone

Detailed geochronology in the adjacent segment of the ABTS belt, the Central Srednogorie, reveals a 14 Ma age progression from north (~92 Ma) to south (~78 Ma), coupled with a southward increase of mantle input recorded by Nd, Sr and Hf isotopes (von Quadt et al., 2005). This is best explained by hinge retreat (roll back) that led to overall crustal thinning and asthenospheric incursion into an extending arc to back-arc environment (von Quadt et al., 2005). Comparison of crystallization ages of rocks from Eastern Srednogorie zone with the published age data from the Central Srednogorie zone (Fig. 7) shows important similarities.

Magmatism in the East Balkan region is initiated at ~94-90 Ma, similar to zircon ages from Elatsite and Chelopech in northernmost Central Srednogorie zone (~92 Ma, von Quadt et al., 2005). Also geochemically, the high K and calc-alkaline, shallow, and mostly intermediate subvolcanic bodies and associated volcanics from the East Balkan are similar to those from the northern part of Central Srednogorie zone (Elatsite, Chelopech, Assarel).

Further south, the 87-85 Ma intrusions and dikes ages in the Strandzha region (Fig. 4) are similar to the 86 Ma age of Elshitsa intrusion in the central part of Central Srednogorie zone. Most intrusions in the Strandzha region crystallized between 82 to 78 Ma; such ages are reported from the southern part of Central and Western Srednogorie zones, for Vurshilo, Vitosha and Capitan Dimitrievo intrusions (Peytcheva et al., 2008). In terms of

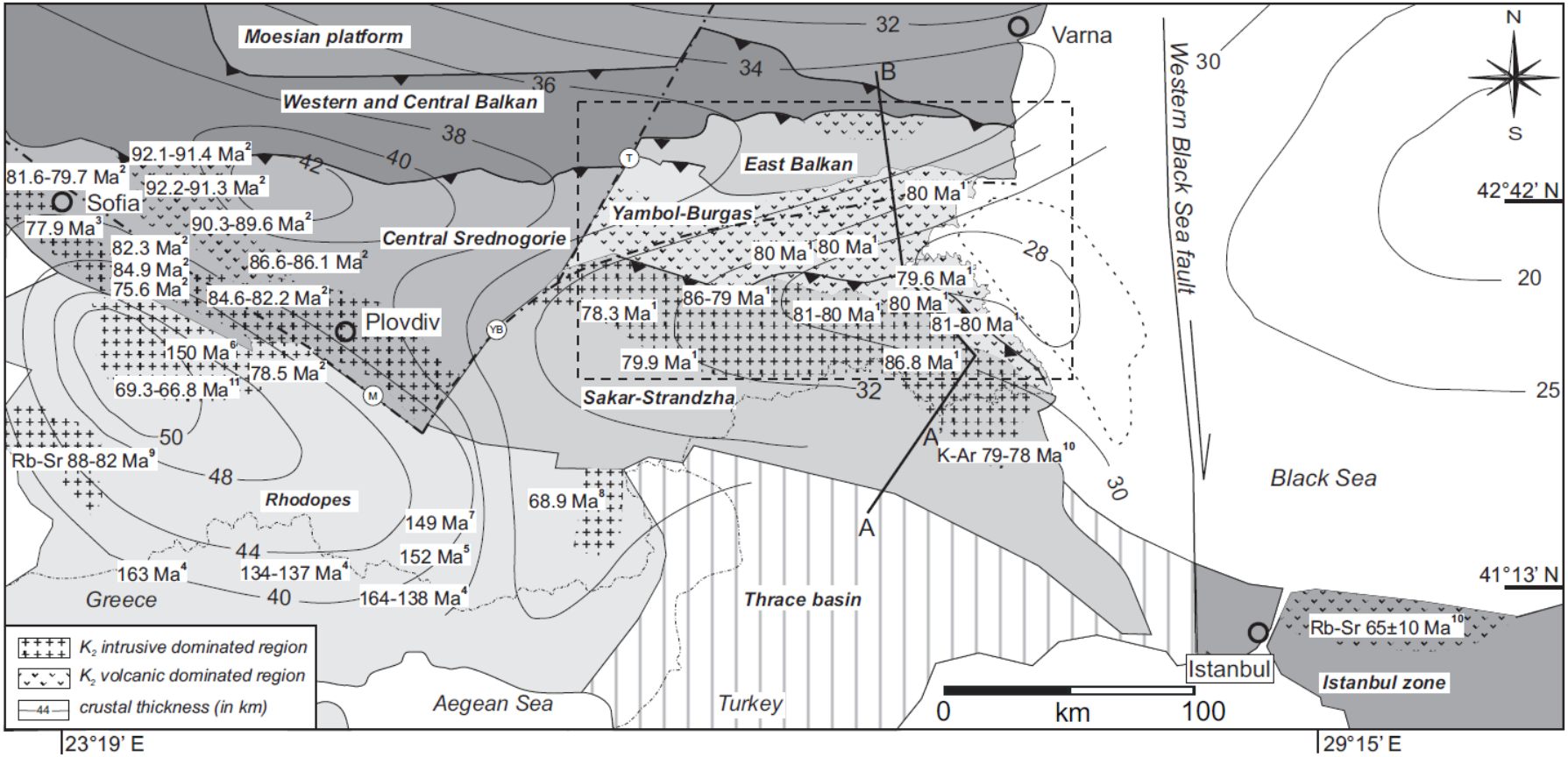

Figure 7. Simplified tectonic map of Eastern Srednogorie zone and surrounding areas, showing crustal thickness (in km) and approximate sample location of published Late-Jurassic to Late Cretaceous magmatic ages discussed in the main text. Superscript numbers are references for radiometric ages as follows: 1 – U-Pb zircon ID-TIMS and LA-ICPMS ages, this study; 2 – U-Pb zircon ID-TIMS (von Quadt et al., 2005); 3 – U-Pb zircon ID-TIMS for Plana pluton (Lora Bidzhova, personal communication); 4 – U-Pb zircon SHRIMP and Pb-Pb evaporation (Turpaud and Reischmann, 2009); 5,6 – U-Pb zircon ID-TIMS (Ovtcharova et al., 2004, Peytcheva et al., 2004); 7 – U-Pb zircon ID-TIMS (Cherneva et al., 2006); 8 – U-Pb zircon ID-TIMS (Marchev et al., 2006); 9 – Rb-Sr whole-rock (Zagorčev and Moorbath, 1983); 10 – K-Ar on Bt and Hb (Moore et al., 1980); 11 – Rb-Sr whole-rock (Öztunali and Satir, 1975). Crustal thickness lines from Yosifov and Pchelarov (1977); Black Sea crustal thickness from Dachev (1988). Stippled field in the Black Sea is the area of most intense magnetic anomalies after Yosifov et al. (1986).

geochemistry and emplacement depth, the deeply eroded middle (?) - crustal gabbroic and granodioritic intrusions with predominantly calc-alkaline affinity in the Strandzha region are similar to the deeply eroded Vurshilo and Capitan Dimitrievo intrusions in the southern Central Srednogorie zone.

Based on the overall similarities in crystallization age, geochemistry and emplacement depth of the magmatism, the East Balkan and Strandzha regions of Eastern Srednogorie zone may be considered eastwards equivalents of the northern and southern parts of Central Srednogorie zone, respectively. We conclude that the large-scale process of slab retreat that operated in Central Srednogorie zone during the Late Cretaceous was probably active also in the Eastern Srednogorie zone, with ages migrating from ca. 90 Ma in the East Balkan to 87-85 Ma and 82-78 Ma in the Strandzha region.

The voluminous mafic to intermediate alkaline magmatism in the central Yambol-Burgas region has no equivalent in Central Srednogorie. Characteristically, the 81-78 Ma old magmatism in the Yambol-Burgas region lacks evidence for the 90-86 Ma events as seen in the East Balkan and Strandzha regions, respectively. The distribution of pre-Cretaceous inherited zircons in this region also clearly differ from those in the East Balkan and Strandzha regions (Figs. 5a, 5b and 6), which is an indication for a possibly different origin of the Yambol-Burgas region. This, combined with the markedly elevated alkalinity of the Yambol-Burgas rocks intermingled with deep marine sediments, are all consistent with the formation of a Late Cretaceous intra-arc rift that separated a previously uniform arc (East Balkan and Strandzha regions) in two parts.

The peak of the magmatism in the Strandzha region overlaps the range of crystallization ages in the Yambol-Burgas region (81-78 Ma). The similar age, but different chemistry and emplacement depth require explanation. One possibility is that rollback caused intra-arc rifting and melting of upper mantle or lower crustal rocks; these newly formed magmas were granted a facilitated access through the thinned crust in the extensional regime of the Yambol-Burgas region. Alternatively, extension in the neighboring Black Sea might have caused rifting and related slab roll back. Regardless of the cause for rifting and slab roll back, our age data show that the thicker crust of the Strandzha region was penetrated by melts simultaneously with the rifting phase in the neighboring Yambol-Burgas region. The abundance of intrusive rocks exposed in the Strandzha region is a result of late exhumation.

The lack of clear along-strike age zonation in Eastern Srednogorie zone does not support the model for east-to-west slab break-off (Neubauer, 2002), which predicts progressively younger magmatic ages along the strike of the ABTS belt in an east-west direction. The overlapping age range of the magmatism in the Central and Eastern Srednogorie zones are also inconsistent with the slab break-off model.

5.3. Eastward continuation and relation to the Black Sea

The Srednogorie zone with its deep marine sedimentary succession (Aiello et al., 1977) is considered as a westerly continuation of the Black Sea basin (Hsü et al., 1977). However, the major subsidence and deepening of the Eastern Srednogorie basin is post-Cenomanian, about 10-30 Ma younger than the mid-Cretaceous opening of the Black sea. A westward propagating rifting was proposed to explain the later opening of the Srednogorie basin (Görür, 1988).

In terms of volume and emplacement mechanisms, the abundant mafic magmatism in the Yambol- Burgas region could represent part of the Black Sea oceanic crust, but its subduction influenced trace element composition clearly differs from typical mid-ocean ridge magmatism (Georgiev et al., 2009). Moreover, geophysical data indicate that large Bouguer anomalies (Dachev, 1988) and positive magnetic anomalies that characterize the oxidized magmatism in the Eastern Srednogorie zone do not continue uninterrupted within the Black Sea (Dachev, 1988; Roussanov and Pchelarov, 1998). They form a zone that bends offshore at almost 90 degrees and runs in a south-southeast direction almost parallel to the present shore (Fig. 7). These features are not consistent with the idea that

the Srednogorie zone magmatism (including the Yambol-Burgas region) represents Black Sea oceanic crust.

The offshore curvature of the Yambol-Burgas region coincides with the observed orientation of the dome-like uplifts in the Strandzha region, which have an east-west orientation in its western part and a NW-SE orientation in the eastern part. This change could have resulted from syn- to post-magmatic dextral strike-slip movements along the Western Black sea fault (Fig. 7), which is considered central for the opening of the Black Sea basin (Okay et al., 1994; Banks and Robinson, 1997; Nikishin et al., 2001; Nikishin et al., 2003). The Western Black sea fault also separates the Srednogorie zone from the Western Pontides Mountains in the Istanbul zone, which host abundant Upper Cretaceous arc magmatism. If movements along this fault caused the separation of a formerly continuous Upper Cretaceous arc comprising the Srednogorie zone and the Western Pontides, our age results imply major movements in the order of 100-150 km along this fault occurred later than the Santonian. The south- southeast curvature of the Srednogorie zone can be explained by the tail effect of southwards syn- to post- magmatic movements of the western Black Sea plate along the Western Black Sea fault, distorting and displacing the easternmost Srednogorie zone southwards. Additionally, paleomagnetic data indicate that the Srednogorie zone drifted 200 to 400 km northwards since the Late Cretaceous (Nozharov et al., 1984) as part of stable Europe. These northward movements may have also contributed to the southward tilting of easternmost Srednogorie.

5.4. Age of basement rocks and inherited zircons

The Late Carboniferous to Early Permian (274-301 Ma) age of intrusive rocks from the Eastern Srednogorie basement (Table 2) confirm that the studied region was actively involved in the Variscan collisional orogeny, which accreted fragments of Gondwanaland (Moesian, Balkan and Thracian terranes) to each other and to Laurasia (Yanev, 2000). Similar to older U-Pb zircon ages are reported for Variscan intrusions from the Central Srednogorie (Peytcheva and von Quadt, 2004; Carrigan et al., 2005; von Quadt et al., 2005), and for metagranites from the neighboring Eastern Rhodopes (Peytcheva and von Quadt, 1995). This age similarity may indicate that the Rhodope Massif, Central Srednogorie and Eastern Srednogorie zones constituted a single terrain during the Permian.

Inherited grains provide additional age constraints for the underlying basement (Fig. 5b). Permian-Carboniferous inherited zircon ages of ~300 Ma are characteristic for the East Balkan and Strandzha regions and probably originate from assimilation of the presently exposed Permian/Carboniferous basements rocks in Strandzha and East Balkan. In contrast, ~460 Ma old inherited zircon grains are found mostly in the Yambol-Burgas region (Fig. 5b), where the pre-Cretaceous basement is not exposed or reached in drill cores in the Yambol-Burgas region. Similar Ordovician ages have been found in Upper Cretaceous intrusions and several Variscan granitoids from the Central Srednogorie zone (Peytcheva and von Quadt, 2004; Carrigan et al., 2005; Peytcheva et al., 2009) and in the Rhodopean metamorphic basement (Bonev et al., 2010). The different inheritance pattern in the Yambol-Burgas region suggests that either the basement here is different, or that the Late Cretaceous magma chambers were situated at a different depth, compared to those in Strandzha and East Balkan. The latter hypothesis is consistent with thermobarometric estimates for olivine and clinopyroxenes crystallization in deep magma chambers, close to the Moho discontinuity (Georgiev et al., 2009). Therefore, the Ordovician inherited ages are a possible indication that the lower crustal rocks in the region have an Ordovician age.

5.5. Tectono-magmatic evolution of a rifted arc

This section integrates the regional geological, geochemical and age information into a model of the geodynamic evolution of the Eastern Srednogorie zone (Fig. 8).

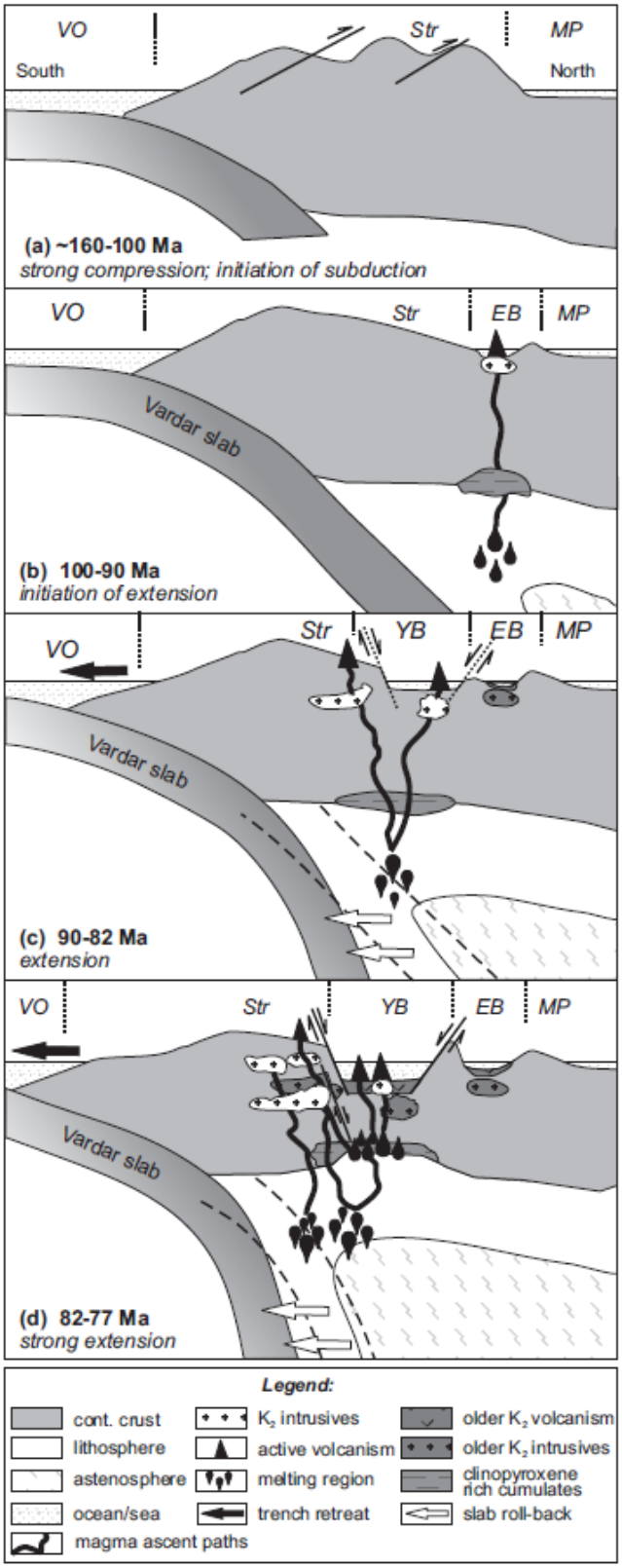

Figure 8. Schematic cartoon, illustrating in a series of diagrams (a-d) our model for the Late Cretaceous geodynamic evolution of Eastern Srednogorie zone. VO – Vardar Ocean; Str – Strandzha region; YB – Yambol-Burgas region; EB – Eastern Balkan region; MP – Moesian platform; Thr – Thrace depression. Note the absence of an absolute scale, due to the contrasting thickness of the upper crust, oceanic and sea depth on one side, and the subducting slab, lithosphere and asthenosphere on the other. The clinopyroxenite cumulates are drawn as products of the magmatism in (b); however, these cumulates may also have formed during an earlier stage. See text for detailed explanation.

The Late Jurassic-Early Cretaceous geodynamic evolution was characterized by successive phases of intense compression, northward thrusting, folding and uplift in the Strandzha region (Banks, 1997; Sunal et al., 2011). Ar/Ar mica ages indicate a ~140 Ma age of the deformation (Neubauer et al., 2010), whereas K-Ar ages of illites/muscovites from phyllites and diabases from the Bulgarian portion of Strandzha Mountains indicate a Jurassic (160-170 Ma) age of the low-grade greenschist facies metamorphism (Lilov et al., 2004). Rb-Sr muscovite and biotite ages from the southern part of Strandzha mountains reveal that peak metamorphic conditions occurred at around 160 Ma (Sunal et al., 2011), supporting earlier biotite whole-rock Rb-Sr Late Jurassic (155 Ma) age of the regional metamorphism (Okay et al., 2001). This compression was most likely related to the subduction/collision system in the southerly lying Rhodope Massif (e.g. Sunal et al., 2011) and resulted in the closure of the Nish-Troyan trough to the northwest of the studied area and folding of its flysch sediments at the end of the Late Jurassic (Nachev and Nachev, 2003). At this time the area of Eastern Srednogorie zone was not magmatically active and was above the sea level (Fig. 8a). The Moesian platform to the north was a shallow epicontinental sea with continuous sedimentation.

Sedimentation in Eastern Srednogorie zone commenced at the end of the Lower Cretaceous and the Cenomanian with deposition of alluvial, lake and swamp sediments, followed by initiation of marine transgression during the Cenomanian - Turonian (Nachev and Dimitrova, 1995b) when marine deposits were formed in a shallow epicontinental sea (Fig. 8b). Magmatic activity was limited to volumetrically minor shallow intrusives, dikes, and associated andesitic lava flows in the present day East Balkan. Their age is considered Late Cenomanian-Early Turonian based on characteristic fauna in associated marls and flysch sediments (Kunchev, 1966; Dabovski et al., 2009b).

The geodynamic setting changed significantly during the Coniacian with the onset of an intra-arc basin formation. The subducting slab migrated southwards, resulting in the formation of 86 Ma old intrusions and probably volcanics (which were later eroded) in the Strandzha region (Fig. 8c). In our model the slab retreat was a continuous process, similar to the slab retreat in the Central Srednogorie zone (von Quadt et al., 2005). Some 93-87 Ma magmatic products may be situated between Strandzha and East Balkan, now covered by sediments and volcanic products deposited during the intra-arc rift phase.

The 82-77 Ma time period was the most intense phase of extension and crustal thinning in the Yambol-Burgas and North-Burgas regions (Fig. 8d). A thick volcano-sedimentary succession was deposited in a deep marine basin (Nachev and Nachev, 2003). Decompression and crustal thinning combined with increased corner flow in the mantle wedge and associated rise in the temperature led to large-scale melting of lower-crustal/upper mantle clinopyroxene-rich and amphibole-bearing cumulates (Georgiev et al., 2009). The crystallization age for the cumulates is unclear: they could have formed during the previous stage of the Late Cretaceous magmatism (e.g. Fig. 8c), or could be significantly older. Melts from such cumulates mixed with mantle-wedge melts produced the mafic and intermediate alkaline magmatism in the Yambol-Burgas region, including the primitive nepheline-normative ankaramites (Georgiev et al., 2009; Marchev et al., 2009). During this period, mantle wedge melts penetrated the thicker crust in the Strandzha region and crystallized as lower-, middle- or upper crustal intrusions (Fig. 8d). Melt access to the crust might have been facilitated by the possible presence of normal faults, parallel to the main rift fault (Fig. 8d). The ~80 Ma old igneous rocks from the Yambol-Burgas and Strandzha regions have notably different geochemistry (e.g. Stanisheva-Vassileva, 1980; Georgiev et al., 2009). One possible explanation for these differences may be the lack of clinopyroxene-rich and amphibole containing cumulates in the lower crust of the Strandzha region. However, a more probable explanation is that the thicker crust in the Strandzha region prevented large-scale decompressional melting of clinopyroxenite cumulates. Rather, mantle-wedge-derived magmas intruded the thicker crust of Strandzha to form tholeiitic, calc-alkaline and partly high-K intrusions. The relatively similar present-day crustal thickness between the Yambol-Burgas and

Strandzha regions (Fig. 8) results from post-magmatic shortening and deformation. In the Late Cretaceous the crust in the Strandzha region was probably much thicker than the crust in the Yambol-Burgas region.

Late Cretaceous magmas in the Yambol-Burgas region erupted on the seafloor or crystallized as shallow intrusives, whereas concomitant intrusions in the Strandzha region crystallized at pressures between 0.7 and 0.2 GPa (Dabovski et al., 2009a). Stronger Cenozoic erosion in the elevated Strandzha region compared to the Yambol-Burgas region may have removed Cretaceous volcanic products. The extensional Late Cretaceous environment in the intermediate Yambol-Burgas region was favorable for the formation of polymetallic vein deposits; submarine volcanogenic-hosted massive sulphide deposits may also be present. In contrast, mostly skarn deposits developed around the deeper intrusions in the Strandzha region.

During the same stage (82-77 Ma), the area of the East Balkan region developed as a separate, non-magmatic deep back-arc basin (Fig. 8d). The lack of volcanic material in the post-Turonian deep-water sediments of East Balkan and their abundance in contemporaneous Yambol-Burgas sediments suggest that both basins were physically separated during the Coniacian-Maastrictian. Nachev and Nachev (2003) proposed the existence of a second elevated arc (in addition to the frontal Rhodope arc) between the Yambol-Burgas and the East Balkan basins. In our model the elevated northern rift shoulder of the Yambol-Burgas intra-arc rift acted as a paleo-relief barrier that prevented the deposition of explosive volcanic material in the deep East Balkan basin.

Sedimentation in the Yambol-Burgas intra-arc rift continued between 77 and 73 Ma (not shown on Fig. 8), probably accompanied by volumetrically small volcanic activity. Towards the end of this period the basin was terminated by uplift, intense thrusting and folding of the sedimentary and volcanic successions, with the total shortening estimated by a factor of three to the original width (Nachev and Nachev, 2003). There is no evidence for magmatic activity in the Strandzha or East Balkan regions at that time. The slab retreat continued further to the south; some younger magmatic products in the southern Strandzha area may be present beneath the younger sediments of the Thrace depression (Fig. 7). At the beginning of Maastrichtian (~73 Ma), shallow water limestones were deposited in the Yambol-Burgas region above the folded Late Cretaceous successions. Sedimentation in the East Balkan continued in a deeper-water environment and the basin was terminated before the Late Paleocene (Nachev and Nachev, 2003). To the south, evidence for further slab retreat and subduction magmatism comes from the Eastern Rhodope and Rila Mountain area where few intrusions have 70-65 Ma ages (Fig. 7). A possible equivalent of this magmatism is a granodiorite from the Istanbul zone in Turkey, which has a Rb-Sr age of 65±10 Ma (Öztunali and Satir, 1975).

The present day structure of the Eastern Srednogorie zone resulted from the multiple northward thrusting during the Early Cretaceous – Paleogene time, which superimposed Strandzha on top of the Yambol-Burgas region, and also parts of North-Burgas region on top of East Balkan (Fig. 3). The East Balkan region itself is thrusted on top of the stable Moesian platform. The surface features are dominated by northward thrusting, which is detected also in the deeper basement. Geophysical data indicate that the rift geometry is preserved only in the deep basement of the Yambol-Burgas, and partly East Balkan zone (Georgiev et al., 2001).

6. Conclusions

U-Pb zircon dating by ID-TIMS and LA-ICPMS methods combined with a synthesis of the regional geology shows that magmatism in the Eastern Srednogorie zone commenced at ca. 90 Ma with volcanism in the northernmost East Balkan region. With time, the magmatic activity migrated southwards, evidenced by several 86 Ma old plutonic bodies that intruded the basement of the present-day Strandzha region. Magmatic activity in the Eastern Srednogorie zone peaked between 81 and 78 Ma, when numerous intrusions crystallized in the Strandzha and Yambol-Burgas regions and abundant volcanics were

formed in the Yambol-Burgas region. The crystallization age of basement granites and gabbros from the Strandzha region is determined as Permian to Carboniferous. Upper Cretaceous rocks from all regions contain abundant inherited zircons. Their age distribution pattern is similar in the Strandzha and East Balkan regions where ca. 300 Ma inherited zircons from the local basement prevail. In contrast, most of the inherited zircons in the Yambol-Burgas region point to an Ordovician age of ca. 450 Ma and few grains have much older ages of 1 to 2 Ga.

Integrating new geochronology results with existing geological and geochemical data, we propose a model for the temporal evolution of the magmatism in the Eastern Srednogorie zone. Our model involves a southward retreating slab and related arc magmatism similar to the one in the Central Srednogorie zone, with older calc-alkaline to high-K shallow intrusions and volcanics in the north (East Balkan) and younger large mid-crustal tholeiitic, calc-alkaline and high-K intrusions in the south (Strandzha). The southward migration of the magmatism lasted from ~ 90 Ma (East Balkan) to ~ 78 Ma (the youngest intrusions in Strandzha). Subduction roll-back, combined with processes of widening of the Black Sea basin and major dextral strike-slip movements along the western Black Sea fault led to the formation of an intra-arc rift basin (Yambol-Burgas) which separated the formerly adjacent East Balkan and Strandzha regions. The main phase of the intra-arc rift alkaline-rich magmatism was from 81 to 78 Ma. Subsequent latest Cretaceous and Cenozoic compression events led to crustal shortening, deformation and northward thrusting, forming the present-day structure of Eastern Srednogorie zone.

Acknowledgements

We thank Ramon Aubert and Elena Stancheva for their help with zircon separation and Kalin Kouzmanov for his generous help with the CL and BSE imaging. We are grateful to Zhivko Ivanov for his advice and guidance during the first field work season in Strandzha Mountains, to Stoimen Bilyarsky for his help in the field and for testing the limits of his limitless Wartburg, and to Dimitar Paskalev for his assistance with field work in the East Balkan. We thank Franz Neubauer and an anonymous reviewer for their constructive reviews, and Nelson Eby for editorial handling. This study represents part of SG's PhD thesis at ETH Zurich supported by the Swiss National Science Foundation Projects No. 200020-100735, 200020-107955 and 200020-116693.

References:

Aiello, E., Bartolini, C., Boccaletti, M., Gočev, P., Karagjuleva, J., Kostadinov, V., Manetti, P., 1977. Sedimentary features of Srednogorie zone (Bulgaria) Upper Cretaceous intra-arc basin. Sedimentary Geology 19, 39-68.

Antonijevic, I., Grubic, A., Djordjevic, M., 1974. The Upper Cretaceous paleorift in Eastern Serbia. In: Karamata, S. (ed.) Metallogeny and Concepts of the Geotectonic development of Yugoslavia, 315-339.

Banks, C. J., 1997., Basins and thrust belts of the Balkan coast of the Black Sea. In: A.G.Robinson (ed.) Regional and petroleum geology of the Black Sea and surrounding region, American Association of Petroleum Geologists Memoir 68, pp. 115-128, Tulsa, OK.

Banks, C. J., Robinson, A., 1997. Mesozoic strike-slip back-arc basins of the Western Black Sea region. In: A.G.Robinson (ed.) Regional and petroleum geology of the Black Sea and surrounding region, American Association of Petroleum Geologists Memoir 68, pp. 53-62, Tulsa, OK.

Berza, T., Constantinescu, E., Vlad, S. N., 1998. Upper Cretaceous magmatic series and associated mineralisation in the Carpathian-Balkan orogen. Resource Geology 48, 291-306.

Boccaletti, M., Manetti, P., Peccerillo.A., 1974. Hypothesis on plate tectonic evolution of Carpatho-Balkan arcs. Earth and Planetary Science Letters 23, 193-198.

Bončev, E., 1971. Lineamenttektonik und Schollengliederung der Erdkruste im ostlichen Teil der Balkanhalbinsel. Annuaire de l'Université de Sofia, Faculté de Géologie et Géographie 63, 287-303.
Bonev N., Marchev, P., Ovtcharova M., Moritz, R., Ulianov, A., 2010. U-Pb LA-ICP/MS zircon geochronology of metamorphic basement and Oligocene volcanic rocks from the SE Rhodopes: inferences for the geological history of the Eastern Rhodope crystalline basement. Geosciences 2010, Sofia. 115-116.
Burg, J.P., 2011. Rhodope: from Mesozoic convergence to Cenozoic extension.
Review of petro-structural data in the geochronological frame. Journal of
Virtual Explorer, 39 (paper 1), 44pp.
Carrigan, C. W., Mukasa, S. B., Haydoutov, I., Kolcheva, K., 2005. Age of Variscan magmatism from the Balkan sector of the orogen, central Bulgaria. Lithos 82, 125-147.
Chang, Z. S., Vervoort, J. D., McClelland, W. C., Knaack, C., 2006. U-Pb dating of zircon by LA-ICP-MS. Geochemistry Geophysics Geosystems, Q05009, doi:10.1029/2005GC001100
Chatalov, G.A., 1990. Geology of the Strandzha Zone in Bulgaria. Geologica Balcanica, Series Operum Singularum 4, Publishing House Bulgarian Academy of Sciences, Sofia, 272 pp (in Bulgarian).
Cherneva, Z., Ovtcharova, M., Dimov, D., von Quadt, A., 2006. "Baby granites" in migmatites from Chepinska river valley, Western Rhodope - geochemistry and U-Pb isotope dating of monazite and zircon. Geosciences 2006, Sofia, 205-208.
Cheshitev, G., Kanchev, I. (eds.), 1989. Geological Map of P. R. Bulgaria, 1:500 000. Sofia, Bulgaria: Supreme Technical Council
Ciobanu, C. L., Cook, N. J., Stein, H., 2002. Regional setting and geochronology of the Late Cretaceous Banatitic Magmatic and Metallogenetic Belt. Mineralium Deposita 37, 541-567.
Dabovski, C., Harkovska, A., Kamenov, B., Mavroudchiev, B., Stanisheva-Vassileva, G. and Yanev, Y., 1991. A geodynamic model of the Alpine magmatism in Bulgaria. Geologica Balcanica 21 (4), 3-15.
Dabovski, C., Boyanov, I., Khrischev, K., Nikolov, T., Sapounov, I., Yanev, Y., Zagorčev, I., 2002. Structure and Alpine evolution of Bulgaria. Geologica Balcanica 32, 9-15.
Dabovski, C., Kamenov, B., Vassilev, E., 2009a. Upper Cretaceous Magmatism. In: Zagorchev, I., Dabovski, C., Nikolov, T. (eds.) Geology of Bulgaria. Volume II. Mesozoic Geology. Sofia: Academic Publishing House "Prof. Marin Drinov", 423-553 (in Bulgarian).
Dabovski, C., Sinyovski, D., Vassilev, E., Dimitrova, E., 2009b. Upper Cretaceous Stratigraphy. In: Zagorchev, I., Dabovski, C., Nikolov, T. (eds.) Geology of Bulgaria, Volume II. Mesozoic Geology. Sofia: Academic Publishing House "Prof. Marin Drinov", 308-422 (in Bulgarian).
Dachev, H., 1988. Structure of the Earth's Crust in Bulgaria. Sofia: Technika (in Bulgarian).
Dewey, J., Pitman, W., Ryan, W., Bonnin, J., 1973. Plate tectonics and the evolution of the Alpine system. Geological Society of America Bulletin 84, 3137-3180.
Georgiev, G., Dabovski, C., Stanisheva-Vassileva, G., 2001. East Srednogorie-Balkan rift zone. In: P.A.Ziegler, Cavazza, W., Robertson, A. H. F., Crasquin-Soleau, S. (eds.) Peri-Tethys Memoir 6: Peri-Tethyan Rift/Wrench Basins and Passive Margins. Paris. Memoires du Museum National d`Histoire Naturelle, 259-293.
Georgiev, S. V., Von Quadt, A., Peytcheva, I., Marchev, P., Heinrich, C. A., 2006. Eastern Srednogorie - new geochemical data for lateral zonation of magmatism. In: Geosciences 2006. Bulgarian Geological Society, Sofia, 197-200.
Georgiev, S., 2008. Sources and evolution of Late Cretaceous magmatism in Eastern Srednogorie, Bulgaria: constraints from petrology, isotope geochemistry and geochronology: PhD thesis, ETH Zurich, 270 pp.
Georgiev, S., Marchev, P., Heinrich, C., Von Quadt, A., Peytcheva, I., Manetti, P., 2009. Origin of Nepheline-Normative High-K Ankaramites and the Evolution of Eastern Srednogorie Arc in Southeastern Europe. Journal of Petrology 50, 1899-1933.

Gerdjikov, I., 2005. Alpine metamorphism and granitoid magmatism in the Strandja Zone: new data from the Sakar unit, SE Bulgaria. Turkish Journal of Earth Sciences 14, 167-183.
Görür, N., 1988. Timing of opening of the Black-Sea basin. Tectonophysics 147, 247-262.
Günther, D., Audetat, A., Frischknecht, R., Heinrich, C. A., 1998. Quantitative analysis of major, minor and trace elements in fluid inclusions using laser ablation inductively coupled plasma mass spectrometry. Journal of Analytical Atomic Spectrometry 13, 263-270.
Heinrich, C. A., Neubauer, F., 2002. Cu-Au-Pb-Zn-Ag metallogeny of the Alpine-Balkan-Carpathian- Dinaride geodynamic province. Mineralium Deposita 37, 533-540.
Heinrich, C. A., Pettke, T., Halter, W. E., Aigner-Torres, M., Audetat, A., Günther, D., Hattendorf, B., Bleiner, D., Guillong, M., Horn, I., 2003. Quantitative multi-element analysis of minerals, fluid and melt inclusions by laser-ablation inductively-coupled-plasma mass-spectrometry. Geochimica et Cosmochimica Acta 67, 3473-3497.
Hsü, K., Nachev, I., Vuchev, V., 1977. Geologic evolution of Bulgaria in the light of plate tectonics. Tectonophysics 40, 245-256.
Ivanov, R., 1979. To the tectonogeochemical analysis of the Upper Cretaceous magmatism in the East Srednogorie. Review of the Bulgarian Geological Society 40, 47-61 (in Bulgarian, with English abstract).
Ivanov, Z. (in press). Geology of Bulgaria (in Bulgarian).
Janković, S., 1997. The Carpatho-Balkanides and adjacent area: a sector of the Tethyan Eurasian metallogenic belt. Mineralium Deposita 32, 426-433.
Kamenov, B., Nedialkov, R., Yanev, Y., Stoykov, S., 2003. Petrology of the Late Cretaceous ore-magmatic centres in the Central Srednogorie, Bulgaria. In: Bogdanov, K., Strashimirov, S. (eds.) Cretaceous porphyry-epithermal systems of the Srednogorie zone, Bulgaria: SEG Guidebook Series, 27-46.
Kamenov, B., Yanev, Y., Nedialkov, R., Moritz, R., Peytcheva, I., Von Quadt, A., Stoykov, S., Zartova, A., 2007. Petrology of Upper Cretaceous island-arc ore-magmatic centers from Central Srednogorie, Bulgaria: Magma evolution and paths. Geochemistry, Mineralogy and Petrology 45, 39-77.
Kaz'min, V. G., Tikhonova, N. F., 2006. Late Cretaceous-Eocene marginal seas in the Black Sea-Caspian region: paleotectonic reconstructions. Geotectonics 40, 169-182.
Krogh, T. E., 1973. Low-contamination method for hydrothermal decomposition of zircon and extraction of U and Pb for isotopic age determinations. Geochimica et Cosmochimica Acta 37, 485-494.
Krogh, T. E., 1982. Improved accuracy of U-Pb zircon ages by the creation of more concordant systems using an air abrasion technique. Geochimica et Cosmochimica Acta 46, 637-649.
Kunchev, I., 1966. Mediterranean type Upper Cretaceous in the Luda Kamchya part of the East Stara Planina. Izvestija NIGI 3, 45-70 (in Bulgarian).
Lilov, P., Maliakov, Y. and Balogh, K., 2004. K-Ar dating of metamorphic rocks from Strandja massif, SE Bulgaria. Geochemistry, mineralogy and petrology, 41, 107-120.
Ludwig, K. R., 1980. Calculation of uncertainties of U-Pb isotope data. Earth and Planetary Science Letters 46, 212-220.
Ludwig, K. R., 1991. ISOPLOT: A plotting program for radiogenic isotope data. U.S. Geological Survey Open-file Report 39.
Ludwig, K. R., 2003. User's manual for Isoplot 3.00. A geochronological toolkit for Microsoft Excel. Berkeley Geochronology Center Special Publication 4.
Marchev, P., Georgiev, S., Zajacz, Z., Raycheva, R., Manetti, P., von Quadt, A., Tomassini, S., 2009. High-K ankaramitic melt inclusions and lavas in the Upper Cretaceous Eastern Srednogorie continental arc, Bulgaria: Implications for the genesis of arc shoshonites. Lithos 113; 228-245.
Marchev, P., Von Quadt, A., Peytcheva, I., Ovtcharova, M., 2006. The age and origin of the Chuchuliga and Rozino granites, Eastern Rhodopes. Geosciences 2006. Sofia, Bulgaria, 213-216.

Mattinson, J. M., 2005. Zircon U-Pb chemical abrasion ("CA-TIMS") method: Combined annealing and multi-step partial dissolution analysis for improved precision and accuracy of zircon ages. Chemical Geology 220, 47-66.
Mitchell, A.H.G., 1996. Distribution and genesis of some epizonal Zn–Pb and Au provinces in the Carpathian–Balkan region. Transactions of the Institution of Mining and Metallurgy (Section B: Applied Earth Sciences) 105, 127– 138.
Moore, W., McKee, E., Akinci, O., 1980. Chemistry and chronology of plutonic rocks in the Pontide mountains, northern Turkey. European Copper Deposits Congress Book. Belgrade, 209-216.
Nachev, I., Dimitrova, E., 1995a. Upper Cretaceous stratigraphy of the Eastern Balkan Mountains. Geologica Balcanica 25, 43-74.
Nachev, I., Dimitrova, E., 1995b. Upper Cretaceous stratigraphy of the Eastern Sredna Gora zone. Geologica Balcanica 25, 3-26.
Nachev, I., Nachev, C., 2003. Alpine plate-tectonic of Bulgaria. Sofia: Artik 2001., 198 pp.
Neubauer, F., 2002. Contrasting Late Cretaceous with Neogene ore provinces in the Alpine-Balkan-Carpathian-Dinaride collision belt. In: Blundell, D. J., Neubauer, F., von Quadt, A. (eds.) The Timing and Location of Major Ore Deposits in an Evolving Orogen, 81-102.
Neubauer F., Bilyarski S., Genser J., Ivanov Z., Peytcheva I., von Quadt A., 2010. Jurassic and Cretaceous tectonic evolution of the Sakar and Srednogorie zones, Bulgaria: $^{40}Ar/^{39}Ar$ mineral ages and structures. Geologica Balcanica, CBGA 2010 meeting, Thessaloniki, abstract volume, 273-274
Nikishin, A. M., Korotaev, M. V., Ershov, A. V., Brunet, M. F., 2003. The Black Sea basin: tectonic history and Neogene-Quaternary rapid subsidence modelling. Sedimentary Geology 156, 149-168.
Nikishin, A. M., Ziegler, P. A., Panov, D. I., Nazarevich, B. P., Brunet, M. F., Stephenson, R. A., Bolotov, S. N., Korotaev, M. V., Tikhomirov, P. L., 2001. Mesozoic and Cainozoic evolution of the Scythian platform - Black Sea - Caucasus domain. In: P.A.Ziegler, Cavazza, W., Robertson, A. H. F., Crasquin-Soleau, S. (eds.) Peri-Tethys Memoir 6: Peri-Tethyan Rift/Wrench Basins and Passive Margins. Memoires du Museum National d`Histoire Naturelle, 186, 295-346.
Nozharov, P., Yosifov, D., Dolapchieva, M., Petkov, N., 1984. Late Alpine paleogeodynamic of the Srednogorie inferred from paleomagnetic data. Bulletin Research Institute Mineral Resources 1, 272-277.
Ogg, J.G., Ogg, G., Gradstein, F.M., 2008. The Concise Geologic Time Scale. Oxford University Press, 184 p.
Okay, A. I., Satir, M., Tüysüz, O., Akyüz, S., Chen, F., 2001. The tectonics of the Strandja Massif: late-Variscan and mid-Mesozoic deformation and metamorphism in the northern Aegean. International Journal of Earth Sciences 90, 217-233.
Okay, A. I., Şengör, A. M. C., Görür, N., 1994. Kinematic history of the opening of the Black Sea and its effect on the surrounding regions. Geology 22, 267-270.
Ovtcharova, M., von Quadt, A., Cherneva, Z., Sarov, S., Heinrich, C., Peytcheva, I., 2004. U-Pb dating of zircon and monazite from granitoids and migmatites in the core and eastern periphery of the Central Rhodopean Dome, Bulgaria. Geochimica et Cosmochimica Acta 68, A664.
Öztunali, Ö., Satir, M., 1975. Rubidium-strontium alterbestimungen des Tiefengesteinen as Çavuşbaşi (Istanbul). Istanbul Üniversiteti Fen Fakültesi Mecmuast Seri B.
Peytcheva, I., von Quadt, A., 1995. U–Pb zircon dating of metagranites from Byala-reka region in the East Rhodopes, Bulgaria. Procedings of XV Congress GBGA, Geoogical Society of Greece Special Publication 4, 627-631.
Peytcheva, I., von Quadt, A., 2004. The Palaeozoic protoliths of Central Srednogorie, Bulgaria: records in zircons from basement rocks and Cretaceous magmatites. 5th International Symposium on Eastern Mediterranean Geology. Thessaloniki, Greece, 392-395.

Peytcheva, I., von Quadt, A., Ovtcharova, M., Handler, R., Neubauer, F., Salnikova, E., Kostitsyn, Y., Sarov, S., Kolcheva, K., 2004. Metagranitoids from the eastern part of the Central Rhodopean dome (Bulgaria): U-Pb, Rb-Sr and $^{40}Ar/^{39}Ar$ timing of emplacement and exhumation and isotope-geochemical features. Mineralogy and Petrology 82, 1-31.
Peytcheva, I., von Quadt, A., Georgiev, N., Ivanov, Z., Heinrich, C. A., Frank,
M., 2008. Combining trace-element compositions, U–Pb geochronology
and Hf isotopes in zircons to unravel complex calcalkaline magma chambers as inferred by mixed gabbros and granodiorites in the Upper Cretaceous Srednogorie zone (Bulgaria). Lithos 104, 405–427
Peytcheva, I., von Quadt, A., Neubauer, F., Frank, M., Nedialkov, R., Heinrich, C., Strashimirov, S., 2009. U-Pb dating, Hf-isotope characteristics and trace-REE-patterns of zircons from Medet porphyry copper deposit, Bulgaria: implications for timing, duration and sources of ore-bearing magmatism. – Mineralogy and Petrology 96, 19-41.
Popov, P., 1981. Magmotectonic features of the Banat-Srednogorie belt. Geologica Balcanica 11, 43-72.
Popov, P., 1987. Tectonics of the Banat Srednogorie rift. Tectonophysics 143, 209-216.
Popov, P., 1996. Characteristic features of the Banat-Srednogorie metallogenic zone. "Plate Tectonic Aspects of the Alpine Metallogeny in the Carpatho-Balkan Region", IGCP Project No. 356. Annual Meet. Sofia 1996, 1, 137-154.
Popov, P., Berza, T., Grubic, A., Ioane, D., 2002. Late Cretaceous Apuseni-Banat-Timok-Srednogorie(ABTS) magmatic and metallogenic belt in the Carpathian-Balkan orogen. Geologica Balcanica 32, 145-162.
Ricou, L. E., Burg, J. P., Godfriaux, I., Ivanov, Z. 1998. Rhodope and Vardar: the metamorphic and the olistostromic paired belts related to the Cretaceous subduction under Europe. Geodinamica Acta 11, 285-309.
Rocholl, A., Dulski, P., Raczek, I., 2000. New ID-TIMS, ICP-MS and SIMS data on the trace element composition and homogeneity of NIST certified reference material SRM 610-611. Geostandards Newsletter 24, 261-274.
Roussanov, I., Pchelarov, V., 1998. Phanerozoic terranes and megastutures of the Balkan peninsula. Geology and Mineral Resources 1, 36-42.
Schmid, S. M., Bernoulli, D., Fugenschuh, B., Matenco, L., Schefer, S., Schuster, R., Tischler, M., Ustaszewski, K., 2008. The Alpine-Carpathian-Dinaridic orogenic system: correlation and evolution of tectonic units. Swiss Journal of Geosciences 101, 139-183.
Slama, J., Kosler, J., Crowley, J. L., Gerdes, A., Hanchar, J., Horstwood, M., Morris, G. A., Nasdala, L., Norberg, N., Schaltegger, U., Tubrett, M. N., Whitehouse, M. J., 2008. Plešovice zircon – a new natural reference material for U-Pb and Hf isotopic microanalysis. Chemical Geology 249, 1-35.
Stacey, J. S., Kramers, J. D., 1975. Approximation of terrestrial lead isotope evolution by a 2-stage model. Earth and Planetary Science Letters 26, 207-221.
Stampfli, G. M., Borel, G., 2004. The TRANSMED transect in space and time: constraints on the paleotectonic evolution of the Mediterranean domain. In: Cawazza, W., Roure, F., Spakman, W., Stampfli, G. M., Ziegler, P. (eds.) The TRANSMED Atlas: the Mediterranean Region from Crust to Mantle. Berlin: Springer Verlag, 53-90.
Stanisheva-Vassileva, G., 1980. The Upper Cretaceous magmatism in Srednogorie zone, Bulgaria: a classification attempt and some implications. Geologica Balcanica 10, 15-36.
Stanisheva-Vassileva, G., 1989. East Srednogorie volcano-intrusive area. In: Stanisheva-Vassileva, G., Strashimirov, S., Yanev, Y. (eds.) Alpine magmatism and related metallogeny in Srednogorie and Eastern Rhodopes-XIV Congress Carpatho-Balkan Geological Association, Sofia, Field Trip Guide Book. Sofia: Sofia University, 27-38 (in Russian).
Starostenko, V., Buryanov, V., Makarenko, I., Rusakov, O., Stephenson, R., Nikishin, A., Georgiev, G., Gerasimov, M., Dimitriu, R., Legostaeva, O., Pehelarov, V. and Sava, C., 2004. Topography of the crust-mantle boundary beneath the Black Sea Basin. Tectonophysics, 381(1-4), 211-233.

Stern, R. A., Amelin, Y., 2003. Assessment of errors in SIMS zircon U-Pb geochronology using a natural zircon standard and NIST SRM 610 glass. Chemical Geology 197, 111-142.
Sunal, G., Satir, M., Natal'in, B.A., Topuz, G. and Vonderschmidt, O., 2011. Metamorphism and diachronous cooling in a contractional orogen: the Strandja Massif, NW Turkey. Geological Magazine 148 (4), 580-596.
Turpaud, Ph., Reischmann, Th., 2009. Characterisation of igneous terranes by zircon dating: implications for UHP occurrences and suture identification in the Central Rhodope, northern Greece. International Journal of Earth Sciences 99, 567-591.
von Quadt, A., Moritz, R., Peytcheva, I., Heinrich, C. A., 2005. Geochronology and geodynamics of Late Cretaceous magmatism and Cu-Au mineralization in the Panagyurishte region of the Apuseni-Banat-Timok-Srednogorie belt, Bulgaria. Ore Geology Reviews 27, 95-126.
von Quadt,A., Sarov, St., Peytcheva, I., Voinova, E., Georgiev,N., 2009. Jurassic metagranitoids south of the West-Rhodope batholith – conventional and in situ U-Pb zircon analyses, Sr-Nd-Hf isotope tracing and geodynamic constraints. Geosciences 2009. Sofia, Bulgaria, 11-12.
von Quadt,A., Erni, M., Martinek, K., Peytcheva, I., Moll, M., Heinrich, C.A., 2011. Zircon crystallization and the life times of magmatic-hydrothermal ore systems. Geology 39 (8), 731–734.
Wiedenbeck, M., Alle, P., Corfu, F., Griffin, W. L., Meier, M., Oberli, F., von Quadt, A., Roddick, J. C., Speigel, W., 1995. Natural zircon standards for U-Th-Pb, Lu-Hf, trace-element and REE analyses. Geostandards newsletter 19, 1-23.
Yanev, S., 2000. Palaeozoic terranes of the Balkan Peninsula in the framework of Pangea assembly. Palaeogeography Palaeoclimatology Palaeoecology 161 (1-2), 151-177.
Yosifov, D., Mirlin, E., Valjashko, G., Pchelarov, V., Brusilovskii, J., 1986. A possible spreading phase in the development of the Srednogorie rift (according to geophysical data). Geologica Balcanica 16, 3-14 (in Russian, with English abstract).
Yosifov, D., Pchelarov, V., 1977. A scheme of the thickness of the Earth's crust in the Balkan Peninsula and some features of its structures. Geologica Balcanica 7, 7-22 (in Russian, with English abstract).
Zagorčev, I., Moorbath., 1983. Rubidium-strontium isotope data on the age of Dautovski pluton (Pirin type granodiorites), southwest Bulgaria. Geologica Balcanica 17, 59-71 (in Russian, with English abstract).
Zimmerman, A., Stein, H. J., Hannah, J. L., Koželj, D., Bogdanov, K., Berza, T., 2008. Tectonic configuration of the Apuseni-Banat-Timok-Srednogorie belt, Balkans-South Carpathians, constrained by high precision Re-Os molybdenite ages. Mineralium Deposita 43, 1-21.
Zonenshain, L. P., Le Pichon, X., (1986). Deep basins of the Black Sea and Caspian Sea as remnants of mesozoic back-arc basins. Tectonophysics 123, 181-211.

Appendix 1. U-Pb zircon analyses by ID-TIMS Abbreviations: Abr – level of pre-treatment where "na" is lack of pre-tratment, "aa" - air abrasion (with the time of air abrasion pecified);"ca" - chemical abrasion. 2σ is the standard analytical error. Str-Strandzha region; YB – Yambol-Burgas region; NB – North Burgas region; EB – East Balkan region.

Sample №	Region	Weight µg	Abr	U ppm	Pb ppm	$^{*206}Pb/^{204}Pb$	$^{206}Pb/^{238}U$	2σ, %	$^{207}Pb/^{235}U$	2σ, %	$^{207}Pb/^{206}Pb$	2σ, %	$^{206}Pb/^{238}U$ age, Ma	$^{207}Pb/^{235}U$ Age, Ma	$^{207}Pb/^{206}Pb$ Age, Ma	Rho
SG 107	Bas	9.5	aa 8h	69.9	3.0	752.1	0.039435	0.24	0.281787	0.90	0.051824	0.83	249.33	252.07	277.68	0.42
SG 068	EB	4.6	aa 3h	495.4	4.9	139.8	0.006461	0.25	0.040809	3.30	0.045812	3.17	41.51	40.61	-12.29	0.55
SG 068	EB	3.1	aa 3h	56.6	0.9	72.2	0.009550	0.72	0.063843	11.16	0.048486	10.57	61.27	62.84	123.09	0.83
SG 068	EB	3.7	aa 3h	304.9	12.6	55.5	0.015096	0.31	0.108698	2.86	0.052224	2.74	96.59	104.77	295.22	0.44
SG 068	EB	3.3	ca	10.7	0.2	275.5	0.015221	0.29	0.104927	3.06	0.049996	2.90	97.38	101.31	194.81	0.58
SG 068	EB	24.9	ca	37.4	0.7	1511.7	0.020214	0.12	0.137219	0.44	0.049233	0.41	129.01	130.56	158.91	0.42
SG 068	EB	24.9	ca	37.4	0.7	1511.7	0.020214	0.12	0.137219	0.44	0.049233	0.41	129.01	130.56	158.91	0.42
SG 068	EB	5.2	ca	200.1	4.2	900.0	0.020651	0.21	0.144223	0.46	0.050652	0.39	131.77	136.80	224.97	0.53
SG 068	EB	5.2	ca	200.1	4.2	900.0	0.020651	0.21	0.144223	0.46	0.050652	0.39	131.77	136.80	224.97	0.53
SG 068	EB	3.6	aa 3h	121.8	4.4	108.8	0.021361	0.42	0.143943	5.44	0.048874	5.14	136.25	136.55	141.74	0.74
SG 068	EB	4.3	aa 3h	382.4	16.2	2215.7	0.041133	0.13	0.297549	0.24	0.052464	0.20	259.85	264.48	305.66	0.56
SG 068	EB	4.3	aa 3h	382.4	16.2	2215.7	0.041133	0.13	0.297549	0.24	0.052464	0.20	259.85	264.48	305.66	0.56
SG 068	EB	2.1	aa 3h	35.0	5.4	42.6	0.046029	1.21	0.329459	15.36	0.051912	14.52	290.10	289.15	281.56	0.71
SG 068	EB	29.5	ca	43.2	2.2	3725.3	0.047451	0.14	0.342796	0.21	0.052395	0.15	298.85	299.29	302.65	0.72
SG 068	EB	10.0	ca	220.8	10.1	2696.6	0.048191	0.12	0.348572	0.16	0.052460	0.10	303.41	303.65	305.52	0.78
SG 068	EB	10.3	ca	37.0	2.0	4916.4	0.055748	0.13	0.412488	0.19	0.053663	0.13	349.72	350.67	356.95	0.71
SG 068	EB	2.5	ca	59.3	3.5	336.6	0.058468	0.18	0.439397	0.93	0.054505	0.87	366.30	369.83	392.00	0.42
SG 069	EB	1.5	ca	105.7	16.1	21.7	0.008122	1.60	0.065627	25.08	0.058603	23.59	52.15	64.54	552.37	0.94
SG 069	EB	2.6	ca	61.0	1.3	126.1	0.015179	0.27	0.104383	3.71	0.049874	3.53	97.12	100.81	189.12	0.67
SG 069	EB	4.7	ca	104.3	8.8	84.8	0.044651	0.39	0.331335	4.10	0.053818	3.85	281.60	290.58	363.47	0.67
SG 093a	EB	6.0	na	61.7	2.7	376.9	0.042886	0.24	0.307902	0.90	0.052072	0.82	270.69	272.55	288.52	0.43
SG 093a	EB	7.2	na	63.2	3.5	620.7	0.055149	0.37	0.417882	1.02	0.054956	0.91	346.05	354.54	410.45	0.48
SG 093a	EB	2.2	na	34.8	2.9	199.2	0.072234	0.27	0.573444	1.70	0.057577	1.59	449.60	460.24	513.73	0.48
SG 085	NB	7.9	na	109.8	1.5	504.1	0.012480	0.20	0.083320	1.22	0.048422	1.15	79.95	81.26	119.94	0.41
SG 085	NB	0.7	na	349.3	7.1	293.5	0.020445	0.28	0.142376	1.78	0.050507	1.69	130.47	135.16	218.40	0.42
SG 085	NB	0.7	na	66.4	7.4	220.8	0.102926	0.26	0.880857	1.96	0.062069	1.83	631.54	641.45	676.50	0.52
SG 087	NB	2.9	na	171.1	13.5	1819.5	0.081240	0.26	0.679642	0.44	0.060675	0.35	503.52	526.56	627.73	0.63
AvQ 054	YB	4.5	a	28.1	0.6	90.3	0.012634	0.68	0.083980	10.35	0.048209	9.82	80.94	81.88	109.58	0.79
AvQ 054	YB	11.2	a	32.9	0.9	75.4	0.012698	1.06	0.082326	4.34	0.047022	4.01	81.34	80.33	50.31	0.42
AvQ 054	YB	6.9	a	33.0	0.6	130.8	0.012702	0.33	0.085819	4.57	0.049002	4.34	81.37	83.60	147.94	0.72
AvQ 054	YB	5.1	a	27.7	0.4	223.3	0.012726	0.42	0.085815	4.18	0.048907	3.96	81.52	83.60	143.36	0.54
AvQ 054	YB	104.0	a	2.3	0.0	243.3	0.012850	0.36	0.085438	3.74	0.048221	3.55	82.31	83.25	110.10	0.57
AvQ 057	YB	38.6	na	218.4	3.4	337.0	0.012471	0.27	0.081888	1.16	0.047624	1.07	79.89	79.92	80.60	0.43
AvQ 057	YB	9.8	aa 2h	21.5	0.8	47.9	0.012513	1.54	0.079119	25.48	0.045858	24.17	80.16	77.32	-9.84	0.86

Sample №	Region	Weight µg	Abr	U ppm	Pb ppm	$^{*206}Pb/^{204}Pb$	$^{206}Pb/^{238}U$	2σ, %	$^{207}Pb/^{235}U$	2σ, %	$^{207}Pb/^{206}Pb$	2σ, %	$^{206}Pb/^{238}U$ age, Ma	$^{207}Pb/^{235}U$ Age, Ma	$^{207}Pb/^{206}Pb$ Age, Ma	Rho
AvQ 057	YB	7.5		17.2	0.8	78.2	0.025168	0.45	0.173601	4.99	0.050027	4.73	160.23	162.54	196.24	0.61
AvQ 057	YB	4.6	na	86.8	8.2	71.6	0.044321	0.36	0.315997	5.03	0.051710	4.74	279.56	278.82	272.59	0.81
AvQ 057	YB	6.2	na	24.3	2.7	61.4	0.045351	1.09	0.830587	6.30	0.132829	5.37	285.92	613.94	2135.71	0.88
AvQ 057	YB	2.3	aa 2h	241.9	16.5	447.5	0.064575	0.34	0.492252	0.93	0.055287	0.82	403.39	406.44	423.86	0.49
AvQ 057	YB	3.6	na	80.0	8.6	107.0	0.064629	0.27	0.489436	2.56	0.054925	2.40	403.71	404.53	409.12	0.62
AvQ 057	YB	2.6	na	690.3	49.6	965.5	0.071794	0.22	0.560381	0.52	0.056610	0.45	446.96	451.77	476.38	0.52
AvQ 057	YB	3.9		40.9	3.7	213.8	0.072789	0.25	0.561907	1.12	0.055988	1.04	452.94	452.77	451.87	0.45
AvQ 057	YB	16.7		21.7	1.6	1061.5	0.073264	0.28	0.571649	0.54	0.056590	0.44	455.79	459.08	475.55	0.59
AvQ 057	YB	12.7		68.7	5.0	1778.1	0.074322	0.26	0.576971	0.40	0.056304	0.30	462.14	462.51	464.37	0.68
AvQ 057	YB	3.5	aa 2h	34.1	3.3	247.1	0.076469	0.61	0.600882	3.25	0.056991	3.01	475.01	477.79	491.17	0.47
AvQ 057	YB	14.0		55.6	5.6	491.2	0.094392	0.33	0.855909	0.54	0.065765	0.40	581.46	627.89	798.90	0.67
AvQ 058	YB	3.5	na	84.9	4.2	246.7	0.046990	0.29	0.341759	2.98	0.052749	2.83	296.01	298.50	318.00	0.55
AvQ 058	YB	1.1	aa 2h	164.0	8.6	307.8	0.047832	0.62	0.352250	2.29	0.053411	2.10	301.20	306.41	346.33	0.42
AvQ 058	YB	1.6	aa 2h	43.8	3.1	72.3	0.071717	0.63	0.577328	10.25	0.058385	9.73	446.49	462.74	544.21	0.85
AvQ 058	YB	2.8	aa 2h	105.7	11.5	191.7	0.100186	0.28	1.290945	1.59	0.093454	1.45	615.50	841.72	1497.10	0.55
SG 044	YB	3.3	aa 3h	589.5	12.4	145.1	0.012354	0.19	0.080022	1.63	0.046978	1.55	79.15	78.17	48.06	0.49
SG 044	YB	5.5	aa 3h	525.1	8.3	429.1	0.012370	0.13	0.082117	0.43	0.048147	0.40	79.25	80.13	106.50	0.41
SG 044	YB	13.5	aa 3h	668.1	9.4	2400.5	0.012371	0.14	0.081569	0.18	0.047820	0.11	79.26	79.62	90.36	0.79
SG 044	YB	3.4	aa 3h	742.8	11.2	766.2	0.012404	0.20	0.082237	0.45	0.048084	0.39	79.47	80.25	103.42	0.47
SG 044	YB	3.7	aa 3h	186.6	4.0	107.8	0.012445	0.18	0.081677	1.88	0.047598	1.78	79.73	79.72	79.38	0.58
SG 044	YB	2.1	aa 3h	1128.7	19.8	264.5	0.012470	0.17	0.083206	0.90	0.048395	0.87	79.89	81.15	118.59	0.27
SG 044	YB	5.0	aa 3h	493.2	11.3	101.9	0.012598	0.26	0.082580	2.96	0.047541	2.80	80.71	80.57	76.51	0.63
SG 044b	YB	2.3	na	150.6	3.9	71.9	0.012406	1.09	0.081772	15.02	0.047806	14.21	79.48	79.81	89.68	0.76
SG 044b	YB	6.6	na	150.3	2.8	581.3	0.013538	0.29	0.090690	0.88	0.048584	0.79	86.69	88.15	127.75	0.45
SG 044b	YB	2.1	na	19.0	2.0	94.9	0.071224	0.44	0.572863	4.74	0.058334	4.46	443.53	459.86	542.35	0.66
SG 044b	YB	4.0	na	18.9	3.4	703.4	0.174703	0.44	1.789964	0.72	0.074309	0.54	1037.97	1041.81	1049.87	0.67
SG 063	YB	7.8	aa 6h	18.9	0.7	216.0	0.027056	0.20	0.193838	2.17	0.051960	2.08	172.10	179.90	283.65	0.47
SG 063	YB	2.6	aa 6h	42.4	2.2	93.4	0.030615	0.26	0.225683	3.66	0.053464	3.48	194.40	206.63	348.54	0.68
SG 063	YB	4.3	aa 6h	21.3	1.3	678.7	0.063063	0.17	0.483446	0.88	0.055599	0.82	394.23	400.43	436.43	0.42
SG 063	YB	5.8	aa 6h	33.7	2.6	447.1	0.068411	0.30	0.577459	0.84	0.061220	0.76	426.57	462.83	646.97	0.43
SG 063	YB	8.7	aa 6h	46.6	3.7	786.0	0.075881	0.15	0.598451	0.30	0.057200	0.25	471.49	476.25	499.24	0.57
SG 102d	YB	6.2	aa 6h	147.8	9.3	32.1	0.012067	0.81	0.073557	15.32	0.044210	14.60	77.32	72.07	-98.98	0.89
SG 102d	YB	4.6	aa 6h	178.3	2.6	330.3	0.012222	0.24	0.082757	1.70	0.049110	1.60	78.31	80.73	153.03	0.47
SG 102d	YB	6.8	aa 6h	135.2	1.9	578.3	0.012428	0.21	0.082602	1.02	0.048205	0.95	79.62	80.59	109.31	0.40
SG 103	YB	2.8	aa 8h	142.8	2.4	169.9	0.012516	0.27	0.084435	2.48	0.048926	2.35	80.19	82.31	144.26	0.53
AvQ 046	Str	6.9	aa 2h	217.1	4.0	133.2	0.012349	0.22	0.081354	2.38	0.047779	2.25	79.12	79.42	88.33	0.63
AvQ 046	Str	1.7	aa 2h	1005.1	14.6	327.0	0.013228	0.39	0.086616	2.86	0.047492	2.69	84.71	84.35	73.98	0.48

Sample №	Region	Weight µg	Abr	U ppm	Pb ppm	$^{*206}Pb/^{204}Pb$	$^{206}Pb/^{238}U$	2σ, %	$^{207}Pb/^{235}U$	2σ, %	$^{207}Pb/^{206}Pb$	2σ, %	$^{206}Pb/^{238}U$ age, Ma	$^{207}Pb/^{235}U$ Age, Ma	$^{207}Pb/^{206}Pb$ Age, Ma	Rho
AvQ 046	Str	0.3	aa 2h	1052.3	56.2	40.2	0.014440	0.37	0.095074	5.74	0.047752	5.46	92.42	92.22	86.97	0.78
AvQ 046	Str	2.3	aa 2h	144.2	4.6	78.4	0.016332	2.40	0.113560	37.42	0.050428	35.88	104.44	109.22	214.77	0.66
AvQ 048	Str	12.0	aa	623.8	8.1	607.2	0.012184	0.19	0.079905	0.87	0.047567	0.82	78.07	78.06	77.75	0.39
AvQ 048	Str	8.2	aa	561.2	9.2	192.1	0.012247	0.22	0.081155	1.63	0.048059	1.53	78.47	79.23	102.22	0.49
AvQ 048	Str	3.9	ca	189.0	5.8	58.1	0.012385	0.23	0.084241	2.17	0.049333	2.07	79.35	82.12	163.71	0.47
AvQ 048	Str	11.2	ca	172.3	2.6	265.4	0.012452	0.43	0.082965	0.86	0.048324	0.73	79.77	80.93	115.13	0.53
AvQ 048	Str	12.0	ca	155.7	2.5	213.3	0.012455	0.54	0.083107	1.10	0.048393	0.94	79.80	81.06	118.59	0.51
AvQ 048	Str	9.7	aa 2h	281.0	4.1	324.3	0.012467	0.13	0.081910	0.50	0.047651	0.46	79.87	79.94	81.95	0.43
AvQ 048	Str	9.0	aa 2h	296.2	4.3	320.8	0.012469	0.28	0.082110	0.63	0.047758	0.54	79.89	80.13	87.28	0.52
AvQ 048	Str	4.2	ca	127.9	2.0	171.5	0.012472	0.52	0.082291	5.21	0.047855	4.96	79.90	80.30	92.09	0.52
AvQ 048	Str	7.8	ca	164.8	2.2	552.0	0.012510	0.18	0.083458	0.86	0.048387	0.83	80.14	81.39	118.21	0.29
AvQ 048	Str	17.7	ca	213.3	3.4	225.9	0.012666	0.39	0.082937	1.06	0.047492	0.94	81.14	80.90	74.03	0.48
AvQ 048	Str	3.8	aa 2h	144.3	2.7	281.2	0.015623	0.39	0.106300	2.30	0.049349	2.16	99.93	102.57	164.45	0.45
AvQ 048	Str	4.7	aa 2h	127.1	3.2	110.7	0.015812	0.23	0.107585	2.44	0.049347	2.32	101.13	103.75	164.38	0.54
AvQ 048	Str	7.4	aa	249.9	5.8	152.7	0.016351	0.19	0.111098	1.47	0.049280	1.38	104.55	106.97	161.16	0.51
AvQ 048	Str	4.2	aa	112.5	2.8	185.9	0.018247	2.25	0.136898	21.76	0.054414	20.46	116.57	130.28	388.23	0.61
AvQ 048	Str	10.5	aa	307.6	6.9	447.8	0.020303	0.27	0.139130	1.55	0.049699	1.44	129.57	132.27	180.98	0.45
AvQ 050	Str	18.2	aa 7h	181.4	2.9	714.4	0.012625	0.17	0.083185	0.33	0.047788	0.28	80.88	81.13	88.78	0.56
AvQ 050	Str	22.8	aa 7h	192.6	2.9	706.9	0.012637	0.19	0.083484	0.47	0.047913	0.43	80.95	81.42	95.01	0.43
AvQ 050	Str	32.1	aa 7h	185.4	3.1	696.7	0.012638	0.51	0.083683	0.66	0.048026	0.41	80.96	81.60	100.57	0.78
AvQ 051	Str	7.2	aa 7h	105.7	2.2	124.2	0.012415	0.19	0.080621	2.07	0.047098	1.96	79.54	78.73	54.27	0.60
AvQ 051	Str	24.7	aa 7h	76.8	1.3	326.1	0.012449	0.30	0.081257	2.20	0.047338	2.08	79.76	79.33	66.28	0.49
AvQ 051	Str	13.9	aa 7h	121.0	2.2	302.9	0.012477	0.15	0.081768	0.69	0.047530	0.64	79.94	79.81	75.89	0.42
AvQ 051	Str	8.5	aa 7h	49.9	1.1	95.3	0.012562	0.22	0.089094	2.24	0.051440	2.16	80.47	86.66	260.59	0.38
AvQ 051	Str	12.1	aa 7h	139.9	2.3	524.6	0.014019	0.24	0.094845	0.66	0.049069	0.61	89.74	92.01	151.14	0.41
AvQ 051	Str	19.7	aa 7h	85.6	3.0	1496.4	0.032830	0.17	0.235510	0.25	0.052027	0.17	208.24	214.74	286.60	0.71
AvQ 052	Str	41.6	aa 6h	174.5	2.2	1801.9	0.012416	0.15	0.081821	0.24	0.047797	0.18	79.54	79.86	89.23	0.66
AvQ 052	Str	4.5	aa 6h	267.4	3.6	820.6	0.012430	0.37	0.082375	0.87	0.048064	0.75	79.64	80.38	102.37	0.50
SG 011	Str	8.4	aa 6h	90.3	5.2	37.4	0.012987	9.80	0.080292	44.50	0.044841	41.39	83.18	78.42	-64.29	0.42
SG 011	Str	2.8	aa 6h	93.0	3.8	47.9	0.013341	0.45	0.089931	7.01	0.048889	6.65	85.43	87.44	142.52	0.81
SG 011	Str	12.2	aa 6h	69.6	1.4	175.4	0.013471	0.15	0.089125	1.27	0.047984	1.23	86.26	86.69	98.49	0.30
SG 011	Str	22.7	aa 6h	62.5	1.0	558.5	0.013481	0.33	0.089045	0.63	0.047904	0.52	86.33	86.61	94.53	0.56
SG 011	Str	13.4	aa 6h	302.9	5.2	2807.2	0.013490	0.28	0.088937	0.46	0.047817	0.36	86.38	86.51	90.19	0.62
SG 021	Str	2.3	aa 6h	185.6	6.2	48.5	0.012272	0.31	0.077540	5.51	0.045826	5.27	78.63	75.83	-11.56	0.81
SG 021	Str	0.8	aa 6h	163.3	4.1	45.9	0.012349	0.89	0.081272	16.59	0.047731	15.82	79.12	79.34	85.92	0.88
SG 021	Str	2.1	na	496.6	10.2	115.7	0.012357	0.21	0.082820	2.26	0.048610	2.14	79.17	80.79	129.11	0.62
SG 021	Str	0.2	na	457.0	36.0	214.8	0.068962	0.39	0.550288	1.44	0.057873	1.31	429.90	445.19	524.96	0.45

Appendix 1.

Sample №	Region	Weight µg	Abr	U ppm	Pb ppm	$^{*206}Pb/^{204}Pb$	$^{206}Pb/^{238}U$	2σ, %	$^{207}Pb/^{235}U$	2σ, %	$^{207}Pb/^{206}Pb$	2σ, %	$^{206}Pb/^{238}U$ age, Ma	$^{207}Pb/^{235}U$ Age, Ma	$^{207}Pb/^{206}Pb$ Age, Ma	Rho
SG 028	Str	9.4	aa 3h	505.7	6.0	1613.0	0.011999	0.15	0.079278	0.45	0.047917	0.41	76.89	77.47	95.14	0.41
SG 028	Str	116.0	aa 3h	31.0	0.4	596.6	0.012103	0.17	0.079798	0.59	0.047817	0.56	77.56	77.96	90.27	0.32
SG 028	Str	6.0	aa 3h	284.9	4.7	164.9	0.012119	0.14	0.080337	0.96	0.048079	0.93	77.65	78.46	103.21	0.28
SG 028	Str	17.0	aa 3h	236.4	2.9	1369.1	0.012215	0.20	0.080181	0.35	0.047608	0.28	78.27	78.32	79.83	0.61
SG 028	Str	4.1	aa 3h	188.9	2.6	315.9	0.012449	0.32	0.082604	3.13	0.048125	2.97	79.76	80.59	105.42	0.55
SG 028	Str	6.4	aa 3h	249.8	3.7	486.1	0.013933	0.36	0.095175	1.62	0.049544	1.50	89.20	92.31	173.67	0.42
SG 028	Str	3.7	aa 3h	242.0	5.6	105.7	0.014238	0.39	0.095998	4.63	0.048900	4.37	91.14	93.08	142.98	0.68
SG 030	Str	19.4	ca	109.0	3.7	589.8	0.030106	0.15	0.210348	0.38	0.050674	0.33	191.21	193.84	225.96	0.50
SG 030	Str	3.5	na	89.5	4.6	485.0	0.050263	0.16	0.371537	0.57	0.053611	0.52	316.13	320.79	354.78	0.43
SG 030	Str	0.8	ca	86.8	5.6	172.3	0.050972	0.36	0.382692	3.03	0.054453	2.85	320.48	329.02	389.79	0.54
SG 030	Str	0.4	ca	81.8	7.5	67.3	0.052973	0.67	0.403065	8.72	0.055185	8.22	332.75	343.87	419.71	0.76
SG 030	Str	1.7	na	36.1	4.2	66.3	0.057441	0.33	0.438711	2.70	0.055393	2.55	360.04	369.34	428.13	0.52
SG 032	Str	3.1	na	162.1	2.8	292.8	0.013322	0.19	0.089690	1.50	0.048830	1.42	85.31	87.21	139.68	0.47
SG 032	Str	2.9	na	72.8	3.6	537.2	0.049839	0.23	0.380508	0.84	0.055373	0.77	313.53	327.41	427.34	0.42
SG 032	Str	1.5	na	126.0	8.1	444.5	0.062869	0.27	0.487873	0.78	0.056282	0.70	393.05	403.46	463.52	0.47
SG 045	Str	12.8	ca	310.8	4.1	548.0	0.012433	0.14	0.081811	0.42	0.047725	0.38	79.65	79.85	85.63	0.46
SG 045	Str	13.1	ca	235.8	2.8	3472.1	0.012438	0.14	0.082195	0.29	0.047929	0.25	79.69	80.21	95.77	0.53
SG 045	Str	25.2	ca	122.4	1.7	2285.8	0.014564	0.13	0.097252	0.28	0.048429	0.23	93.21	94.24	120.26	0.55
SG 045	Str	5.6	ca	281.1	4.8	320.4	0.014774	0.15	0.099369	0.87	0.048783	0.82	94.54	96.19	137.42	0.43
SG 051	Str	2.1	na	426.8	19.2	40.5	0.011944	1.32	0.095941	16.07	0.058257	15.07	76.54	93.02	539.46	0.77
SG 051	Str	3.0	aa 2h	191.6	8.6	69.9	0.021440	0.31	0.158645	1.85	0.053666	1.76	136.75	149.52	357.09	0.35
SG 051	Str	4.1	aa 2h	192.2	7.2	108.8	0.021633	0.25	0.153903	1.14	0.051597	1.08	137.97	145.35	267.60	0.36
SG 051	Str	5.7	na	145.1	4.9	367.7	0.030026	0.21	0.212930	1.00	0.051433	0.93	190.71	196.01	260.28	0.43
SG 051	Str	2.2	aa 2h	191.0	8.2	150.2	0.030422	0.55	0.216528	2.11	0.051621	2.01	193.19	199.02	268.63	0.30
SG 051	Str	2.6	aa 2h	189.6	9.8	323.1	0.042523	4.43	0.314674	6.54	0.053670	4.78	268.46	277.80	357.19	0.68
SG 052	Str	0.8	na	705.0	133.3	531.2	0.011662	0.25	0.076129	1.46	0.047346	1.38	74.74	74.50	66.67	0.40
SG 052	Str	65.6	aa 6h	344.2	4.4	7995.9	0.012113	0.19	0.081388	0.22	0.048733	0.11	77.61	79.45	135.03	0.87
SG 052	Str	38.8	aa 6h	246.1	3.2	2200.6	0.012259	0.49	0.079972	1.01	0.047315	0.88	78.54	78.12	65.12	0.49
SG 052	Str	38.6	aa 6h	309.8	4.0	2716.3	0.012316	0.22	0.080667	0.40	0.047505	0.33	78.91	78.77	74.65	0.55
SG 057	Str	2.5	aa 3h	242.4	3.9	144.6	0.011873	0.26	0.080477	1.68	0.049160	1.58	76.09	78.59	155.45	0.45
SG 057	Str	4.3	aa 3h	231.0	6.9	165.4	0.021584	0.23	0.145177	1.44	0.048783	1.35	137.66	137.64	137.38	0.46
SG 057	Str	4.2	aa 3h	194.2	4.7	1828.6	0.025387	0.21	0.179774	0.47	0.051359	0.40	161.61	167.87	256.98	0.52
SG 057	Str	2.5	aa 3h	97.1	6.4	75.8	0.034169	0.58	0.237420	8.19	0.050395	7.73	216.58	216.31	213.29	0.80
SG 057	Str	6.0	aa 3h	103.9	6.0	260.2	0.046157	0.16	0.332327	0.63	0.052219	0.58	290.88	291.34	295.02	0.43
SG 057	Str	22.8	aa 6h	132.7	8.6	5570.1	0.069391	0.13	0.532733	0.15	0.055681	0.06	432.48	433.62	439.69	0.91
ST 25	Str	7.0	ca	116.2	3.7	71.4	0.013513	0.21	0.091246	2.61	0.048973	2.48	86.53	88.66	146.51	0.60
ST 25	Str	3.8	ca	93.4	4.4	44.9	0.013562	0.44	0.092518	6.87	0.049476	6.51	86.84	89.85	170.43	0.84
ST 25	Str	11.3	ca	136.8	5.0	60.5	0.013573	0.23	0.091276	2.97	0.048774	2.81	86.91	88.69	136.99	0.71
ST 25	Str	9.4	ca	121.2	5.0	53.5	0.013576	0.25	0.093452	3.36	0.049923	3.20	86.93	90.71	191.42	0.68

Appendix 1. U-Pb zircon analyses by LA-ICPMS Abbreviations : EB – East Balkan region; NB – North Balkan region; YB – Yambol-Burgas region; Str – Strandzha region; Bas – basement rocks; P % - for samples where common Pb correction was applied this is the age difference in percentage between the common Pb corrected age, presented here and the uncorrected age; Rho-correlation coefficient ; R – number of readings integrated from the signal ; S – seconds integrated from the signal ; A/In – the ratio of the age calculated using the average approach (similar to LAMTRACE program) versus the calculated age using the intercept regression approach (used in this study), i.e. this ratio is an estimation of the degree of elemental fractionation in the course of the analyses; C (concordance) – within their analytical errors samples marked with * cross the concordia band.

sample #					Isotope ratios					Apparent ages							
crystal #	Region	block		P%	$^{207}Pb/^{235}U$	2σ,%	$^{206}Pb/^{238}U$	2σ,%	Rho	$^{206}Pb/^{238}U$	2σ,Ma	$^{207}Pb/^{235}U$	2σ,Ma	R	S	A/In	C
SG 047-cr1	Bas	ja12e	5	2.3	0.5409	13.53	0.0486	4.64	0.34	299.0	13.9	430.84	58.3	31	4.2	1.03	
SG 047-cr10	Bas	ja12e	14		0.3759	4.45	0.0503	2.27	0.51	316.6	7.2	324.01	14.4	146	19.7	0.91	*
SG 047-cr2	Bas	ja12e	6		0.3303	7.10	0.0462	2.06	0.29	290.9	6.0	289.82	20.6	280	37.5	1.05	*
SG 047-cr3	Bas	ja12e	7	2.4	0.5810	10.67	0.0734	5.86	0.55	445.6	26.1	455.94	48.6	272	36.4	0.94	*
SG 047-cr4	Bas	ja12e	8		0.3630	9.93	0.0432	4.35	0.44	275.2	12.0	316.91	31.5	163	21.8	1.06	*
SG 047-cr5	Bas	ja12e	9		0.3347	10.52	0.0445	5.96	0.57	280.4	16.7	293.13	30.8	185	24.8	1.08	*
SG 047-cr6	Bas	ja12e	10		11.1622	10.94	0.3862	5.25	0.48	2105.3	110.6	2536.76	277.5	125	16.8	1.28	
SG 047-cr7	Bas	ja12e	11		0.3559	8.29	0.0480	3.81	0.46	302.3	11.5	309.16	25.6	207	27.7	1.07	*
SG 047-cr8	Bas	ja12e	12		0.3551	12.00	0.0502	6.98	0.58	315.8	22.1	308.58	37.0	67	9.0	0.98	*
SG 047-cr9	Bas	ja12e	13		0.4062	14.42	0.0488	8.65	0.60	306.9	26.6	346.15	49.9	115	15.4	1.01	*
SG 070-cr1	Bas	ja12d	5	4.4	0.1996	72.48	0.0417	5.56	0.99	263.4	14.6	184.80	133.9	255	34.2	1.40	*
SG 070-cr10	Bas	ja12d	17	2.4	0.4658	9.64	0.0419	3.34	0.35	258.4	8.6	380.37	36.7	126	16.9	1.14	
SG 070-cr11	Bas	ja12d	4		0.3969	8.42	0.0409	2.91	0.35	261.7	7.6	343.06	28.9	160	21.6	1.16	
SG 070-cr2	Bas	ja12d	6		0.3735	8.49	0.0513	1.94	0.23	322.5	6.3	322.24	27.4	250	33.5	1.02	*
SG 070-cr3	Bas	ja12d	7		0.7535	6.41	0.0840	1.94	0.30	520.0	10.1	570.26	36.6	110	14.7	1.00	
SG 070-cr4	Bas	ja12d	8		0.5780	6.15	0.0735	1.74	0.28	457.5	8.0	463.16	28.5	245	32.8	1.07	*
SG 070-cr5-c	Bas	ja12d	10	4.8	-0.1007	36.69	0.0409	6.78	0.18	258.7	17.5	-107.74	-39.5	120	16.1	1.41	
SG 070-cr5-r	Bas	ja12d	9		0.3049	15.20	0.0433	3.64	0.24	273.9	10.0	270.66	41.1	151	20.2	1.16	*
SG 070-cr6-r	Bas	ja12d	11		0.3114	12.79	0.0432	3.05	0.24	272.2	8.3	275.06	35.2	112	15.0	1.23	*
SG 070-cr7	Bas	ja12d	12		0.2778	19.30	0.0388	4.14	0.21	241.5	10.0	245.56	47.4	55	7.4	1.16	*
SG 070-cr8-c	Bas	ja12d	14		0.2061	18.79	0.0404	2.91	0.15	254.4	7.4	189.54	35.6	88	11.8	1.10	
SG 070-cr8-r	Bas	ja12d	13		0.3597	10.86	0.0445	2.97	0.27	280.6	8.3	311.99	33.9	99	13.3	1.06	*
SG 070-cr9-c	Bas	ja12d	16	2.6	0.5688	10.53	0.0464	3.67	0.35	285.0	10.5	447.44	47.1	120	16.1	1.09	
SG 070-cr9-r	Bas	ja12d	15		0.1374	134.28	0.0428	5.72	0.04	270.0	15.4	130.74	175.6	86	11.5	1.19	*
SG 068-cr1-c	EB	ma04c	4		0.3161	25.23	0.0444	6.06	0.24	264.8	16.0	265.35	67.0	73	10.0	1.06	*
SG 068-cr3-r	EB	ma04c	6		0.3445	19.55	0.0475	4.02	0.21	299.0	12.0	300.61	58.8	120	16.4	1.10	*
SG 068-cr4-c	EB	ma04c	7	5.8	0.1979	11.75	0.0218	3.11	0.26	139.3	4.3	183.35	21.5	133	18.2	1.05	
SG 068-cr5	EB	ma04c	8	3.6	0.1579	10.56	0.0151	3.54	0.33	93.2	3.3	143.81	15.2	270	37.0	1.06	
SG 068-cr6	EB	ma04c	9		0.1643	21.45	0.0244	3.86	0.18	155.1	6.0	154.50	33.1	128	17.5	1.03	*
SG 068-cr7-r	EB	ma04c	11	1.9	0.0925	13.10	0.0114	2.61	0.20	71.8	1.9	88.14	11.5	140	19.2	1.12	
SG 068-cr7-r?	EB	ma04c	10	16.2	0.0929	16.17	0.0123	4.12	0.25	66.1	2.7	76.09	12.3	139	19.0	1.07	*
SG 068-cr8-r	EB	ma04c	12		0.0384	37.56	0.0076	9.09	0.24	48.8	4.4	38.31	14.4	180	24.7	1.17	*

sample #					Isotope ratios					Apparent ages							
crystal #	Region	block		P%	$^{207}Pb/^{235}U$	2σ,%	$^{206}Pb/^{238}U$	2σ,%	Rho	$^{206}Pb/^{238}U$	2σ,Ma	$^{207}Pb/^{235}U$	2σ,Ma	R	S	A/In	C
SG 068-cr9	EB	ma04c	13		0.0929	7.70	0.0124	1.99	0.26	79.6	1.6	90.16	6.9	314	43.0	1.08	
SG 069-cr1	EB	jn08a	13	8.6	0.3464	12.60	0.0121	6.47	0.51	71.0	4.6	279.30	35.2	137	17.0	1.14	
SG 069-cr13	EB	jn08b	5		0.2718	3.97	0.0375	1.37	0.35	237.3	3.3	244.16	9.7	380	47.1	1.03	*
SG 069-cr14	EB	jn08b	6	2.5	0.3568	10.32	0.0392	2.45	0.24	241.6	5.9	303.06	31.3	90	11.2	1.19	
SG 069-cr16	EB	jn08b	7		0.0549	3.72	0.0084	1.28	0.34	53.7	0.7	54.26	2.0	384	47.6	1.00	*
SG 069-cr17-r	EB	jn08b	8		0.3777	3.46	0.0486	1.35	0.39	305.8	4.1	325.38	11.3	370	45.9	0.99	
SG 069-cr2	EB	jn08a	14	6.0	0.9233	15.58	0.0757	3.77	0.24	443.3	16.7	634.38	98.8	181	22.4	1.04	
SG 069-cr5	EB	jn08a	16	2.0	0.4068	14.35	0.0536	3.52	0.25	329.9	11.6	340.74	48.9	60	7.4	1.05	*
SG 069-cr6	EB	jn08a	17		0.3201	3.94	0.0434	1.59	0.40	273.8	4.4	281.98	11.1	430	53.3	0.96	*
SG 069-cr7	EB	jn08b	4		0.3644	4.45	0.0489	1.45	0.33	307.5	4.5	315.47	14.0	248	30.8	1.00	*
SG 085-cr1	NB	jn15b	11	5.5	0.4607	10.80	0.0449	2.54	0.24	267.9	6.8	366.94	39.6	226	28.0	1.19	
SG 085-cr2	NB	jn15b	12	9.8	0.5648	7.15	0.0223	3.59	0.50	128.2	4.6	417.88	29.9	120	14.9	1.09	
SG 085-cr4	NB	jn15b	13	10.4	1.6583	7.08	0.0815	1.88	0.27	454.7	8.6	924.85	65.4	334	41.4	0.96	
SG 094-9	NB	jn15b	15		0.4216	16.09	0.0516	3.65	0.23	324.4	11.8	357.22	57.5	146	18.1	1.22	*
AvQ 046-cr5-c	Str	ar01c	7		0.1255	22.27	0.0203	4.61	0.21	114.5	5.3	106.88	23.8	132	18.1	0.97	*
AvQ 046-cr7-c	Str	ar01c	10	2.4	0.1158	14.83	0.0157	4.10	0.28	100.6	4.1	111.28	16.5	67	9.2	1.02	*
AvQ 046-cr7-r	Str	ar01c	11	2.7	0.0231	93.10	0.0086	6.90	0.07	55.4	3.8	23.16	21.6	80	11.0	1.58	
AvQ 046-cr8-r	Str	ar01c	9		1.1952	8.58	0.0894	2.64	0.31	551.8	14.6	798.35	68.5	117	16.0	1.06	
AvQ 046-cr9-c	Str	ar01c	12		0.1284	16.83	0.0116	5.35	0.32	74.2	4.0	122.69	20.6	89	12.2	1.13	
AvQ 048-cr10r	Str	ar01d	13		0.1179	16.45	0.0164	3.66	0.22	104.8	3.8	113.14	18.6	97	13.3	1.01	*
AvQ 048-cr2-c	Str	ar01c	13		0.05958	157.22	0.0208	6.88	0.04	132.9	9.1	58.8	92.4	237	33	1.17	*
AvQ 048-cr2-r	Str	ar01c	14		0.0842	8.20	0.0127	2.33	0.28	81.5	1.9	82.07	6.7	387	53.0	1.17	*
AvQ 048-cr3-r	Str	ar01c	15	16.9	0.1098	11.40	0.0106	4.54	0.40	68.0	3.1	105.78	12.1	239	32.7	1.17	
AvQ 048-cr4-c	Str	ar01c	17	8.0	0.0981	18.70	0.0130	4.03	0.22	76.4	3.1	87.67	16.4	336	46.0	1.29	*
AvQ 048-cr4-r	Str	ar01c	16		0.0983	12.14	0.0118	3.13	0.26	76.7	2.4	96.56	11.7	157	21.5	1.14	
AvQ 048-cr5-c	Str	ar01d	4		0.0893	10.16	0.0132	2.36	0.23	84.5	2.0	86.87	8.8	169	23.2	1.19	*
AvQ 048-cr5-r	Str	ar01d	5	3.2	0.1042	10.44	0.0129	2.85	0.27	80.1	2.3	97.57	10.2	128	17.5	1.07	
AvQ 048-cr6-c	Str	ar01d	6		0.2301	14.24	0.0345	3.19	0.22	218.7	7.0	210.31	30.0	53	7.3	1.09	*
AvQ 048-cr6-r	Str	ar01d	7		0.0946	9.24	0.0122	2.53	0.27	78.1	2.0	91.79	8.5	111	15.2	1.15	
AvQ 048-cr7-c	Str	ar01d	8		0.3378	17.38	0.0442	5.51	0.32	278.6	15.3	295.53	51.4	32	4.4	1.12	*
AvQ 048-cr7-r	Str	ar01d	9		0.0701	10.31	0.0128	2.12	0.21	81.8	1.7	68.81	7.1	77	10.5	1.05	
AvQ 048-cr8-c	Str	ar01d	10		0.0940	21.58	0.0125	5.19	0.24	79.9	4.1	91.25	19.7	329	45.1	1.37	*
AvQ 048-cr8-r	Str	ar01d	11		0.0812	14.37	0.0115	4.25	0.30	73.7	3.1	79.32	11.4	60	8.2	1.12	*
AvQ 048-cr9-r	Str	ar01d	12	18.2	0.1063	14.78	0.0140	5.03	0.34	73.6	3.7	84.72	12.5	221	30.3	1.15	*
AvQ 050-cr10	Str	ja21f	14		0.1470	26.53	0.0119	7.30	0.28	76.1	5.6	139.28	36.9	77	9.5	1.18	
AvQ 050-cr10r	Str	ja21f	13		0.1037	48.04	0.0134	10.39	0.22	85.7	8.9	100.21	48.1	78	9.7	1.07	*
AvQ 050-cr3-c	Str	ja21f	16		0.0894	22.35	0.0124	5.12	0.23	79.2	4.1	86.99	19.4	248	30.8	1.19	*
AvQ 050-cr4-c	Str	ja21f	17	1.9	0.1318	19.29	0.0123	7.32	0.38	78.6	5.8	125.74	24.3	204	25.3	1.24	
AvQ 050-cr5-c	Str	ja21f	15	15.9	0.0998	15.82	0.0107	5.30	0.34	68.4	3.6	96.55	15.3	272	33.7	1.21	

sample #					Isotope ratios					Apparent ages							
crystal #	Region	block		P%	$^{207}Pb/^{235}U$	2σ,%	$^{206}Pb/^{238}U$	2σ,%	Rho	$^{206}Pb/^{238}U$	2σ,Ma	$^{207}Pb/^{235}U$	2σ,Ma	R	S	A/In	C
AvQ 050-cr8-c	Str	ja21f	9	34.4	0.0745	183.63	0.0092	7.39	0.04	59.0	4.4	72.95	134.0	231	28.6	1.01	*
AvQ 050-cr8-r	Str	ja21f	10	27.0	0.0980	28.05	0.0094	6.55	0.23	60.3	4.0	94.97	26.6	194	24.1	1.16	
AvQ 050-cr9-c	Str	ja21f	11		0.0430	97.00	0.0137	7.29	0.08	87.5	6.4	42.75	41.5	218	27.0	1.21	*
AvQ 050-cr9-r	Str	ja21f	12		0.0809	36.43	0.0146	6.06	0.17	93.5	5.7	78.98	28.8	152	18.8	0.97	*
AvQ 051-cr10	Str	ja21g	4		0.1961	46.41	0.0429	5.88	0.13	270.7	15.9	181.84	84.4	60	7.4	1.14	*
AvQ 051-cr10	Str	ja21g	5	5.0	0.4341	25.68	0.0534	4.77	0.19	319.1	15.2	350.49	90.0	302	37.4	1.15	*
AvQ 051-cr1-c	Str	ja21g	7	8.3	0.0812	32.36	0.0132	5.98	0.18	77.4	4.6	72.89	23.6	178	22.1	1.13	*
AvQ 051-cr1-r	Str	ja21g	8		0.1026	19.02	0.0127	5.07	0.27	81.1	4.1	99.14	18.9	133	16.5	1.13	*
AvQ 051-cr5	Str	ja21g	9	3.2	0.0426	81.06	0.0155	5.72	0.07	96.0	5.5	41.06	33.3	129	16.0	0.93	
AvQ 051-cr8-r	Str	ja21g	6	2.8	0.0928	11.87	0.0130	2.68	0.23	83.1	2.2	90.14	10.7	203	25.2	1.10	*
SG 001-cr11	Str	jn07a	11	8.5	0.2009	6.06	0.0132	2.10	0.35	84.6	1.8	185.93	11.3	315	39.1	1.00	
SG 001-12-c?	Str	jn07a	12	7.6	0.0606	22.80	0.0104	3.54	0.16	66.9	2.4	59.75	13.6	419	52.0	1.07	*
SG 001-12-r	Str	jn07a	13		0.0833	8.74	0.0126	2.16	0.25	80.9	1.7	81.27	7.1	290	36.0	1.02	*
SG 001-1-c	Str	jn07a	4	2.0	0.0630	22.74	0.0130	3.16	0.14	81.8	2.6	60.87	13.8	458	56.8	0.96	
SG 001-1-r	Str	jn07a	5		0.0810	10.41	0.0126	2.85	0.27	80.5	2.3	79.09	8.2	315	39.1	1.06	*
SG 001-5-r	Str	jn07a	6		0.0877	9.86	0.0132	2.16	0.22	85.7	1.9	86.32	8.5	231	28.6	1.03	*
SG 001-6-c?	Str	jn07a	7		0.0750	14.95	0.0125	2.43	0.16	80.3	2.0	73.40	11.0	420	52.1	1.03	*
SG 001-7-r	Str	jn07a	8	2.4	0.1119	15.64	0.0123	4.05	0.26	77.2	3.1	105.23	16.5	229	28.4	1.18	
SG 001-cr8	Str	jn07a	9		0.1067	8.32	0.0137	2.34	0.28	87.5	2.1	102.90	8.6	176	21.8	0.98	
SG 001-cr9	Str	jn07a	10	1.9	0.1693	5.38	0.0132	2.20	0.41	83.1	1.8	156.00	8.4	360	44.6	1.02	
SG 011-cr1	Str	ja12b	4		0.0958	7.76	0.0129	1.78	0.23	82.8	1.5	92.92	7.2	76	10.2	1.10	
SG 011-cr10	Str	ja12b	14		0.0985	10.88	0.0122	3.18	0.29	78.3	2.5	95.39	10.4	158	21.2	1.14	
SG 011-cr11	Str	ja12b	15		0.0938	9.34	0.0140	2.32	0.25	89.9	2.1	91.01	8.5	394	52.8	1.03	*
SG 011-cr12	Str	ja12b	16		0.0927	6.75	0.0126	2.00	0.30	80.9	1.6	90.05	6.1	125	16.8	1.10	
SG 011-cr2	Str	ja12b	5		0.0980	8.68	0.0135	2.43	0.28	86.5	2.1	94.90	8.2	122	16.3	1.05	*
SG 011-cr3	Str	ja12b	6		0.0899	11.53	0.0136	2.72	0.24	86.9	2.4	87.45	10.1	116	15.5	1.05	*
SG 011-cr4	Str	ja12b	7		0.0765	13.12	0.0124	2.85	0.22	79.2	2.3	74.83	9.8	79	10.6	1.11	*
SG 011-cr5	Str	ja12b	8		0.0969	6.28	0.0147	1.76	0.28	94.5	1.7	94.07	5.9	114	15.3	1.02	*
SG 011-cr6	Str	ja12b	9		0.0948	8.34	0.0132	2.42	0.29	84.4	2.0	91.98	7.7	201	26.9	1.03	*
SG 011-cr7	Str	ja12b	10	2.1	0.0959	8.08	0.0140	2.41	0.30	87.9	2.1	91.09	7.4	313	41.9	1.07	*
SG 011-cr7	Str	ja12b	11	9.1	0.0774	20.73	0.0118	4.27	0.21	75.4	3.2	75.66	15.7	311	41.7	1.18	*
SG 011-cr8	Str	ja12b	12		0.0865	11.89	0.0137	3.27	0.27	87.8	2.9	84.27	10.0	36	4.8	1.00	*
SG 011-cr9	Str	ja12b	13	3.0	0.1215	12.25	0.0148	3.65	0.30	91.6	3.3	113.19	13.9	198	26.5	1.15	
SG 021-cr1	Str	jn15a	12		0.0753	5.86	0.0124	1.31	0.22	79.4	1.0	73.68	4.3	364	45.1	1.04	
SG 021-11	Str	jn15a	15		0.0754	8.60	0.0121	1.88	0.22	77.5	1.5	73.80	6.3	97	12.0	1.05	*
SG 021-12	Str	jn15a	16		0.0858	6.89	0.0113	1.63	0.24	72.7	1.2	83.62	5.8	343	42.5	1.07	
SG 021-2-r	Str	jn15a	13		0.0684	7.89	0.0103	1.76	0.22	66.0	1.2	67.14	5.3	224	27.8	1.09	*
SG 021-cr8	Str	jn15a	14		0.0853	6.43	0.0122	1.52	0.24	77.8	1.2	82.65	5.3	336	41.7	1.05	*
SG 028-cr1-c	Str	ma04c	14	5.0	0.2989	13.91	0.0418	3.71	0.27	250.8	9.3	253.83	35.3	113	15.5	1.22	*
SG 028-cr1-r	Str	ma04c	14		0.1402	18.44	0.0127	7.33	0.40	81.5	6.0	133.22	24.6	68	9.3	1.07	

sample #				Isotope ratios					Apparent ages							
crystal #	Region	block	P%	$^{207}Pb/^{235}U$	2σ,%	$^{206}Pb/^{238}U$	2σ,%	Rho	$^{206}Pb/^{238}U$	2σ,Ma	$^{207}Pb/^{235}U$	2σ,Ma	R	S	A/In	C
SG 028-cr2-c	Str	ma04c 17	7.4	0.1082	38.32	0.0129	7.10	0.19	76.7	5.4	96.91	37.1	167	22.9	1.14	*
SG 028-cr2-r	Str	ma04c 16		0.1077	21.11	0.0131	5.74	0.27	79.4	4.6	98.72	20.8	251	34.4	1.23	*
SG 028-cr3-c	Str	ma04d 4		0.3500	18.21	0.0467	3.91	0.21	296.1	11.6	306.19	55.8	156	21.4	1.28	*
SG 028-cr3-r	Str	ma04d 5		0.0758	15.12	0.0127	2.76	0.18	81.8	2.3	74.71	11.3	242	33.2	1.08	*
SG 028-cr4	Str	ma04d 6	5.1	0.0984	10.51	0.0117	3.91	0.37	74.7	2.9	95.34	10.0	164	22.5	1.09	
SG 028-cr4-c?	Str	ma04d 7		0.3345	13.66	0.0358	5.26	0.39	225.4	11.9	291.64	39.8	86	11.8	1.10	
SG 028-cr5	Str	ma04d 8		0.0833	7.52	0.0123	1.90	0.25	78.0	1.5	80.25	6.0	503	68.9	1.09	*
SG 028-cr6	Str	ma04d 9	8.5	0.1185	26.05	0.0119	6.43	0.25	76.3	4.9	113.74	29.6	266	36.4	1.26	
SG 028-cr6-r	Str	ma04d 10		0.0826	10.68	0.0116	3.14	0.29	74.4	2.3	80.61	8.6	156	21.4	1.13	*
SG 028-cr7	Str	ma04d 11		0.0915	6.81	0.0123	2.05	0.30	79.3	1.6	89.63	6.1	444	60.8	1.03	
SG 028-cr8	Str	ma04d 13	8.9	0.0802	11.35	0.0112	2.66	0.23	71.9	1.9	78.33	8.9	325	44.5	1.13	*
SG 028-cr8-c	Str	ma04d 12	1.9	0.0853	14.54	0.0124	3.30	0.23	79.3	2.6	83.12	12.1	280	38.4	1.07	*
SG 028-cr-r	Str	ma04c 15		0.0978	6.82	0.0151	1.73	0.25	94.1	1.6	92.32	6.3	195	26.7	0.91	*
SG 051-cr1	Str	ja12c 5	16.5	1.6938	5.32	0.0416	6.95	0.99	220.2	15.3	894.73	47.6	247	33.1	1.39	
SG 051-cr10	Str	ja12c 17		0.5588	2.96	0.0497	1.80	0.61	312.9	5.6	450.73	13.3	456	61.1	1.03	
SG 051-cr11-c	Str	ja12d 4		0.0848	12.80	0.0133	5.63	0.44	85.2	4.8	82.66	10.6	375	50.3	1.03	*
SG 051-cr1	Str	ja12c 4		0.6230	7.41	0.0543	9.98	0.99	340.9	34.0	491.74	36.4	101	13.5	1.28	
SG 051-cr1-r	Str	ja12b 17	7.2	0.1148	59.14	0.0285	7.09	0.12	168.5	11.9	102.77	60.8	220	29.5	1.17	*
SG 051-cr2-c	Str	ja12c 7	2.3	0.3091	5.24	0.0292	2.61	0.50	181.6	4.7	268.03	14.1	186	24.9	0.99	
SG 051-cr2-r	Str	ja12c 6	74.6	8.2247	8.12	0.0885	6.77	0.83	143.2	9.7	1144.68	93.0	240	32.2	1.10	
SG 051-cr3-c	Str	ja12c 8	7.0	0.4269	6.25	0.0240	5.31	0.85	142.6	7.6	339.56	21.2	208	27.9	0.83	
SG 051-cr3-r	Str	ja12c 9	19.0	0.2993	15.00	0.0105	13.08	0.87	67.1	8.8	265.83	39.9	33	4.4	1.19	
SG 051-cr4-c	Str	ja12c 10	4.1	0.1568	11.59	0.0149	4.15	0.36	95.6	4.0	147.89	17.1	85	11.4	0.94	
SG 051-cr5-c	Str	ja12c 12	2.0	0.5241	4.87	0.0483	3.80	0.78	298.3	11.3	420.91	20.5	418	56.0	1.17	
SG 051-cr5-r	Str	ja12c 11		0.4444	10.76	0.0524	6.61	0.61	329.3	21.8	373.33	40.2	175	23.5	1.32	*
SG 051-cr6-c	Str	ja12c 13	10.4	0.5582	15.88	0.0361	10.46	0.66	205.3	21.5	411.85	65.4	103	13.8	1.22	
SG 051-cr7-c	Str	ja12c 14	56.4	2.2579	16.44	0.0499	6.66	0.41	138.8	9.2	695.47	114.3	100	13.4	1.04	
SG 051-cr8	Str	ja12c 15	12.7	0.7476	9.21	0.0274	4.30	0.47	174.0	7.5	566.85	52.2	394	52.8	0.91	
SG 051-cr9-r	Str	ja12c 16	66.8	2.9015	3.30	0.0353	2.46	0.75	75.2	1.9	685.41	22.6	292	39.1	1.07	
SG 052-1-c	Str	jn08d 12		0.0925	7.66	0.0154	3.45	0.45	98.3	3.4	89.60	6.9	370	45.9	0.95	*
SG 052-1-r	Str	jn08d 13	26.5	0.1727	17.28	0.0093	5.64	0.33	59.8	3.4	161.78	28.0	386	47.9	1.31	
SG 052-cr3	Str	jn08d 14	9.1	0.0158	155.78	0.0135	5.22	0.03	78.6	4.1	14.47	22.5	245	30.4	1.15	
SG 052-5-c	Str	jn08d 17	10.4	0.0742	47.01	0.0139	6.11	0.13	79.6	4.9	65.30	30.7	290	36.0	1.11	*
SG 052-6-c	Str	jn08d 16	1.9	0.3728	12.64	0.0537	3.89	0.31	330.8	12.9	316.40	40.0	343	42.5	1.04	*
SG 052-cr7	Str	jn08d 15	2.1	0.0332	58.65	0.0124	5.15	0.09	77.9	4.0	32.51	19.1	268	33.2	1.17	
SG 053-10-c	Str	jn15b 9	12.9	0.4232	7.66	0.0143	4.14	0.54	79.9	3.3	318.50	24.4	260	32.2	1.13	
SG 053-11	Str	jn15b 10		0.1004	11.14	0.0114	2.99	0.27	70.5	2.1	93.60	10.4	200	24.8	1.02	
SG 053-1-c?	Str	jn15b 4		0.4167	12.12	0.0439	3.11	0.26	275.8	8.6	352.74	42.8	190	23.6	1.11	
SG 053-cr2	Str	jn15b 5		0.0859	26.28	0.0112	4.81	0.18	71.1	3.4	82.78	21.8	151	18.7	1.31	*
SG 053-3-c	Str	jn15b 6	3.5	0.1610	6.83	0.0195	1.75	0.26	120.0	2.1	146.68	10.0	237	29.2	1.21	

sample #					Isotope ratios					Apparent ages							
crystal #	Region	block		P%	$^{207}Pb/^{235}U$	2σ,%	$^{206}Pb/^{238}U$	2σ,%	Rho	$^{206}Pb/^{238}U$	2σ,Ma	$^{207}Pb/^{235}U$	2σ,Ma	R	S	A/In	C
SG 053-cr5	Str	jn15a	17		0.5320	9.47	0.0623	2.22	0.23	393.5	8.7	437.06	41.4	115	14.3	1.09	*
SG 053-cr7-c	Str	jn15b	7		0.0983	17.55	0.0126	3.77	0.22	81.0	3.1	95.19	16.7	154	19.1	1.19	*
SG 053-cr9	Str	jn15b	8		0.1177	10.59	0.0120	3.49	0.33	76.8	2.7	112.97	12.0	235	29.1	1.21	
SG 057-cr1-r?	Str	ma04e	11		0.3580	9.05	0.0437	2.28	0.25	278.1	6.3	313.23	28.3	458	62.7	1.13	
SG 057-cr2-r	Str	ma04e	12	7.4	0.2102	6.06	0.0203	1.69	0.28	129.3	2.2	193.76	11.7	356	48.8	0.98	
SG 057-cr2-r	Str	ma04e	13		0.1666	8.17	0.0232	2.40	0.29	147.6	3.5	156.44	12.8	176	24.1	1.02	*
SG 057-cr3	Str	ma04e	10	2.2	0.2923	6.26	0.0368	1.85	0.30	227.8	4.2	255.32	16.0	288	39.5	0.99	
SG 057-cr4	Str	ma04e	14		0.6086	3.40	0.0731	1.30	0.38	453.3	5.9	481.60	16.4	347	47.5	1.04	
SG 057-cr5-r	Str	ma04e	16		0.0439	17.27	0.0073	4.47	0.26	47.4	2.1	44.42	7.7	78	10.7	1.21	*
SG 057-cr5-r?	Str	ma04e	15		0.1408	7.13	0.0209	2.25	0.32	133.2	3.0	133.78	9.5	81	11.1	1.13	*
SG 057-cr6-r	Str	ma04e	17	4.4	0.1563	19.62	0.0231	4.75	0.24	141.1	6.7	141.40	27.7	304	41.6	1.21	*
SG 057-cr7-c	Str	ma04f	6	7.1	-0.5236	14.75	0.0405	6.51	0.44	238.0	15.5	-677.10	-99.9	117	16.0	1.21	
SG 057-cr8	Str	ma04f	5		0.1045	15.44	0.0160	2.95	0.19	102.2	3.0	100.91	15.6	110	15.1	1.20	*
SG 057-cr8-c	Str	ma04f	4		0.2008	17.63	0.0284	3.92	0.22	183.2	7.2	188.25	33.2	121	16.6	1.01	*
ST-cr25-cr10	Str	jn08c	10		0.0968	6.53	0.0135	1.79	0.27	86.4	1.5	93.78	6.1	316	39.2	1.07	*
ST-25-12-c?	Str	jn08c	11		0.0845	8.39	0.0139	1.88	0.22	88.9	1.7	82.35	6.9	377	46.7	0.98	*
ST-cr25-cr15	Str	jn08c	12		0.0952	9.68	0.0136	2.73	0.28	86.9	2.4	92.37	8.9	106	13.1	1.04	*
ST-cr25-cr6	Str	jn08c	8	2.9	0.0716	10.65	0.0131	1.87	0.18	81.2	1.5	68.25	7.3	447	55.4	1.04	
ST-cr25-cr8	Str	jn08c	9		0.0911	6.50	0.0136	1.55	0.24	87.0	1.3	88.52	5.8	445	55.2	1.04	*
AvQ 054-cr6	YB	ja21g	17		-0.0097	3.75	0.0125	10.67	2.85	80.3	8.6	-9.94	-0.4	154	19.1	1.08	
AvQ 054-cr8	YB	ja21g	16	3.8	0.0588	32.14	0.0108	7.35	0.23	68.9	5.1	58.02	18.6	35	4.3	1.01	*
AvQ 055-cr1	YB	ma04f	7		-0.0307	17.71	0.0151	7.89	0.45	96.6	7.6	-31.61	-5.6	236	32.3	1.06	
AvQ 055-cr2	YB	ma04f	8	3.6	0.0733	27.97	0.0115	4.98	0.18	70.9	3.5	69.35	19.4	115	15.8	1.08	*
AvQ 055-cr5	YB	ma04f	10		1.0023	7.36	0.1014	2.42	0.33	624.4	15.1	706.36	52.0	318	43.6	1.17	
AvQ 055-cr5	YB	ma04f	11	5.4	5.9504	2.95	0.1202	4.16	1.41	694.2	28.9	1920.31	56.7	405	55.5	1.56	
AvQ 055-cr5-c	YB	ma04f	12		1.0784	19.95	0.1217	2.45	0.12	740.6	18.1	742.84	148.2	282	38.6	1.34	*
AvQ 057-cr1-c	YB	ja21g	14	8.5	0.5365	17.71	0.0647	3.65	0.21	404.3	14.7	436.11	77.2	178	22.1	1.16	*
AvQ 057-cr1-r	YB	ja21g	15		0.5867	29.52	0.0676	4.51	0.15	421.5	19.0	468.71	138.4	120	14.9	1.19	*
AvQ 057-cr2-r	YB	ja21g	13	3.2	0.0194	105.72	0.0713	3.54	0.03	430.3	15.2	18.92	20.0	264	32.7	1.18	
AvQ 057-cr6-c	YB	ja21g	11		0.1752	9.62	0.0277	2.24	0.23	176.0	3.9	163.93	15.8	200	24.8	1.00	*
AvQ 057-cr6-r	YB	ja21g	12		0.1991	8.27	0.0228	2.35	0.28	146.6	3.4	185.63	15.3	65	8.1	1.06	
AvQ 057-cr7	YB	ja21g	10	5.6	0.9900	14.38	0.0669	4.95	0.34	417.7	20.7	698.73	100.5	71	8.8	0.99	
AvQ 058-cr1	YB	jn15a	10		0.0813	11.50	0.0113	3.37	0.29	72.5	2.4	79.35	9.1	328	40.7	1.07	*
AvQ 058-cr10	YB	jn15a	7		0.0685	18.21	0.0107	3.22	0.18	69.7	2.2	68.18	12.4	78	9.7	1.19	*
AvQ 058-cr12	YB	jn15a	8		0.0856	9.72	0.0125	2.23	0.23	78.6	1.8	82.19	8.0	384	47.6	1.01	*
AvQ 058-cr14	YB	jn15a	5		0.0846	6.29	0.0127	1.49	0.24	81.6	1.2	82.95	5.2	373	46.3	1.00	*
AvQ 058-cr15	YB	jn15a	4		0.0796	7.39	0.0110	1.73	0.23	70.8	1.2	77.81	5.8	438	54.3	1.06	
AvQ 058-cr9	YB	jn15a	6	2.7	0.0531	21.37	0.0090	3.81	0.18	57.5	2.2	52.56	11.2	215	26.7	1.18	*
AvQ 142	YB	ja21f	8		0.0897	12.64	0.0113	3.77	0.30	72.1	2.7	87.19	11.0	235	29.1	1.18	

sample #				Isotope ratios					Apparent ages							
crystal #	Region	block	P%	$^{207}Pb/^{235}U$	2σ,%	$^{206}Pb/^{238}U$	2σ,%	Rho	$^{206}Pb/^{238}U$	2σ,Ma	$^{207}Pb/^{235}U$	2σ,Ma	R	S	A/In	C
AvQ 142	YB	ja21f	7 17.8	0.0940	10.16	0.0124	3.73	0.37	65.4	2.4	75.56	7.7	272	33.7	1.10	*
AvQ 142	YB	ja21f	6 3.5	0.6091	16.25	0.0768	3.53	0.22	461.2	16.3	469.60	76.3	190	23.6	1.15	*
SG 040-cr1	YB	jn15c	8 13.5	0.1574	9.20	0.0099	3.91	0.42	55.0	2.2	129.68	11.9	80	9.9	1.21	
SG 040-cr2	YB	jn15c	9 32.0	0.1888	15.62	0.0088	8.01	0.51	56.4	4.5	175.63	27.4	120	14.9	1.03	
SG 040-cr3	YB	jn15c	10 10.1	0.1696	22.47	0.0104	4.79	0.21	66.9	3.2	159.09	35.7	29	3.6	1.11	
SG 040-cr4-r	YB	jn15c	11 3.0	0.0822	26.66	0.0124	5.87	0.22	79.3	4.7	80.20	21.4	195	24.2	0.92	*
SG 040-cr5	YB	jn15c	12	0.0952	13.79	0.0122	5.82	0.42	77.3	4.5	91.20	12.6	107	13.3	1.12	*
SG 040-cr6	YB	jn15c	13 3.0	0.1122	6.48	0.0124	2.93	0.45	79.4	2.3	108.00	7.0	446	55.3	0.95	
SG 040-cr7	YB	jn15c	14 2.4	0.0860	7.21	0.0119	3.49	0.48	76.1	2.7	83.76	6.0	163	20.2	1.07	*
SG 040-cr8	YB	jn15c	15	0.0941	3.22	0.0130	1.67	0.52	83.5	1.4	91.32	2.9	326	40.4	0.99	
SG 040-cr9	YB	jn15c	16	0.1735	8.29	0.0225	3.26	0.39	143.3	4.7	162.46	13.5	450	55.8	1.23	
SG 041-cr10	YB	jn07b	7	0.0904	3.19	0.0132	1.09	0.34	84.7	0.9	87.90	2.8	320	39.7	1.01	*
SG 041-cr12	YB	jn07a	17 21.3	0.1681	6.74	0.0106	1.78	0.26	67.8	1.2	157.75	10.6	97	12.0	1.18	
SG 041-cr13	YB	jn07b	8 13.0	0.2826	7.00	0.0129	2.64	0.38	71.9	1.9	223.26	15.6	302	37.4	1.07	
SG 041-cr3	YB	jn07b	4 3.1	0.1132	2.65	0.0137	0.82	0.31	85.0	0.7	105.68	2.8	383	47.5	1.01	
SG 041-cr4	YB	jn07a	16	0.0953	3.62	0.0134	0.89	0.25	85.8	0.8	92.40	3.3	374	46.4	1.01	
SG 041-cr6	YB	jn07b	5	0.0825	3.06	0.0126	0.86	0.28	81.0	0.7	80.46	2.5	398	49.4	1.05	*
SG 041-7-r	YB	jn07a	14	0.0924	5.23	0.0144	1.45	0.28	91.7	1.3	89.45	4.7	275	34.1	1.00	*
SG 041-8-r	YB	jn07a	15 5.0	0.0413	20.46	0.0115	1.70	0.08	70.0	1.2	39.11	8.0	183	22.7	1.20	
SG 041-cr9	YB	jn07b	6	0.0849	7.32	0.0121	1.88	0.26	78.0	1.5	82.97	6.1	56	6.9	1.06	*
SG 044-cr1	YB	ma04d	14	0.0789	9.73	0.0123	2.26	0.23	78.7	1.8	77.14	7.5	270	37.0	1.08	*
SG 044-cr10	YB	ma04e	9	0.0802	4.49	0.0125	1.29	0.29	80.0	1.0	78.33	3.5	402	55.1	1.00	*
SG 044-cr2	YB	ma04d	15	0.0906	5.92	0.0130	1.71	0.29	83.2	1.4	88.03	5.2	270	37.0	1.03	*
SG 044-cr3	YB	ma04d	16	0.0733	26.79	0.0120	4.85	0.18	76.8	3.7	71.96	19.3	135	18.5	1.19	*
SG 044-cr4	YB	ma04d	17	0.0733	6.63	0.0121	1.63	0.25	77.8	1.3	72.28	4.8	235	32.2	1.11	*
SG 044-cr5	YB	ma04e	4	0.0883	16.83	0.0110	4.08	0.24	70.5	2.9	85.88	14.5	61	8.4	1.06	*
SG 044-cr6	YB	ma04e	5	0.0730	7.74	0.0110	2.02	0.26	70.2	1.4	71.57	5.5	57	7.8	1.10	*
SG 044-cr7	YB	ma04e	6	0.0808	8.51	0.0124	1.97	0.23	79.7	1.6	79.32	6.8	149	20.4	1.03	*
SG 044-cr8	YB	ma04e	7	0.0839	4.86	0.0123	1.49	0.31	78.5	1.2	81.83	4.0	208	28.5	1.04	*
SG 044-cr9-r	YB	ma04e	8	0.0883	4.00	0.0125	1.42	0.35	80.0	1.1	85.93	3.4	328	44.9	1.00	
SG 063-cr10	YB	jn12a	17	0.1557	7.97	0.0194	4.00	0.50	123.6	4.9	146.91	11.7	100	13.4	0.90	
SG 063-cr1	YB	jn12a	4	0.0723	20.95	0.0107	5.28	0.25	68.4	3.6	70.83	14.8	118	15.8	1.20	*
SG 063-cr2-c	YB	jn12a	6	0.8584	30.25	0.0344	16.61	0.55	217.9	36.2	629.24	190.4	23	3.1	1.18	
SG 063-cr2-r	YB	jn12a	5	0.1014	13.98	0.0112	4.76	0.34	71.6	3.4	98.07	13.7	80	10.7	1.17	
SG 063-cr3	YB	jn12a	7	0.6738	11.49	0.0866	3.59	0.31	537.0	19.3	524.18	60.2	110	14.7	1.04	*
SG 063-cr4	YB	jn12a	8	0.2692	16.54	0.0330	4.24	0.26	209.3	8.9	242.04	40.0	70	9.4	1.15	*
SG 063-cr5	YB	jn12a	9 17.7	0.0668	422.57	0.0261	5.95	0.01	166.4	9.9	65.65	277.4	200	26.8	0.99	*
SG 063-cr6-c	YB	jn12a	11	0.5356	18.40	0.0656	4.64	0.25	410.9	19.1	436.67	80.4	67	9.0	1.09	*
SG 063-cr6-r	YB	jn12a	10	0.4998	29.24	0.0553	7.76	0.27	346.9	26.9	411.54	120.3	44	5.9	1.25	*

sample #					Isotope ratios					Apparent ages							
crystal #	Region	block		P%	$^{207}Pb/^{235}U$	2σ,%	$^{206}Pb/^{238}U$	2σ,%	Rho	$^{206}Pb/^{238}U$	2σ,Ma	$^{207}Pb/^{235}U$	2σ,Ma	R	S	A/In	C
SG 063-cr7	YB	jn12a	12		0.5513	17.84	0.0808	4.38	0.25	498.8	21.9	444.19	79.2	50	6.7	1.03	*
SG 063-cr8-c	YB	jn12a	14		0.6075	4.73	0.0745	3.04	0.64	463.4	14.1	481.95	22.8	190	25.5	1.09	*
SG 063-cr8-r	YB	jn12a	13		0.3199	3.64	0.0416	2.55	0.70	262.6	6.7	281.85	10.3	325	43.6	1.09	
SG 063-cr9-c	YB	jn12a	15		0.3199	5.88	0.0417	2.94	0.50	264.1	7.8	282.83	16.6	245	32.8	1.06	*
SG 063-cr9-r	YB	jn12a	16		0.2837	4.78	0.0316	2.73	0.57	203.5	5.5	257.01	12.3	431	57.8	1.18	
SG 066-cr10	YB	jn07b	13		0.2877	7.09	0.0340	2.68	0.38	216.3	5.8	257.87	18.3	188	23.3	1.01	
SG 066-cr11	YB	jn07b	14		0.2256	4.80	0.0257	1.77	0.37	163.8	2.9	206.57	9.9	427	52.9	1.08	
SG 066-12-c	YB	jn07b	15		0.1734	6.76	0.0251	2.34	0.35	158.8	3.7	161.65	10.9	136	16.9	1.14	*
SG 066-12-r	YB	jn07b	16		0.1377	4.11	0.0196	1.16	0.28	125.2	1.4	131.19	5.4	227	28.1	1.01	*
SG 066-cr13	YB	jn07b	17		0.1504	5.48	0.0203	1.62	0.30	129.6	2.1	142.27	7.8	404	50.1	0.99	
SG 066-cr6	YB	jn07b	9		0.1123	8.68	0.0157	4.13	0.48	100.3	4.1	108.21	9.4	199	24.7	1.17	*
SG 066-7-c	YB	jn07b	10	6.9	0.2248	6.16	0.0174	2.42	0.39	111.3	2.7	205.86	12.7	142	17.6	1.08	
SG 066-8-r	YB	jn07b	11	3.6	0.1376	12.37	0.0220	4.44	0.36	140.3	6.2	130.93	16.2	101	12.5	1.02	*
SG 066-cr9	YB	jn07b	12		0.2573	5.34	0.0258	1.92	0.36	167.0	3.2	235.86	12.6	336	41.7	1.01	
SG 078-cr1	YB	jn08b	9	6.7	0.1720	20.50	0.0228	4.01	0.20	135.9	5.5	151.08	31.0	95	11.8	1.03	*
SG 078-12-c	YB	jn08b	16	2.0	0.3114	5.94	0.0368	2.87	0.48	228.4	6.5	270.49	16.1	80	9.9	1.05	
SG 078-12-r	YB	jn08b	17		0.4193	4.03	0.0433	1.98	0.49	273.5	5.4	355.58	14.3	111	13.8	1.04	
SG 078-cr13	YB	jn08b	14	34.2	2.4211	5.85	0.0460	3.48	0.59	192.1	6.7	967.31	56.6	77	9.5	1.05	
SG 078-cr14	YB	jn08b	13		0.2122	9.82	0.0306	2.86	0.29	194.3	5.6	195.40	19.2	100	12.4	1.09	*
SG 078-3-c	YB	jn08b	10		0.1030	8.17	0.0154	2.91	0.36	98.7	2.9	99.58	8.1	122	15.1	1.21	*
SG 078-cr7	YB	jn08b	11	28.9	2.3462	1.68	0.0599	1.78	1.06	268.9	4.8	996.53	16.8	378	46.9	0.99	
SG 078-cr8	YB	jn08b	12	3.3	0.6287	4.48	0.0460	2.52	0.56	280.6	7.1	482.05	21.6	270	33.5	1.09	
SG 078-cr9	YB	jn08b	15	68.0	5.4543	4.72	0.0656	4.58	0.97	134.1	6.1	1026.41	48.4	153	19.0	1.13	
SG 079-cr1	YB	jn08c	14		0.3439	3.72	0.0466	1.13	0.30	293.4	3.3	300.09	11.2	307	38.1	1.09	*
SG 079-2-c	YB	jn08c	13	4.5	0.1170	6.96	0.0123	1.89	0.27	75.5	1.4	107.62	7.5	287	35.6	1.00	
SG 079-cr5	YB	jn08c	15	3.1	0.0966	7.36	0.0121	2.13	0.29	75.1	1.6	90.79	6.7	285	35.3	1.01	
SG 079-cr5	YB	jn08c	16		0.0990	9.75	0.0123	2.61	0.27	78.5	2.0	95.88	9.3	210	26.0	1.01	
SG 079-cr7	YB	jn08c	17	2.1	0.0725	10.65	0.0123	2.31	0.22	77.0	1.8	69.59	7.4	160	19.8	1.00	*
SG 090-cr1	YB	jn15b	16	4.2	0.1217	20.07	0.0148	6.57	0.33	90.9	6.0	111.94	22.5	118	14.6	1.40	*
SG 090-cr2	YB	jn15b	17		0.0576	49.54	0.0137	4.64	0.09	87.7	4.1	56.90	28.2	465	57.7	1.10	*
SG 090-cr6	YB	jn15b	4	2.6	0.2781	16.18	0.0357	3.76	0.23	220.3	8.3	243.46	39.4	166	20.6	1.20	*
SG 090-cr7	YB	jn15b	5		0.6603	15.45	0.0744	3.75	0.24	462.4	17.3	514.78	79.5	117	14.5	1.08	*
SG 090-cr8	YB	jn15c	6		0.2260	8.26	0.0304	2.27	0.27	193.2	4.4	206.87	17.1	216	26.6	1.02	*
SG 090-cr9	YB	jn15c	7		0.1250	15.87	0.0182	3.68	0.23	116.4	4.3	119.56	19.0	150	18.6	1.16	*
SG 102d-cr1	YB	jn08a	4		0.3051	7.57	0.0401	1.99	0.26	253.5	5.0	270.41	20.5	350	43.4	0.98	*
SG 102d-cr10	YB	jn08a	10	1.9	0.0713	11.25	0.0110	2.54	0.23	69.0	1.8	68.67	7.7	301	37.3	1.08	*
SG 102d-cr11	YB	jn08a	11	4.2	0.2458	3.83	0.0247	1.41	0.37	150.5	2.1	214.66	8.2	130	16.1	1.13	
SG 102d-cr12	YB	jn08a	12	2.7	0.0904	8.13	0.0125	2.30	0.28	78.0	1.8	85.56	7.0	285	35.3	0.98	*
SG 102d-cr3	YB	jn08a	5		0.0530	17.76	0.0094	2.84	0.16	60.5	1.7	52.44	9.3	232	28.8	1.28	*

sample # / crystal #	Region	block		P%	Isotope ratios $^{207}Pb/^{235}U$	2σ,%	$^{206}Pb/^{238}U$	2σ,%	Rho	Apparent ages $^{206}Pb/^{238}U$	2σ,Ma	$^{207}Pb/^{235}U$	2σ,Ma	R	S	A/In	C
SG 102d-cr5	YB	jn08a	7		0.0875	4.68	0.0128	1.40	0.30	81.8	1.1	85.17	4.0	292	36.2	1.00	*
SG 102d-cr7	YB	jn08a	8		0.0892	7.39	0.0122	2.21	0.30	78.1	1.7	86.74	6.4	300	37.2	0.97	
SG 102d-cr8	YB	jn08a	9		0.2560	4.54	0.0353	1.41	0.31	223.7	3.1	231.42	10.5	427	52.9	1.03	*
SG 103-cr10	YB	jn08d	10		0.0933	5.80	0.0126	2.72	0.47	81.0	2.2	90.56	5.3	377	46.7	1.01	
SG 103-cr11	YB	jn08d	11		0.0673	14.35	0.0127	3.39	0.24	81.3	2.8	66.13	9.5	362	44.9	1.08	
SG 103-cr2-c	YB	jn08d	4		0.0608	22.19	0.0115	3.61	0.16	74.0	2.7	59.90	13.3	401	49.7	1.14	*
SG 103-cr3	YB	jn08d	5		0.0799	10.30	0.0118	3.46	0.34	75.7	2.6	78.03	8.0	403	50.0	1.05	*
SG 103-cr6	YB	jn08d	6		0.0805	13.79	0.0113	3.51	0.25	72.3	2.5	78.65	10.8	363	45.0	1.06	*
SG 103-cr7	YB	jn08d	7		0.0832	13.15	0.0122	3.62	0.28	78.1	2.8	81.10	10.7	374	46.4	1.07	*
SG 103-cr8	YB	jn08d	8	3.4	0.0657	16.01	0.0126	3.71	0.23	78.0	2.9	62.50	10.0	316	39.2	1.03	
SG 103-cr9	YB	jn08d	9		0.0755	10.95	0.0116	3.26	0.30	74.2	2.4	73.91	8.1	369	45.8	1.15	*

Additional sphene analyses

sample # / crystal #	Region	block		P%	Isotope ratios $^{207}Pb/^{235}U$	2σ,%	$^{206}Pb/^{238}U$	2σ,%	Rho	Apparent ages $^{206}Pb/^{238}U$	2σ,Ma	$^{207}Pb/^{235}U$	R	S	A/In	C
SG 063-3-sphene	YB	jn08a	15	49.4	1.8025	15.52	0.0261	5.58	0.36	84.7	4.7	658.03	187	23.2	0.83	
ST-25-1-sphene	Str	jn08c	4	7.7	0.1743	7.50	0.0128	2.75	0.37	75.6	2.1	151.52	458	56.8	1.01	
ST-25-2-sphene	Str	jn08c	5	23.8	0.2718	21.75	0.0135	7.03	0.32	65.8	4.6	191.21	251	31.1	1.09	
ST-25-4-sphene	Str	jn08c	6	11.4	0.5314	12.58	0.0164	4.10	0.33	93.3	3.8	391.92	456	56.5	1.01	
ST-25-5-sphene	Str	jn08c	7	17.4	0.2195	14.23	0.0143	3.22	0.23	75.9	2.4	169.18	412	51.1	1.00	
SG 068-sphene-cr3	EB	ma04f	15	43.6	0.7555	12.14	0.0154	5.96	0.49	55.7	3.3	360.38	65	8.9	1.03	
SG 068sphene-cr5	EB	ma04f	16	11.2	0.7060	8.19	0.0137	4.61	0.56	87.9	4.1	542.40	210	28.8	1.02	

Appendix 3. U-Pb age results by sample

U-Pb age results for Eastern Srednogorie zone are presented below, starting with the southernmost Strandzha region through the intermediate Yambol-Burgas and North Burgas regions and finally for the northernmost East Balkan region. Location of samples and regions is shown on ***Figure 3-1***. For each sample the data are presented as a series of graphs, constructed with the ISOPLOT add-in for Excel (Ludwig, K. R., 2003, *Berkeley Geochronology Center Special Publication* 4). We gave preference to ID-TIMS ages over LA-ICPMS data, where sufficient numbers of zircon grains were analyzed by both methods. Depending on sample population and number of studied grains, concordia ages were preferred rather than upper - or lower intercept ages or weighted averages of $^{206}Pb/^{238}U$ ages. Intercept ages and weighted $^{206}Pb/^{238}U$ ages were filtered based on the number of grains and MSWD values.

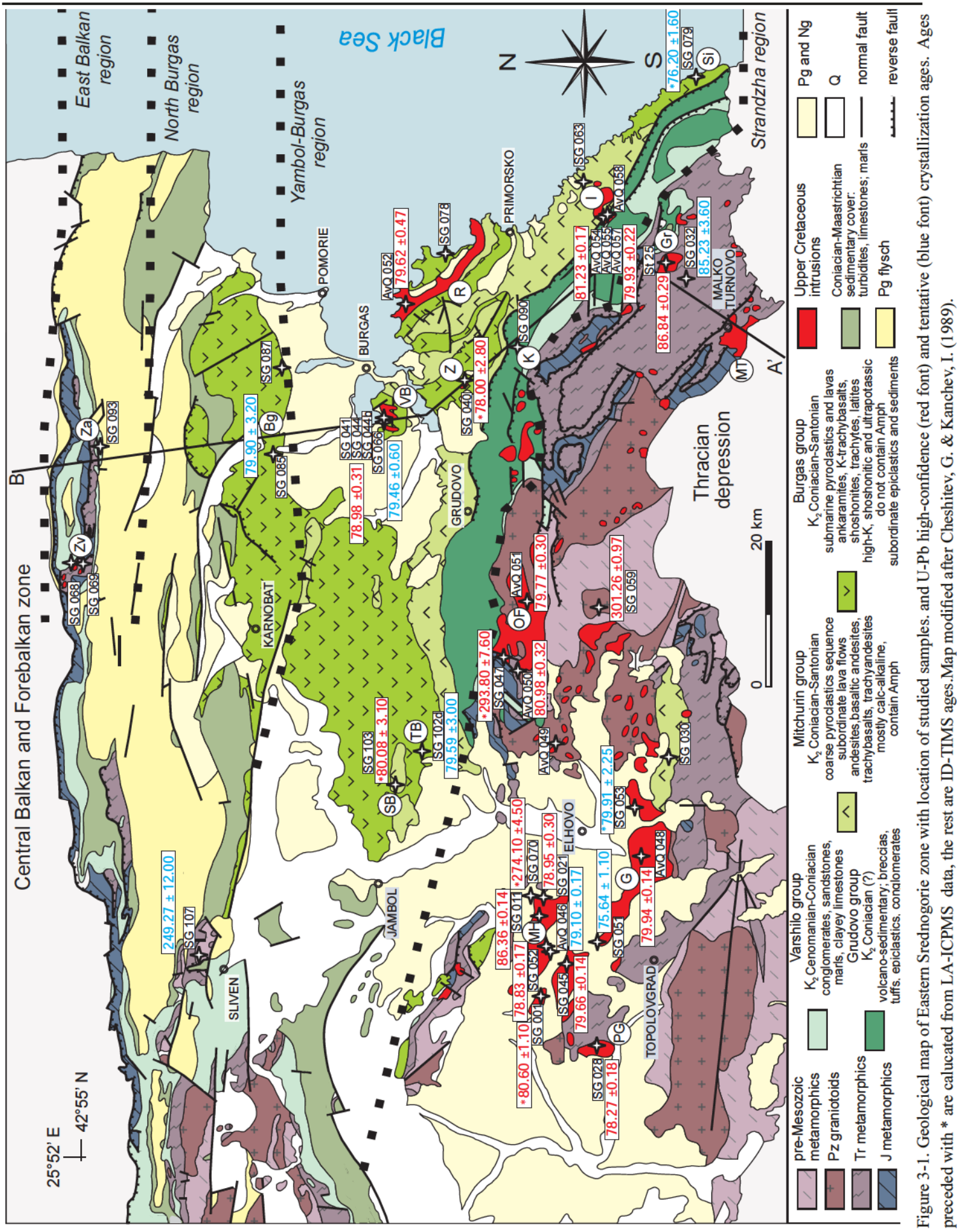

Figure 3-1. Geological map of Eastern Srednogorie zone with location of studied samples. and U-Pb high-confidence (red font) and tentative (blue font) crystallization ages. Ages preceded with * are calucated from LA-ICPMS data, the rest are ID-TIMS ages.Map modified after Cheshitev, G. & Kanchev, I. (1989).

1.1. STRANDZHA REGION

AvQ 046 – Gabbro, Monastery Heights

The sample is taken close to the village of Goljam Manastir, and is representative for the basic intrusive phase of Monastery Heights pluton. Four zircons air-abraded for 2 hours and analyzed by ID-TIMS plot on the concordia band between 79 and 105 Ma, without overlapping, and with increasing $^{207}Pb/^{235}U$ errors from the youngest to the oldest (***Figure 3-2***a). The youngest zircon has the smallest errors, and its concordia age of 79.10 ± 0.17 Ma most likely represents the crystallization age of the sample (***Figure 3-2***b). The remaining three zircons were probably entrapped during assimilation of host rocks from the gabbroic magma. It remains unclear whether the 92.4 Ma and especially the 104.4 Ma $^{206}Pb/^{238}U$ ages represent magmatic events, or the U-Pb systematic of the grains had been disturbed by the presence of older component or Pb loss (large $^{207}Pb/^{235}U$ errors prevent further interpretation). LA-ICPMS results on 5 zircons generally agree with the ID-TIMS age range, except for one grain with considerably older age (***Figure 3-3***).

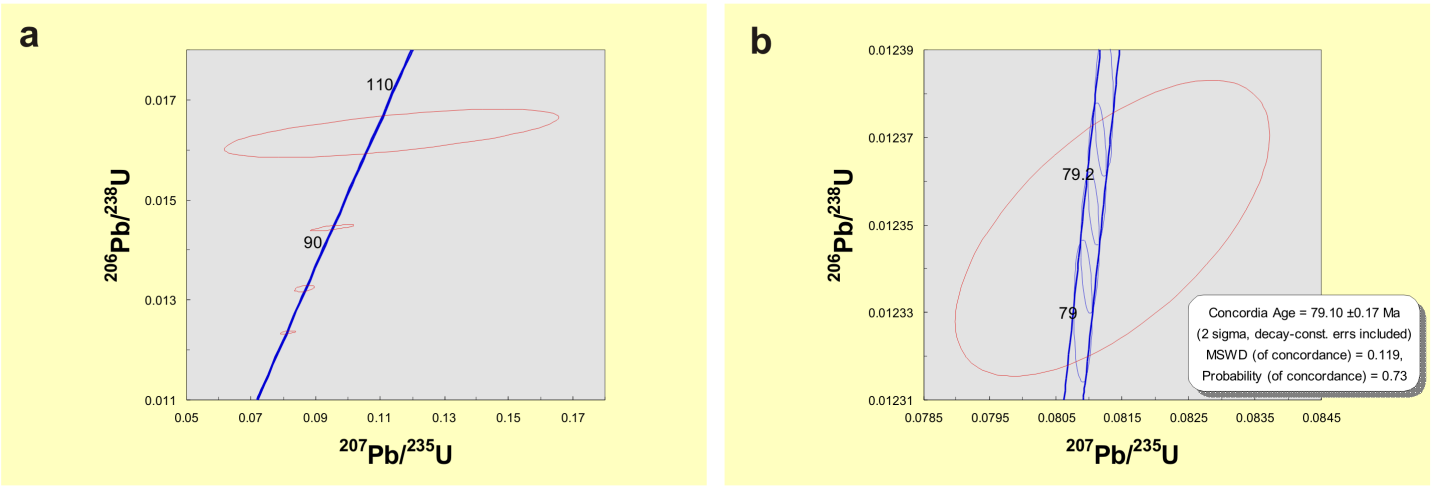

Figure 3-2. Results from single zircon U-Pb ID-TIMS dating for sample AvQ 046

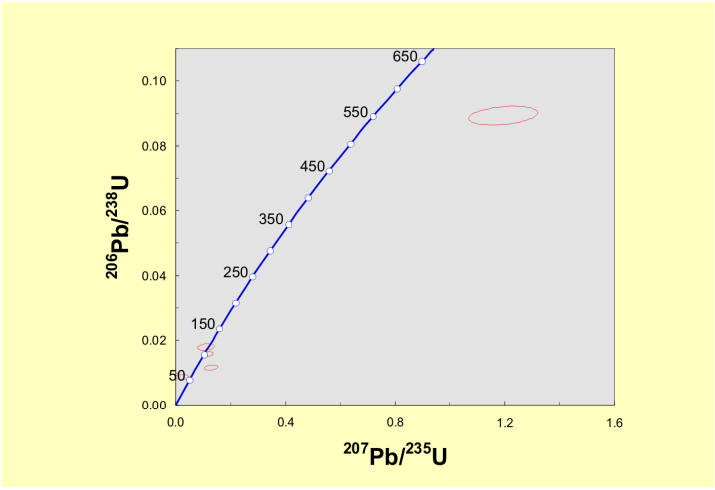

Figure 3-3. Results from single zircon U-Pb LA-ICPMS dating for sample AvQ 046

AvQ 048 – Granodiorite, Granitovo

Granitovo pluton is the largest granitic intrusion in the Strandzha region and the whole Eastern Srednogorie. Fifteen zircons were analyzed by ID-TIMS. Five of them show evidence for incorporation of older component and lie to the right of the concordia band with $^{206}Pb/^{238}U$ ages ranging from 100 to 130 Ma (***Figure 3-4***a). Four air abraded zircons yield two possible ages, one at 78 Ma and another one at 80 Ma with unclear relations (***Figure 3-4***b). Six chemically abraded zircons plot closer to the older, ~80 Ma age. The chemically

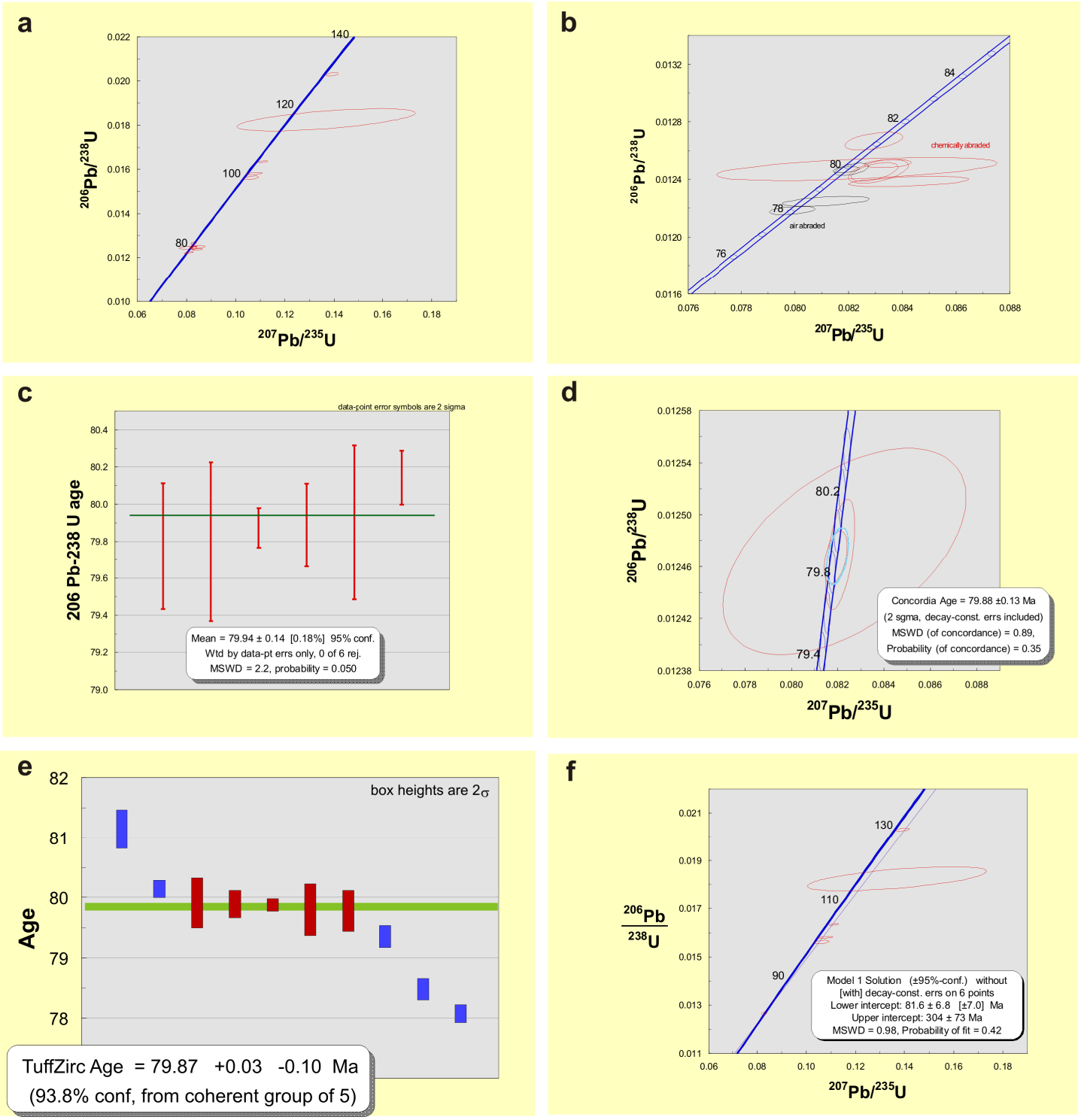

Figure 3-4. Results from single zircon U-Pb ID-TIMS dating for sample AvQ 048

abraded zircons show some discordance signaling insufficient annealing/leaching steps; the chemical abrasion procedure was being established establishing at the time. Nevertheless, they all have consistent $^{206}Pb/^{238}U$ ages coinciding with the ages of the two older air abraded zircons and therefore we consider the weighted average 79.94 ± 0.14 Ma $^{206}Pb/^{238}U$ age of 6 zircons to represent the crystallization age of the granite (***Figure 3-4***c). Similar age and error are obtained if we use the concordia age of three zircons (***Figure 3-4***d), or the zircon age extractor algorithm for all Late Cretaceous zircons (***Figure 3-4***e). The constructed discordia chord from the older zircons and either of the Late Cretaceous zircons indicate a Carboniferous/Permian inherited component in those zircon grains (***Figure 3-4***f). Most of the fifteen grains, analyzed by LA ICPMS form a coherent group with a weighed average $^{206}Pb/^{238}U$ age of 79.8 ± 2.4 Ma (***Figure 3-5***a). The larger spread of the LA-ICPMS individual ages compared to the TIMS data is reflected in the higher MSWD value of 7.9. The relative

probability plot of the LA-ICPMS zircon data and the applied unmixing of ages show a prominent peak at 80.35 ± 0.71 Ma (***Figure 3-5***b). The zircon age extractor algorithm gives a slightly younger, but nevertheless overlapping within the error age (***Figure 3-5***c). The oldest analyzed zircon core has a Permian age.

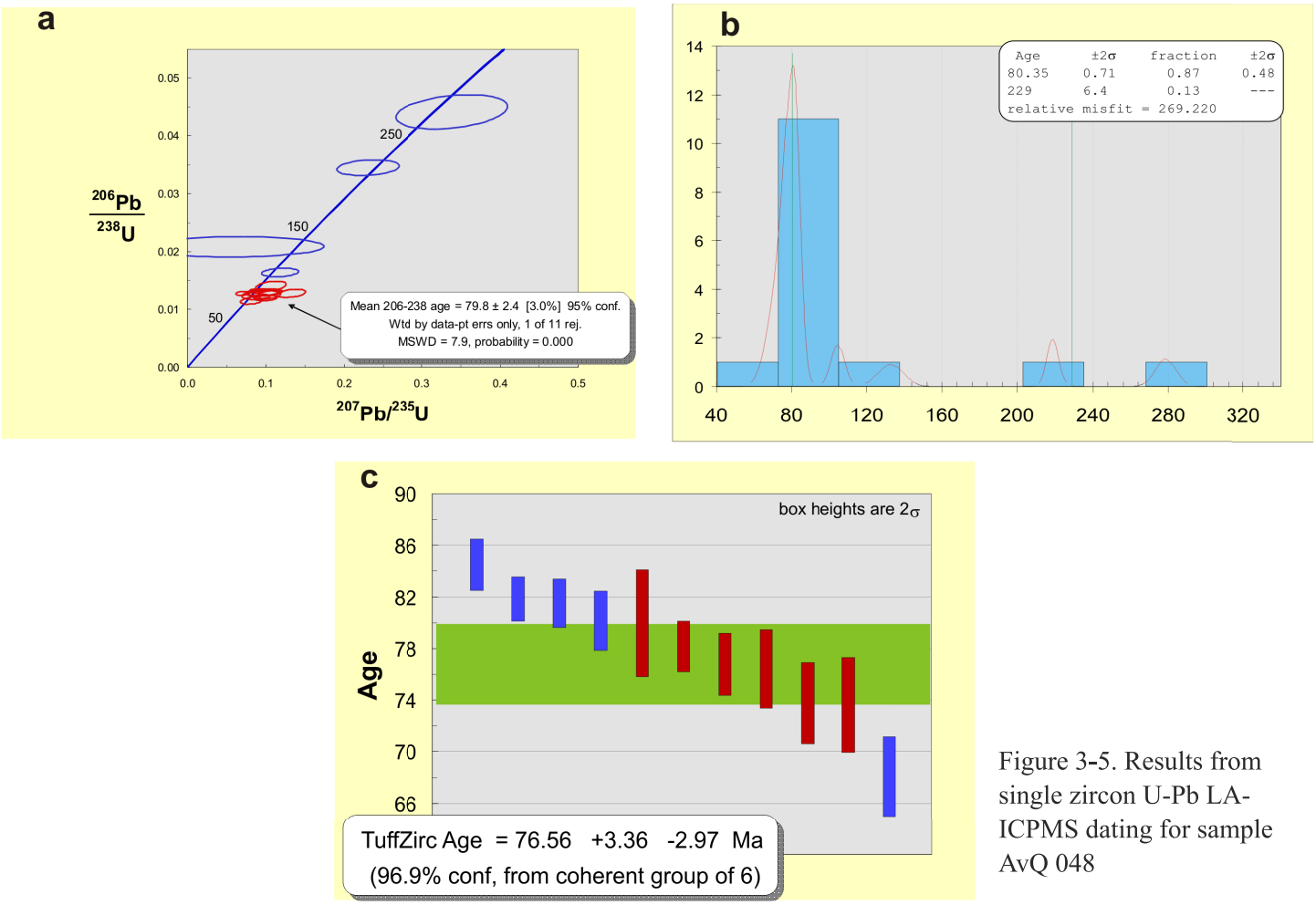

Figure 3-5. Results from single zircon U-Pb LA-ICPMS dating for sample AvQ 048

AvQ 050 – Amph Gabbro, Oman-Fakya

Three zircon grains were air-abraded for 7 hours and analyzed by ID-TIMS. The zircons still show minimal evidence of Pb loss but nevertheless yield a concordant age of 80.98 ± 0.32 Ma at the 95% confidence level (***Figure 3-6***), which we consider to be the crystallization age of the rock. The weighted average $^{206}Pb/^{238}U$ age is 80.91 ± 0.09 Ma, which equivalent within errors to the Concordia age.

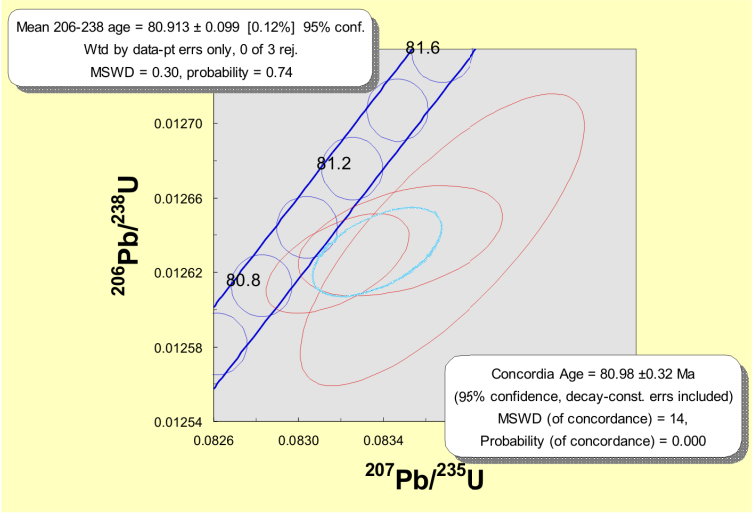

Figure 3-6. Results from single zircon U-Pb ID-TIMS dating for sample AvQ 050

Nine grains dated by LA-ICPMS all show Late Cretaceous ages (***Figure 3-7***a). Although individual measurement errors are high, the probability plot indicates a peak at ca. 80 Ma (***Figure 3-7***b) and the zircon age extraction algorithm also yields an age consistent with the TIMS data, but with larger errors (***Figure 3-7***c).

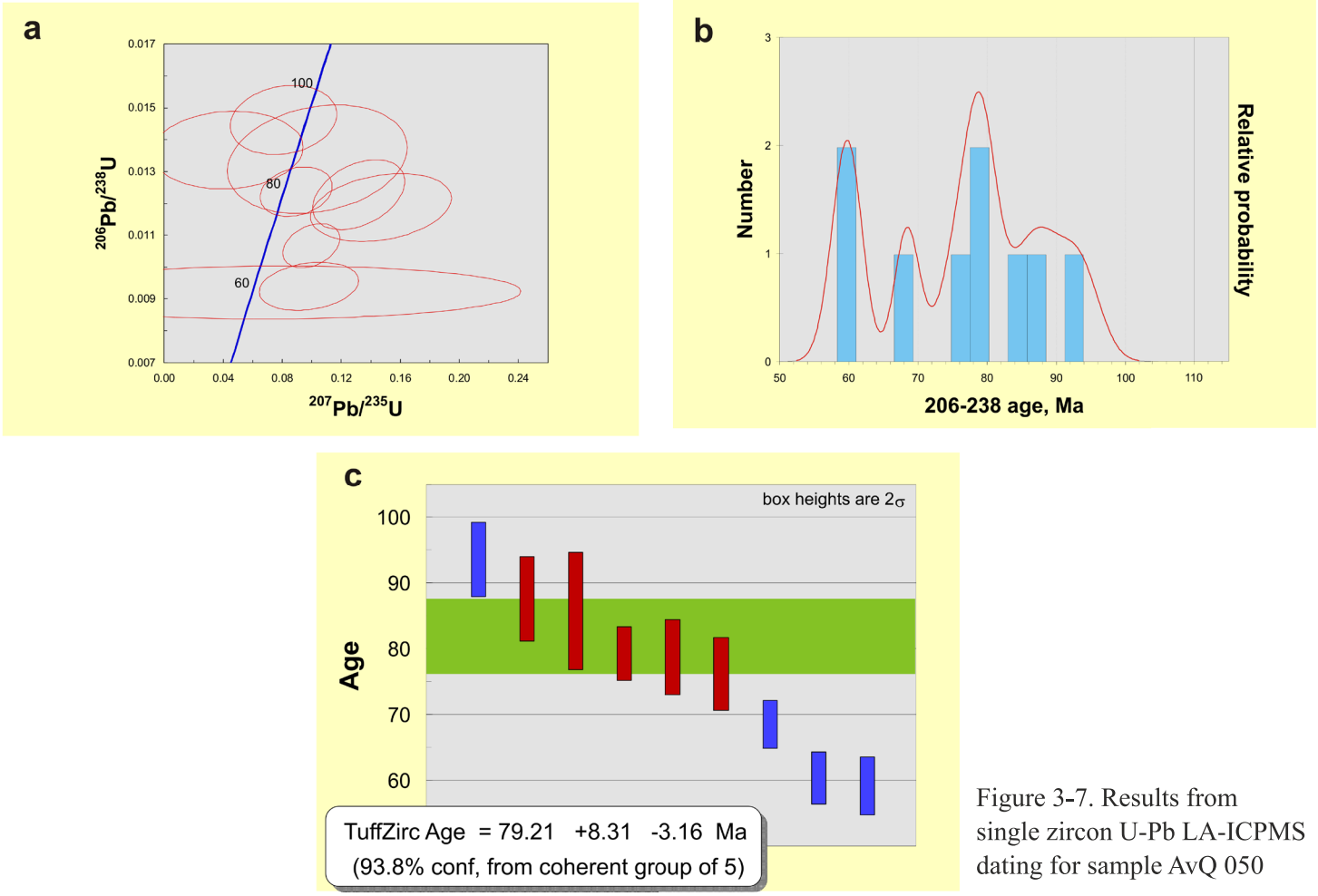

Figure 3-7. Results from single zircon U-Pb LA-ICPMS dating for sample AvQ 050

AvQ 051 – Qz leucosyenite, Oman-Fakya

Six zircons were air-abraded for 7 hours and analyzed by ID-TIMS. Five zircons form a discordia line with a lower intercept at 82.2 ± 3.9 Ma and upper intercept at 332.8 ± 9.0 Ma, MSWD = 0.42 (***Figure 3-8***a). Three grains are concordant at 79.77 ± 0.30 Ma at the 95% confidence level (***Figure 3-8***b). The two zircons with larger errors and slightly lower $^{206}Pb/^{238}U$ age on the diagram may have experienced minor Pb loss.

Additional six grains were dated by LA-ICPMS (***Figure 3-9***a). Three zircons yield a concordant age of 81.8 ± 3.5 Ma at the 95% confidence level, which overlaps with the ID-TIMS age. The weighted average $^{206}Pb/^{238}U$ age and the zircon extraction age are also similar (***Figure 3-9***a, c). Two iherited grains have Carboniferous/Permian ages (***Figure 3-9***a, c, d).

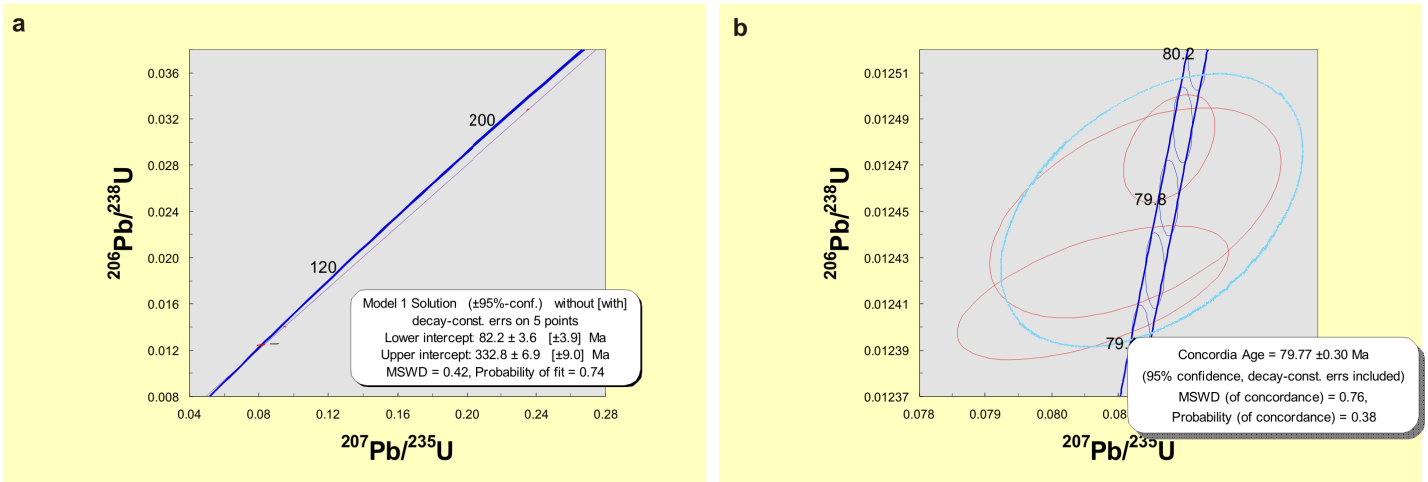

Figure 3-8. Results from single zircon U-Pb ID-TIMS dating for sample AvQ 051

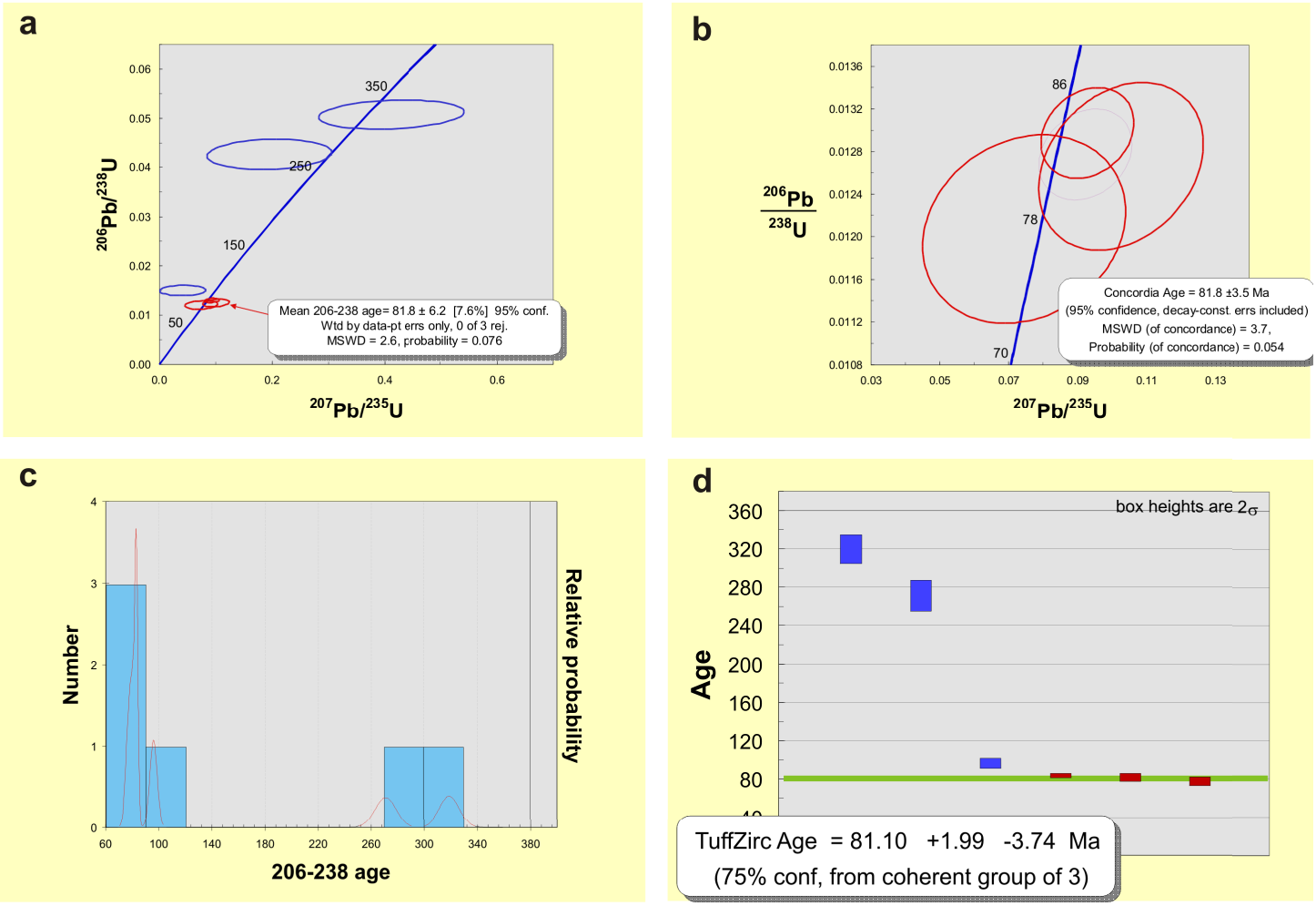

Figure 3-9. Results from single zircon U-Pb LA-ICPMS dating for sample AvQ 051

SG 001 – Granodiorite, Monastery Heights

The sample is collected near the village of Ovtchi Kladenetz and represents the granodioritic phase of the Monastery Heights intrusion. Results for ten zircons dated by LA-ICPMS are presented on ***Figure 3-10***. The concordia age formed by three grains at 80.6 ± 1.1 Ma, 2 sigma errors (***Figure 3-10***b) is considered as the best estimate for the crystallization age of the granodiorite. Discernibly older inherited components are not detected in this sample. One grain shows younger age of 66 Ma, which is probably a result of overcorrection for common Pb.

SG 011 – Diorite, Monastery Heights

This sample, collected between the villages of Goljam Manastir and Krumovo is representative of the diorite phase of the Monastery Heights pluton. Five zircon grains, air abraded for 6 hours, were analyzed by ID-TIMS and they all yield similar ages (***Figure 3-11***a). Three of the zircons yield a well defined concordia age of 86.31 ± 0.14 Ma, which is considered as the crystallization age of the rock. The remaining two grains have slightly younger ages with larger errors. Their anomalously low $^{206}Pb^{*}/^{204}Pb$ ratios of 37 and 47 which indicates a large proportion of common Pb either from within the grain, or from contamination.

LA-ICPMS age results for thirteen zircons from this sample are presented on ***Figure 3-12***a. The mean $^{206}Pb/^{238}U$ age for the whole population is 85.3 ± 3.2 Ma at the 95% confidence level and the MSWD is high (26). The relative probability is highest at 87 Ma (***Figure 3-12***c), and this is the age resulting from the zircon tuff age algorithm as well (***Figure 3-12***d). Five grains are concordant within their errors at 87.8 ± 1.0 Ma (***Figure 3-12***b), an age similar to the well defined ID-TIMS concordia age.

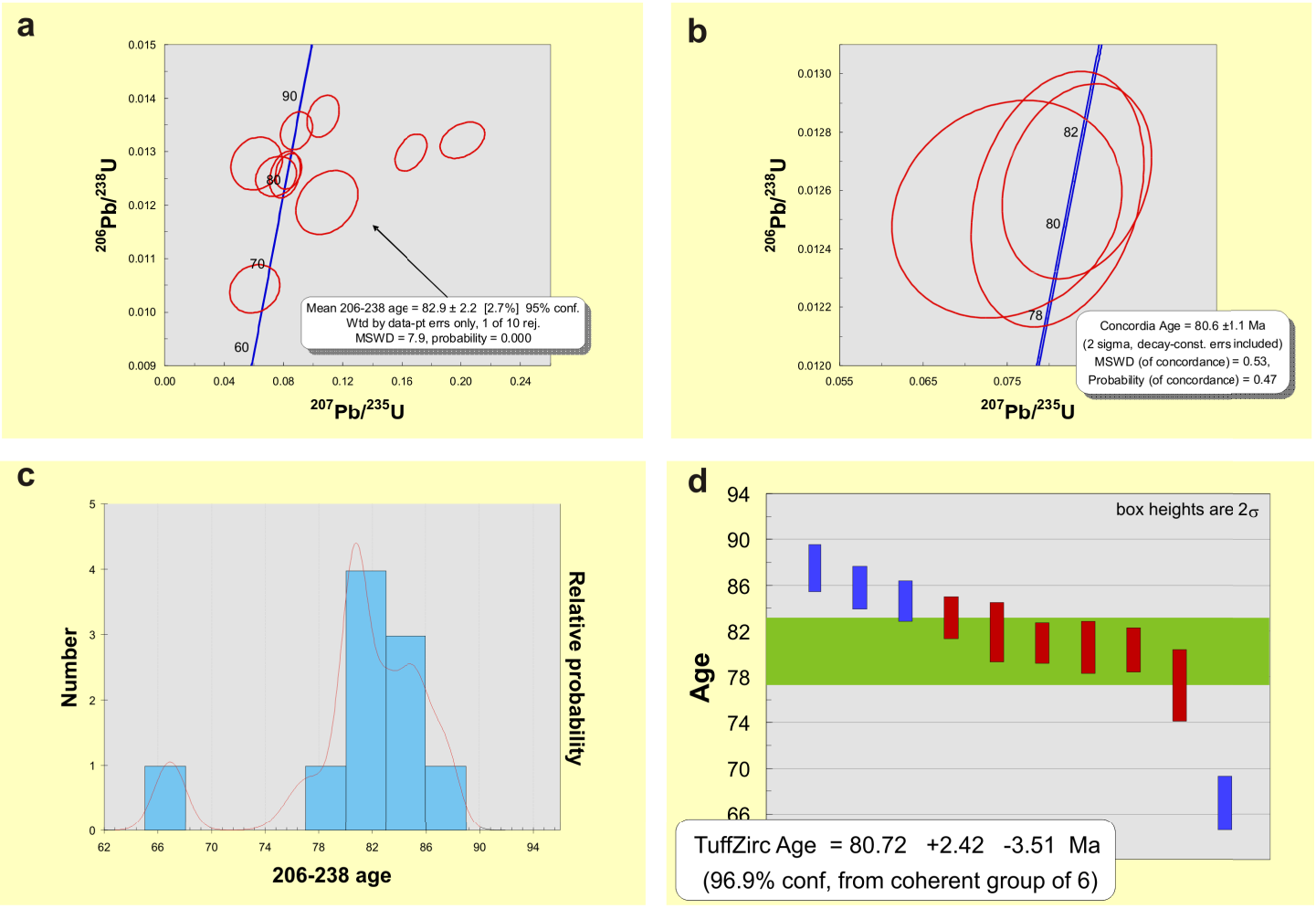

Figure 3-10. Results from single zircon U-Pb LA-ICPMS dating for sample SG 001

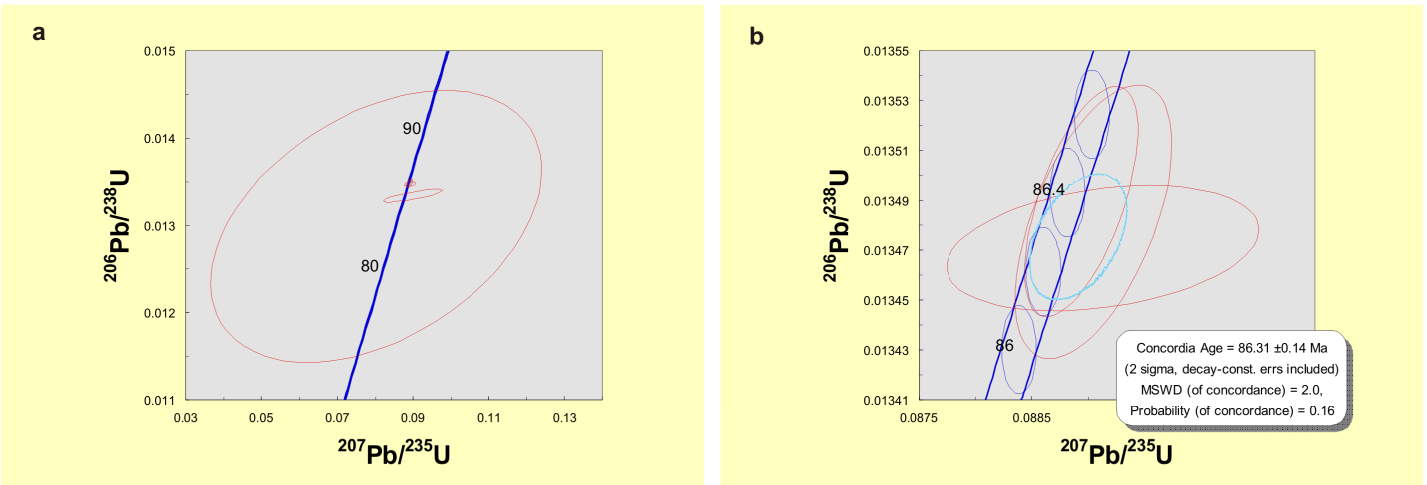

Figure 3-11. Results from single zircon U-Pb ID-TIMS dating for sample SG 011

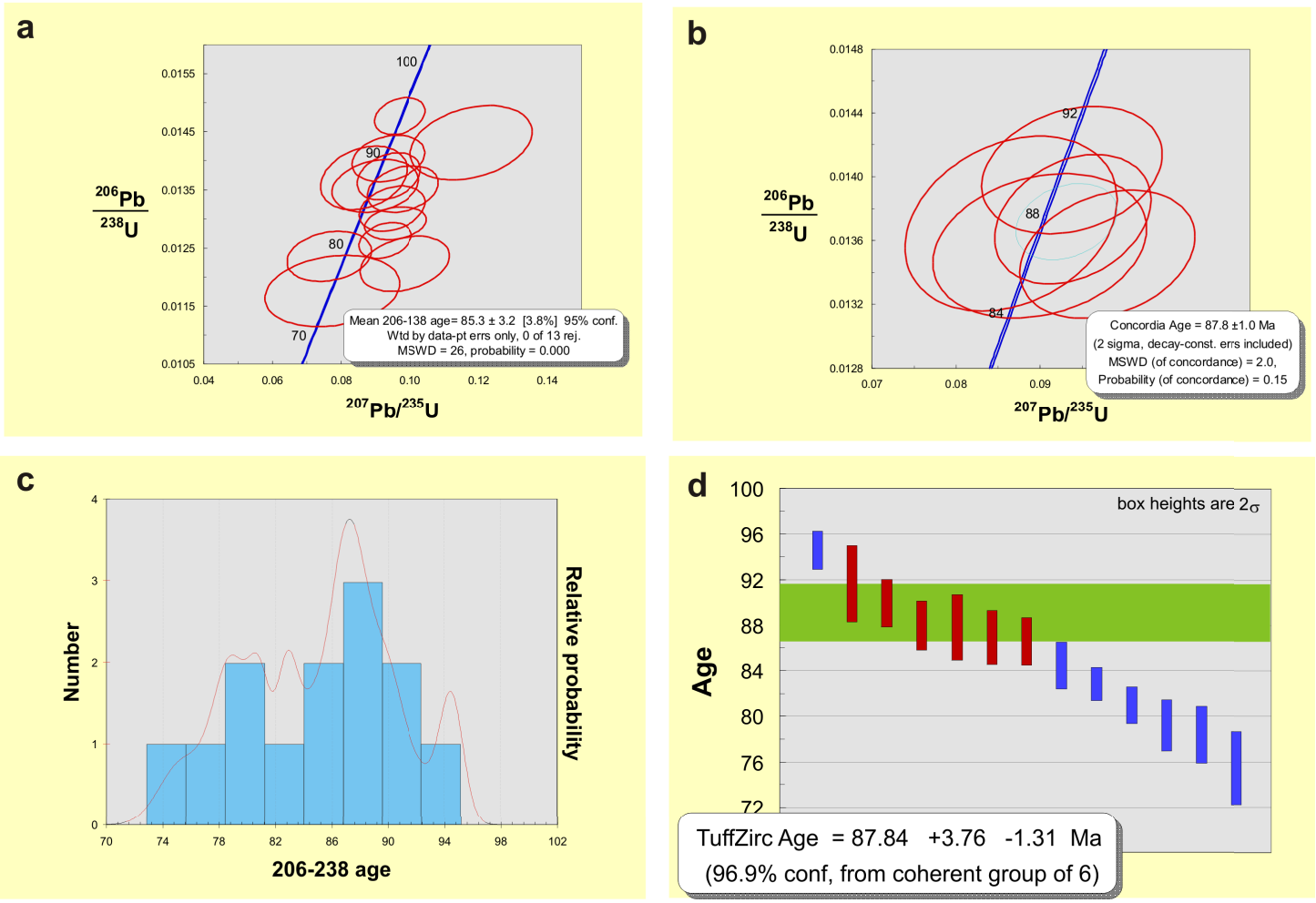

Figure 3-12. Results from single zircon U-Pb LA-ICPMS dating for sample SG 011

SG 021 – Basaltic andesite dike, Monastery Heights

The dike crosscuts a basic medium-grained intrusion near the Drama village, at the eastern part of Monastery Heights pluton. Four zircons were analyzed by ID-TIMS (***Figure 3-13***a). Three zircons are concordant within their errors and yield a 78.95 ± 0.30 Ma concordia age at the 95% confidence limit (***Figure 3-13***b). Two of the concordant zircons have low $^{206}Pb^{*}/^{204}Pb$ ratios of 46 and 48 and the zircon with highest $^{206}Pb^{*}/^{204}Pb$ ratios has the oldest $^{206}Pb/^{238}U$ age within this group. One grain has older discordant ages and together with the remaining zircons forms a discordia line with an upper intercept age of 546 ± 35 Ma,

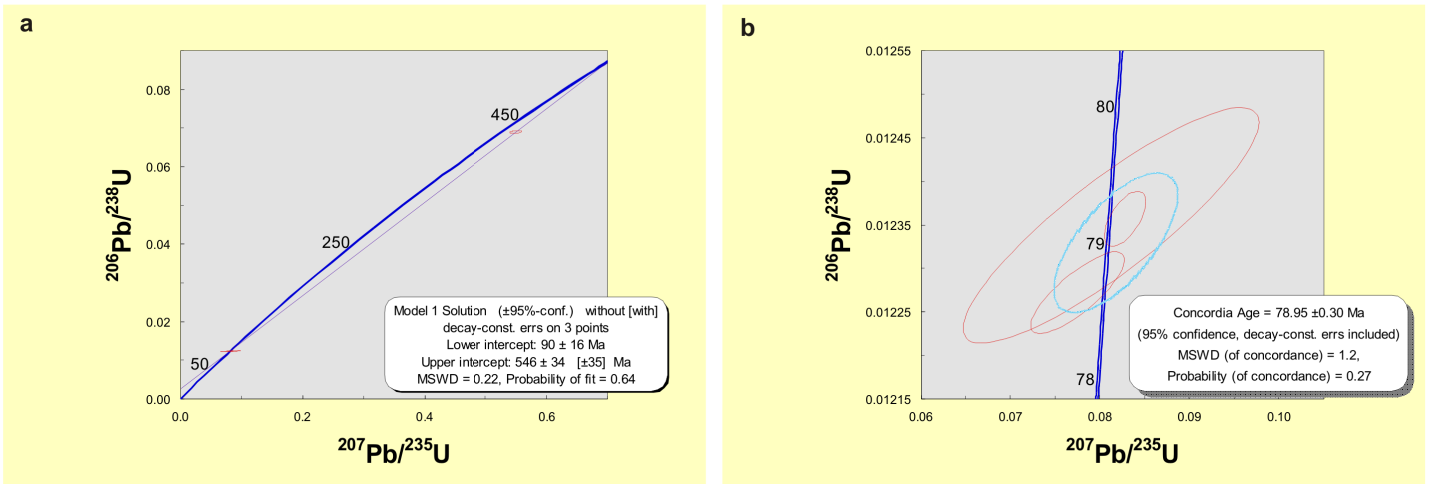

Figure 3-13. Results from single zircon U-Pb ID-TIMS dating for sample SG 021

indicating a possible Neoproterozoic/Cambrian inheritance. Five zircons were dated by LA-ICPMS, which proved insufficient for a confident age determination (***Figure 3-14***a, b).

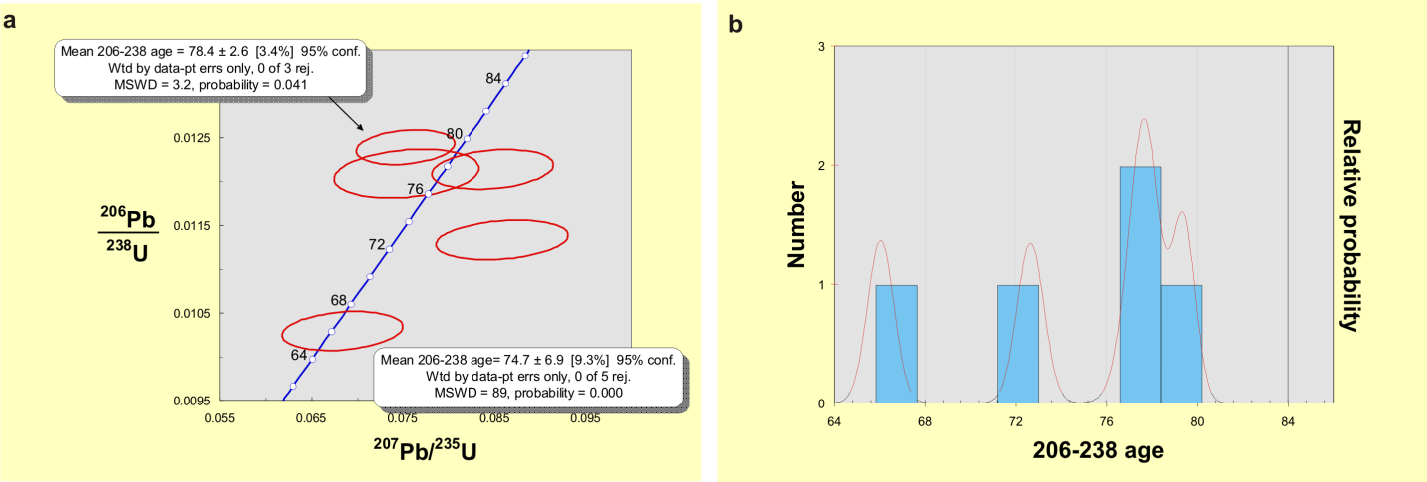

Figure 3-14. Results from single zircon U-Pb LA-ICPMS dating for sample SG 021

SG 028 – Granodiorite, Polski Gradetz pluton

Seven zircon grains were air abraded for 3 hours and dated by U-Pb ID-TIMS. On a concordia plot, four grains are situated around 78 Ma and three grains have older $^{206}Pb/^{238}U$ ages from 80 to 90 Ma (***Figure 3-15***a). When regressed together, all zircons form a chord with MSWD of 4 and very imprecise and geologically unreasonable upper intercept age. The most concordant zircon yields a concordia age of 78.27 ± 0.18 Ma, 2 sigma errors (***Figure 3-15***b). Two other zircons are overstepping partly the concordia band and yield a 77.63

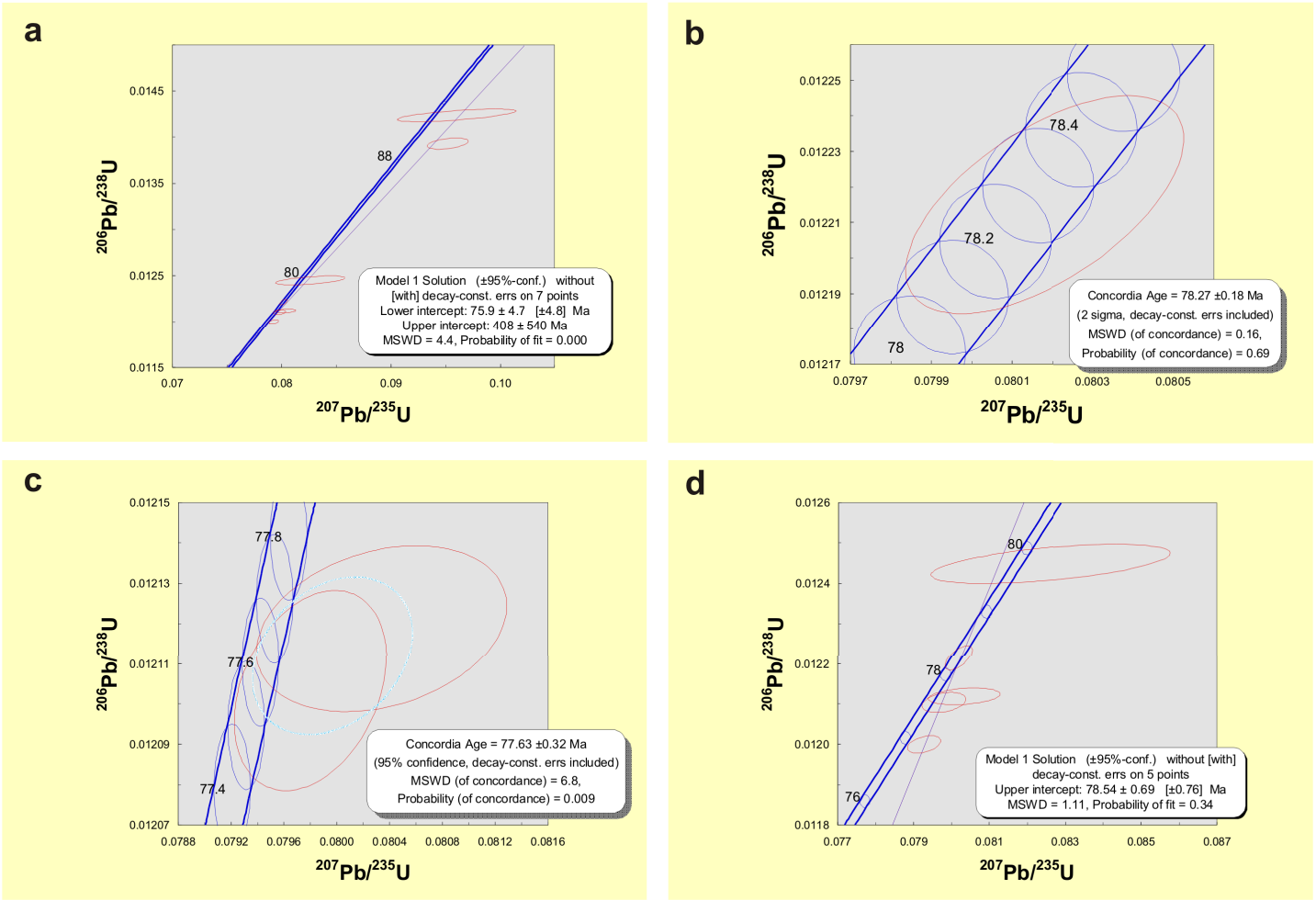

Figure 3-15. Results from single zircon U-Pb ID-TIMS dating for sample SG 028

± 0.32 Ma concordia age at the 95% confidence limit (***Figure 3-15***c). These two grains may be younger than the concordant zircon at 78.27 ± 0.18 Ma (***Figure 3-15***b), but their limited overlap with the concordia band suggests that their slightly younger ages may reflect minor Pb loss. Indeed, together with the remaining Campanian zircons they lie on a discordia chord with MSWD of 1.1 and upper intercept age very close to the age of the most concordant zircon, at 78.54 ± 0.76 Ma (***Figure 3-15***d). Therefore we consider the age of 78.27 ± 0.18 Ma to be the best estimate of the crystallization age of the granodiorite.

Fifteen zircons were analyzed by LA-ICPMS (***Figure 3-16***a). Eleven grains form a coherent group at about 78 Ma and three analyses detect Permian cores in Late Cretaceous zircons (***Figure 3-16***a, b). The crystallization age of 78.63 +0.74 -2.32 Ma calculated with the TuffZircAge algorithm of ISOPLOT (***Figure 3-16***c) is similar to the ID-TIMS estimate for crystallization age of the rock (78.27 ± 0.18 Ma).

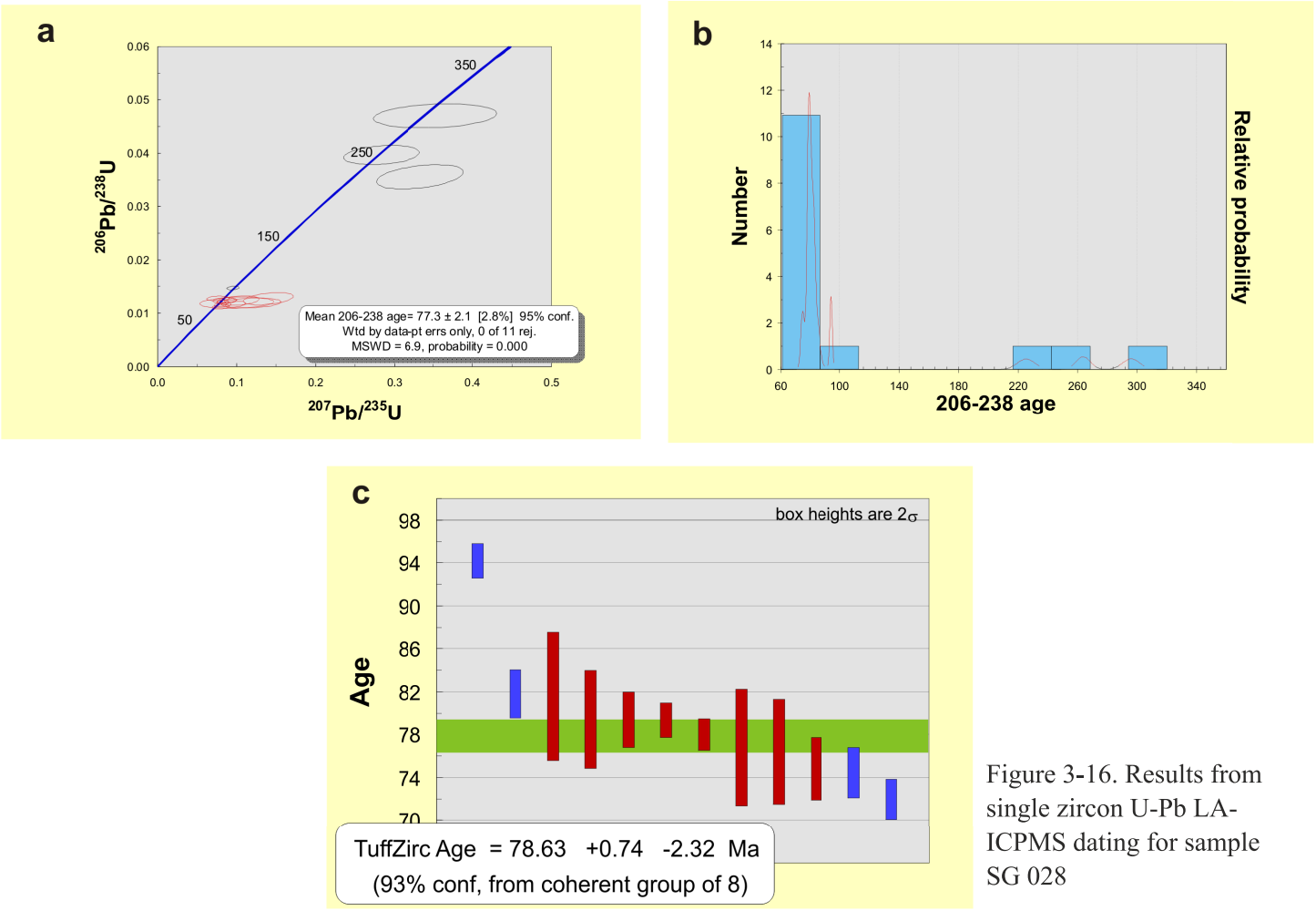

Figure 3-16. Results from single zircon U-Pb LA-ICPMS dating for sample SG 028

SG 030 – Latite, Southern Strandzha

This rock is from the southernmost occurrence of basic/intermediate lavas in Eastern Srednogorie, south of Razdel village, and represents the only sizeable outcrop of volcanic rocks preserved in the Strandzha region. Five zircons grains were analyzed by ID-TIMS; three of them chemically abraded, the other two were not abraded. All grains are variably discordant and have $^{206}Pb/^{238}U$ ages distinctly older than Late Cretaceous, some zircons overlap slightly the concordia band (***Figure 3-17***).

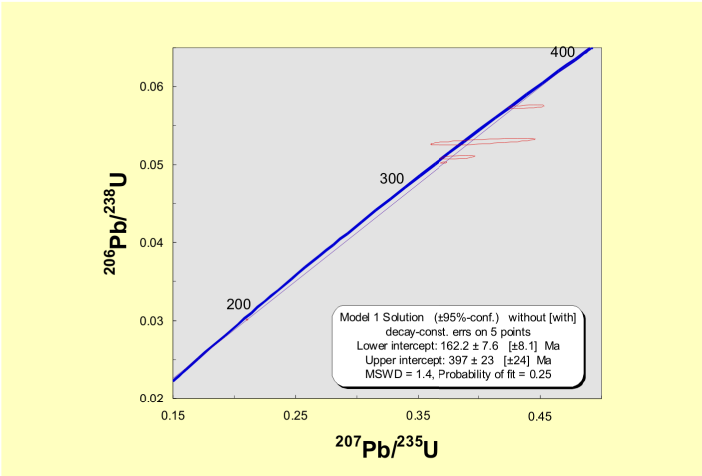

Figure 3-17. Results from single zircon U-Pb ID-TIMS dating for sample SG 030

The discordance of chemically abraded zircons can be explained with the presence of older inherited cores. A model 1 discordia line calculated with all five points has an MSWD of 1.4 and upper intercept of 397 ± 24 Ma. The lower intercept gives an age of 162.2 ± 8.1 Ma, suggesting that Devonian inherited cores were overgrown by variable amounts of Middle to Upper Jurassic rims.

SG 032 – Basaltic dike, Gramatikovo pluton?

The dike crosscuts the low-grade metamorphic rocks from the Strandzha allochtonous unit, south of the village of Gramatikovo. Three unabraded zircons analyzed by ID-TIMS have discordant ages (***Figure 3-18***). One grain with a $^{206}Pb/^{238}U$ age of 85.31 Ma indicates a possible Late Cretaceous event. The three zircons form a discordia chord with lower intercept of 75.1 ± 6.6 Ma and an upper intercept of 470 ± 15 Ma indicating an Ordovician magmatic event. The Late Cretaceous lower intercept is based on 3 points only (and only one of the Cretaceous) and therefore not considered a robust age estimate. Considering the proximity of Gramatikovo pluton and its 86 Ma well defined crystallization age (see sample ST 25), it not unlikely that the studied dike is genetically related to the pluton and its single zircon poor-defined concordia age of 85.23 ± 3.6 Ma at the 95% confidence level represents better the crystallization age of the dike than the lower intercept age. Additional analyses are needed to better constrain the crystallization age of the sample.

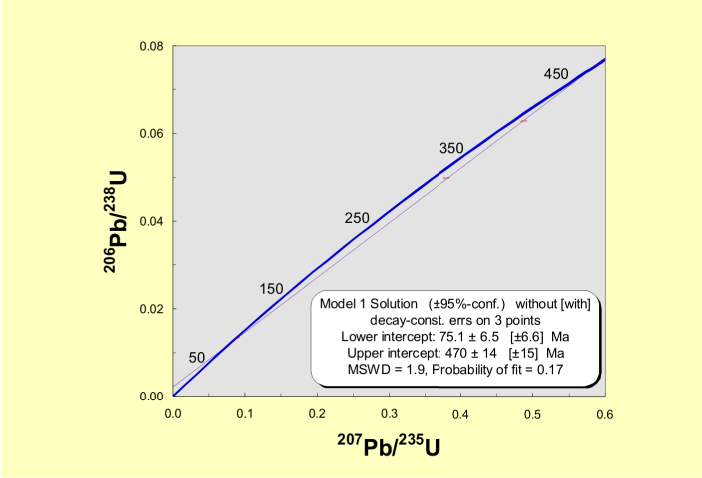

Figure 3-18. Results from single zircon U-Pb ID-TIMS dating for sample SG 032

SG 045 – Granite, Granitovo

The sample is from a quarry near the village of Kamenna Reka. Four chemically abraded zircons were dated by ID-TIMS (***Figure 3-19***a). One zircon yields a concordant age of 79.66 ± 0.14 Ma, 2 sigma errors (***Figure 3-19***b), which is just slightly younger than the 79.94 ± 0.14 Ma age of the granodiorite phase from the same pluton (see sample AvQ 048). A second zircon with almost identical $^{206}Pb/^{238}U$ age is discordant, having a slightly older $^{207}Pb/^{235}U$ age of 80.21 Ma. Two discordant zircons with clearly older $^{206}Pb/^{238}U$ ages the Late Cretaceous concordant zircon lie on a chord with upper intercept of 246 ± 52 Ma suggesting the presence of Permian inherited cores.

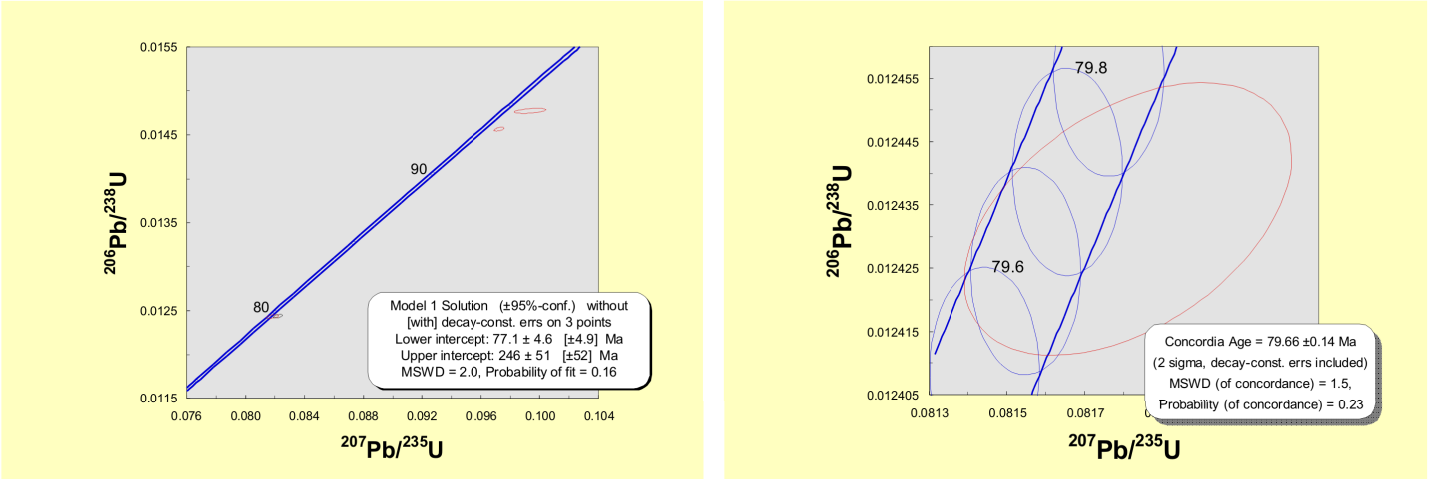

Figure 3-19. Results from single zircon U-PB ID-TIMS dating for sample SG 045

SG 047 – Gneiss-granite, Oman-Fakya

The sample, taken between the villages of Dennitsa and Oman, is representative of the frame into which the Late Cretaceous Oman-Fakya pluton intruded. Ten zircon grains dated by U-Pb LA-ICPMS (***Figure 3-20***a-d) have a Permian/ Carboniferous concordant age of 293.8 ± 7.6 Ma at the 95% confidence limit. One older grain is concordant at 450 Ma.

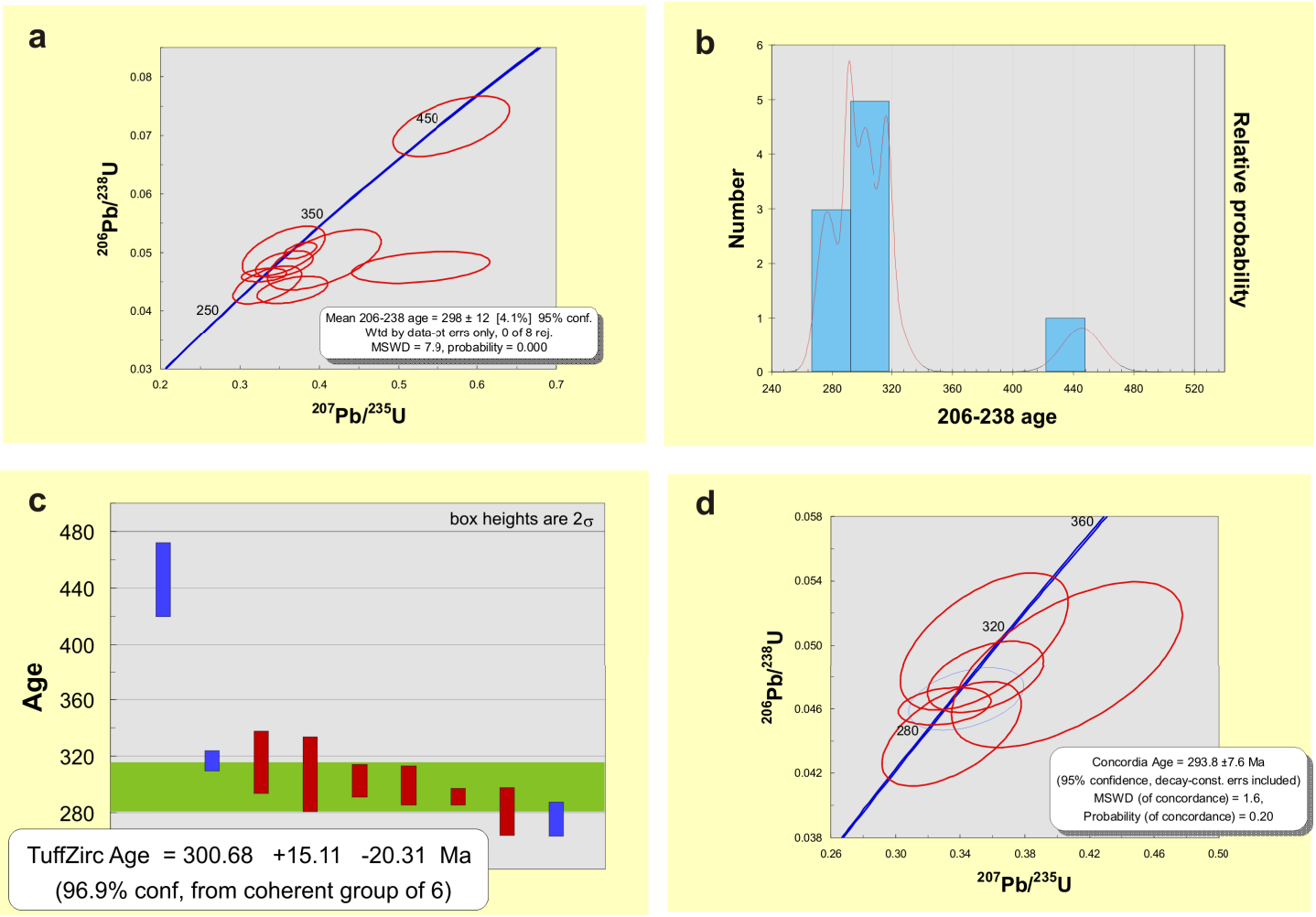

Figure 3-20. Results from single zircon U-Pb LA-ICPMS dating for sample SG 047

SG 051 – hydrothermally altered granite, Granitovo

Six unabraded and air abraded for two hours zircon grains dated by ID-TIMS all show disturbed U-Pb systematics (***Figure 3-21***a). The youngest zircon has a $^{206}Pb/^{238}U$ age of 76.54 ± 1.01 Ma, with an imprecise $^{207}Pb/^{235}U$ age. Four of the remaining zircons lie on a discordia line with an MSWD = 1.5 and upper intercept at 268 ± 37 Ma, pointing towards a possible Permian age and recent Pb loss (lower intercept close to present). Sixteen LA-ICPMS analyses have grossly disturbed U-Pb systematics (***Figure 3-22***). No meaningful age could be extracted from this population.

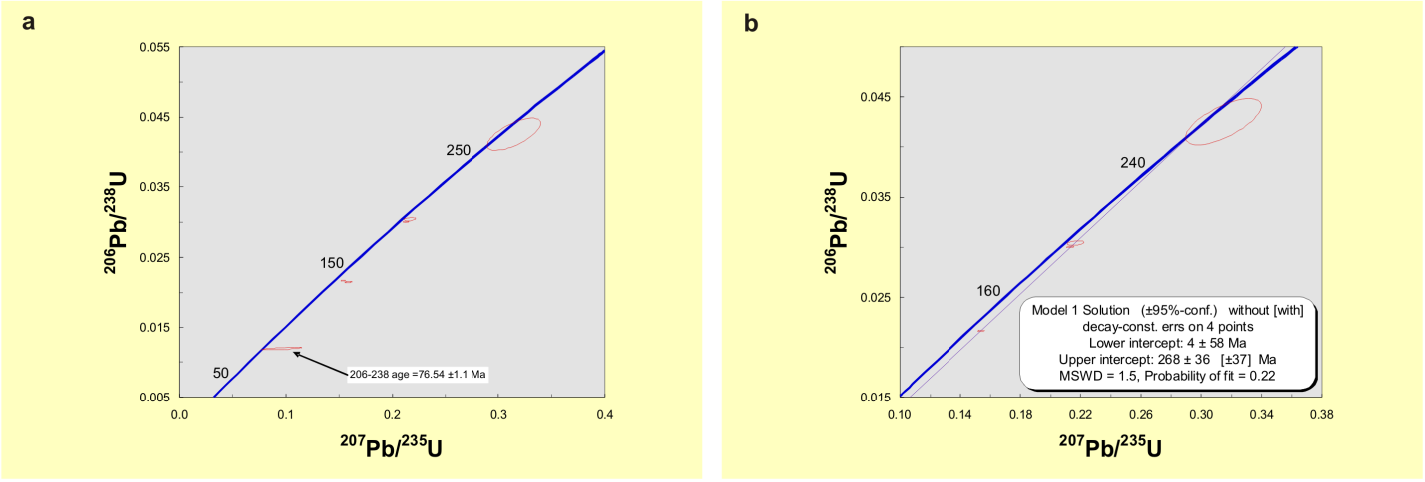

Figure 3-21. Results from single zircon U-Pb ID-TIMS dating for sample SG 051

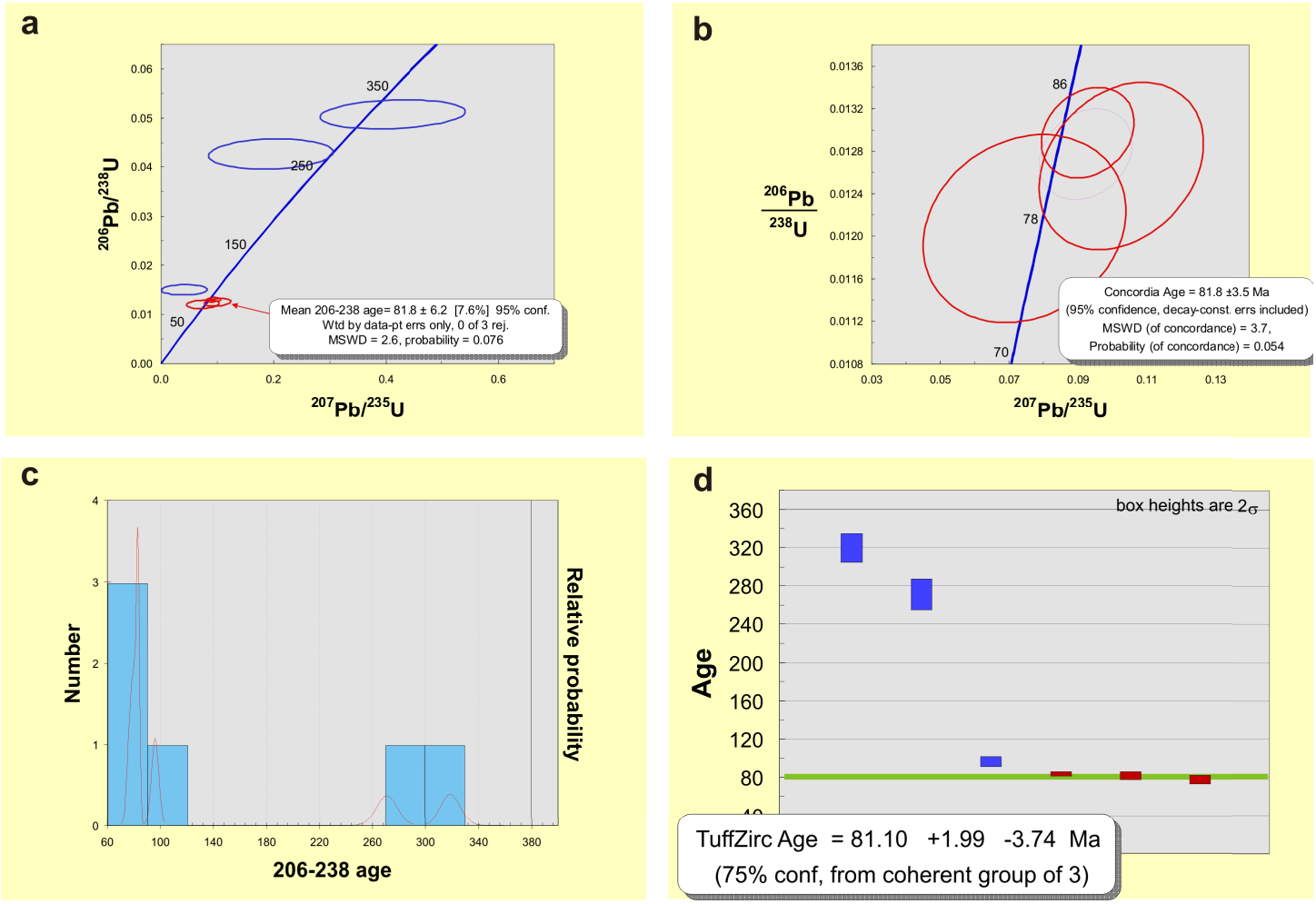

Figure 3-22. Results from single zircon U-Pb LA-ICPMS dating for sample SG 051

SG 052 – Aplitic dike, Monastery Heights

Three zircons and one monazite were analyzed by ID-TIMS (***Figure 3-23***a). The error ellipses of two zircons overlap, yielding a concordant age of 78.83 ± 0.17 Ma, 2 sigma error (***Figure 3-23***b). The monazite is concordant at 74.75 ± 0.20 Ma, while the third zircon is discordant, with unclear relations to the other grains.

Additional six zircons were dated by LA-ICPMS (***Figure 3-24***a). The unmix ages algorithm of ISOPLOT yields a $^{206}Pb/^{238}U$ age of 78.76 ± 1.7 Ma for five zircons from the population (***Figure 3-24***b). One grains has a concordant Carboniferous age.

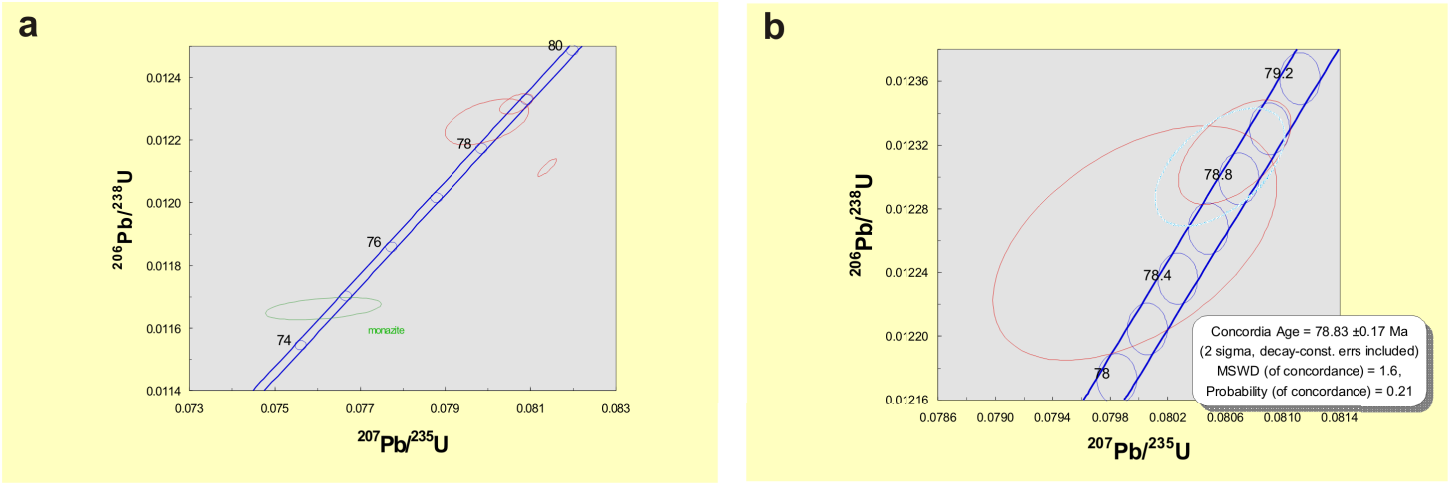

Figure 3-23. Results from single zircon U-Pb ID-TIMS dating for sample SG 052

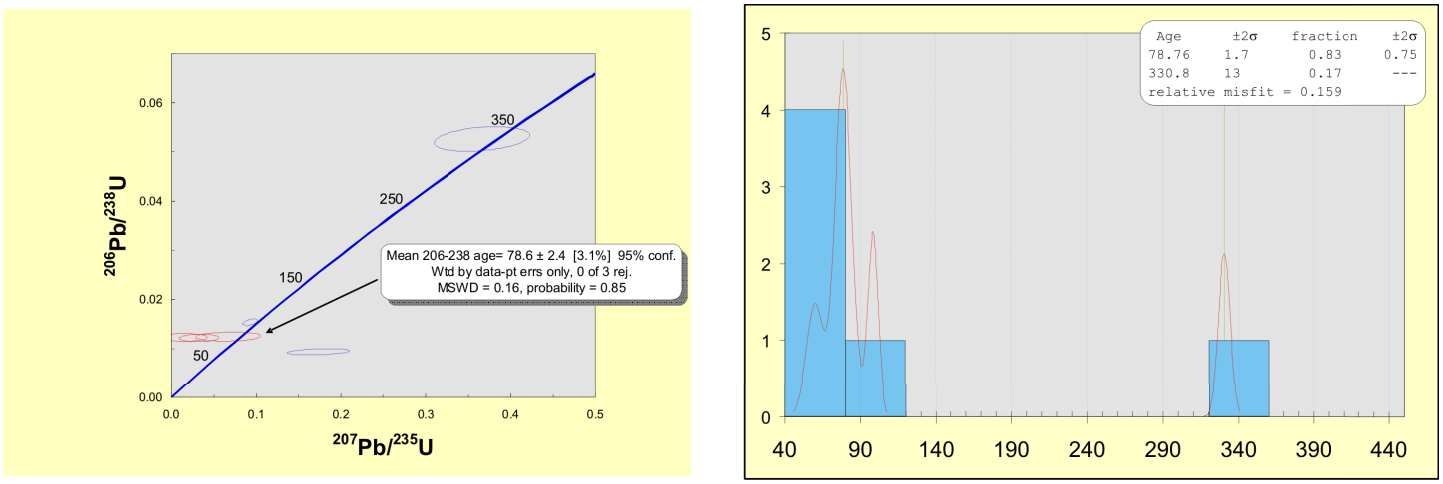

Figure 3-24. Results from single zircon U-Pb LA-ICPMS dating for sample SG 052

SG 053 – Gabbro, Chernozem-Razdel

Eight zircons were analyzed by U-Pb LA-ICPMS (***Figure 3-25***a). The zircon age extractor algorithm gives an age of 79.91 +1.07 -3.09 Ma (***Figure 3-25***b). Three grains have older $^{206}Pb/^{238}U$ ages of 120, 276 and 396 Ma.

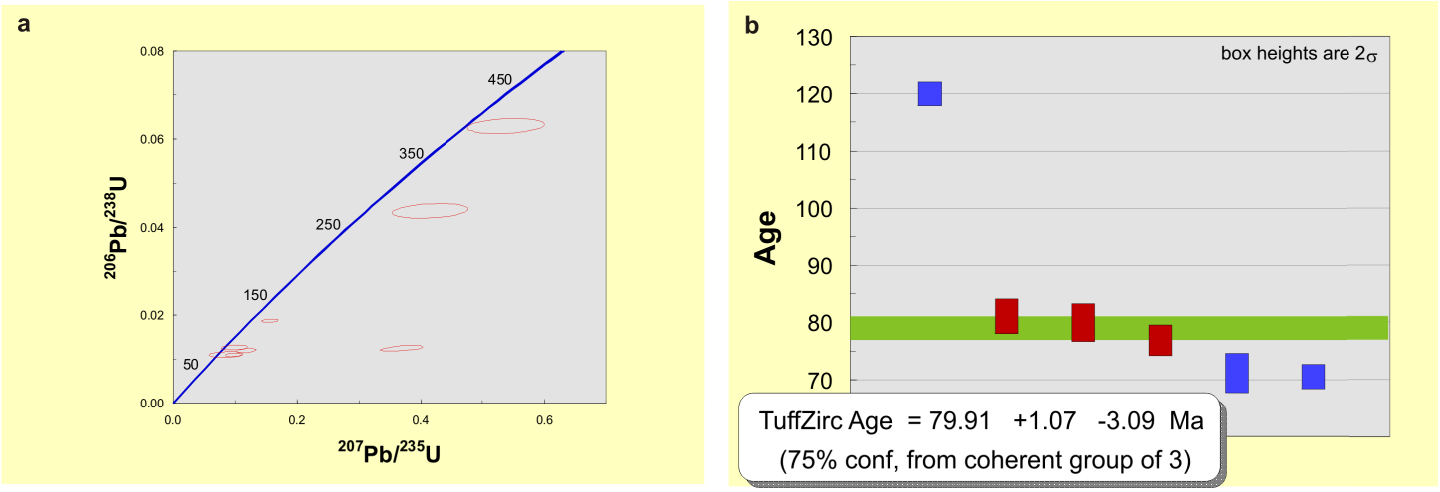

Figure 3-25. Results from single zircon U-Pb LA-ICPMS dating for sample SG 053

SG 057– Gabbro-diorite, southern Strandzha

Six grains were analyzed by ID-TIMS, five air abraded for 3 hours and one grain air abraded for 6 hours. A wide spread of ages is observed (***Figure 3-26***a) and crystallization oag of the rock could not be determined. Three grains are concordant within their errors at 138, 291 and 433 Ma (***Figure 3-26*** b, c, d). An additional grain is concordant at 216 Ma, but with a high error on the $^{207}Pb/^{235}U$ ratio. Together with two other grains it lies on a discordia line with a MSWD = 2, lower intercept at 111.5 ± 5.2 Ma and upper intercept at 441.8 ± 6.1 Ma (***Figure 3-26***e). One discordant grain has a Late Cretaceous $^{206}Pb/^{238}U$ age but this does not necessarily imply a Late Cretaceous age of the sample, because the analysis lies on the line of recent Pb loss of the 138 Ma old concordant zircon.

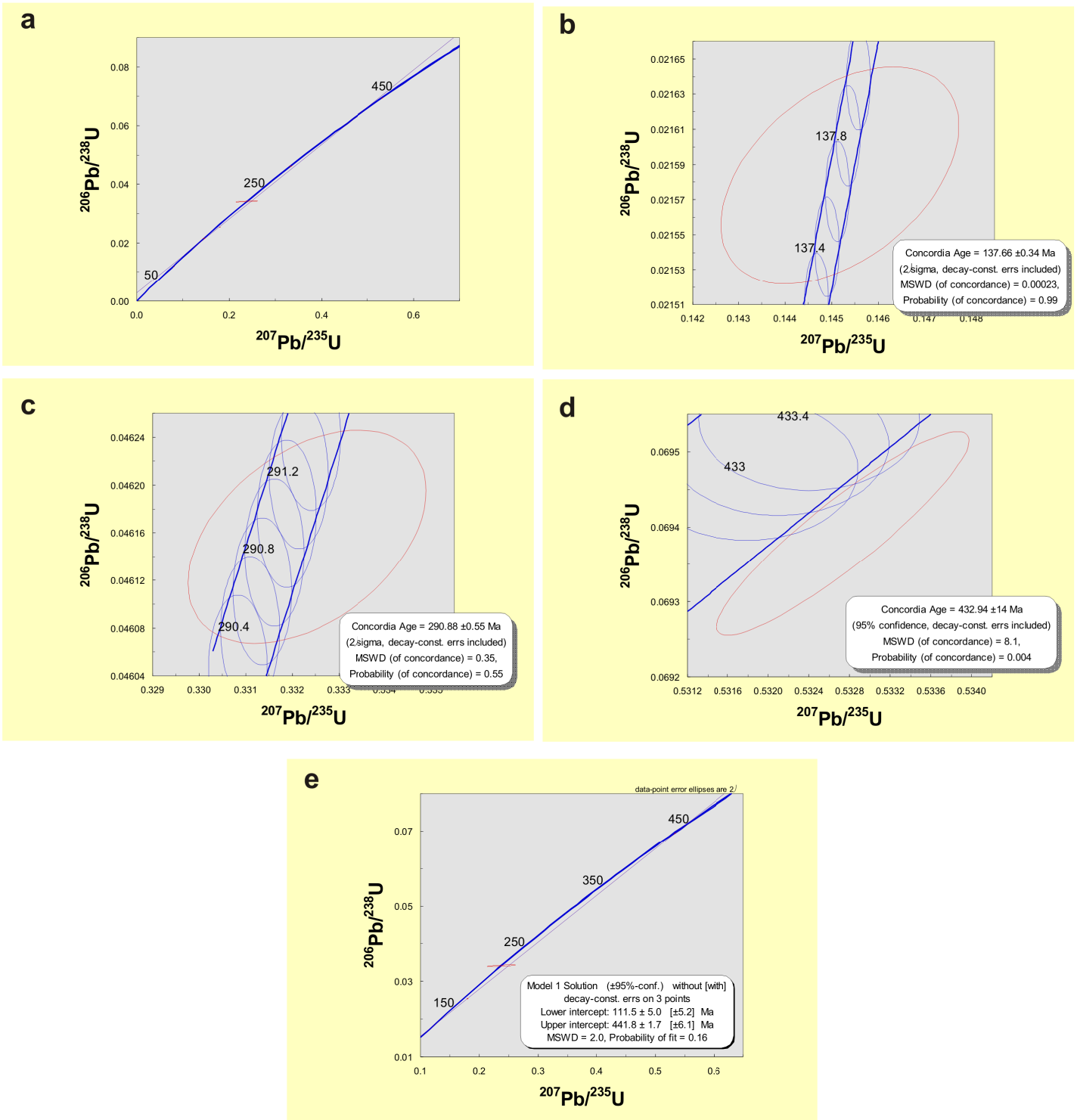

Figure 3-26. Results from single zircon U-Pb ID-TIMS dating for sample SG 057

LA-ICPMS U-Pb ages of 11 zircons from this sample also show wide scatter (***Figure 3-27***) and do not resolve the age of the rock. Late Cretaceous ages are not detected by the LA dating; one grain has a $^{206}Pb/^{238}U$ age of 47 Ma with a slight reverse discordance. Four grains give a weighted average $^{206}Pb/^{238}U$ age of 134 ± 13 Ma at the 95% confidence level and high scatter (MSWD = 27). More analyses are needed for confident age determination of this sample.

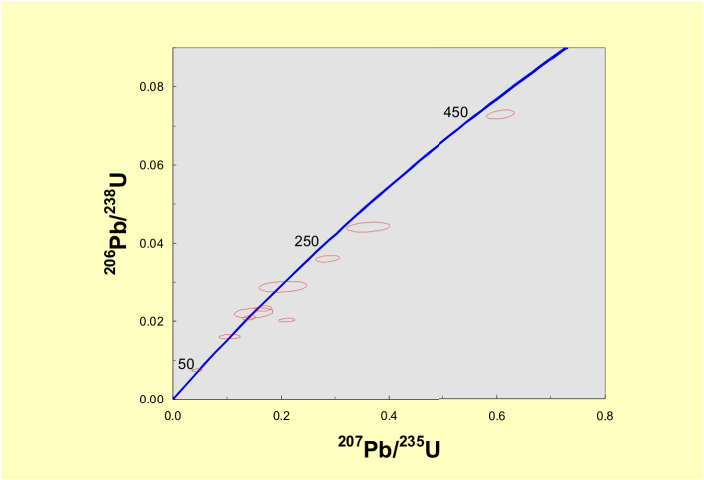

Figure 3-27. Results from single zircon U-Pb LA-ICPMS dating for sample SG 057

SG 059– Gabbro, Zheljazkovo

Four zircons dated by ID-TIMS are situated at or close to the concordia, and three of them yield a Carboniferous concordant age of 301.26 ± 0.97 Ma, 2 sigma errors (***Figure 3-28***).

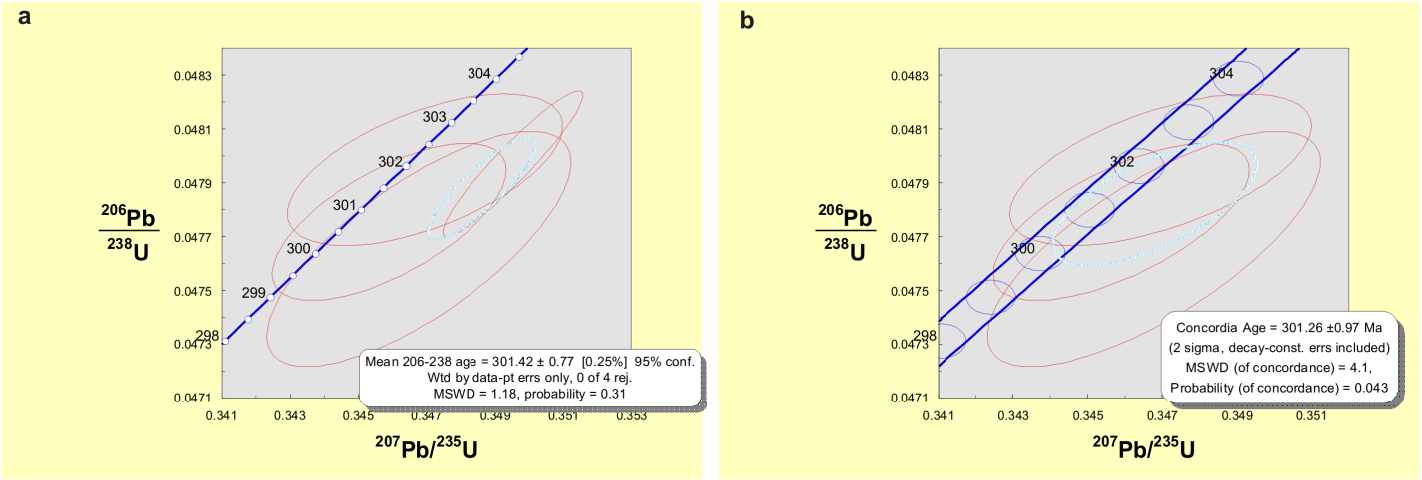

Figure 3-28. Results from single zircon U-Pb ID-TIMS dating for sample SG 059

SG 070 – Gneiss-granite, Monastery Heights

This sample is taken as representative for the basement rocks, into which the Late Cretaceous Monastery Heights pluton was intruded. Eleven zircons dated by LA-ICPMS are presented on ***Figure 3-29***. Most grains have coherent $^{206}Pb/^{238}U$ ages of about 270 Ma (***Figure 3-29***b, c.). Five zircons overlap within their assigned errors with the concordia curve and yield a concordia age of 274.1 ± 4.5 Ma, which is considered to represent the crystallization age of the granite (***Figure 3-29***d).

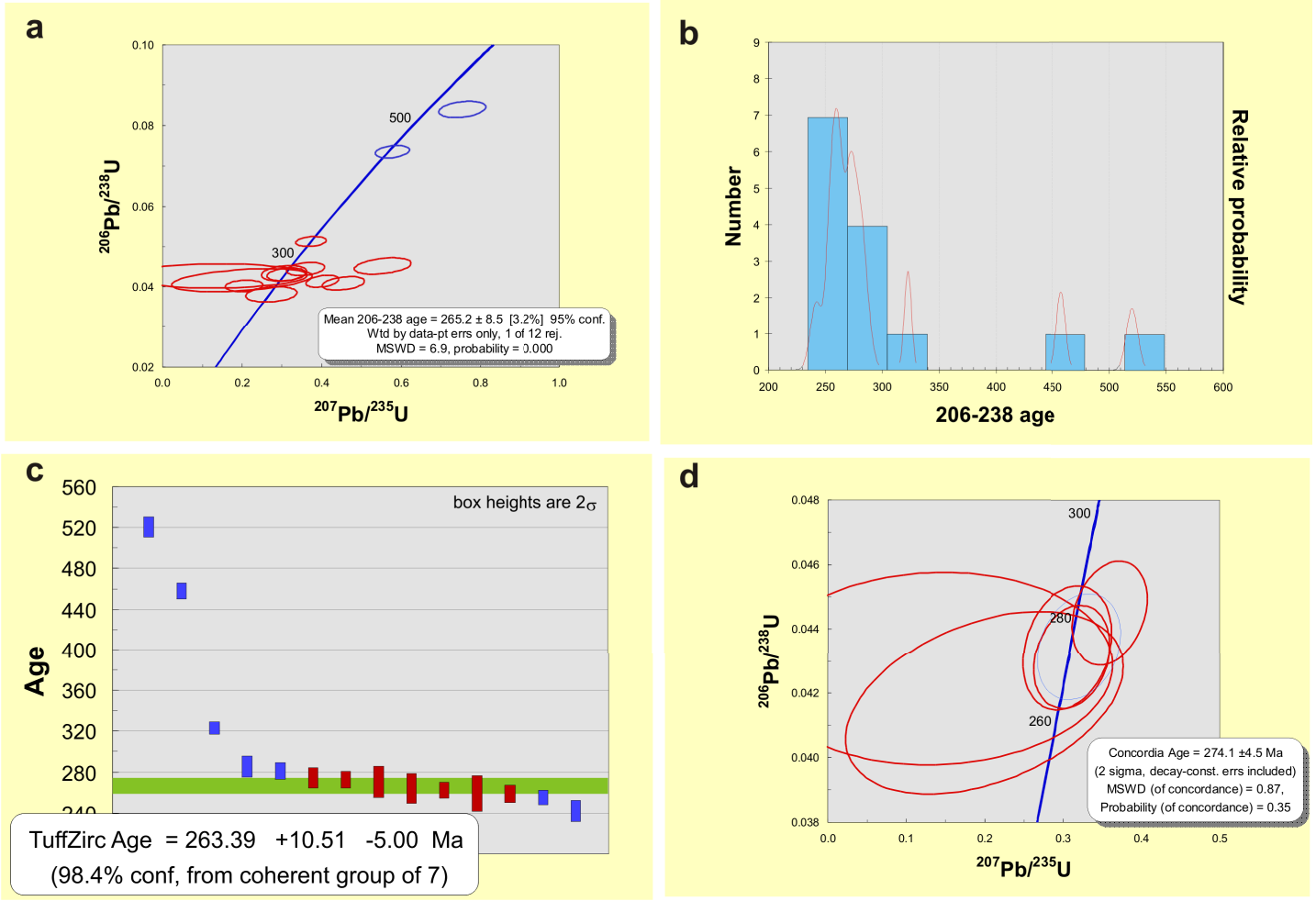

Figure 3-29. Results from single zircon U-Pb LA-ICPMS dating for sample SG 070

ST 25 – Gabbro, Gramatikovo

Four zircons analyzed by ID-TIMS yield a concordia age of 86.84 ± 0.29 Ma, 95% confidence limits, and a slightly older weighted average $^{206}Pb/^{238}U$ age of 87.02 ± 0.29 (***Figure 3-30***). All grains have rather low $^{206}Pb^{*}/^{204}Pb$ ratios from 45 to 70, which indicates a large proportion of common Pb. Ages were calculated with an increased blank proportion of 6pg/g, and the zircon with highest $^{206}Pb^{*}/^{204}Pb$ has the lowest $^{206}Pb/^{238}U$ age which suggests that the concordia age is more representative for the age of the rock compared to the weighted average $^{206}Pb/^{238}U$ age.

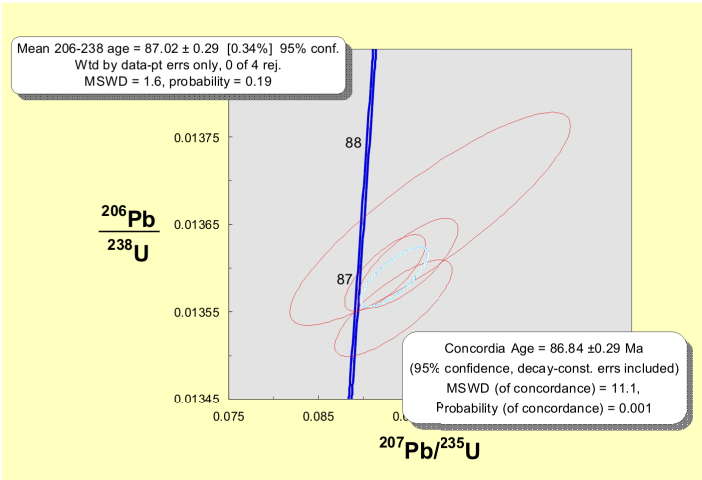

Additional five zircon and four sphene grains were dated by LA-ICPMS (***Figure 3-31***a). Four zircons yield a concordia age of 87.28 ± 1.6 Ma (***Figure 3-31***b), in good agreement with the ID-TIMS age. The sphenes are largely discordant, even after applying ^{204}Pb correction.

Figure 3-30. Results from single zircon U-Pb ID-TIMS dating for sample ST 25

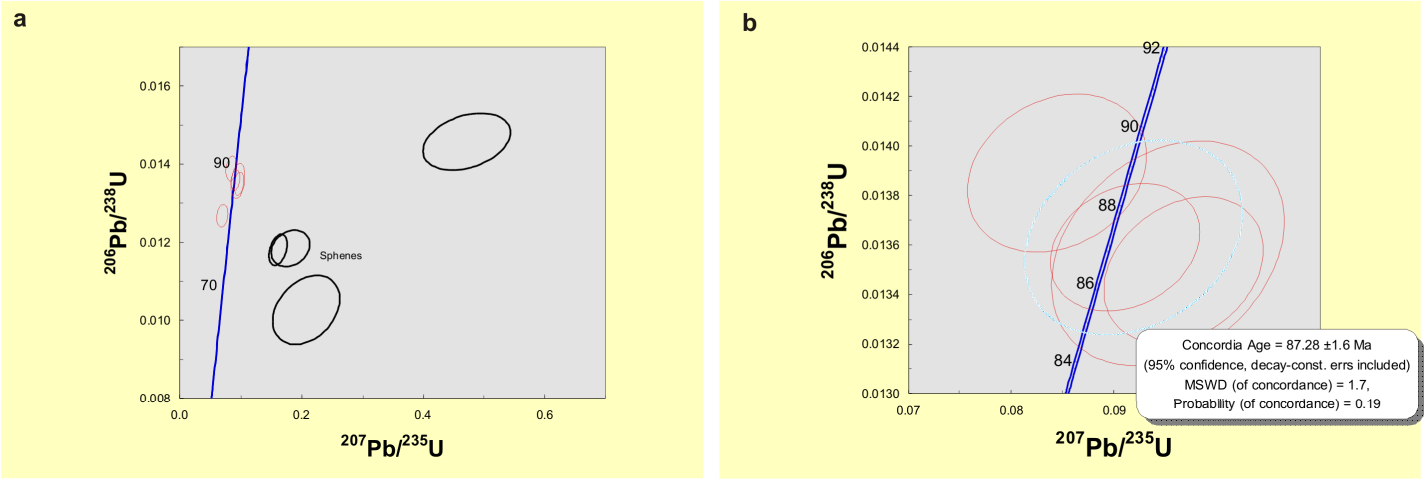

Figure 3-31. Results from single zircon U-PB LA-ICPMS dating for sample ST 25

1.2. YAMBOL-BURGAS region

AvQ 052 – Monzo-syenite, Rossen

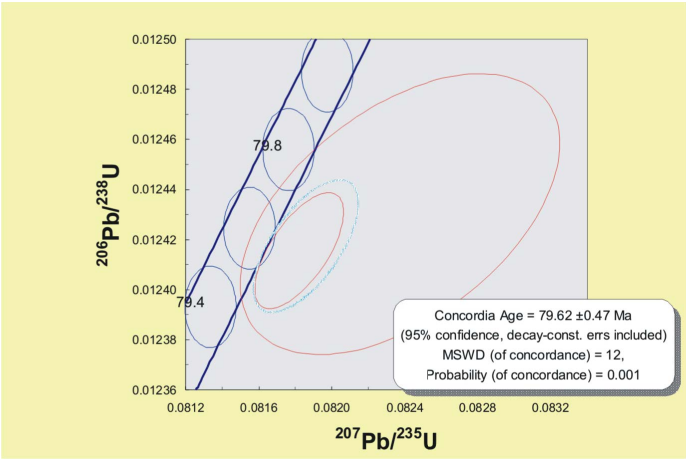

This monzo-syenite from Rossen volcano-intrusive center is taken from the quarry near the village of Chernomoretz. The two zircons analyzed by U-Pb ID-TIMS (***Figure 3-32***) yield a Late Cretaceous concordant age of 79.62 ± 0.47 Ma (95% confidence level interval). Additional analyses are needed to better constrain the crystallization age.

Figure 3-32. Results from single zircon U-Pb ID-TIMS dating for sample AvQ 052

AvQ 054 – Amphibole gabbro, Izgrev

The sample was collected in the quarry of Izgrev pluton. Five zircon grains analyzed by ID-TIMS have concordant Late Cretaceous ages (***Figure 3-33***). Four zircons are concordant at 81.27 ± 0.17 Ma; this age is interpreted to be the crystallization age of the rock. One grain has a $^{206}Pb/^{238}U$ age slightly older than the four concordand zircons, probably due to incorporation of minor inherited component. The weighted average $^{206}Pb/^{238}U$ age of all five zircons is 81.64 ± 0.64 Ma, with a MSWD value of 8.1. Only two prismatic grains were analyzed by LA ICPMS. Although this is insufficient for age calculation, they do have a Late Cretaceous $^{206}Pb/^{238}U$ ages.

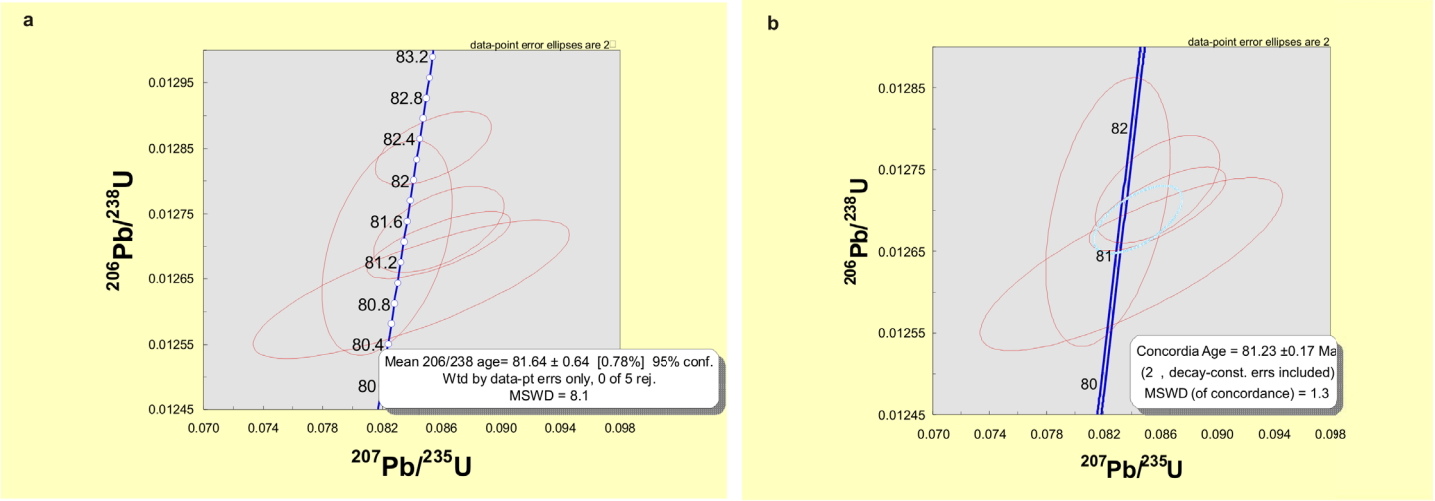

Figure 3-33. Results from single zircon U-Pb ID-TIMS dating for sample AvQ 054

AvQ 055 – Amph gabbro, Izgrev

The sample is taken close to the locality where AvQ 054 is sampled; it represents a more finer-grained variety of the same rock as AvQ 054. Six zircons analyzed by LA-ICPMS are variably discordant. The relative probability distribution of the $^{206}Pb/^{238}U$ ages indicates an old inherited age within 650-750 Ma (***Figure 3-34***). Three zircons have younger ages with limited overlap between two of them. Additional analyses are needed for age calculation. The TIMS crystallization age of 81.27 ± 0.17 Ma of sample AvQ 054 is most likely representative also for the finer-grained variety in AvQ 055.

Figure 3-34. Results from single zircon U-Pb LA-ICPMS dating for sample AvQ 055

AvQ 057 – Olivine-Gabbro, Izgrev

This sample is from Izgrev pluton, and was collected just outside of the quarry where AvQ 054 and AvQ 055 were sampled. We analyzed 13 zircons using conventional U-Pb ID-TIMS. The gabbro has a complicated inheritance pattern, with most of the points being concordant or lying close to the concordia curve (***Figure 3-35***a). The resulting precise zircon ages cover a wide range from ca. 80 to 460 Ma, and there is also an indication for a possible Mesoproterozoic magmatic event. The concordia age of the two youngest zircons at 79.93 ± 0.22 Ma (***Figure 3-35***b) is considered as the crystallization age of the rock.

The most prominent group of inherited zircons is clustered around 460 Ma and four of them lie on a discordia line with upper intercept age of 464 ± 14 Ma (***Figure 3-35***c). The uppermost zircon on ***Figure 3-35***c lies almost entirely within the concordia band and yields a well-defined Ordovician concordia age of 462.2 ± 1.2 Ma (***Figure 3-35***f). The remaining zircons on ***Figure 3-35***c have slightly younger U-Pb ages probably reflecting minor Pb loss. Two zircons have older $^{206}Pb/^{238}U$ and $^{207}Pb/^{235}U$ ages and together with the Ordovician concordant zircon form a discordia line with lower intercept in the Ordovician, and an upper intercept at 1353 ± Ma (***Figure 3-35***d). The two older zircons probably crystallized in the Mesoproterozoic and were later overgrown by Ordovician rims. Two long prismatic grains are concordant at 403.63 ± 0.86 Ma, indicative of a Lower Devonian magmatic event (***Figure 3-35***e). Additional two inherited zircon concordant ages can be recognized at 160.11 ± 0.63 Ma and 279.61 ± 0.70 Ma (***Figure 3-35***g,h). The relatively large errors on the Jurassic and Permian single zircons questions their concordance and their geologic meaning. However, part of

the age data obtained from six LA ICPMS analyses (only single age domains) confirm a Jurassic event at 159 ± 2.6 Ma (***Figure 3-36***). The LA-ICPMS dating also reveal 417.9 ± 8.5 Ma age(***Figure 3-36***) which is close to the ID-TIMS well defined Devonian age of inherited grains.

In summary, the Izgrev gabbro AvQ 057 that crystallized in the Late Cretaceous carries evidence for a broad range of age events within the basement rocks of Izgrev pluton: Jurassic, Permian, Devonian, Ordovician and possibly Mesoproterozoic.

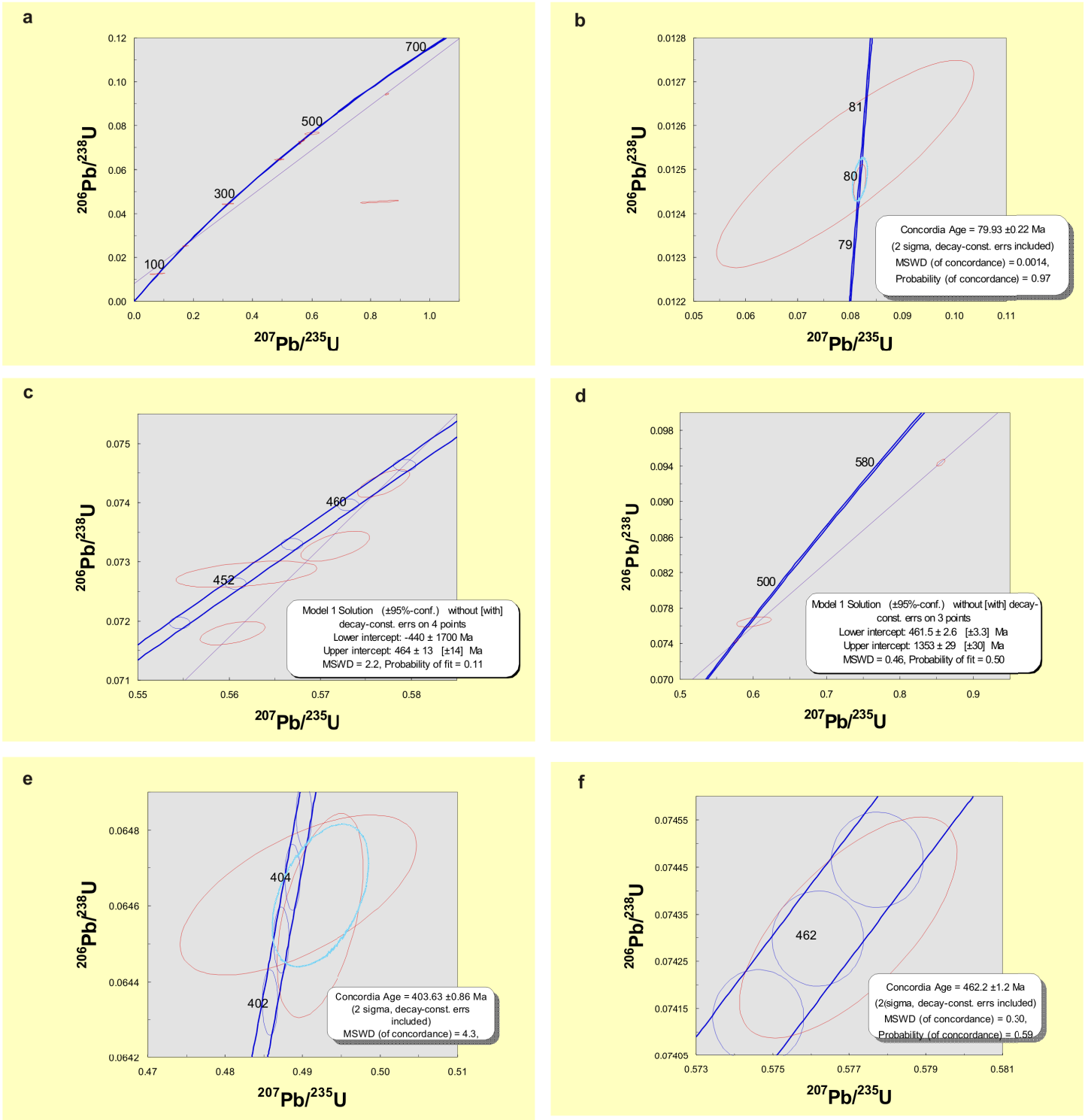

Figure 3-35. Results from single zircon U-Pb ID-TIMS dating for sample AvQ 057

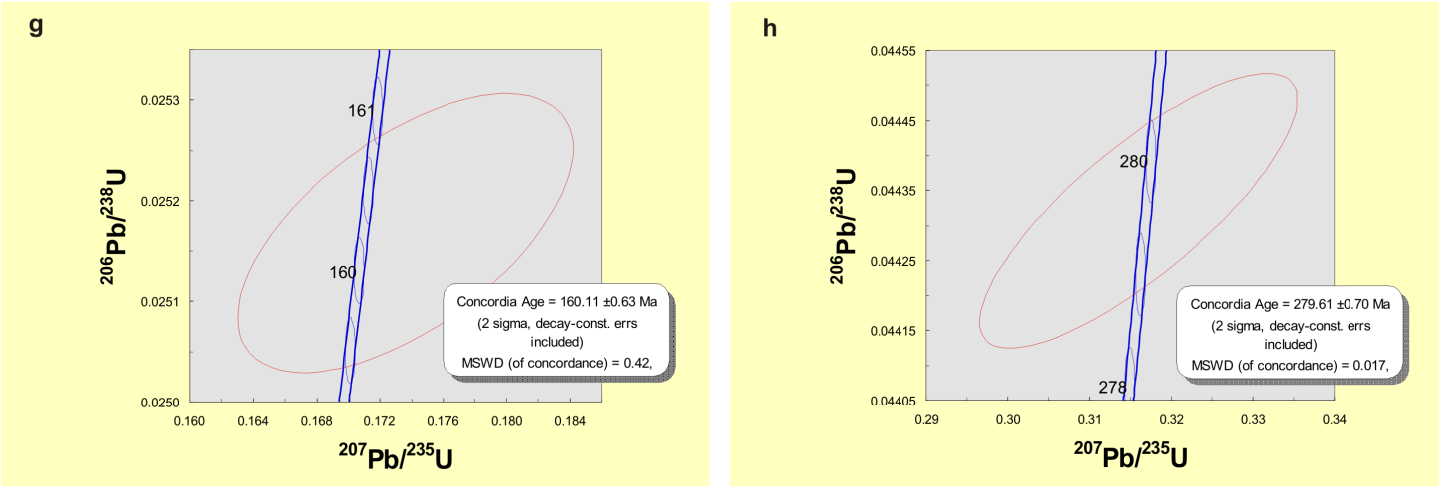

Figure 3-35-continued. Results from single zircon U-Pb ID-TIMS dating for sample AvQ 057

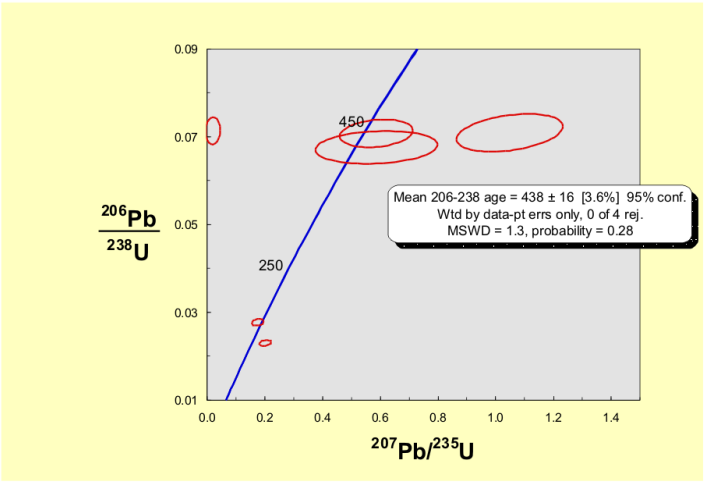

Figure 3-36. Results from single zircon U-Pb LA-ICPMS dating for sample AvQ 057

AvQ 058 – Ankaramite, Izgrev

The sample is taken from a small quarry exploiting volcanic rocks in Izgrev. All four ID-TIMS dated zircons exhibit an inherited age component (***Figure 3-37***a). Two grains are concordant at ca. 300 Ma (***Figure 3-37*** b), but they do not overlap each other. Together with a discordant older grain they form a discordia line with lower intercept at 295.6 ± 3.7 Ma and upper intercept at 1948 ± 37 Ma and a MSWD of 0.6 (***Figure 3-37***c). One zircon is concordant at 445.5 ± 1.6 Ma (***Figure 3-37***d) but with a large $^{207}Pb/^{235}U$ errorIt is possible that this zircon experienced some Pb loss and its crystallization age could be the 462.2 ± 1.2 Ma age observed in sample AvQ 057 (mafic intrusive from a nearby locality). In fact, this zircon lies on the discordia line formed by the Ordovician zircons from AvQ 057 which also show evidence of Pb loss. Five grains dated by LA-ICPMS have Late Cretaceous ages with limited overlap (***Figure 3-38***). Their weighted average $^{206}Pb/^{238}U$ age of 75.7 ± 7.0 at the 95% confidence limit has a high MSWD of 51 reflecting the data scatter. Additional analyses are needed to better constrain the crystallization age of the sample.

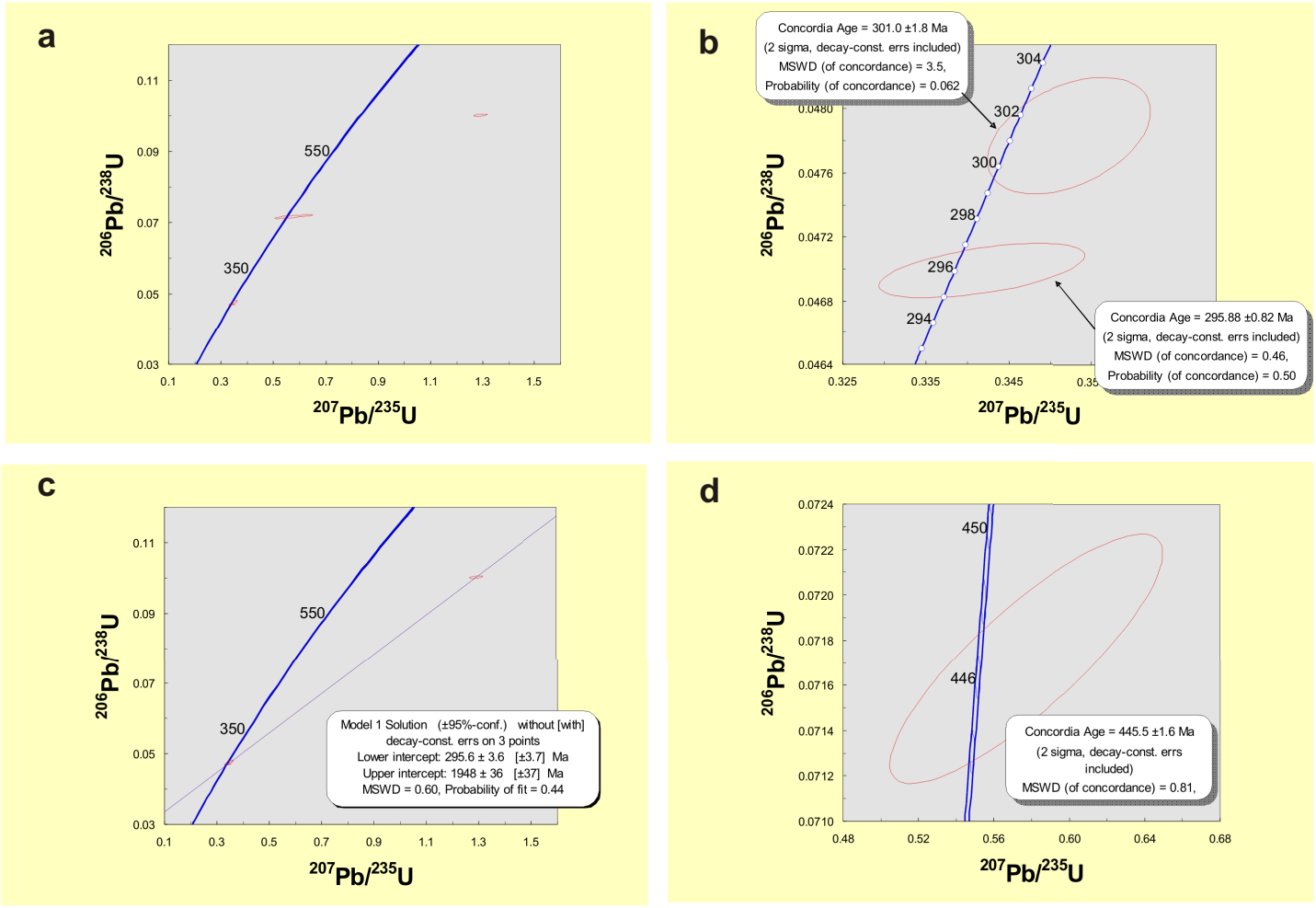

Figure 3-37. Results from single zircon U-Pb ID-TIMS dating for sample AvQ 058

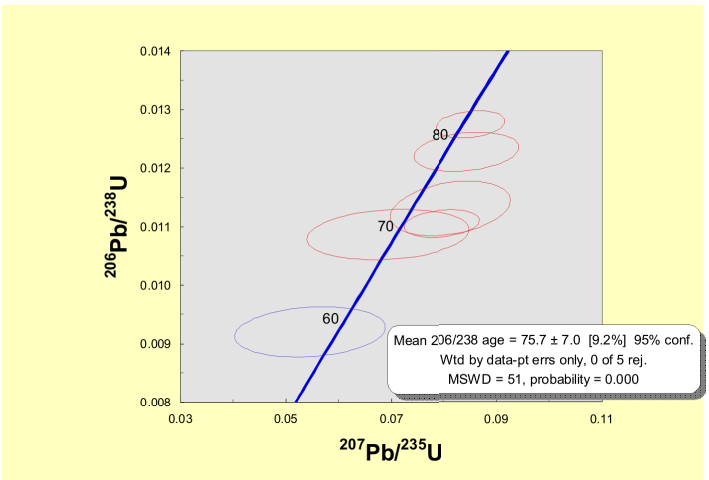

Figure 3-38. Results from single zircon U-Pb LA-ICPMS dating for sample AvQ 058

AvQ 142 – Gabbro, Vurshilo

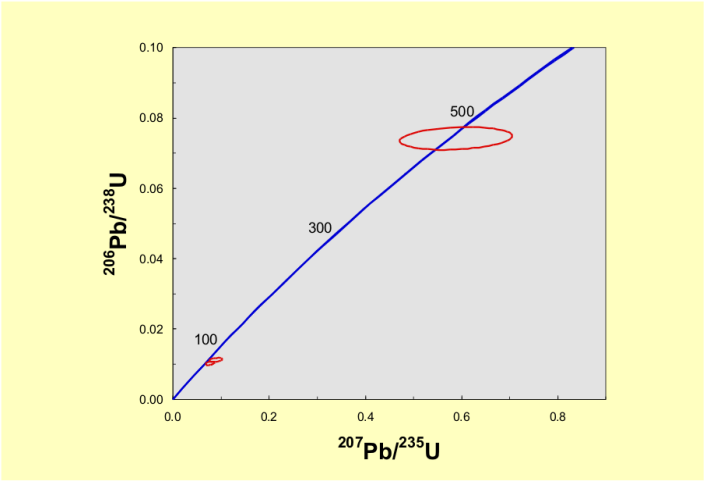

Three zircons were analyzed by LA-ICPMS U-Pb method. One is concordant with large errors at ca. 450 Ma, and the remaining two have Late Cretaceous $^{206}Pb/^{238}U$ ages (***Figure 3-39***). Additional analyses are needed to constrain the crystallization age of the sample.

Figure 3-39. Results from single zircon U-Pb LA-ICPMS dating for sample AvQ 142

SG 040 – Diorite, Zidarovo pluton

Nine zircons dated by LA-ICPMS suggestt a Late Cretaceous crystallization age of the sample (***Figure 3-40***a,b). One grain gives indication for an older component, while three grains are largely discordant (***Figure 3-40***a). The remaining four zircons form a somewhat coherent group at or near the concordia with a weighted average $^{206}Pb/^{238}U$ age of 78.0 ± 2.8 Ma at the 95% confidence level and with a MSWD of 1.3. The use of the zircon age extraction algorithm also yields a similar Late Cretaceous age with a smaller error (***Figure 3-40***b).

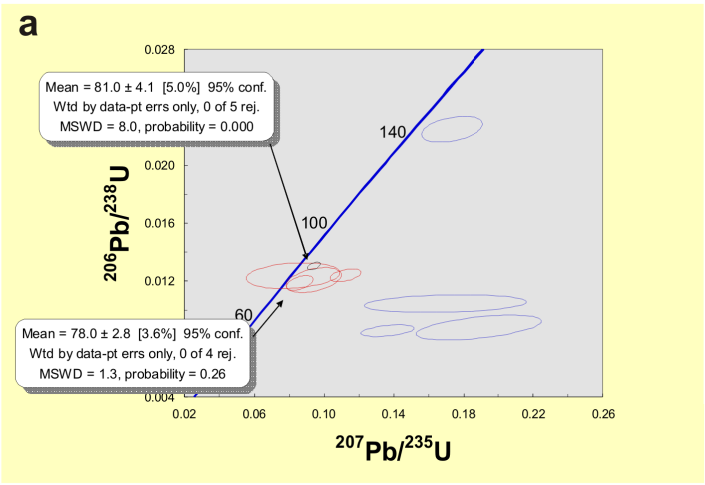

Figure 3-40. Results from single zircon U-Pb LA-ICPMS dating for sample SG 040

SG 041 – fine-grained syenite, Vurli Brjag pluton

LA-ICPMS dating on nine zircons shows disturbed U-Pb systematics (***Figure 3-41***a). The relative probability is highest for the group at 85Ma and this is also the age given by the zircon extraction age algorithm of ISOPLOT (***Figure 3-41***b, c). One grain with smaller errors is concordant at 80.97 ± 0.70 Ma and based on this age, it can be speculated that this syenite represents an earlier phase of the Vurli Brjag pluton (earlier compared to the SG 044 monzonite). However, the number of dated grains and their U-Pb systematics do not permit calculation of confident crystallization age of the sample.

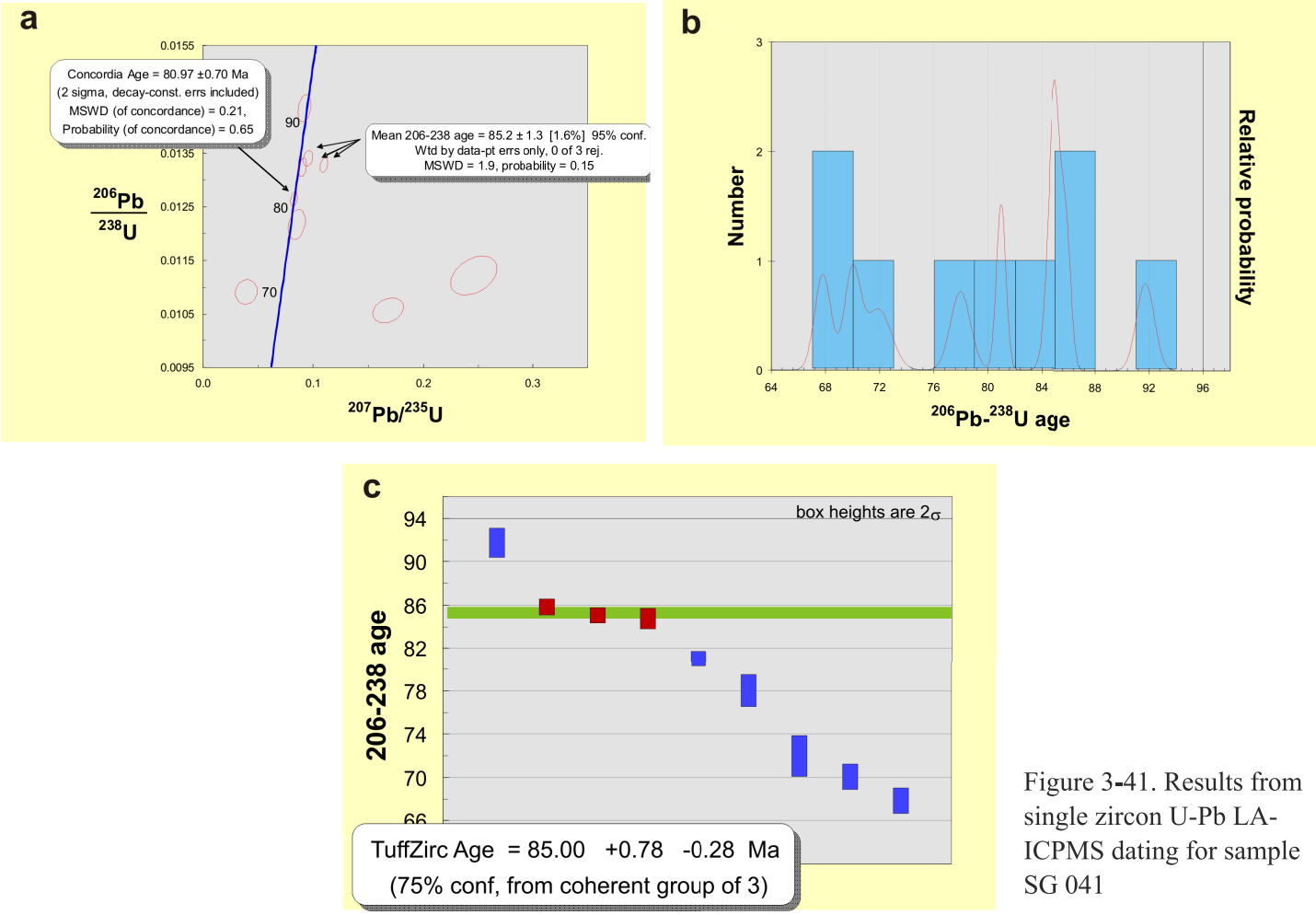

Figure 3-41. Results from single zircon U-Pb LA-ICPMS dating for sample SG 041

SG 044 – Monzonite, Vurli Brjag pluton

The sample is collected from a large quarry near the village of Gorno Ezerovo, close to the town of Burgas. The monzonite is intruded in a sequence of basalt and andesite lava flows and pyroclastic products with geochemically similar composition. Seven zircons air abraded for 3 hours were dated by ID-TIMS. They all have Late Cretaceous ages and lie at or next to the concordia band (***Figure 3-42***a). One grain apparently has a slightly older component and has a $^{206}Pb/^{238}U$ age of ~80.8 Ma. All remaining six zircons have $^{206}Pb/^{238}U$ ages from 79.15 to 79.89 Ma with a weighted average of 79.43 ± 0.30 Ma. Four analyses form a discordia line with lower intercept of 78.98 ± 0.31 Ma and a MSWD of 1.5. Considering the large uncertainty of the upper

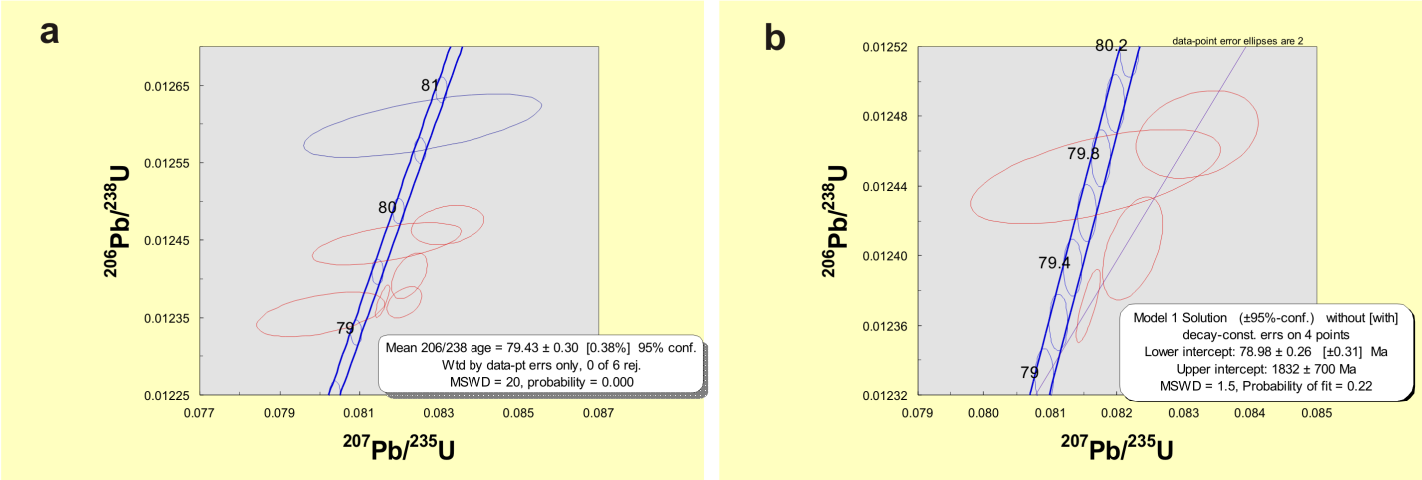

Figure 3-42. Results from single zircon U-Pb ID-TIMS dating for sample SG 044

intercept and the evidence from CL and BSE imaging for homogeneous grains, we consider the weighted average $^{206}Pb/^{238}U$ age of 79.43 ± 0.30 Ma a better estimate for the crystallization age of the rock than the lower intercept age. The relatively large scatter and small degree of discordance of the U-Pb ages could be due to limited amount of Pb loss.

Ten additional grains were analyzed by LA-ICPMS (***Figure 3-43***a). Seven grains overlap within their errors and give a concordia age of 79.42 ± 0.96 Ma at the 95% confidence limit (***Figure 3-43***b), which is in agreement with the ID-TIMS age of the rock.

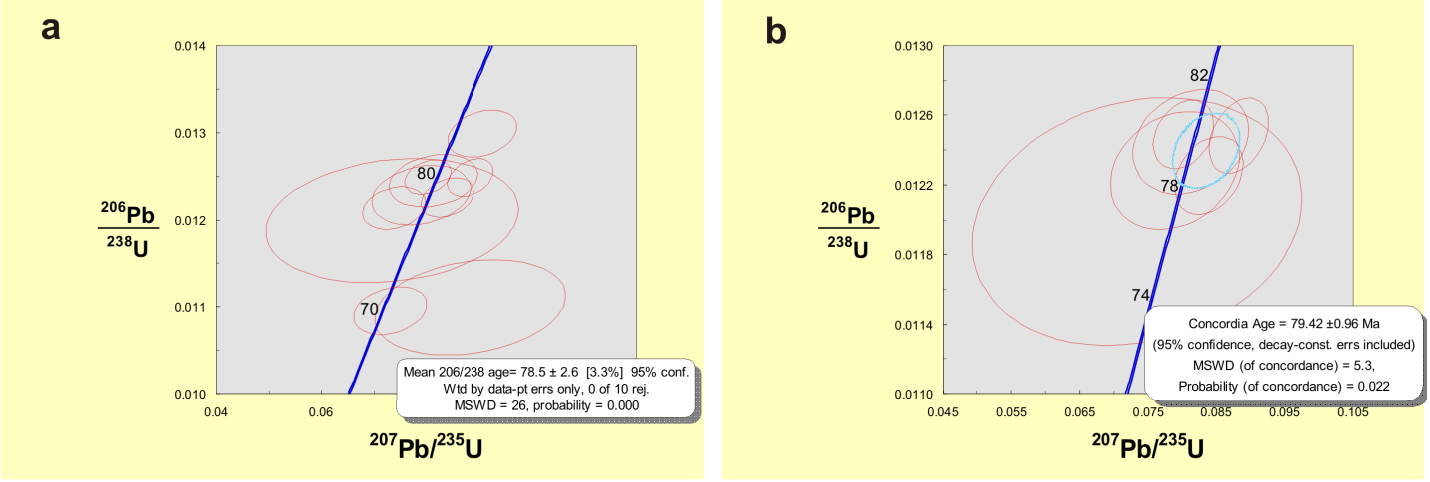

Figure 3-43. Results from single zircon U-Pb LA-ICPMS dating for sample SG 044

SG 044b – Latite, Vurli Brjag

The sample is from the same quarry as the SG 044 monzonite, from the volcanic sequence into which the monzonite was intruded. Four unabraded zircons were dated by ID-TIMS (***Figure 3-44***a). Two grains have Late Cretaceous ages: one discordant at ~87 Ma, and one concordant with a larger error at 79.46 ± 0.60 Ma (***Figure 3-44***b). From the two older grains, one is broadly concordant at ca. 440 Ma with a large $^{207}Pb/^{235}U$ error, and one grain is concordant at 1039.3 ± 4.2 Ma (***Figure 3-44***c). If the concordant grain at 1039 Ma is excluded, the remaining three zircons form three different discordia chords with a Late Cretaceous lower intercept (***Figure 3-44***d, e, f). The constructed discordia line is not anchored on ***Figure 3-44***d, anchored at the 443.53 Ma $^{206}Pb/^{238}U$ age of the zircon (***Figure 3-44***e), or anchored at 462 Ma (***Figure 3-44***f, 462 Ma is the Ordovician age well documented in sample AvQ 057). The latter may be the most reliable age estimate, because it has the best MSDW from the three regressions. Regardless of whether we assume the concordant Late Cretaceous age (based on 1 grain), or either of the lower intercepts (based on 3-point regressions), we conclude that the SG 044b latite crystallization was broadly coeval with but still older than the intrusion of SG 044 monzonite. Additional analyses are needed to better constrain the age of the rock.

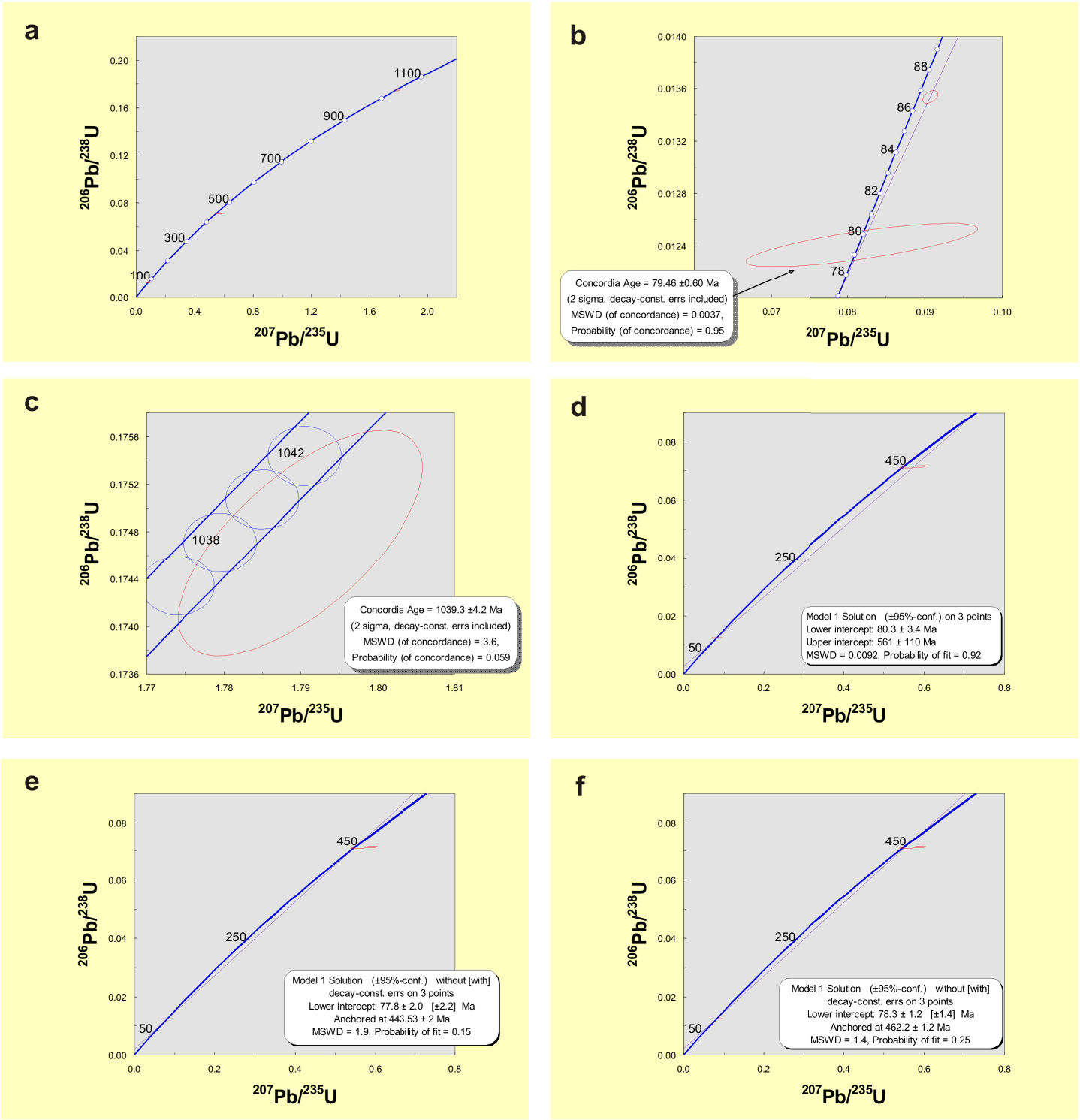

Figure 3-44. Results from single zircon U-Pb ID-TIMS dating for sample SG 044b

SG 063 – Latite dike, near Izgrev

This dike cuts Late Cretaceous sediments from the Mitchurin group near the town of Tsarevo. Five air abraded for 6h zircons analyzed by ID-TIMS all show discordant ages (***Figure 3-45***a) ranging from 170 to 470 Ma ($^{206}Pb/^{238}U$ ages). Currently, the best estimate for the crystallization age is the lower intercept age a three-point discordia line with a MSWD value of 0.56 that crosses the concordia at 104 ± 28 and 450 ± 26 Ma (***Figure 3-45***b). The Ordovician upper intercept age is relatively well defined and coincides within errors with the ~460 Ma inherited Ordovician ages observed in most studied rocks from the Yambol-Burgas region. The lower intercept however, with its large errors gives a broad range of ages from 76 to 132 Ma. Given the fact that the dike is intruded into Late Cretaceous sediments, its crystallization age has to be near the lower limit of this range. Additional analyses are needed to better constrain the age of the rock.

LA-ICPMS data for 14 zircon grains and one sphene are scattered along the concordia line with various degree of discordance and large errors (***Figure 3-46***a). Of them, two zircons and the sphene grain have Late Cretaceous $^{206}Pb/^{238}U$ ages with a mean value of 73 ± 19 Ma with a high MSWD of 16. The relative age probability plot of all grains graphically shows the large age spread and limited overlap (***Figure 3-46***b).

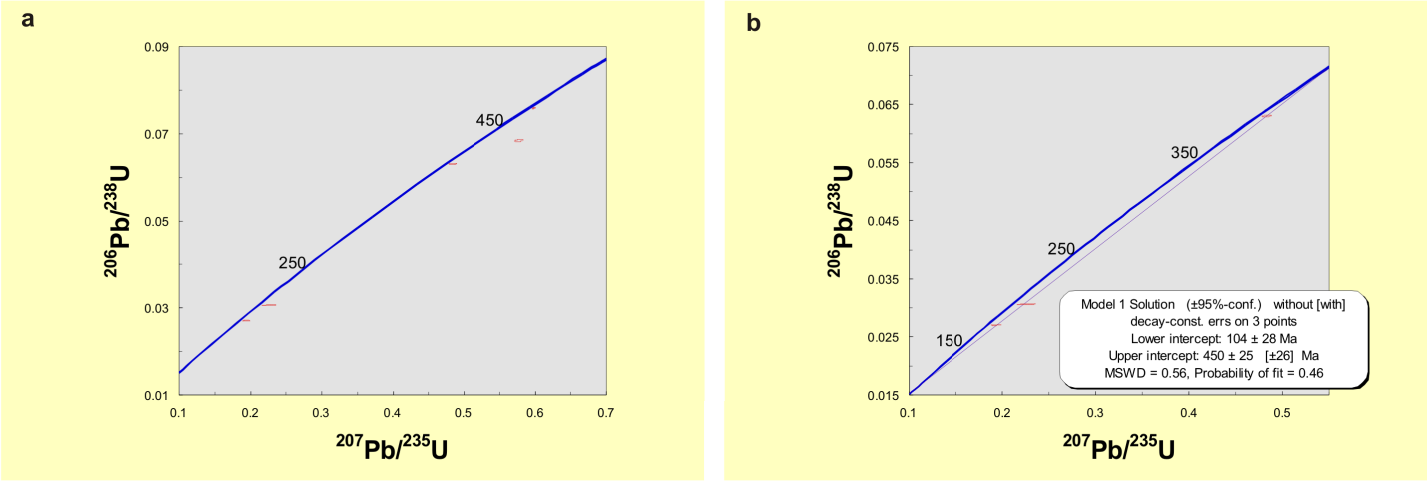

Figure 3-45. Results from single zircon U-Pb ID-TIMS dating for sample SG 063

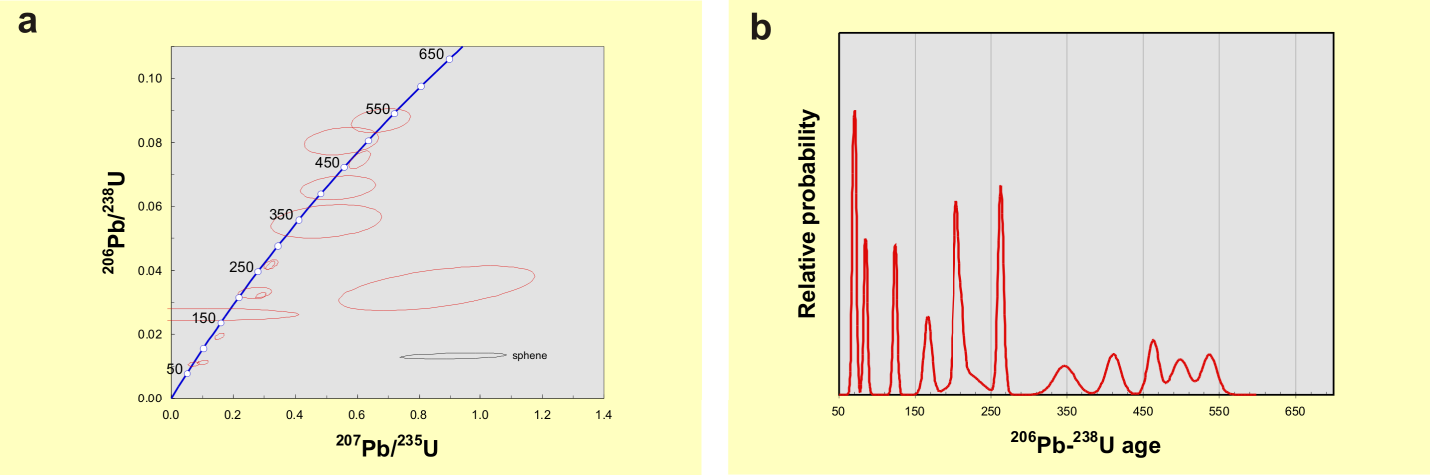

Figure 3-46. Results from single zircon U-Pb LA-ICPMS dating for sample SG 063

SG 066 – Qz-syenite dike, Vurli Brjag

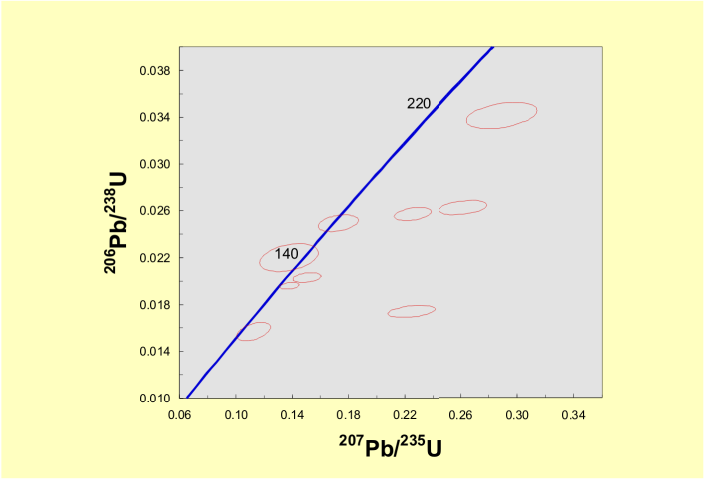

Nine variably discordant zircons dated by LA-ICPMS show scattered $^{206}Pb/^{238}U$ ages (Figure 3-47). Additional analyses are needed to constrain the age of the rock.

Figure 3-47. Results from single zircon U-PB LA-ICPMS dating for sample SG 066

SG 078 – Sub-alkaline granite, Rossen

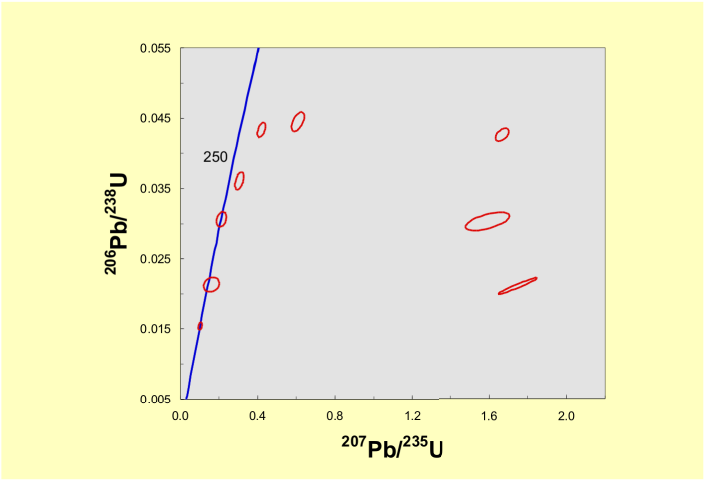

Nine zircons dated by LA-ICPMS show disturbed U-Pb systematics and some of the analyses plot away from the concordia band (***Figure 3-48***). Three grains are concordant within their assigned errors at ca. 99, 136 and 194 Ma. Additional analyses are needed to constrain the age of the rock. This sample has unusually radiogenic whole-rock Pb and Sr isotopes resembling the values of the Variscan basement in the Strandzha region. However, the zircon data provide indications that its age is younger than Carboniferous/Permian.

Figure 3-48. Results from single zircon U-Pb LA-ICPMS dating for sample SG 078

SG 079 – Diorite, Silistar

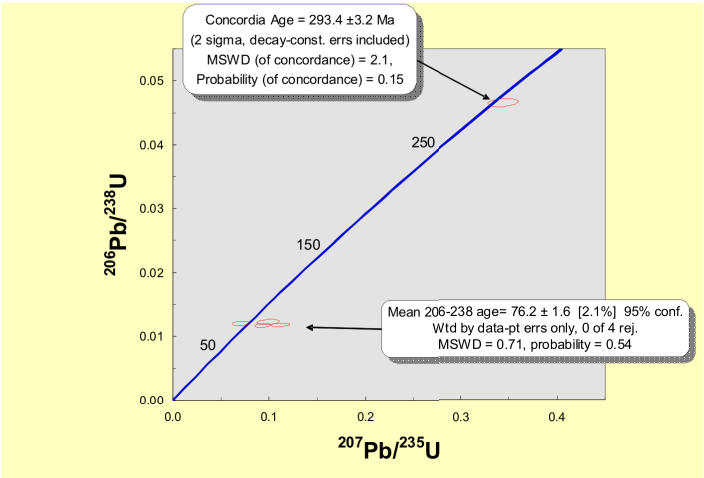

Five zircon were dated by LA-ICPMS. Four of them have similar $^{206}Pb/^{238}U$ ages with a weighted average of 76.2 ± 1.6 Ma and MSWD of 0.71 (***Figure 3-49***), which is considered to be the crystallization age of the rock. One older grain is concordant at 293.4 ± 3.2 Ma, 2 sigma level.

Figure 3-49. Results from single zircon U-Pb LA-ICPMS dating for sample SG 079

SG 090 – Ankaramite, Krushevets

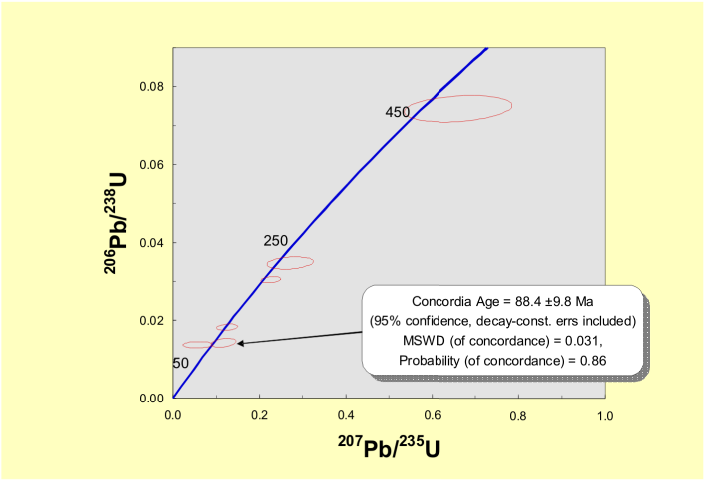

Six zircons analyzed by LA-ICPMS have $^{206}Pb/^{238}U$ ages ranging from Late Cretaceous to Ordovician (***Figure 3-50***). The two youngest zircons have limited overlap and yield a poorly defined concordia age of 88.4 ± 9.8 Ma at the 95% confidence level. Additional analyses are needed to better constrain the age of the rock.

Figure 3-50. Results from single zircon U-Pb LA-ICPMS dating for sample SG 090

SG 102d – Dacite, Tamarino Bakadzhik

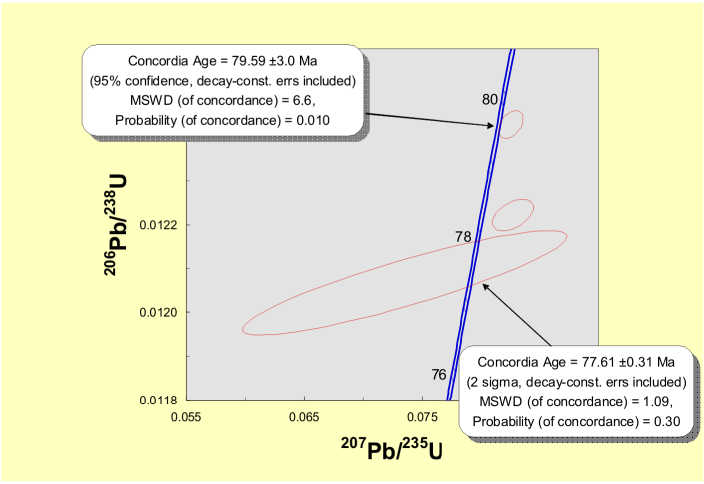

Figure 3-51. Results from single zircon U-PB ID-TIMS dating for sample SG 102d

The sample is from a weathered and altered dacite from the Tamarino Bakadzhik center. Three air abraded for 6 hours grains measured by ID-TIMS all show evidence of Pb loss (***Figure 3-51***) Two zircons overlap with the concordia band, one with larger error gives a concordia age of 77.61 ± 0.31 Ma at the 2 sigma level; the second zircon has smaller errors but overlaps only slightly with the concordia and yields an age of 79.59 ± 3.0 Ma at the 95% confidence levels. Published K_Ar ages for the Tamarino Bakadzhik are ~80 Ma. The three studied zircons may also have crystallized at ~80 Ma but later experienced small amounts of Pb loss which shifted their position off the concordia. Additional analyses are needed to better constrain the age of the rock.

LA-ICPMS data for eight zircons show $^{206}Pb/^{238}U$ ages ranging from 60 to 80 Ma (***Figure 3-52***a). Three grains overlap at ~80 Ma and yield a weighted average $^{206}Pb/^{238}U$ age of 80.1 ± 5.6 Ma. If all younger grains are considered, a discordia line can be constructed 73.0 ± 6.6 Ma and 1469 ± 240 Ma for the lower and upper intercept, respectively. The relative probability plot shows a Late Cretaceous peak, in addition to indications of a Permian-Triassic event (***Figure 3-52***c), whereas the Jurassic peak comes from a single, largely discordant zircon and is therefore less informative.

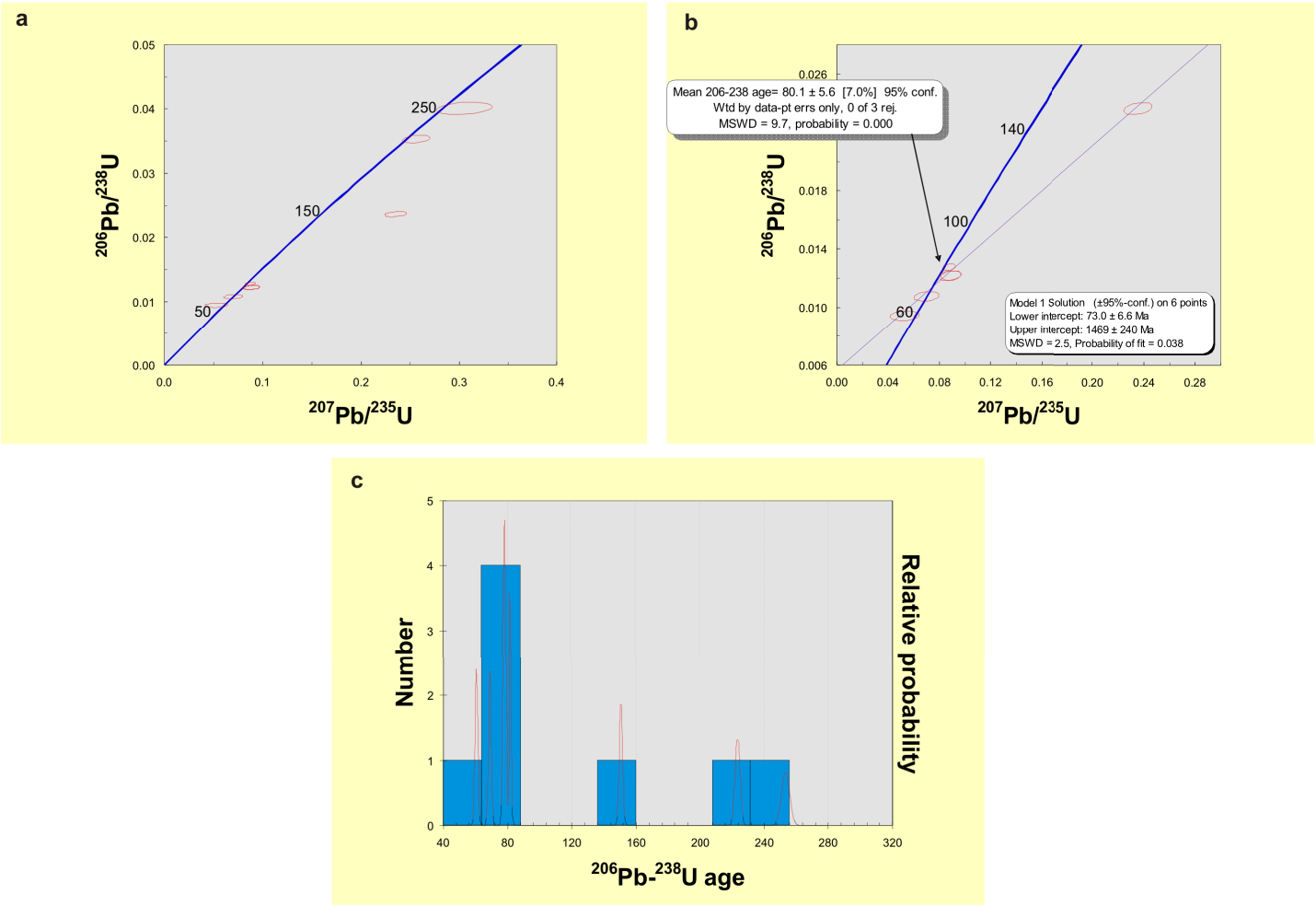

Figure 3-52. Results from single zircon U-Pb LA-ICPMS dating for sample SG 102d

SG 103 – Latite, Sv.Spaski Bakadzhik

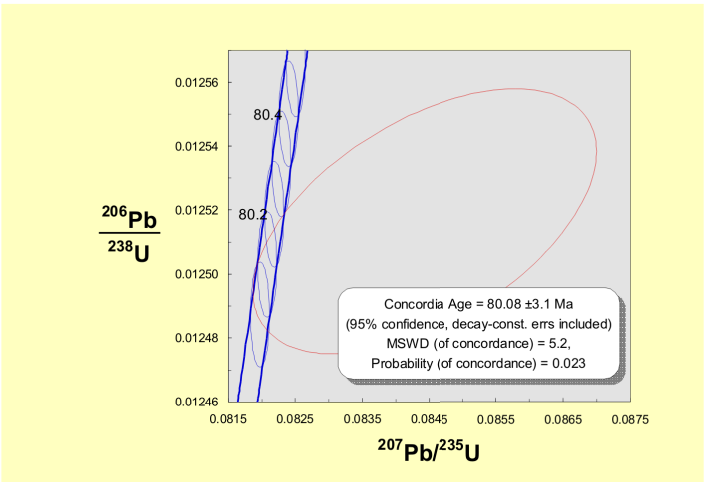

Figure 3-53. Results from single zircon U-Pb ID-TIMS dating for sample SG 103

The single grain analyzed by ID-TIMS has a concordia age of 80.08 ± 3.1 Ma, 95% confidence level (***Figure 3-53***), with a slight discordance.

Eight zircons dated by LA-ICPMS all show Late Cretaceous ages and plot at or near the concordia curve (***Figure 3-54***a). Their $^{206}Pb/^{238}U$ ages range from 72.3 to 81.3 Ma and produce a wide peak on the probability plot (***Figure 3-54***b). Five of the grains overlap within their error and yield a concordia age of 74.7 ± 1.9 Ma at the 95% confidence level (***Figure 3-54***c). A slightly older age of 75.69 Ma is given by the zircon age extraction algorithm (***Figure 3-54***d).

Given that the only ID-TIMS analyses has an older $^{206}Pb/^{238}U$ age of ~80 Ma, we consider the 76.8 ± 2.9 Ma weighted average $^{206}Pb/^{238}U$ age of all analyzed grains (***Figure 3-54***a) as the best

estimate for the crystallization age of the sample, regardless of the high MSWD value of 7. Additional analyses are needed to better constrain the age of the rock.

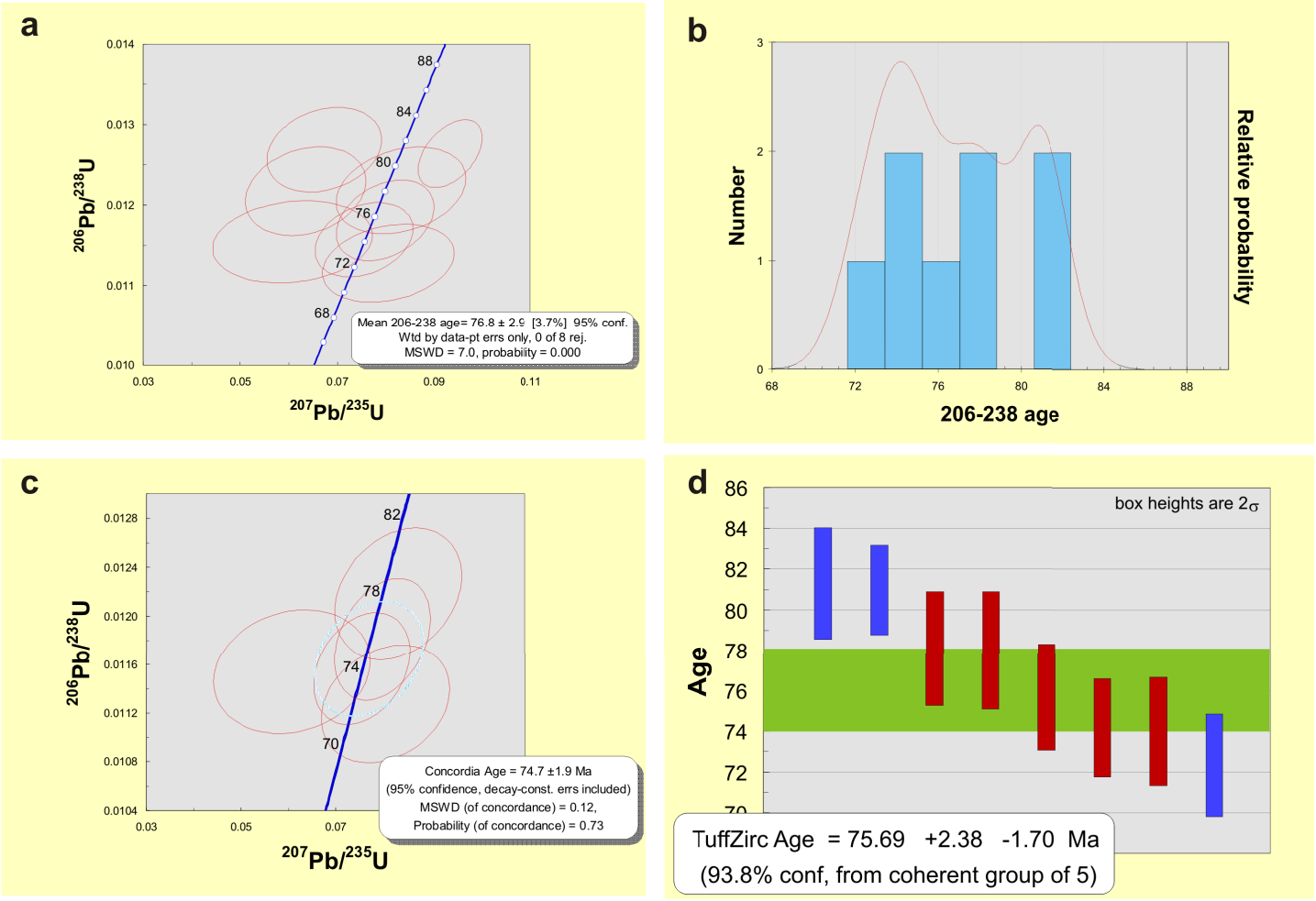

Figure 3-54. Results from single zircon U-Pb LA-ICPMS dating for sample SG 103

1.3. NORTH BURGAS region

SG 085 – Alkaline trachyte, Balgarovo

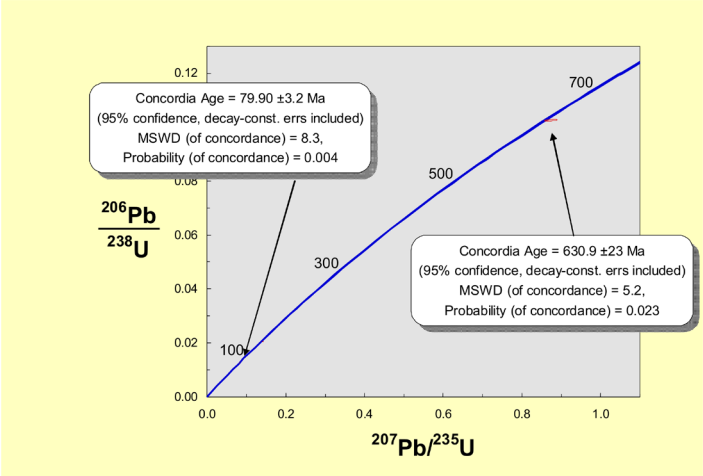

Figure 3-55. Results from single zircon U-Pb ID-TIMS dating for sample SG 085

Three grains analyzed by ID-TIMS yielded three different and slightly discordant ages (***Figure 3-55***). At the 95% confidence limit one zircon has a concordia age of 79.90 ± 3.2 Ma and the oldest grain yields a concordia age of 630.9 ± 23 Ma (***Figure 3-55***).

Both grains have older $^{207}Pb/^{235}U$ ages and it is possible that they experienced Pb loss, or that they have an older inherited component. Three zircons and one apatite grain, analyzed by LA-ICPMS have largely discordant and older than Late Cretaceous ages. Additional analyses are needed to constrain the age of the rock.

1.4. EAST BALKAN region

SG 068 – Diorite porphyry

The sample is collected at Assara peak in the Eastern Balkan Mountains, near the village of Zvezda. Thirteen zircon grains and four monazites were analyzed by ID-TIMS. The analyzed air abraded and chemically abraded zircons show a wide range of $^{206}Pb/^{238}U$ ages from ca. 41 to 366 Ma (***Figure 3-56***a). Four zircons are concordant within their relatively large errors at 41.55 ± 0.10 Ma, 61.18 ± 0.27 Ma, 136.23 ± 0.44 Ma and 290.7 ± 2.9 Ma respectively (***Figure 3-57***).

Two chemically abraded zircons are concordant with considerably smaller error ellipses at 298.98 ± 0.50 Ma, 303.49 ± 0.45 Ma respectively and demonstrate the upper limits of precision and concordance achieved in this study (***Figure 3-58***, b). The zircons with the oldest $^{206}Pb/^{238}U$ ages are slightly displaced from the concordia band and yield concordia ages of 349.94 ± 9.6 Ma and 366.20 ± 12 Ma within their 95% confidence interval (***Figure 3-58***c, d). Despite the large number of concordant grains, the analyses do not overlap and the age of the rock cannot be determined. There seem to be no systematic relation between the $^{206}Pb/^{238}U$ age and the variable external morphology of the zircons.

None of the chemically abraded zircons shows the Eocene-Paleocene (42 and 61 Ma) ages. The younger 42 and 61 Ma zircons have comparatively larger errors, which hinders detail age interpretation. An attempt was made to calculate possible discordia lines with the remaining discordant zircons. The three scenarios that yield statistically reasonable MSWD (***Figure 3-56*** b, c, d) indicate a possible Early Cretaceous event in addition to the well defined from the concordant zircons Carboniferous/Permian inheritance. In an unsuccessful attempt to determine the age of the rock, additional ten zircons (***Figure 3-59***) and two sphene grains were analyzed by

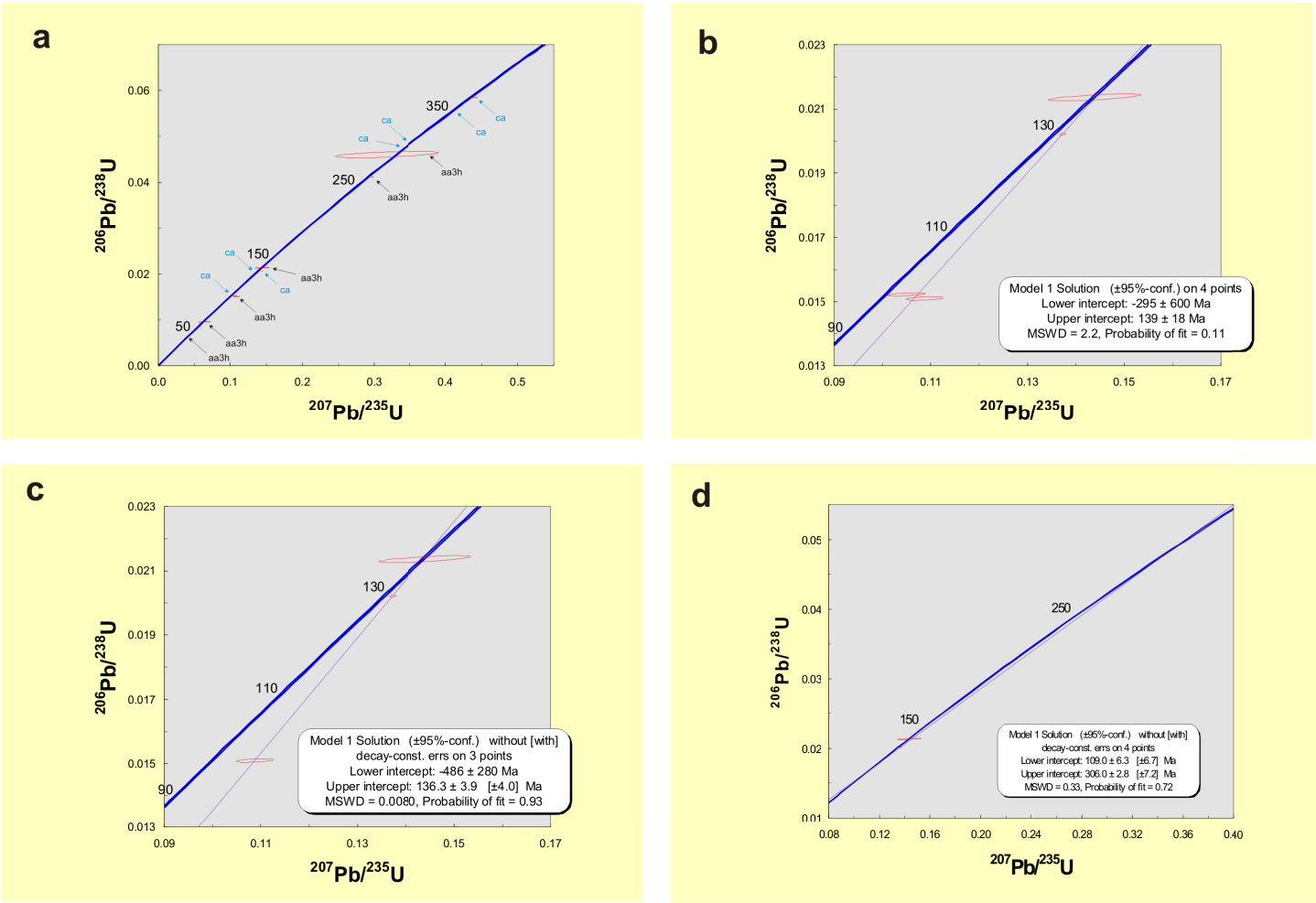

Figure 3-56. Results from single zircon U-Pb ID-TIMS dating for sample SG 068

LA-ICPMS. Zircon data is scattered and several possible groups can be recognized based on their $^{206}Pb/^{238}U$ age, including the clustering of three data points at ca. 80 Ma. The sphene grains are grossly discordant.

The combined ID-TIMS and LA-ICPMS age data for SG 068 zircons are presented on ***Figure 3-60***. The relative probability of the zircon measurements indicates peaks at ca. 61, 96 and 131 Ma in addition to the Variscan peaks. The position and height of the peaks are controlled dominantly the more precise ID-TIMS data.

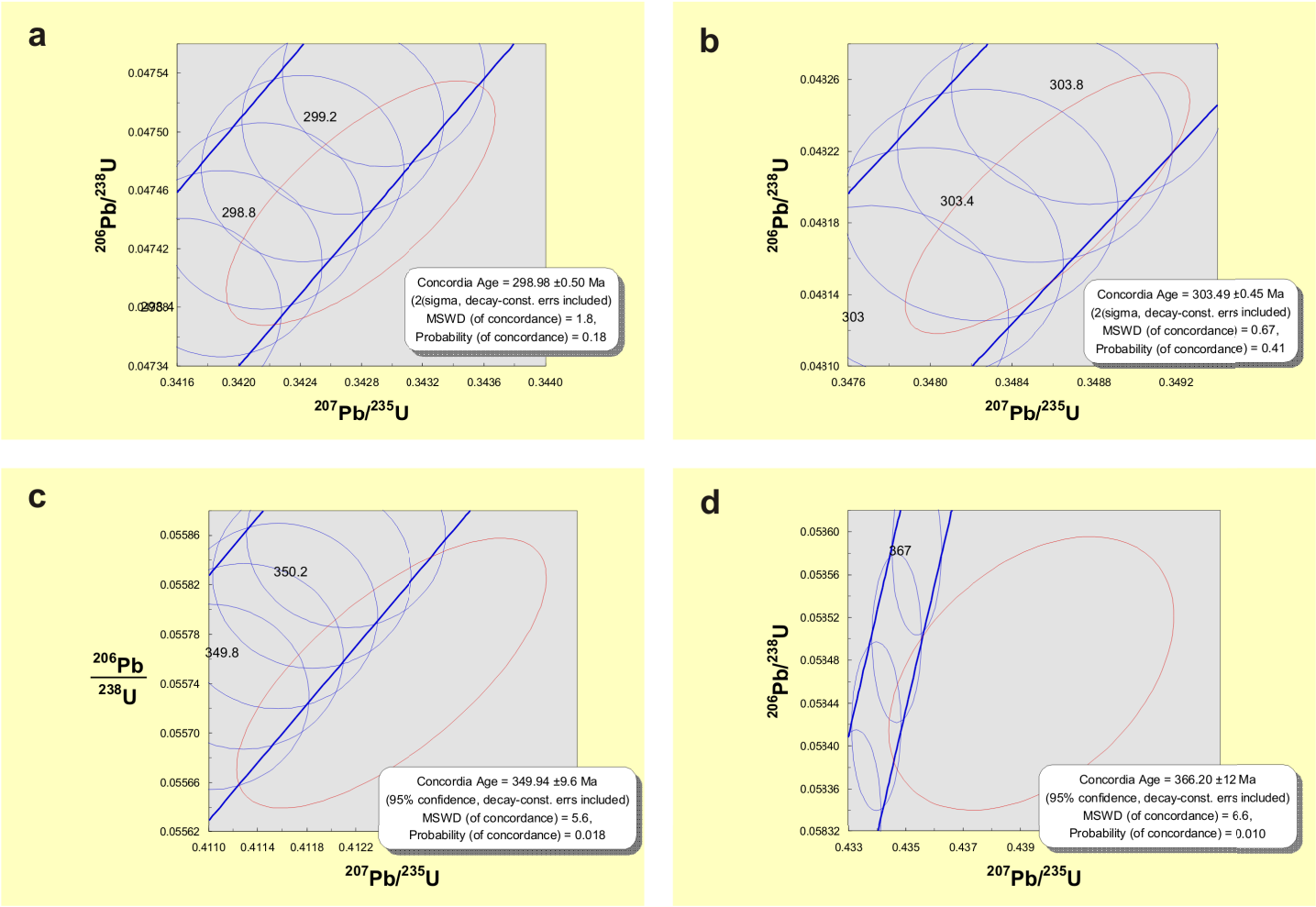

Figure 3-57. Results from single zircon U-Pb ID-TIMS dating for sample SG 068

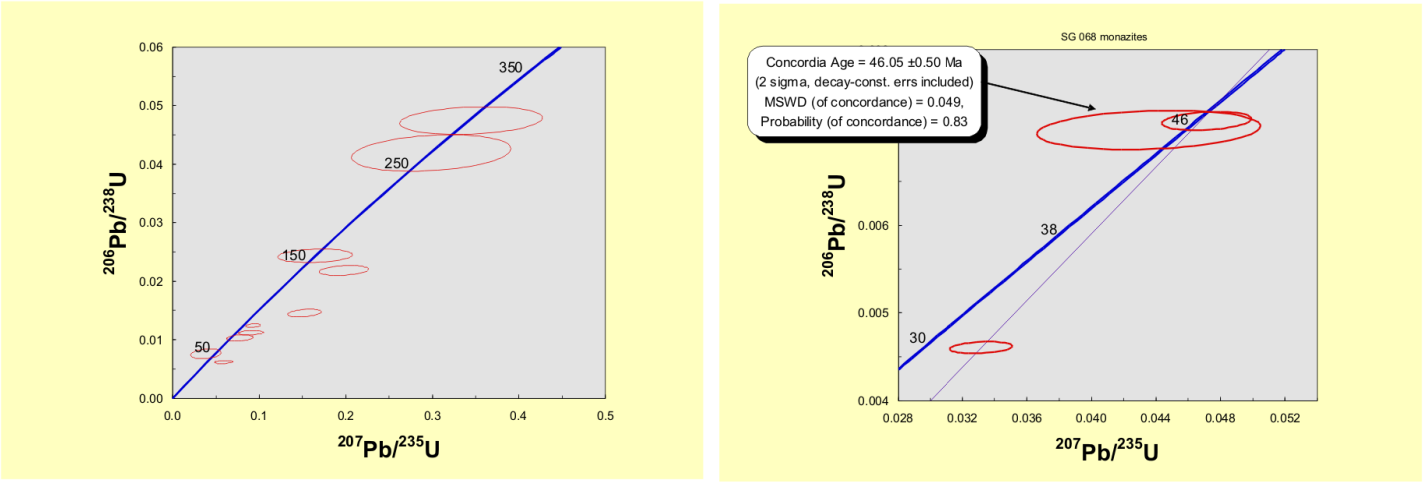

Figure 3-59. Results from single zircon U-PB LA-ICPMS dating for sample SG 068

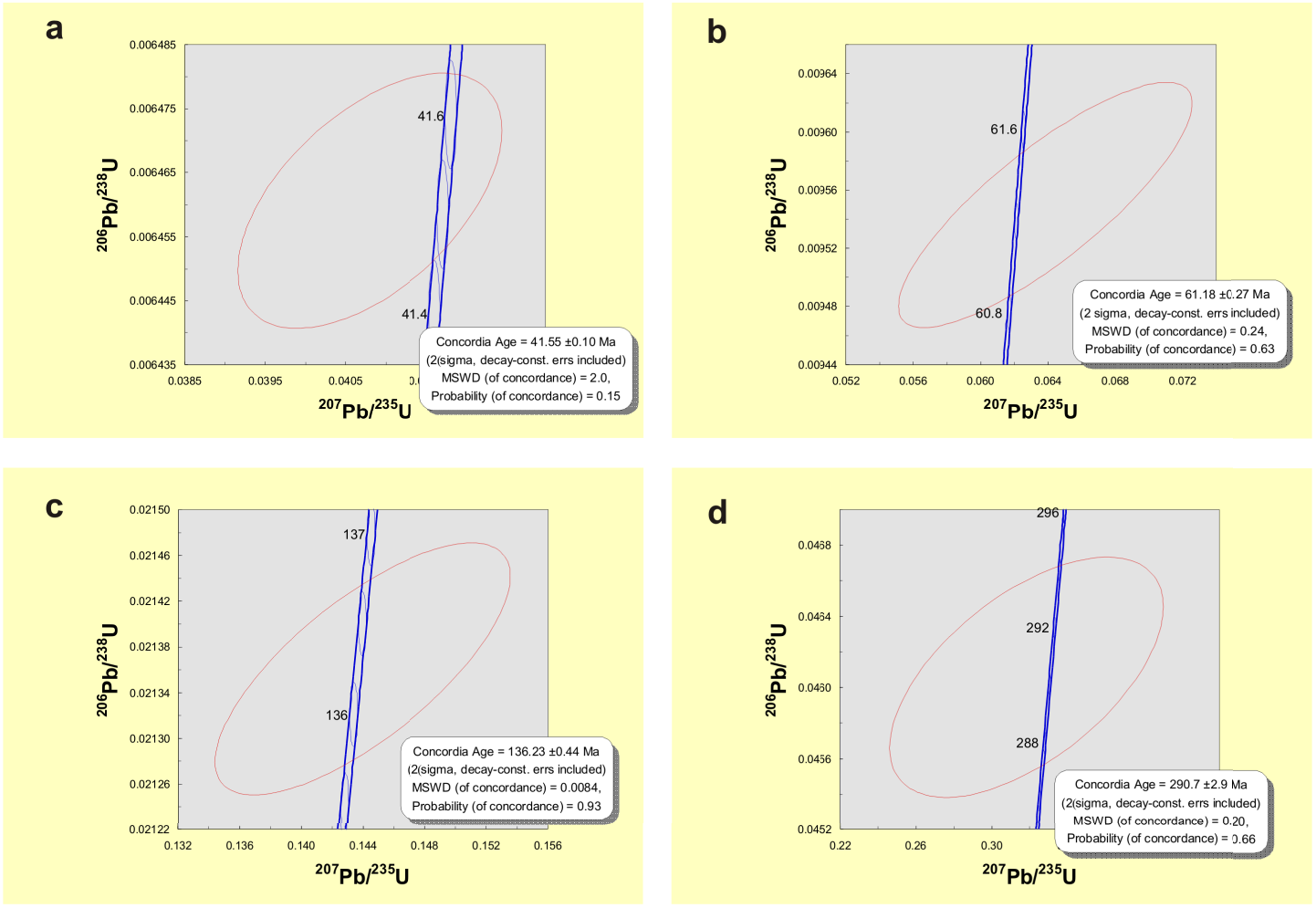

Figure 3-58. Results from single zircon U-Pb ID-TIMS dating for sample SG 068

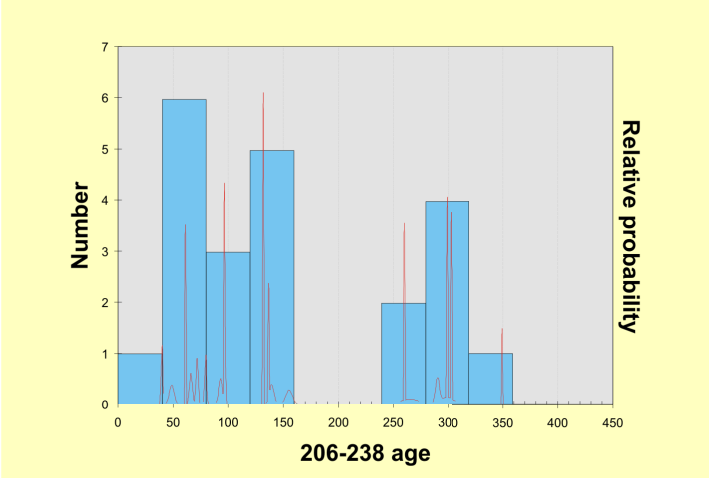

Figure 3-60. Combined results from single zircon U-PB ID-TIMS and LA-ICPMS dating for sample SG 068

SG 069 – Qz-diorite dike

The studied dike cut Triassic flysch sediments near the village of Zvezda. Three chemically abraded zircons analyzed by ID-TIMS all cross the concordia line and single zircon concordia ages can be calculated at ~52, 97 and 281 Ma for each analysis (***Figure 3-61***). The zircon with the youngest age has high Pb content and anomalously low $^{206}Pb^{*}/^{204}Pb$ ratios and was probably contaminated with common Pb.

The measurements do not lie on a discordia line and the crystallization age of the dike cannot be determined. LA-ICPMS data for 9 zircons indicate the presence of a 250-350 Ma old inherited component (***Figure 3-62***). One zircon has a $^{206}Pb/^{238}U$ age of 71 Ma, while the youngest grain is concordant at 53.71 ± 0.69 Ma, two sigma errors. This age alone cannot be confidently considered as a crystallization age of the sample, but nevertheless indicates, in a similar way as data for sample SG 068 that compared to the other regions of Eastern Srednogorie, the rocks from the East Balkan region were affected by some younger, post-Late Cretaceous event.

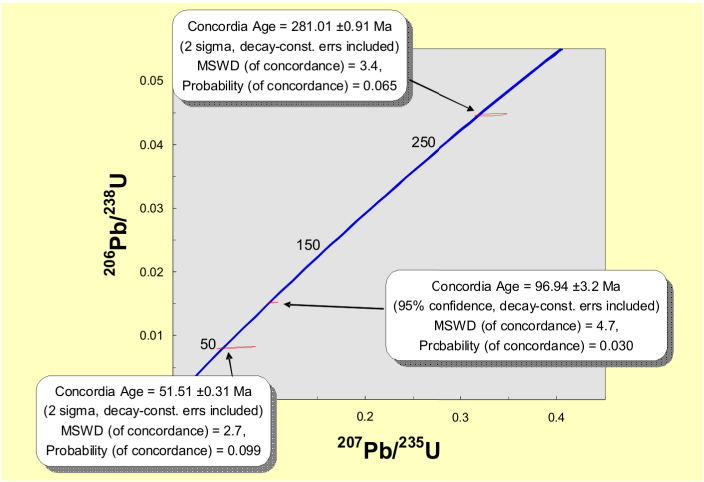

Figure 3-61. Results from single zircon U-PB ID-TIMS dating for sample SG 069

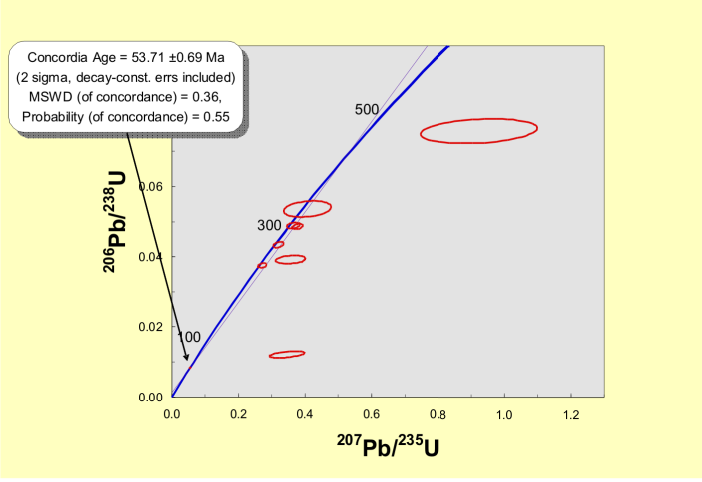

Figure 3-62. Results from single zircon U-PB LA-ICPMS dating for sample SG 069

SG 093 – Andesite, Zaimchevo

This sample is collected between the villages of Zaimchevo and Kamnjak. The three non-abraded zircons dated by ID-TIMS lie on a discordia with an upper intercept of 577 ± 57 Ma and a lower intercept at 258 ± 15 Ma, with a MSWD of 0.13 (***Figure 3-63***a). The youngest grain alone yields a concordia age of 270.65 ± 0.69 Ma, 2 sigma errors, reflecting assimilation of Variscan basement by the Late Cretaceous magmas.

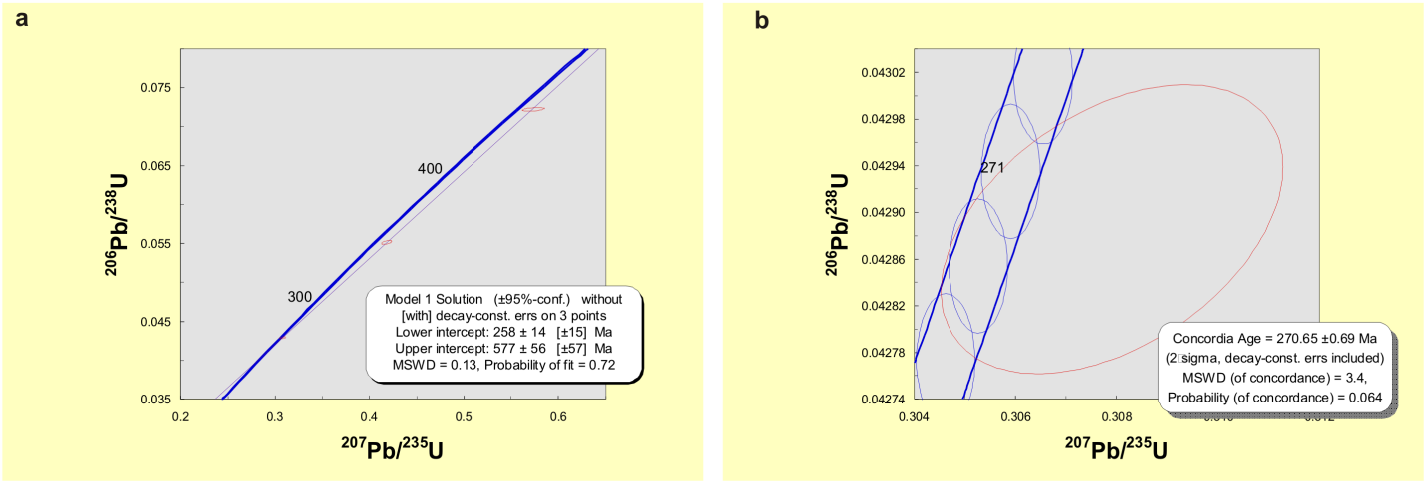

Figure 3-63. Results from single zircon U-PB ID-TIMS dating for sample SG 093

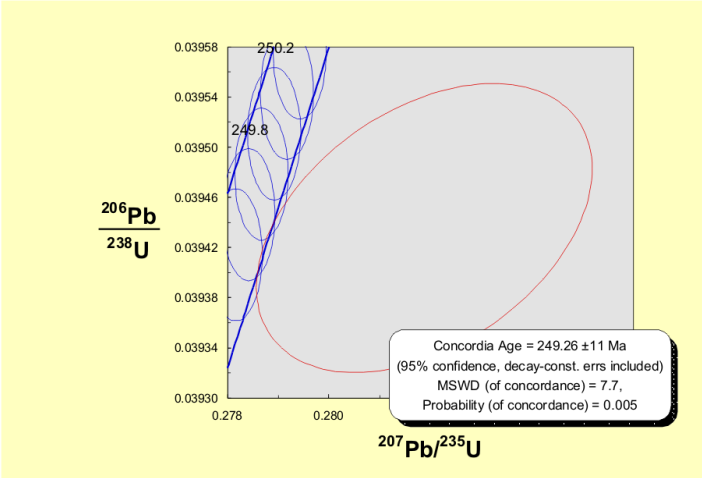

Figure 3-64. Results from single zircon U-PB ID-TIMS dating for sample SG 107

SG 107 – Rhyolite, Karandila

A single zircon dated by ID-TIMS shows slight discordance, but crosses the concordia band and gives and age of 249.26 ± 1 Ma at the 95 % confidence limit (***Figure 3-64***). Additional analyses are needed to constrain the age of the rock.

Appendix 4. CL and BSE images with LA-ICPMS ^{206}Pb-^{238}U ages

Cathodoluminiscence (CL) and backscattered images (BSE) of zircons, showing the location and diameter of laser craters (solid circles) and the calculated ^{206}Pb-^{238}U age with corresponding 2σ uncertainties. The grain number (lower right) and lab number of the LA-ICPMS dating analyses (e.g. Ar01c04) are also provided, as a reference to Appendix 2. Samples are arranged alphabetically, starting with AvQ samples (pages 1-6) followed by SG-samples (pages 7-19) and sample St 25 (page 19).

AvQ 046

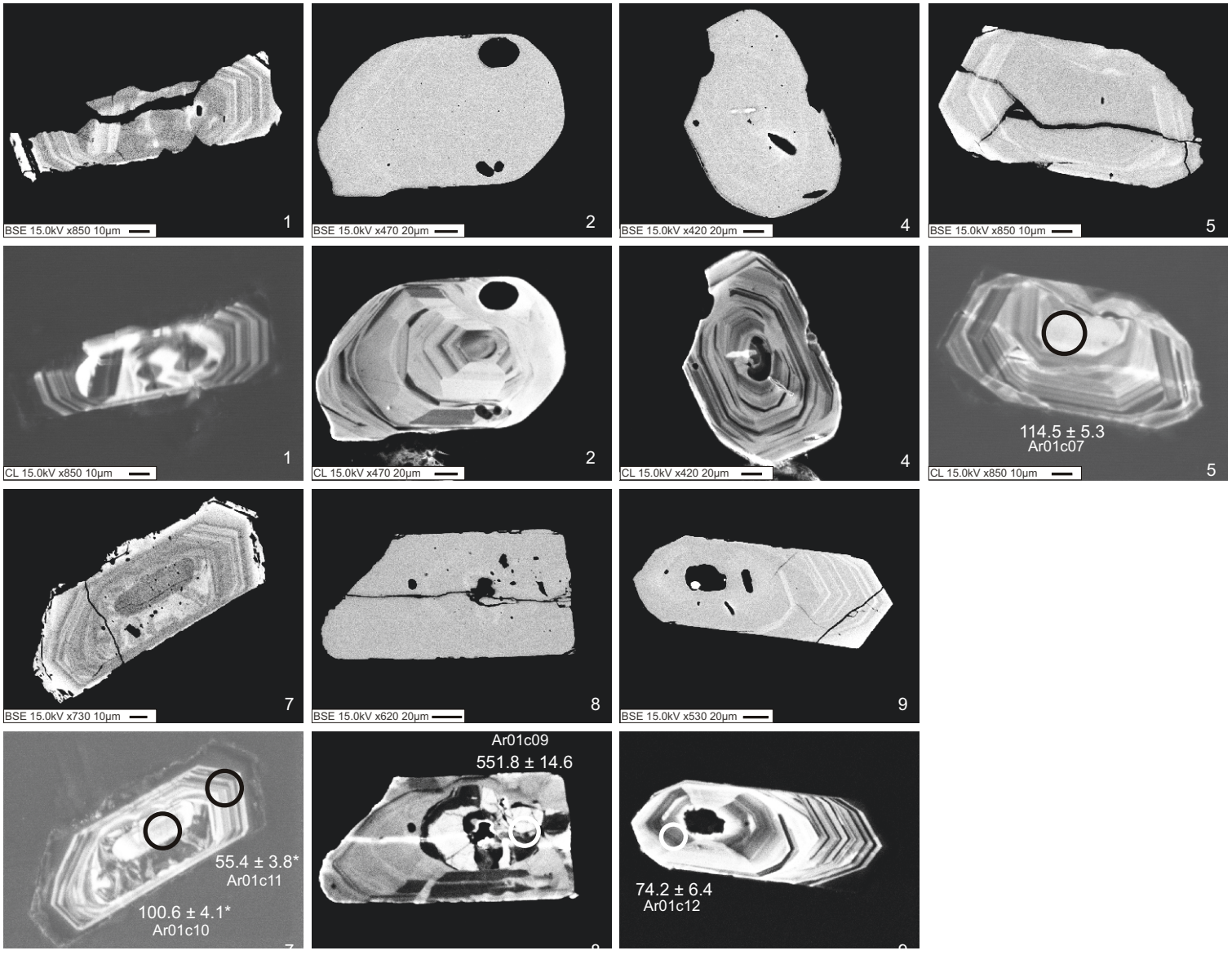

AvQ 048

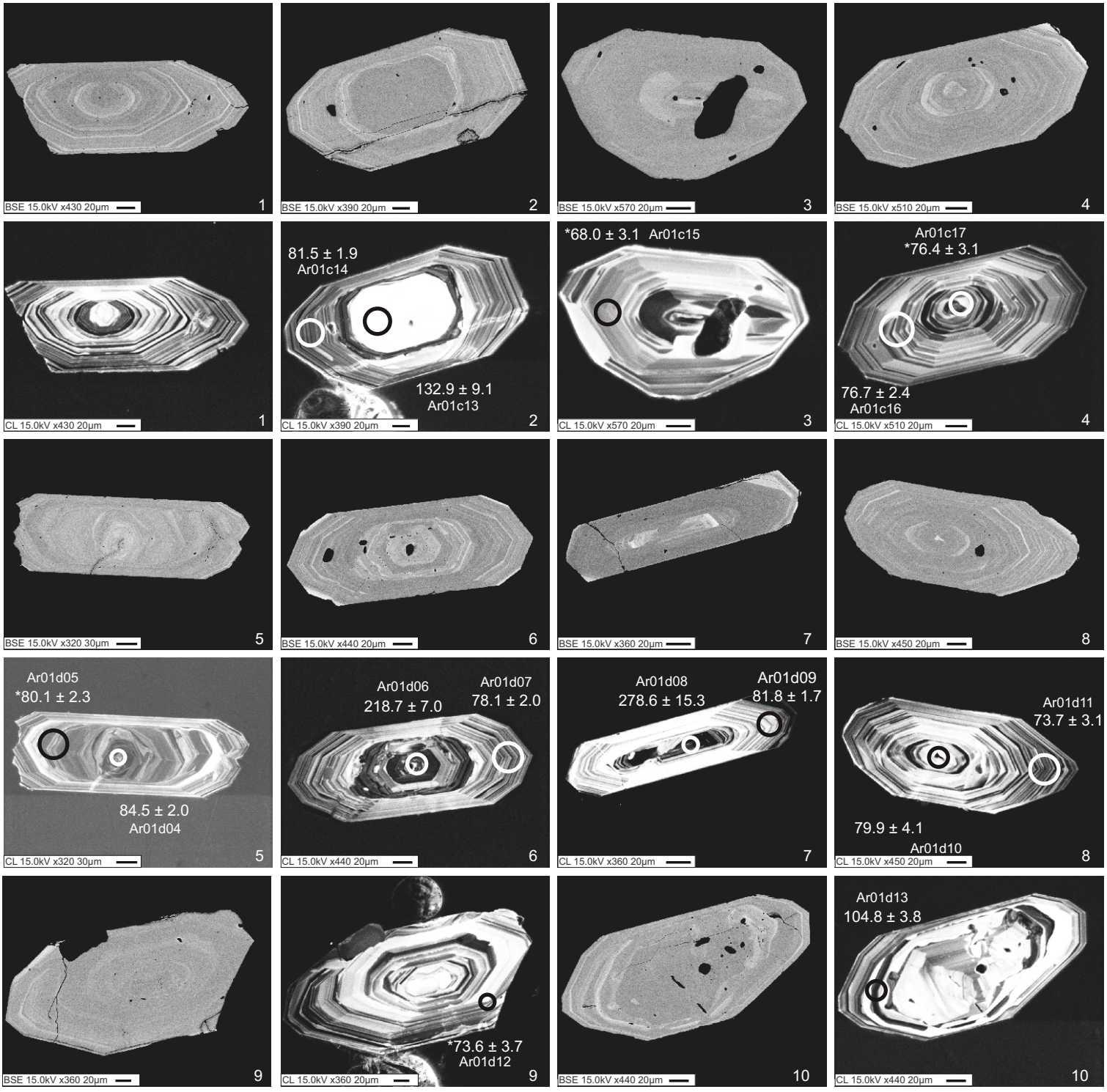

AvQ 050

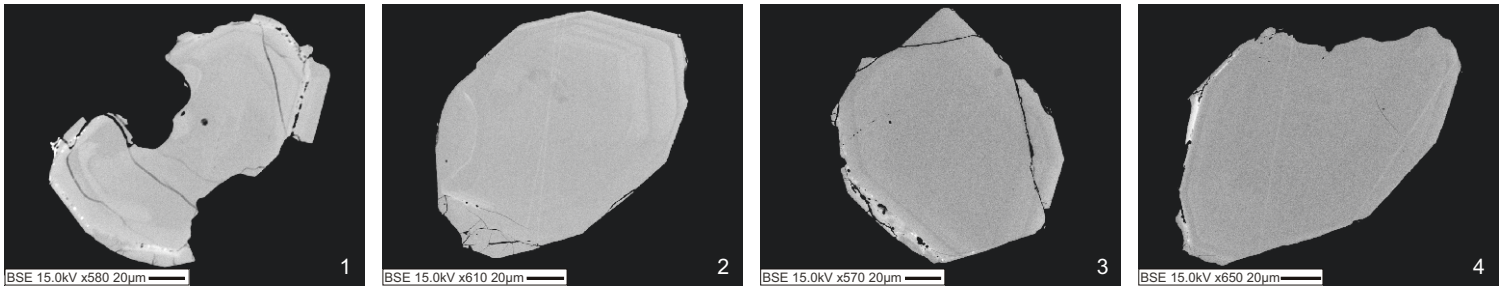

AvQ 050-continued

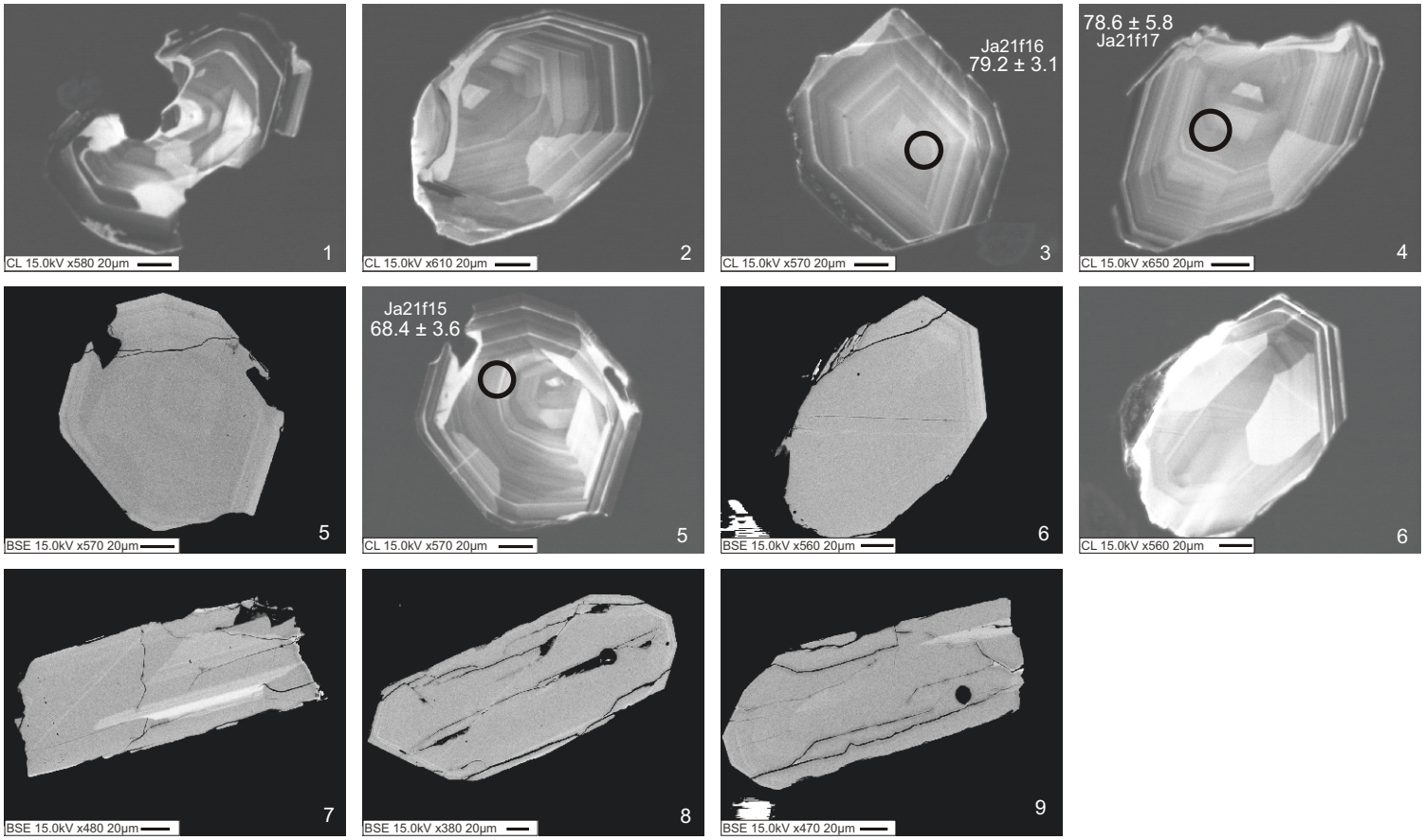

AvQ 051

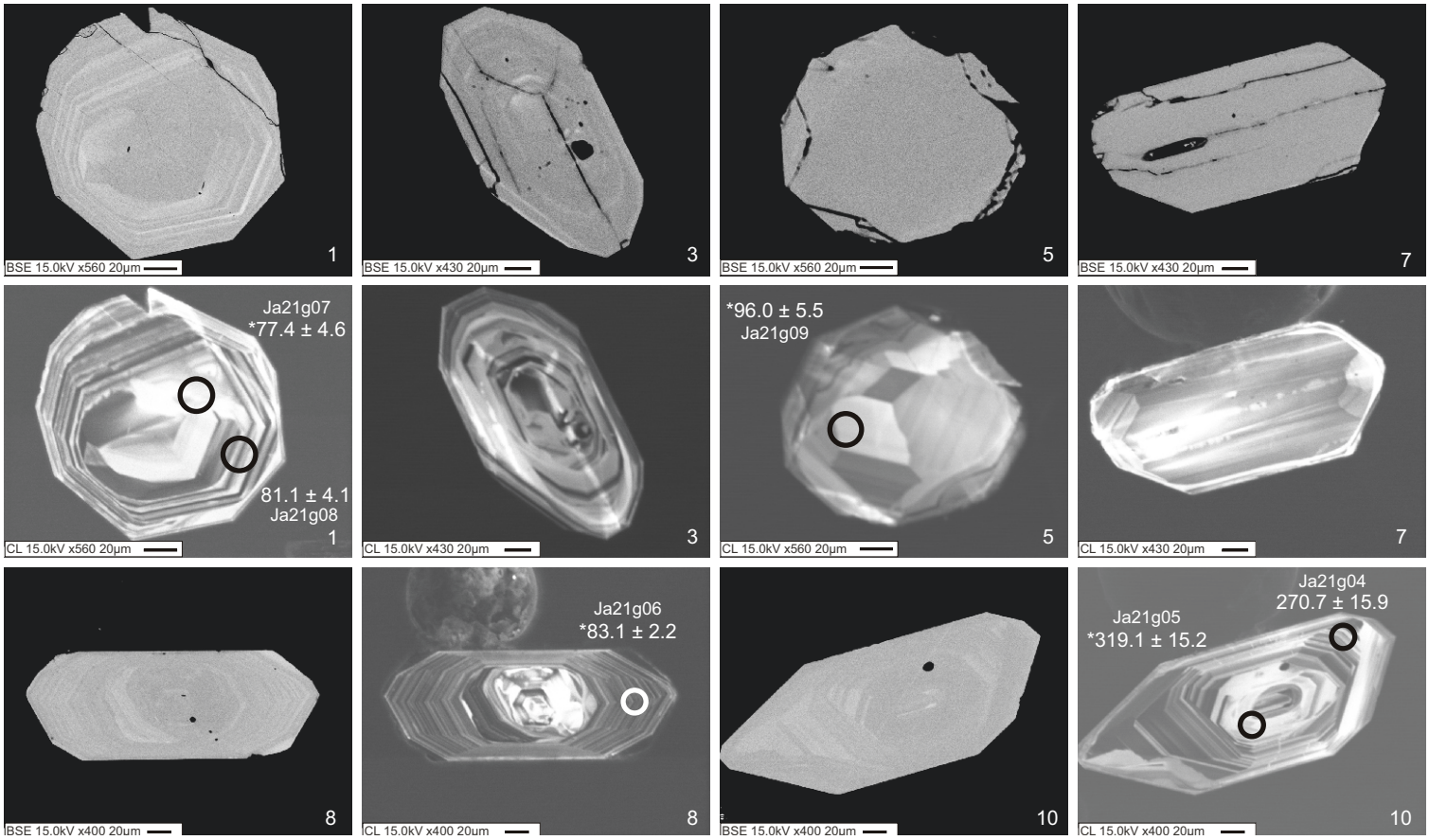

AvQ 054

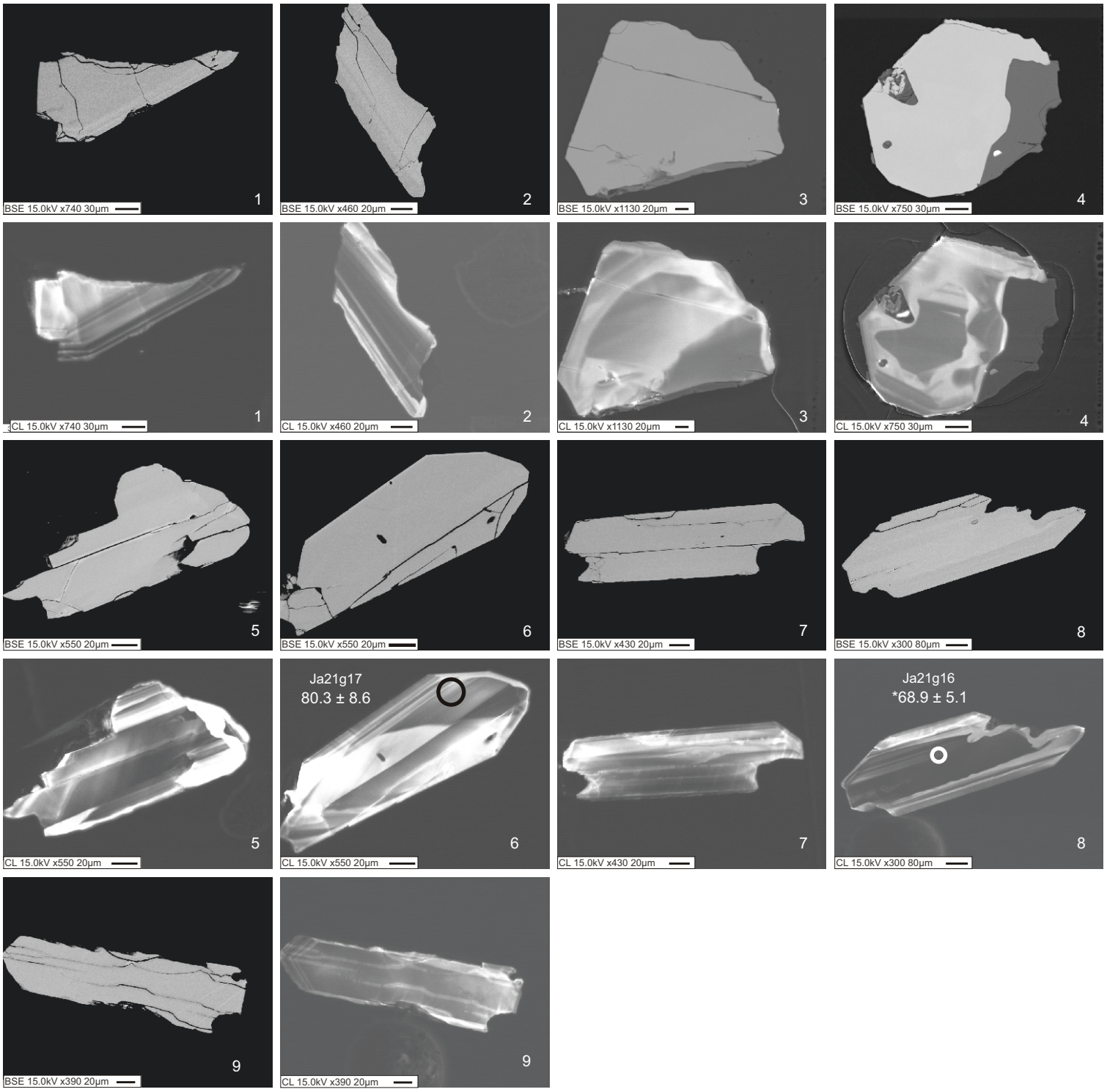

AvQ 055

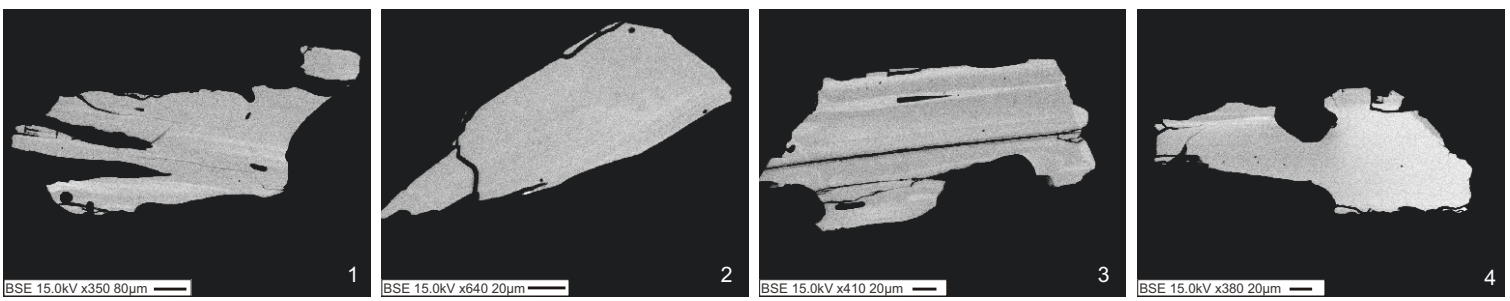

AvQ 055-continued

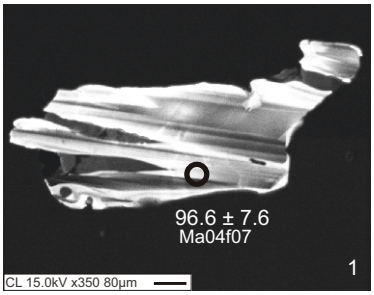

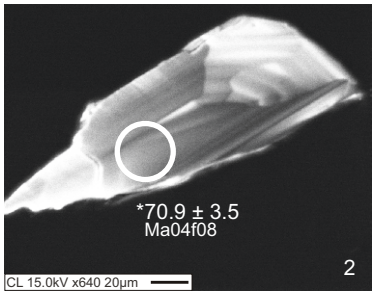

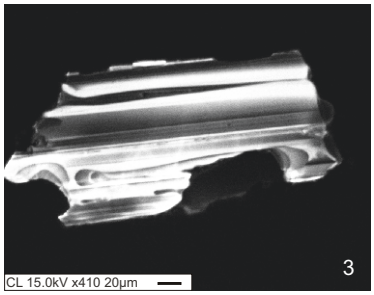

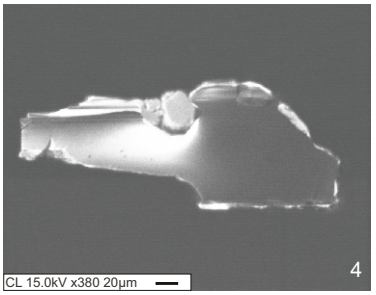

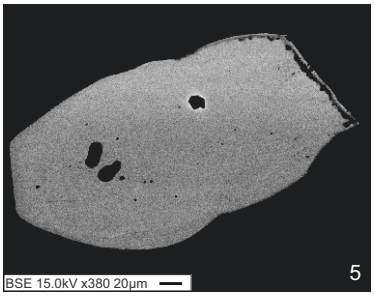

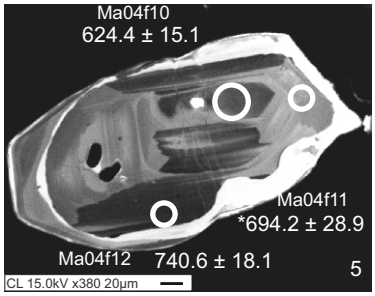

AvQ 057

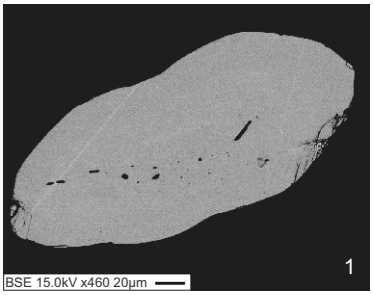

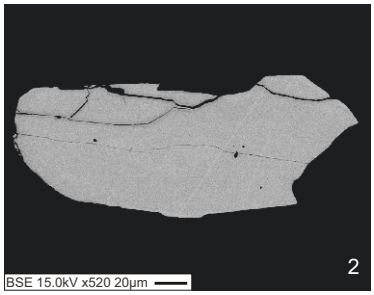

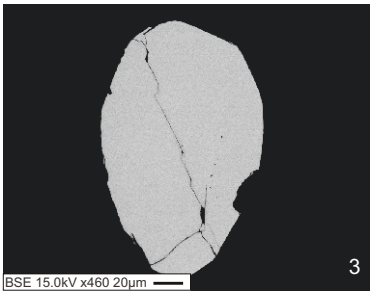

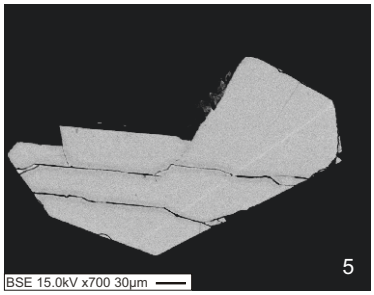

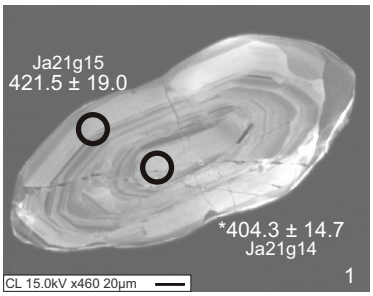

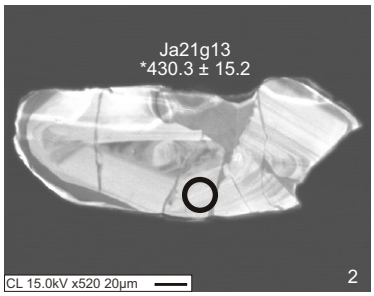

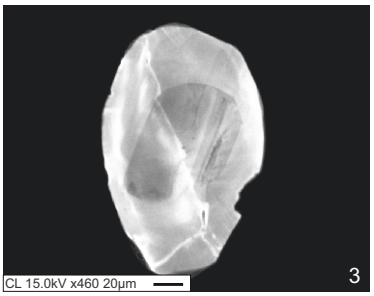

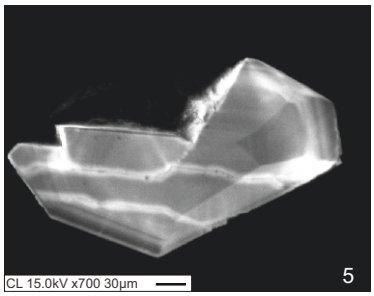

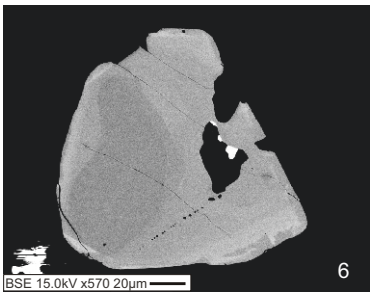

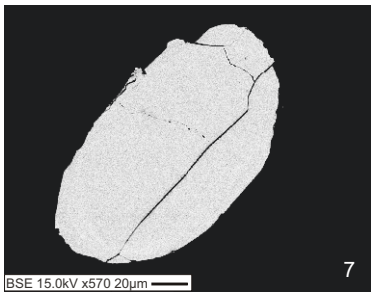

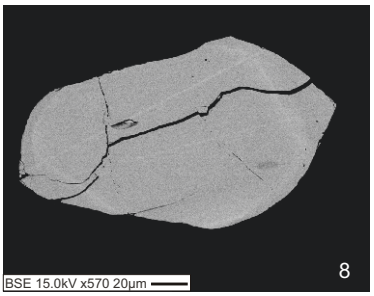

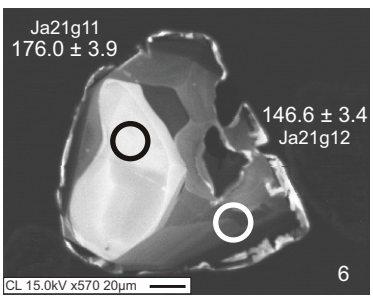

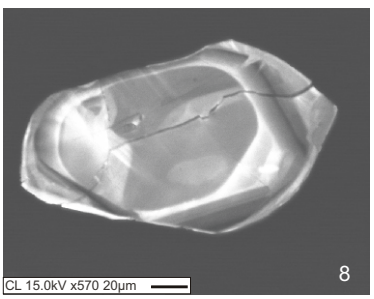

AvQ 058

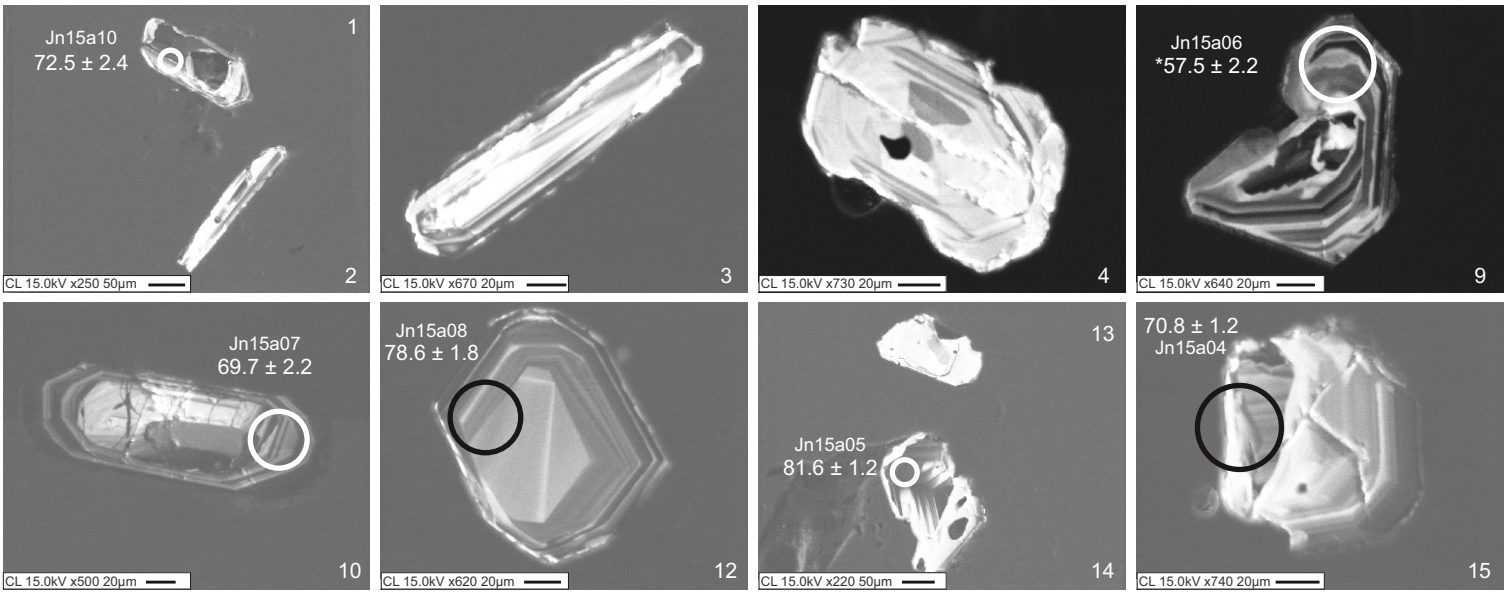

AvQ 142

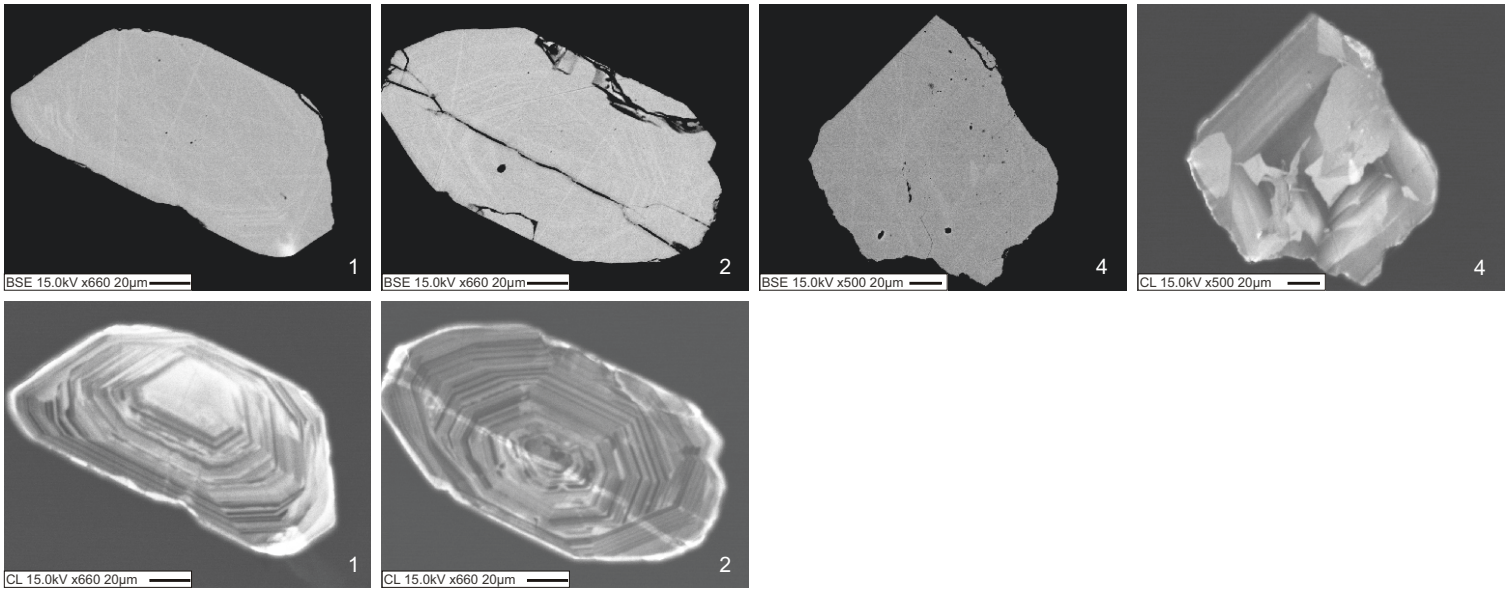

SG 001

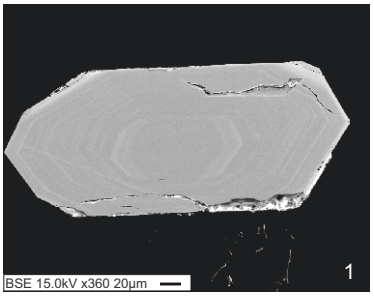
BSE 15.0kV x360 20µm
1

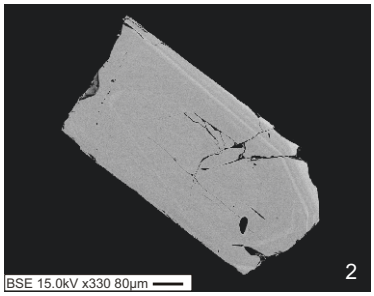
BSE 15.0kV x330 80µm
2

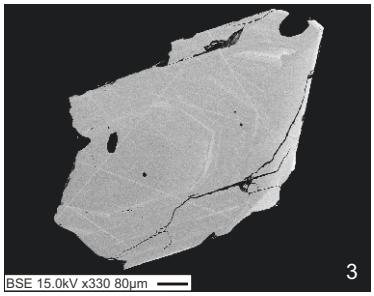
BSE 15.0kV x330 80µm
3

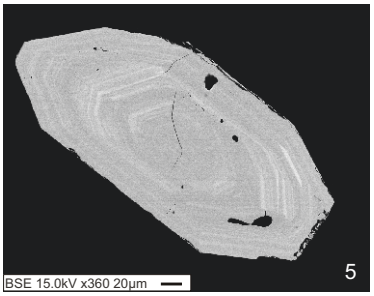
BSE 15.0kV x360 20µm
5

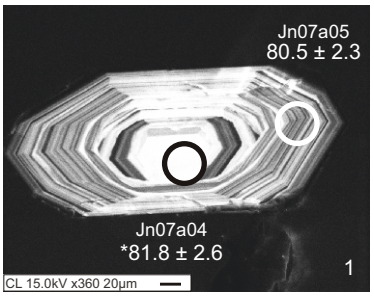
Jn07a05
80.5 ± 2.3
Jn07a04
*81.8 ± 2.6
CL 15.0kV x360 20µm
1

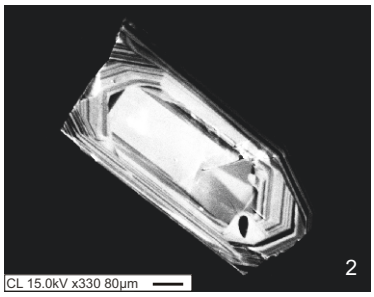
CL 15.0kV x330 80µm
2

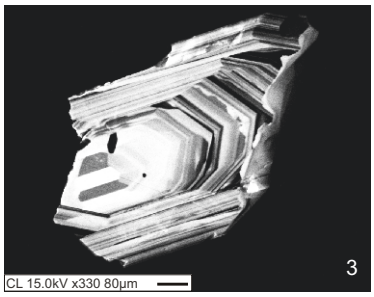
CL 15.0kV x330 80µm
3

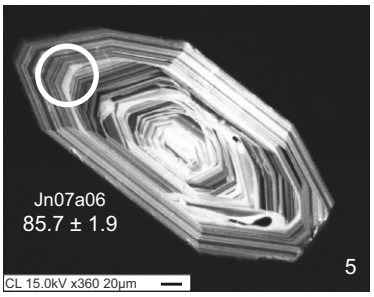
Jn07a06
85.7 ± 1.9
CL 15.0kV x360 20µm
5

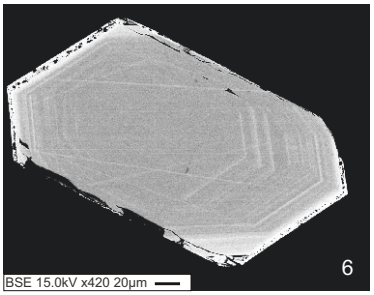
BSE 15.0kV x420 20µm
6

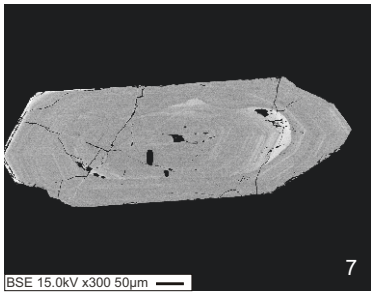
BSE 15.0kV x300 50µm
7

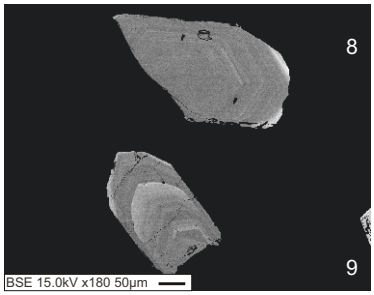
8
BSE 15.0kV x180 50µm
9

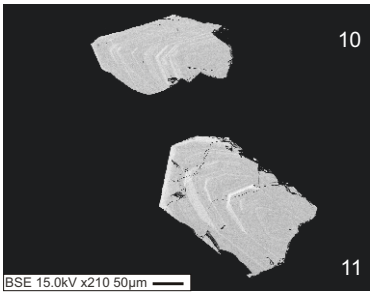
10
BSE 15.0kV x210 50µm
11

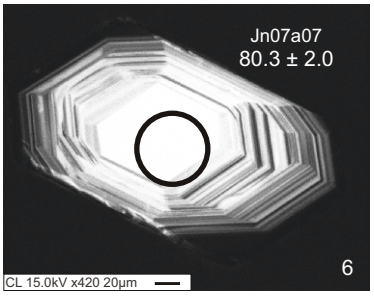
Jn07a07
80.3 ± 2.0
CL 15.0kV x420 20µm
6

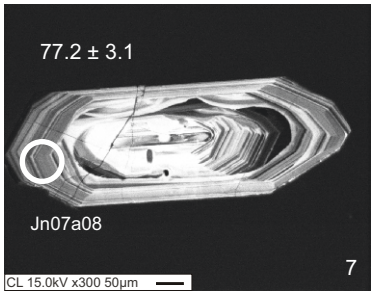
77.2 ± 3.1
Jn07a08
CL 15.0kV x300 50µm
7

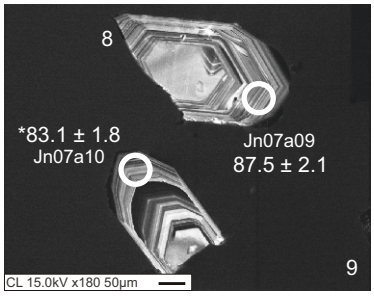
8
*83.1 ± 1.8
Jn07a10
Jn07a09
87.5 ± 2.1
CL 15.0kV x180 50µm
9

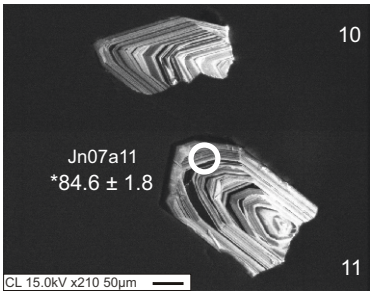
10
Jn07a11
*84.6 ± 1.8
CL 15.0kV x210 50µm
11

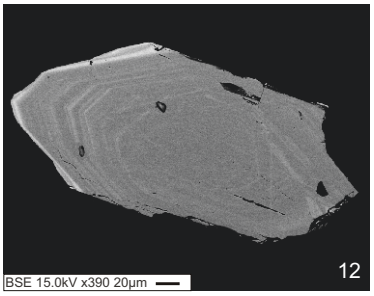
BSE 15.0kV x390 20µm
12

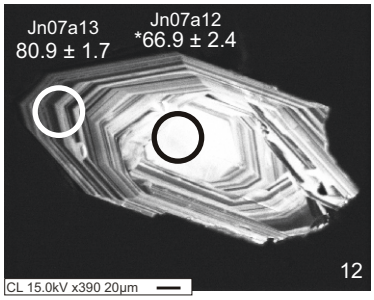
Jn07a13
80.9 ± 1.7
Jn07a12
*66.9 ± 2.4
CL 15.0kV x390 20µm
12

SG 011

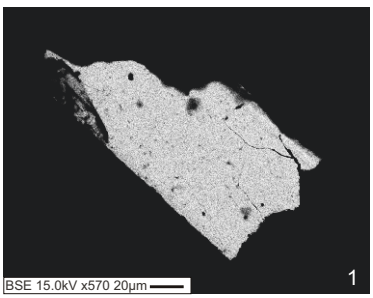
BSE 15.0kV x570 20µm
1

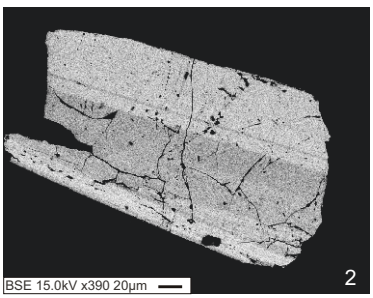
BSE 15.0kV x390 20µm
2

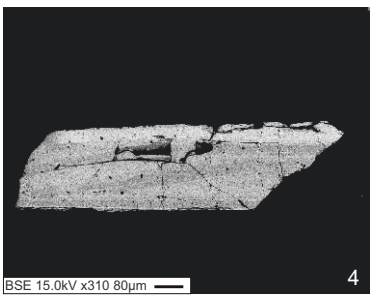
BSE 15.0kV x310 80µm
4

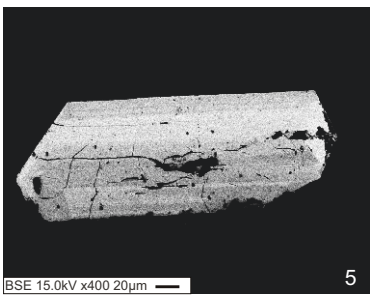
BSE 15.0kV x400 20µm
5

SG 011-continued

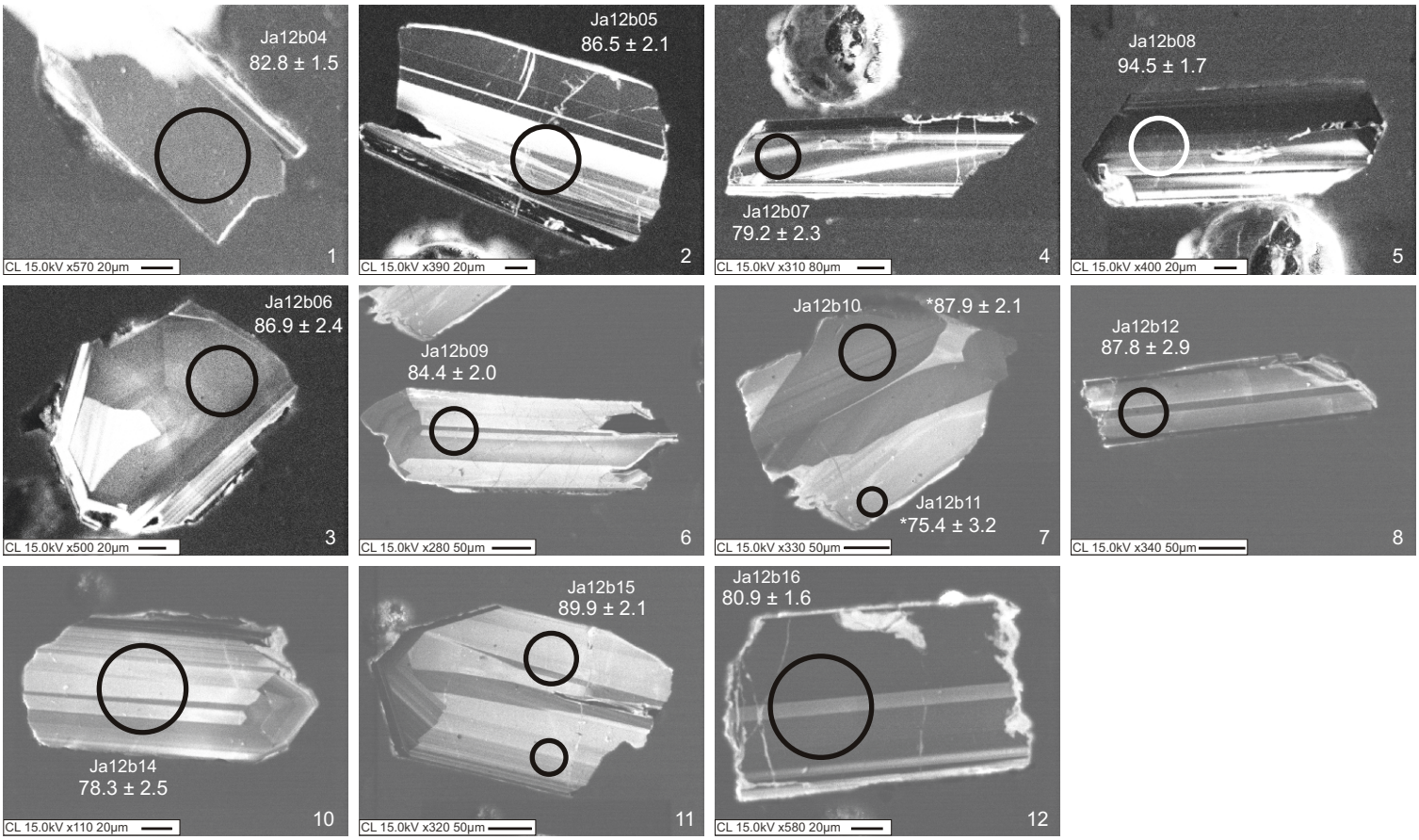

SG 028

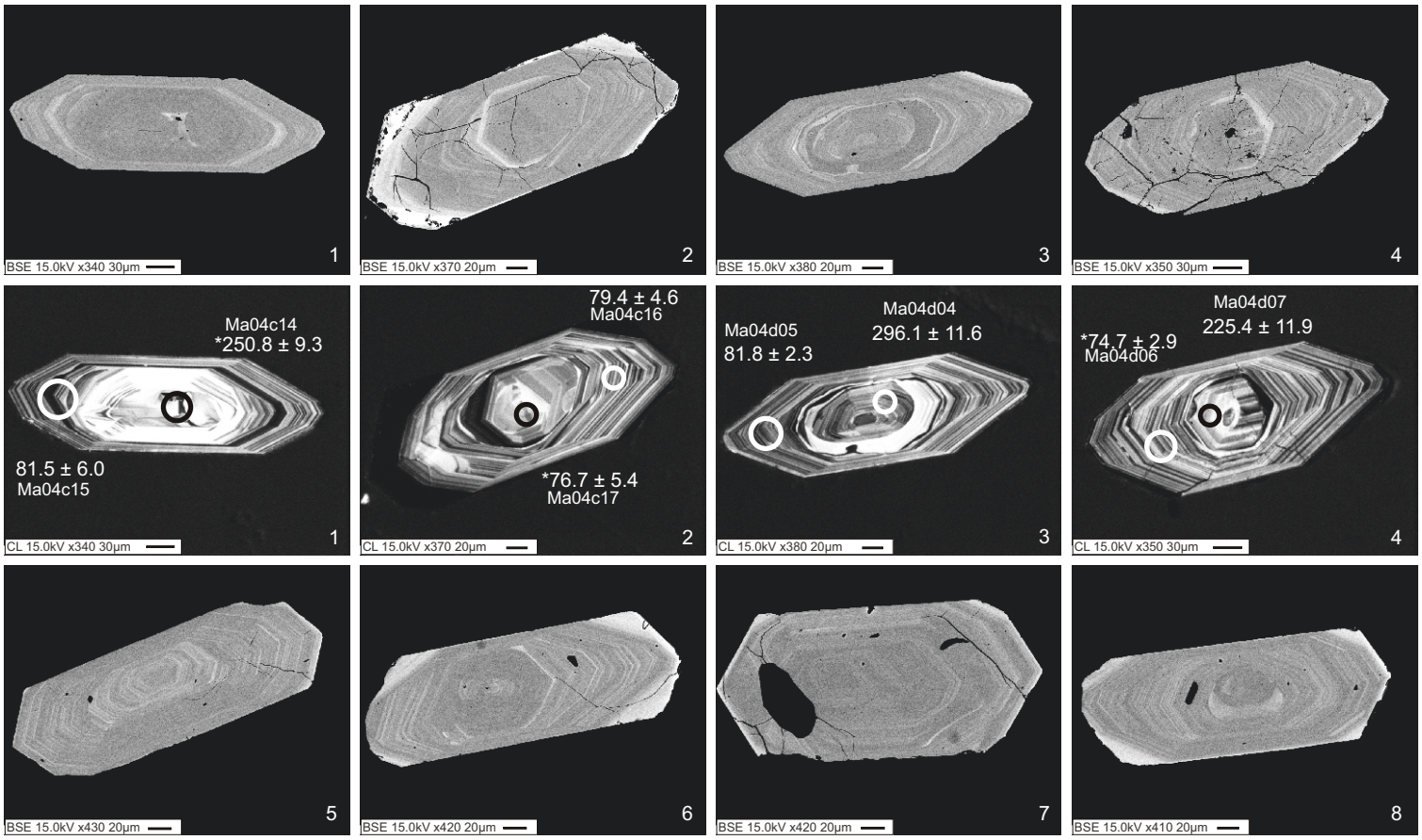

SG 028-continued

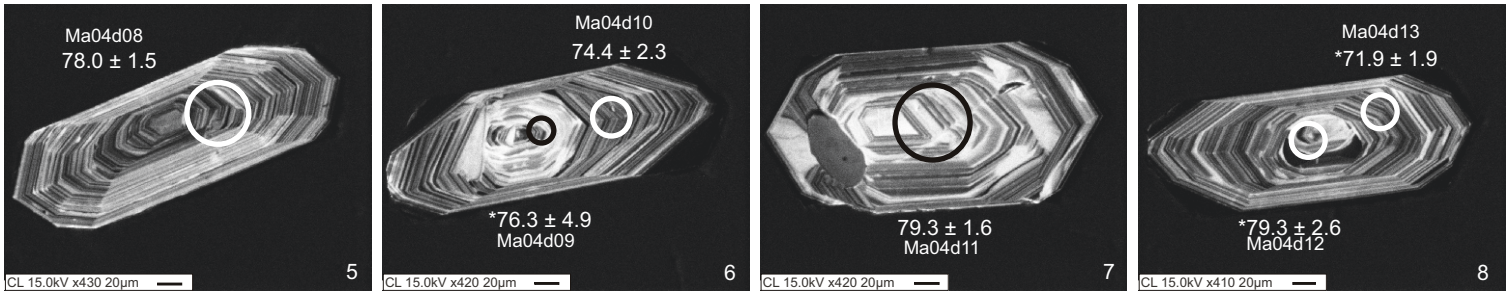

SG 040

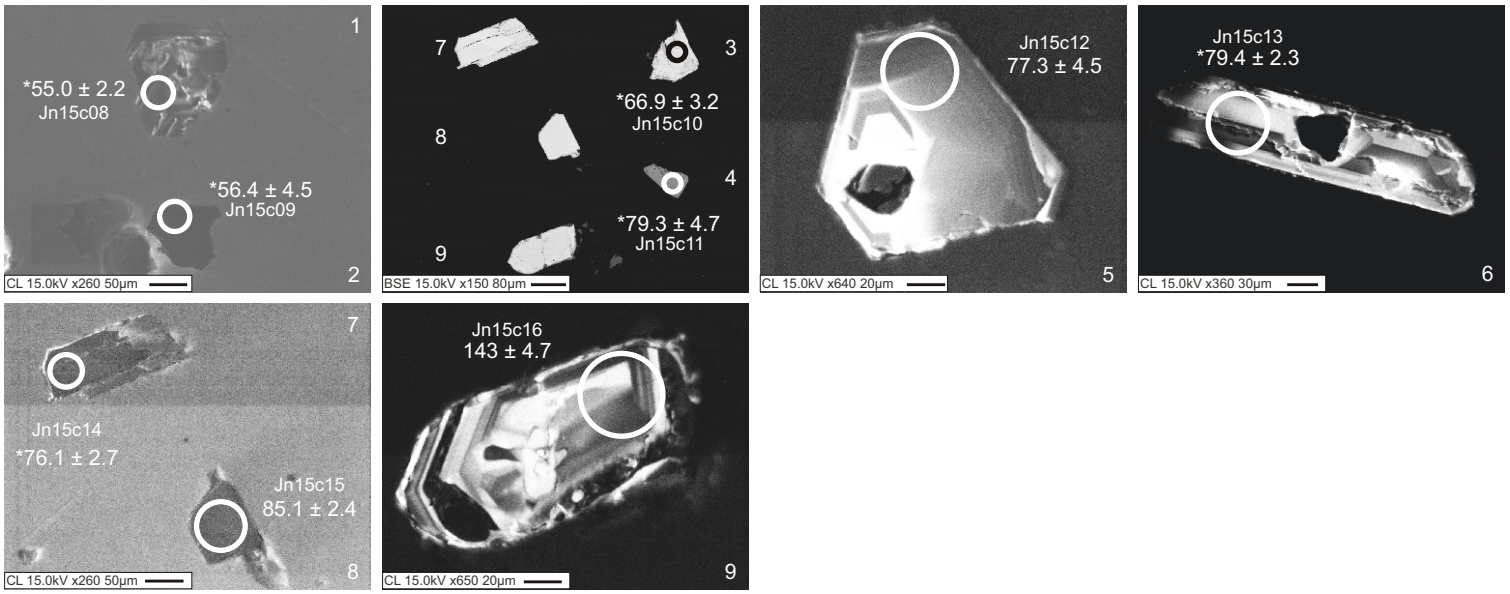

SG 041

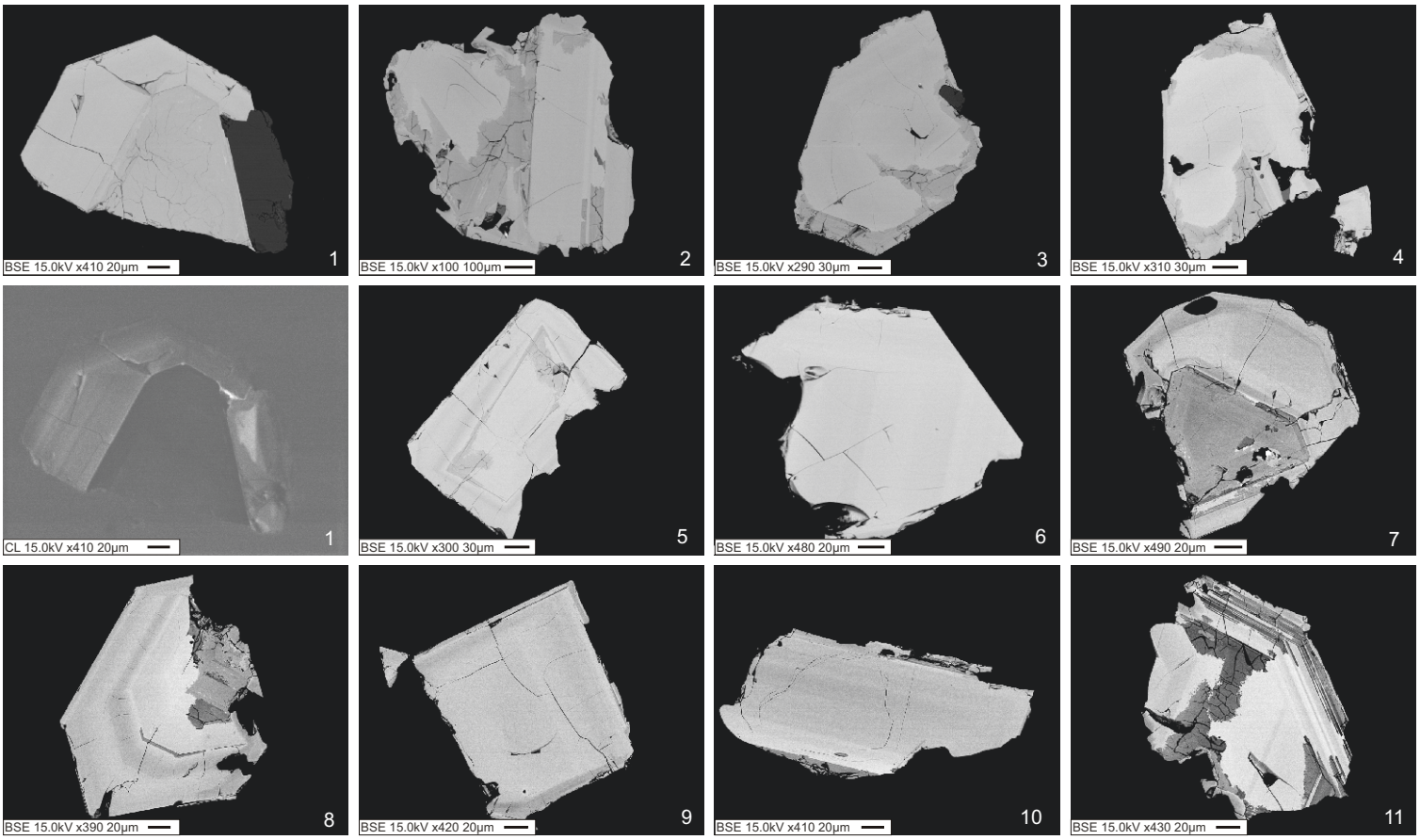

SG 041-continued

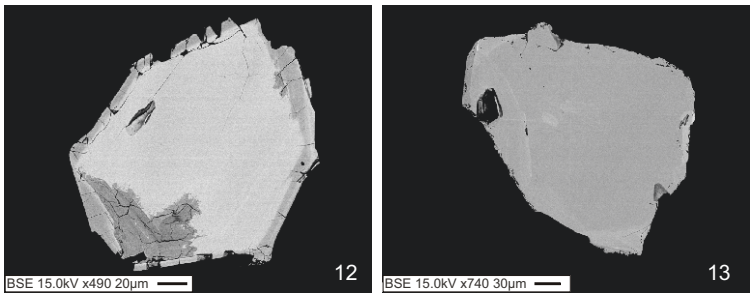

SG 044

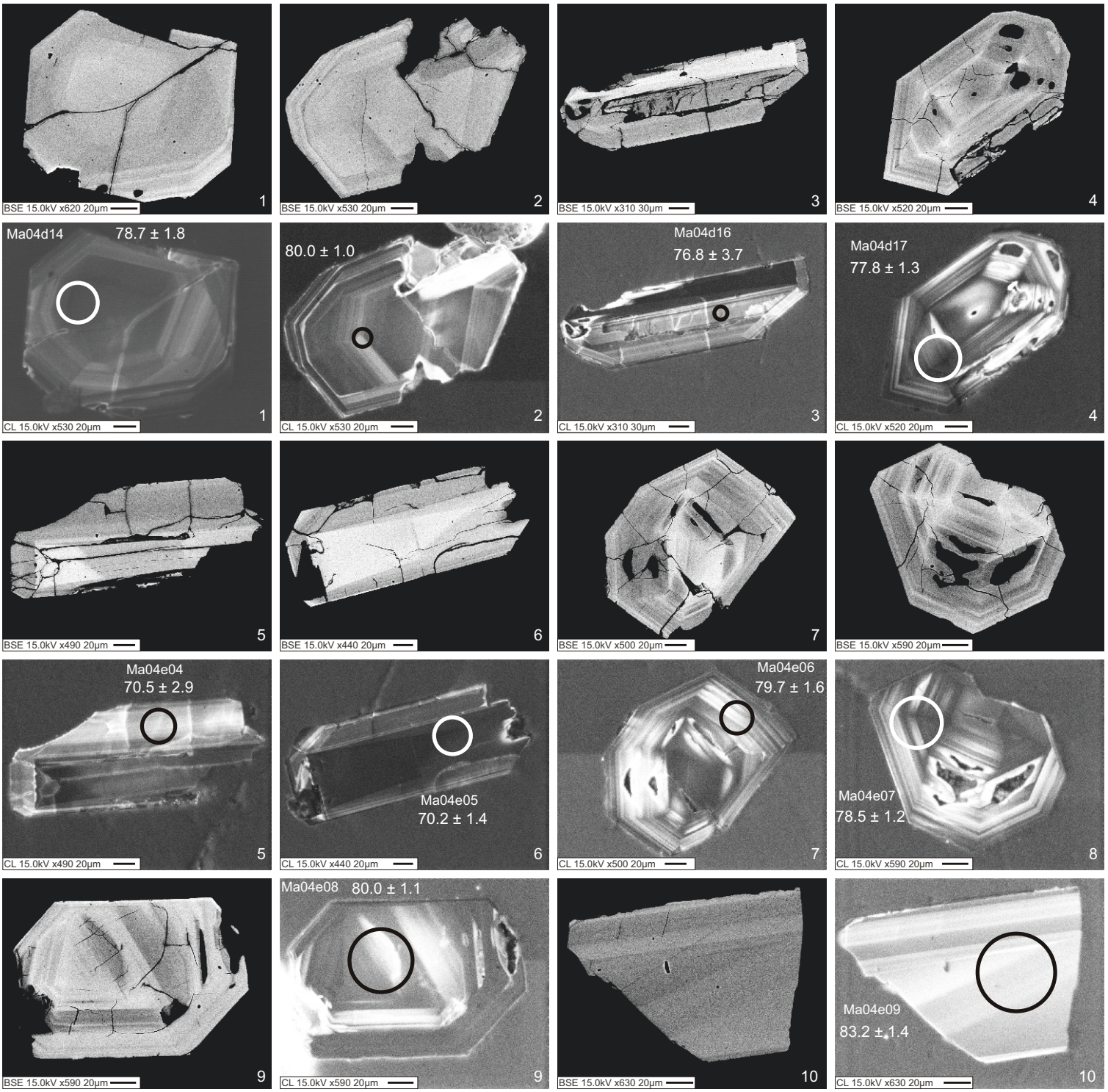

SG 047

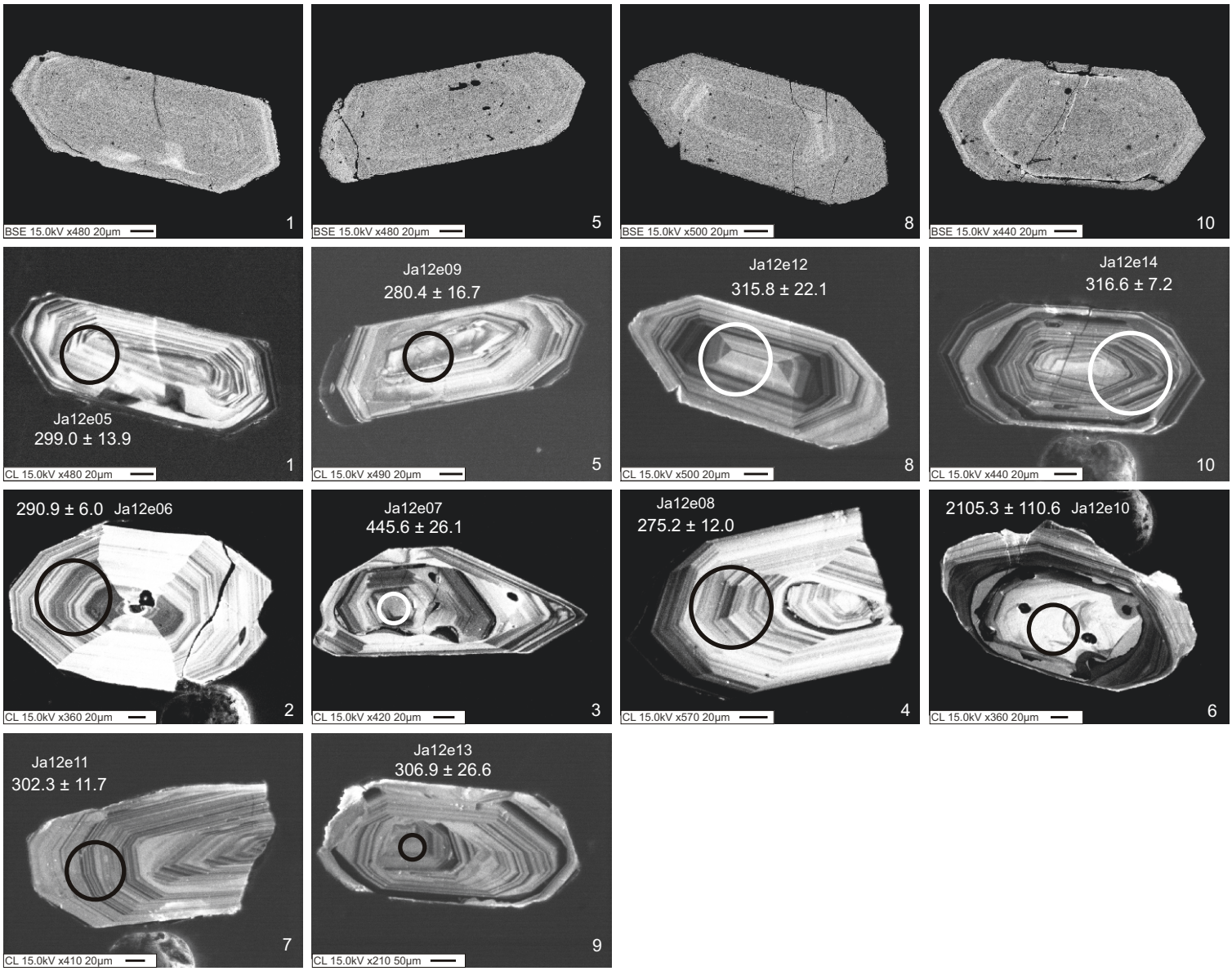
BSE 15.0kV x480 20µm
1
BSE 15.0kV x480 20µm
5
BSE 15.0kV x500 20µm
8
BSE 15.0kV x440 20µm
10
Ja12e05
299.0 ± 13.9
CL 15.0kV x480 20µm
1
Ja12e09
280.4 ± 16.7
CL 15.0kV x490 20µm
5
Ja12e12
315.8 ± 22.1
CL 15.0kV x500 20µm
8
Ja12e14
316.6 ± 7.2
CL 15.0kV x440 20µm
10
290.9 ± 6.0 Ja12e06
CL 15.0kV x360 20µm
2
Ja12e07
445.6 ± 26.1
CL 15.0kV x420 20µm
3
Ja12e08
275.2 ± 12.0
CL 15.0kV x570 20µm
4
2105.3 ± 110.6 Ja12e10
CL 15.0kV x360 20µm
6
Ja12e11
302.3 ± 11.7
CL 15.0kV x410 20µm
7
Ja12e13
306.9 ± 26.6
CL 15.0kV x210 50µm
9

SG 051

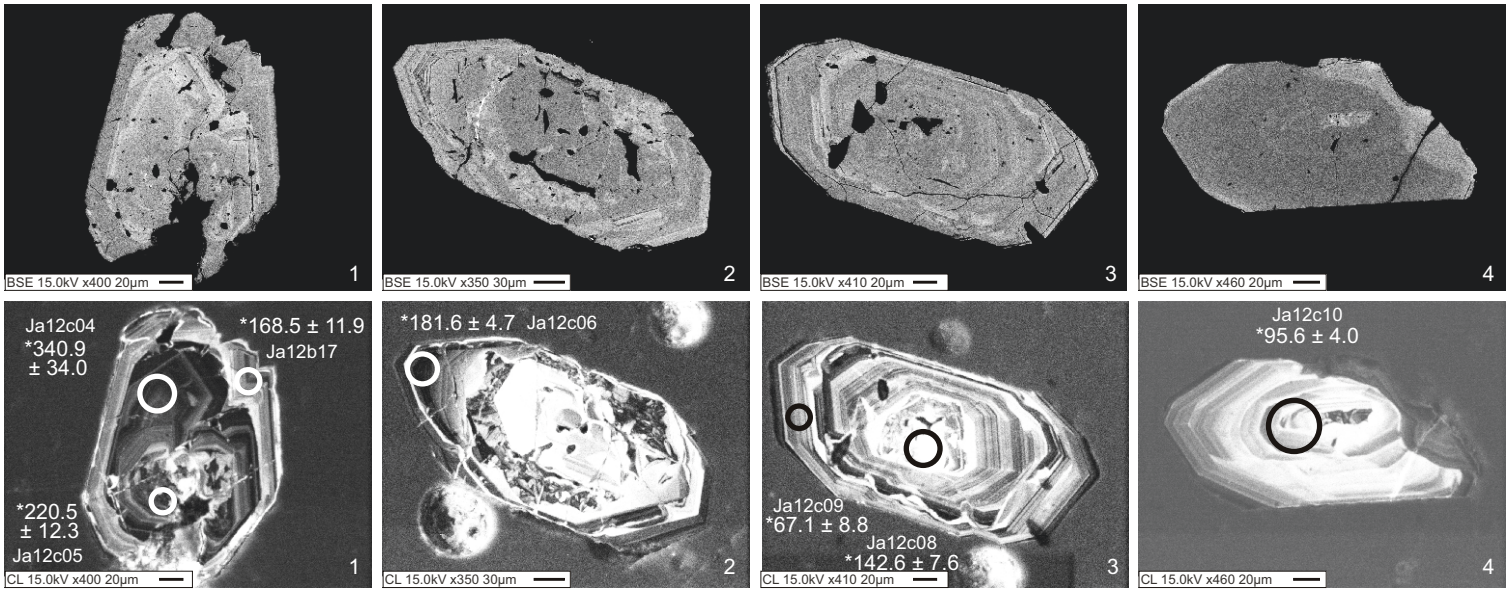
BSE 15.0kV x400 20µm
1
BSE 15.0kV x350 30µm
2
BSE 15.0kV x410 20µm
3
BSE 15.0kV x460 20µm
4
Ja12c04
*340.9
± 34.0
*168.5 ± 11.9
Ja12b17
*220.5
± 12.3
Ja12c05
CL 15.0kV x400 20µm
1
*181.6 ± 4.7 Ja12c06
CL 15.0kV x350 30µm
2
Ja12c09
*67.1 ± 8.8
Ja12c08
*142.6 ± 7.6
CL 15.0kV x410 20µm
3
Ja12c10
*95.6 ± 4.0
CL 15.0kV x460 20µm
4

SG 051-continued

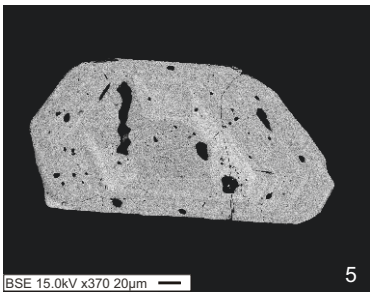

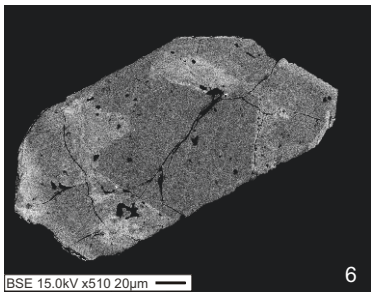

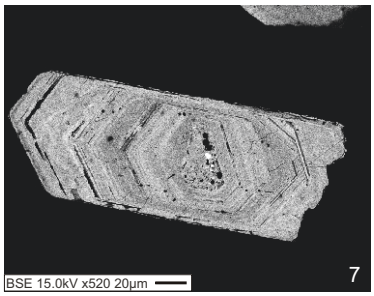

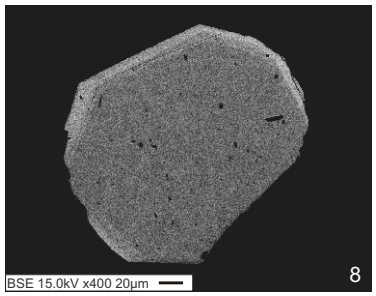

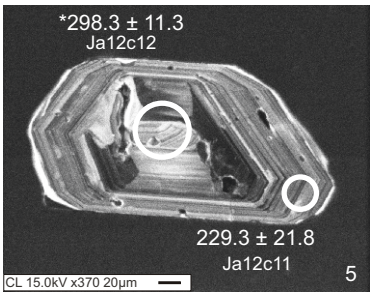

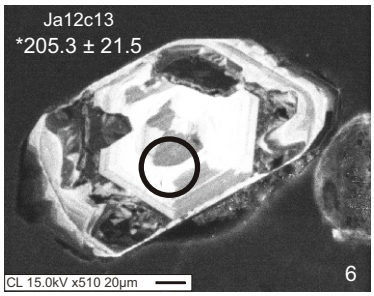

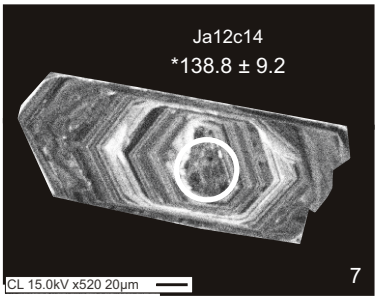

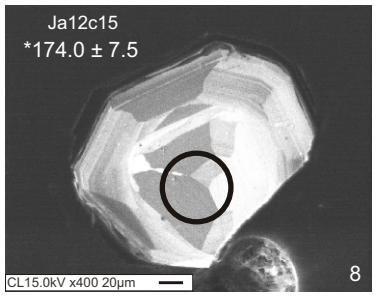

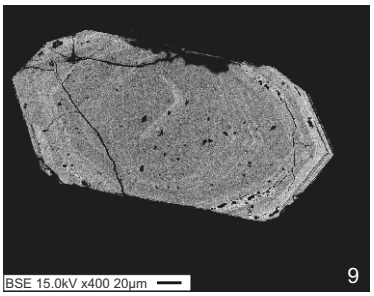

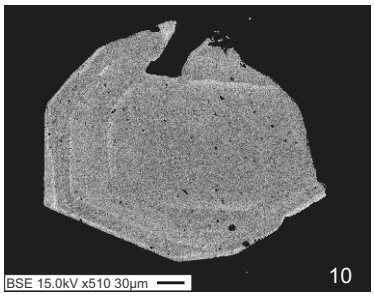

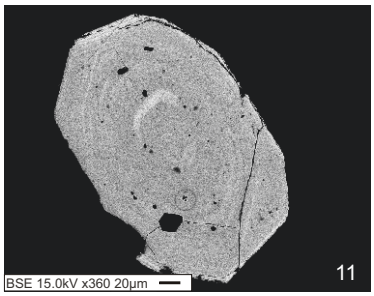

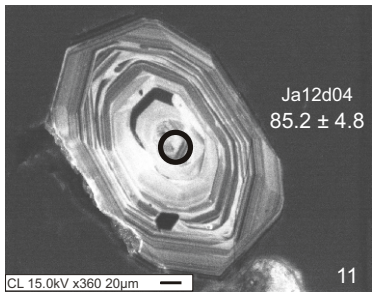

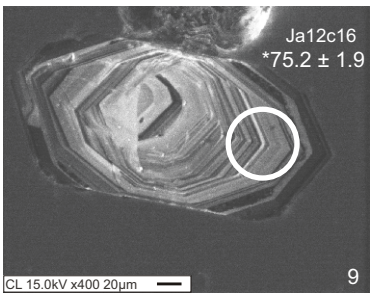

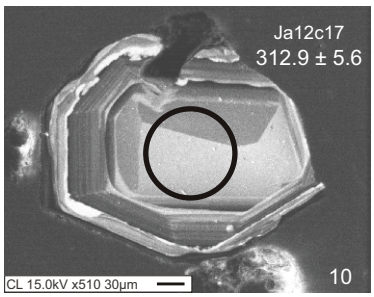

SG 052

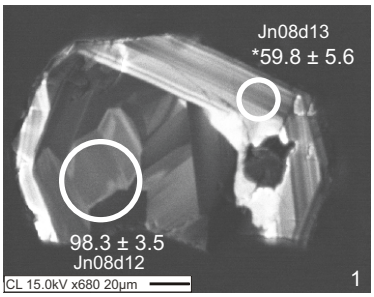

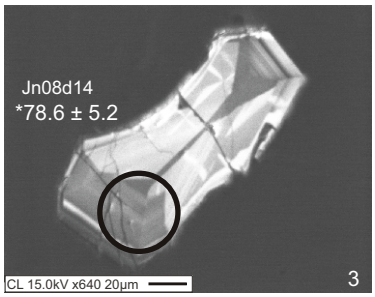

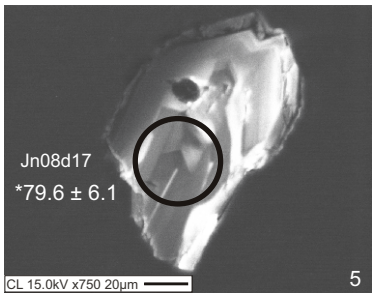

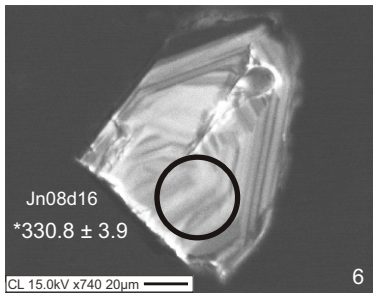

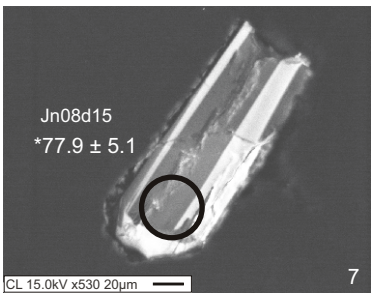

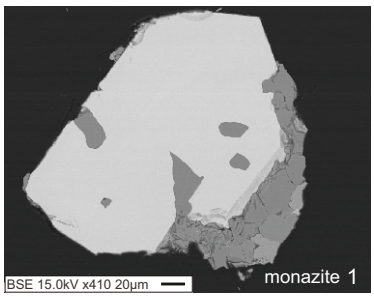

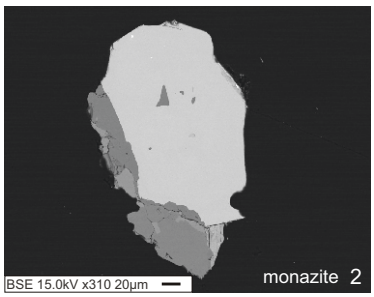

SG 053

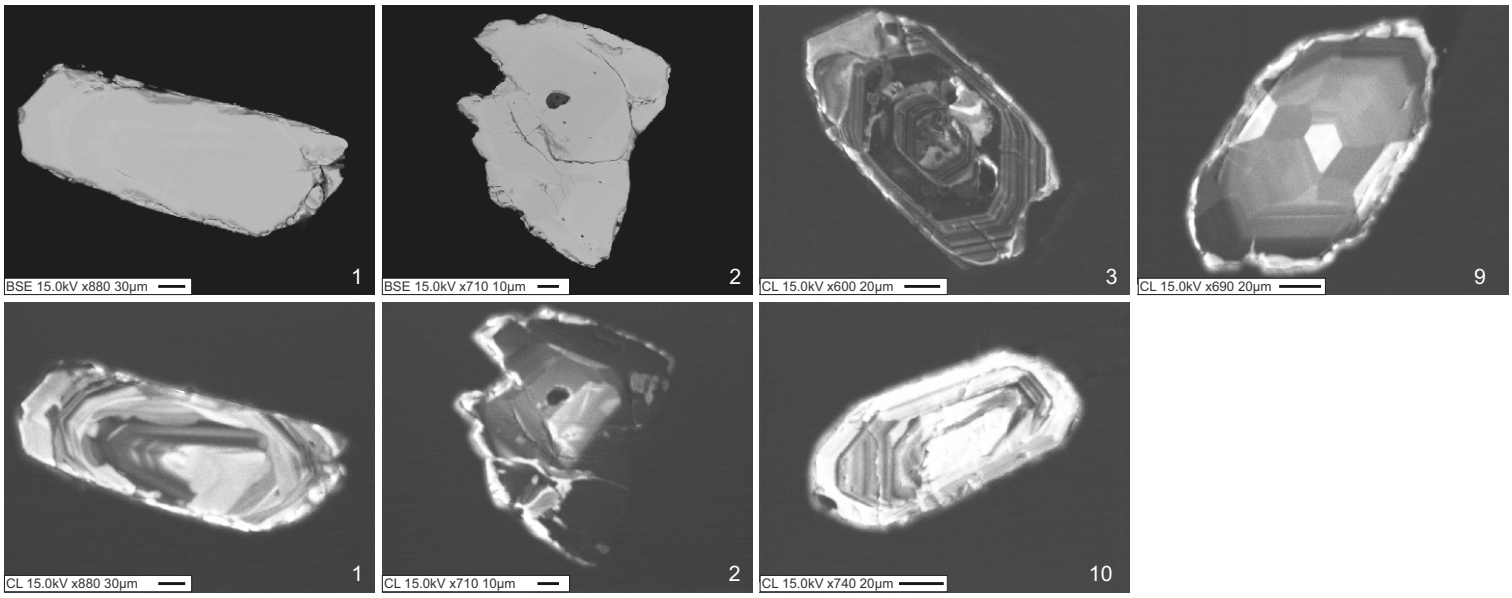
BSE 15.0kV x880 30µm
1
BSE 15.0kV x710 10µm
2
CL 15.0kV x600 20µm
3
CL 15.0kV x690 20µm
9
CL 15.0kV x880 30µm
1
CL 15.0kV x710 10µm
2
CL 15.0kV x740 20µm
10

SG 057

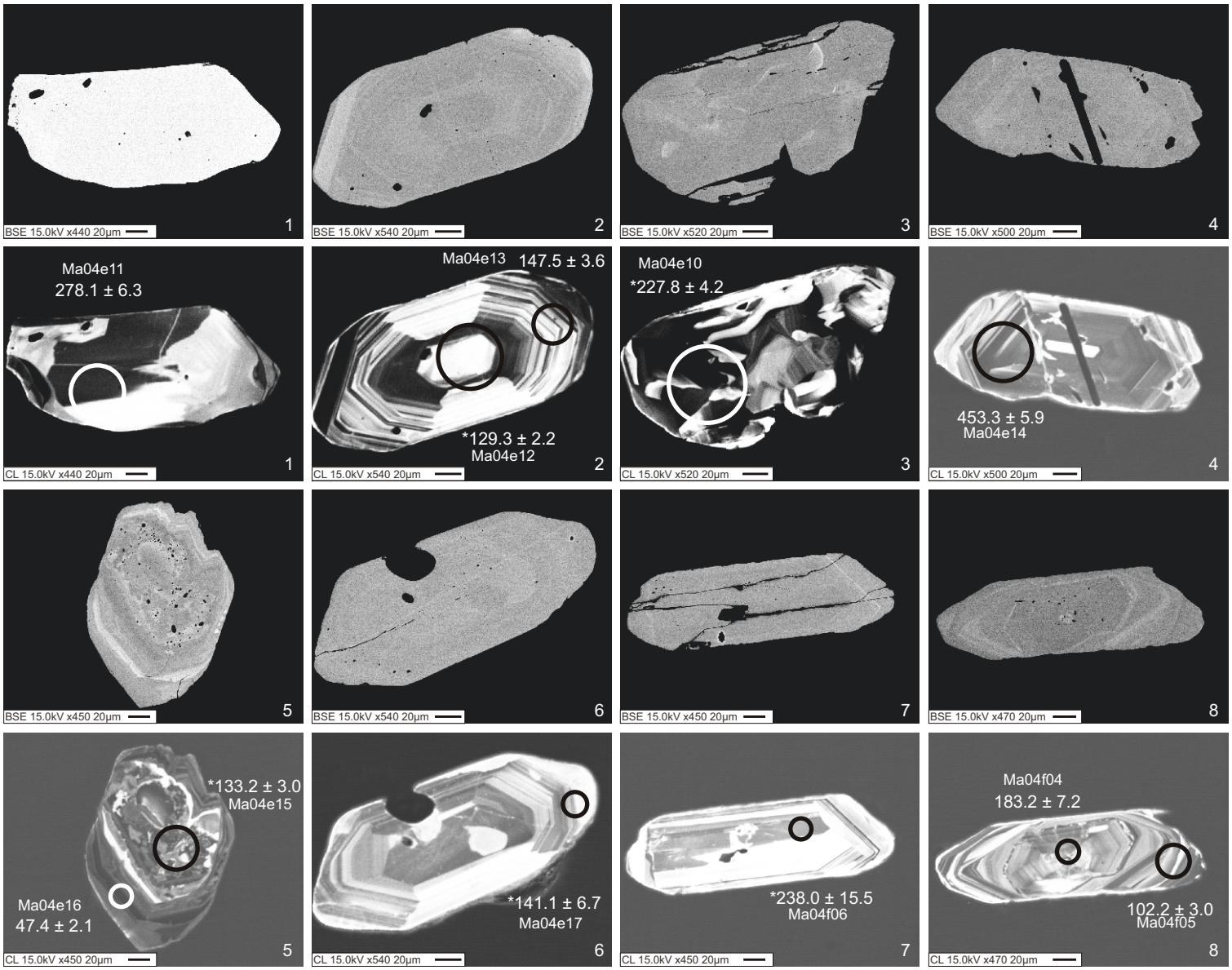
BSE 15.0kV x440 20µm
1
BSE 15.0kV x540 20µm
2
BSE 15.0kV x520 20µm
3
BSE 15.0kV x500 20µm
4
Ma04e11
278.1 ± 6.3
CL 15.0kV x440 20µm
1
Ma04e13
147.5 ± 3.6
*129.3 ± 2.2
Ma04e12
CL 15.0kV x540 20µm
2
Ma04e10
*227.8 ± 4.2
CL 15.0kV x520 20µm
3
453.3 ± 5.9
Ma04e14
CL 15.0kV x500 20µm
4
BSE 15.0kV x450 20µm
5
BSE 15.0kV x540 20µm
6
BSE 15.0kV x450 20µm
7
BSE 15.0kV x470 20µm
8
*133.2 ± 3.0
Ma04e15
Ma04e16
47.4 ± 2.1
CL 15.0kV x450 20µm
5
*141.1 ± 6.7
Ma04e17
CL 15.0kV x540 20µm
6
*238.0 ± 15.5
Ma04f06
CL 15.0kV x450 20µm
7
Ma04f04
183.2 ± 7.2
102.2 ± 3.0
Ma04f05
CL 15.0kV x470 20µm
8

SG 063

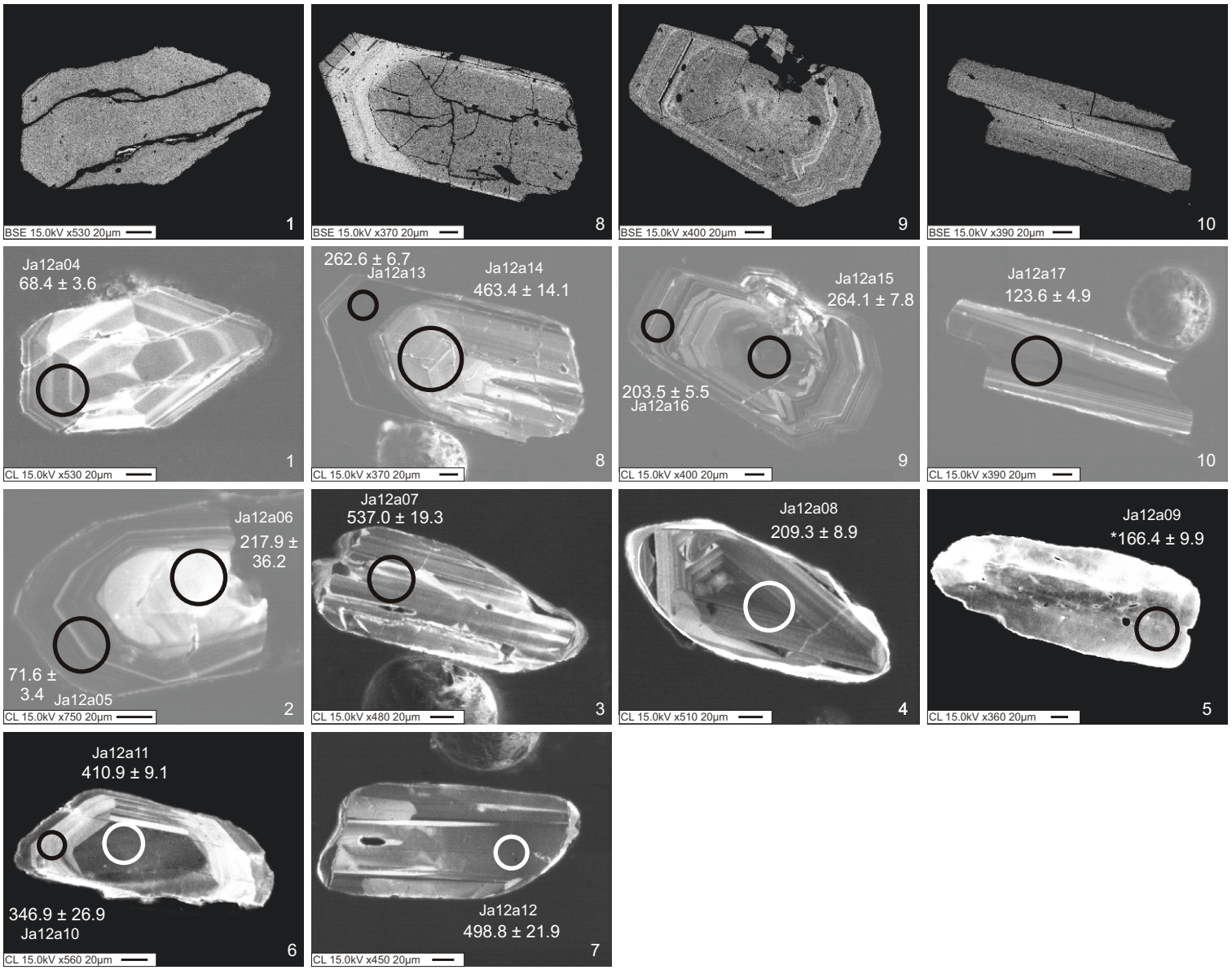
BSE 15.0kV x530 20µm
1
BSE 15.0kV x370 20µm
8
BSE 15.0kV x400 20µm
9
BSE 15.0kV x390 20µm
10
Ja12a04
68.4 ± 3.6
CL 15.0kV x530 20µm
1
262.6 ± 6.7
Ja12a13
Ja12a14
463.4 ± 14.1
CL 15.0kV x370 20µm
8
Ja12a15
264.1 ± 7.8
203.5 ± 5.5
Ja12a16
CL 15.0kV x400 20µm
9
Ja12a17
123.6 ± 4.9
CL 15.0kV x390 20µm
10
Ja12a06
217.9 ±
36.2
71.6 ±
3.4
Ja12a05
CL 15.0kV x750 20µm
2
Ja12a07
537.0 ± 19.3
CL 15.0kV x480 20µm
3
Ja12a08
209.3 ± 8.9
CL 15.0kV x510 20µm
4
Ja12a09
*166.4 ± 9.9
CL 15.0kV x360 20µm
5
Ja12a11
410.9 ± 9.1
346.9 ± 26.9
Ja12a10
CL 15.0kV x560 20µm
6
Ja12a12
498.8 ± 21.9
CL 15.0kV x450 20µm
7

SG 066

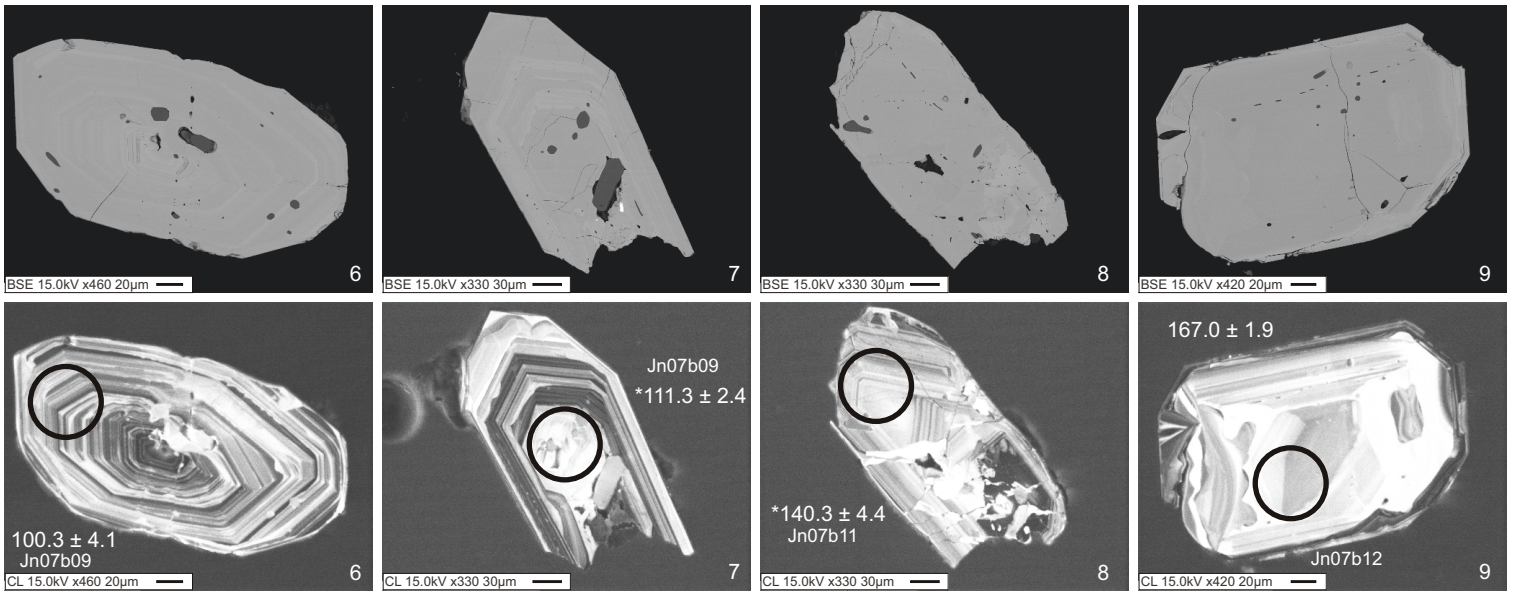
BSE 15.0kV x460 20µm
6
BSE 15.0kV x330 30µm
7
BSE 15.0kV x330 30µm
8
BSE 15.0kV x420 20µm
9
100.3 ± 4.1
Jn07b09
CL 15.0kV x460 20µm
6
Jn07b09
*111.3 ± 2.4
CL 15.0kV x330 30µm
7
*140.3 ± 4.4
Jn07b11
CL 15.0kV x330 30µm
8
167.0 ± 1.9
Jn07b12
CL 15.0kV x420 20µm
9

SG 066-continued

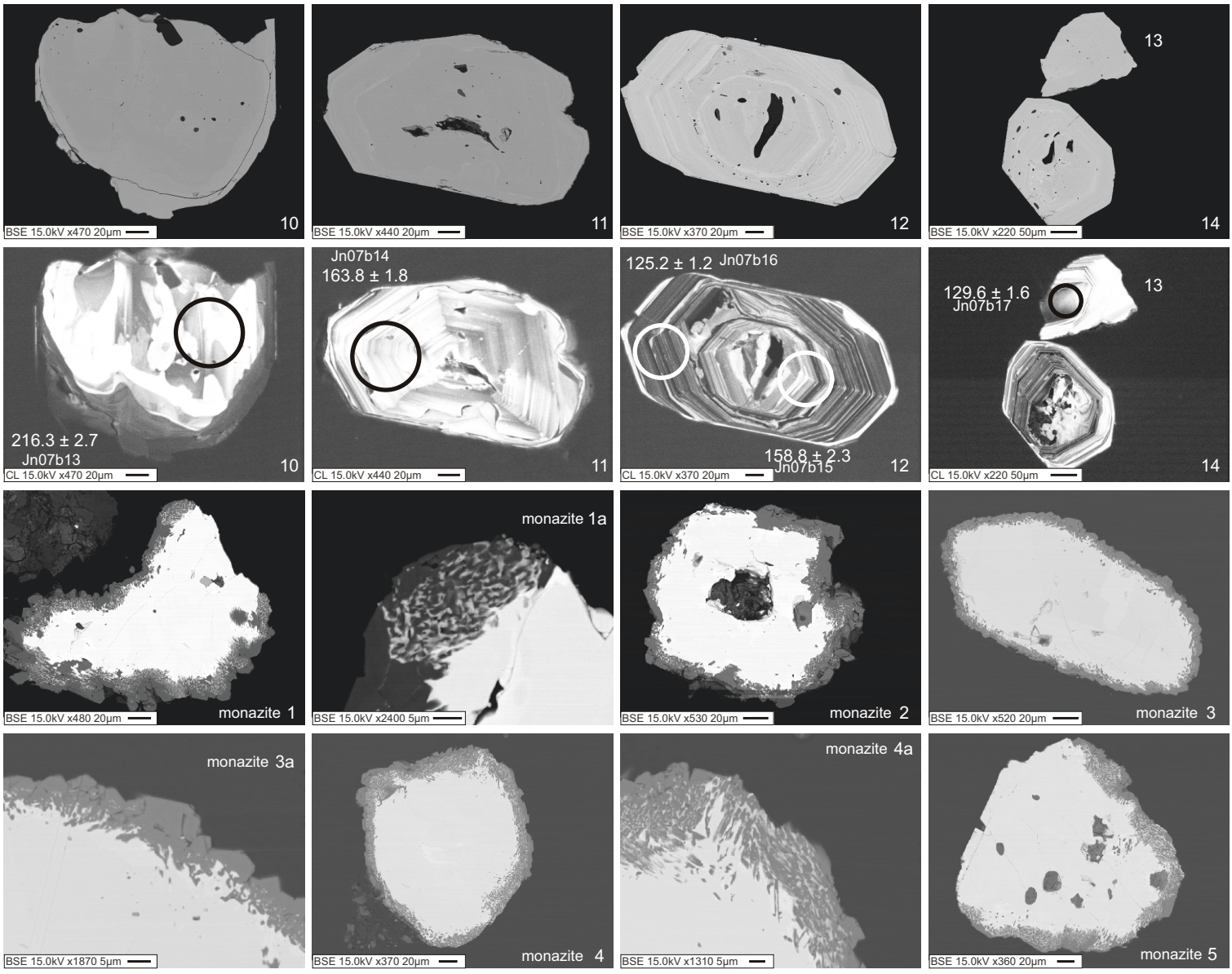

SG 068

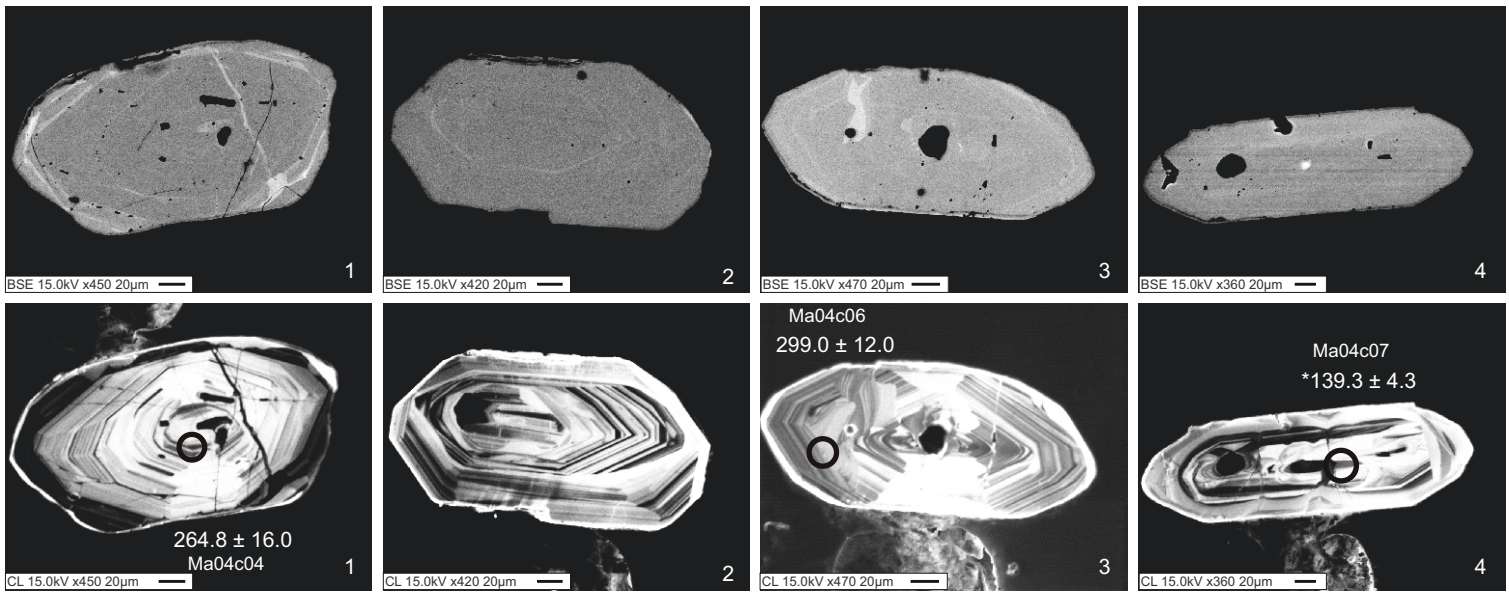

SG 068-continued

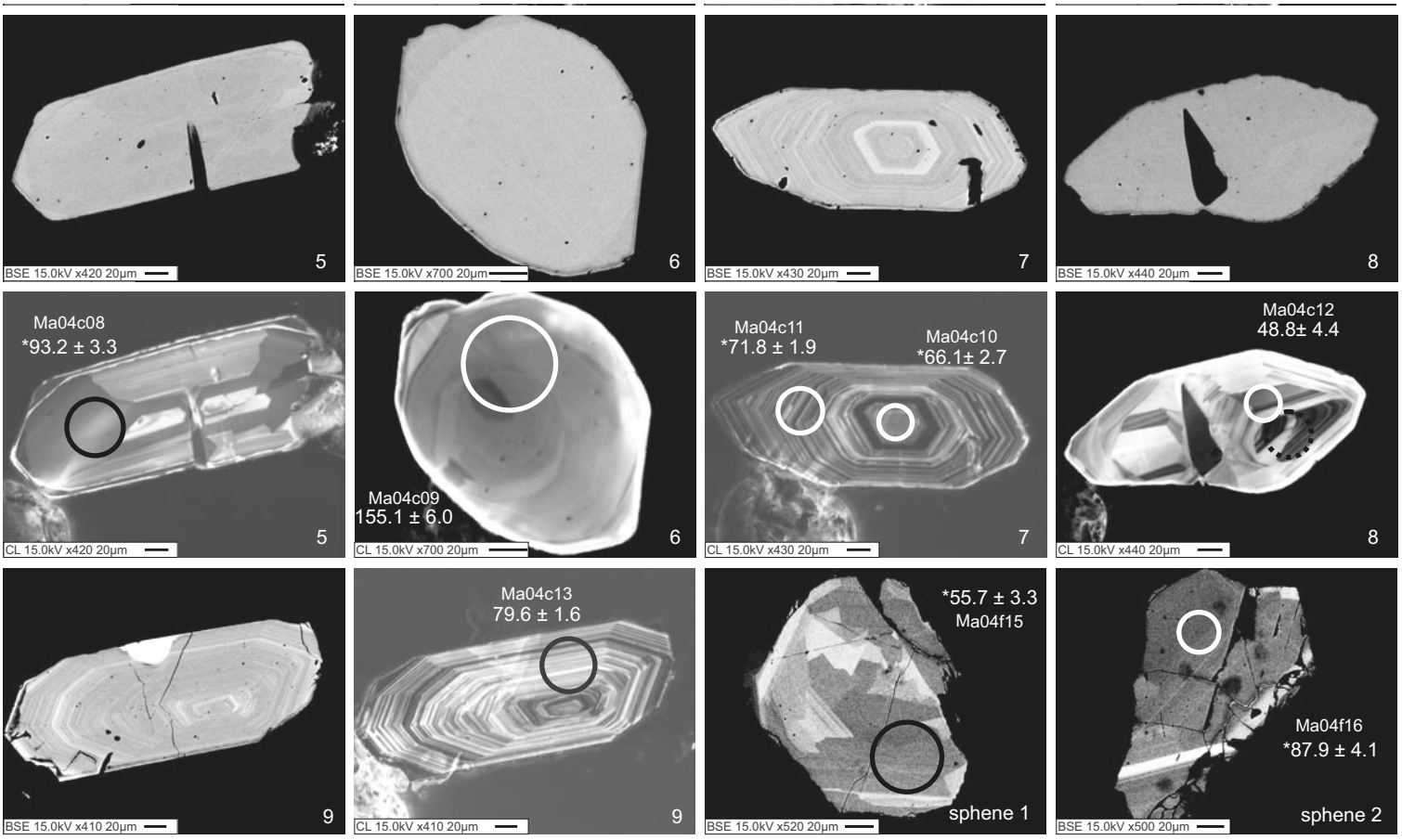

SG 069

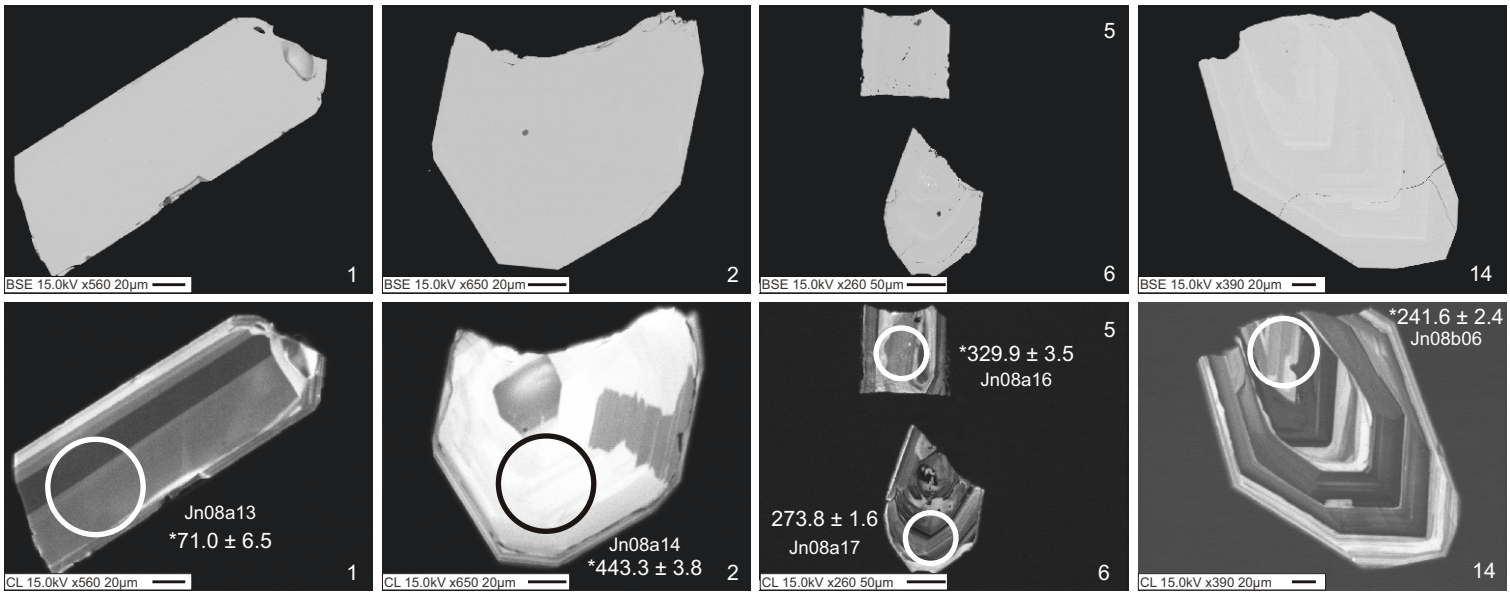

SG 069-continued

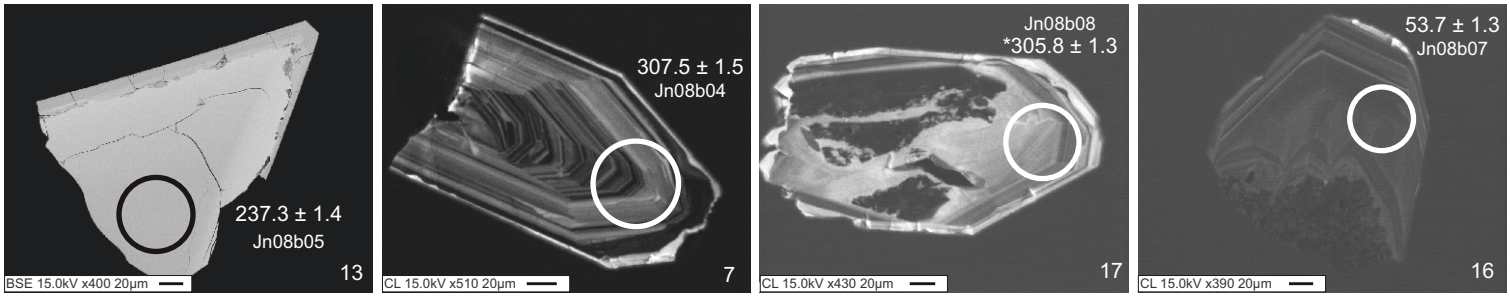

SG 070

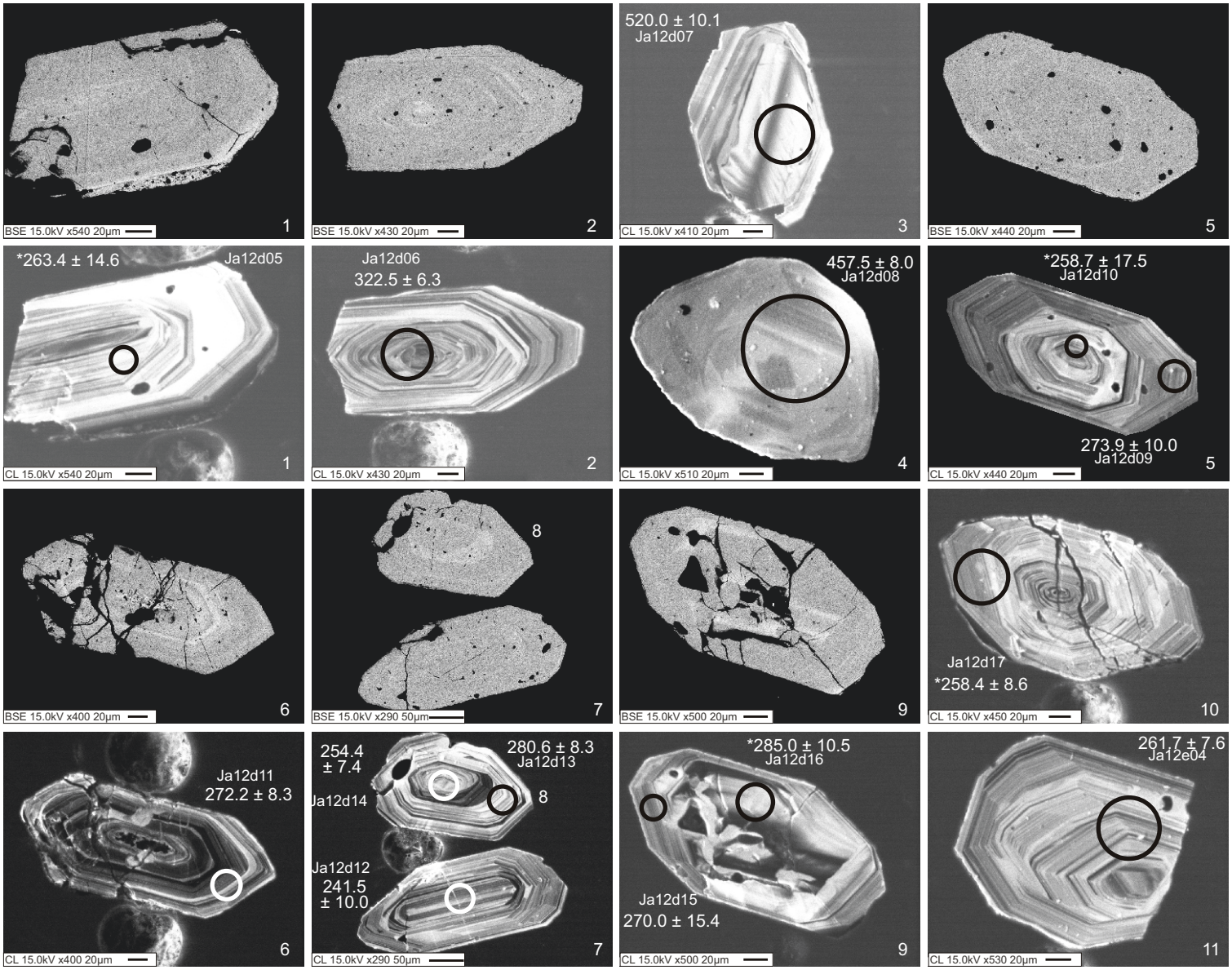

SG 078

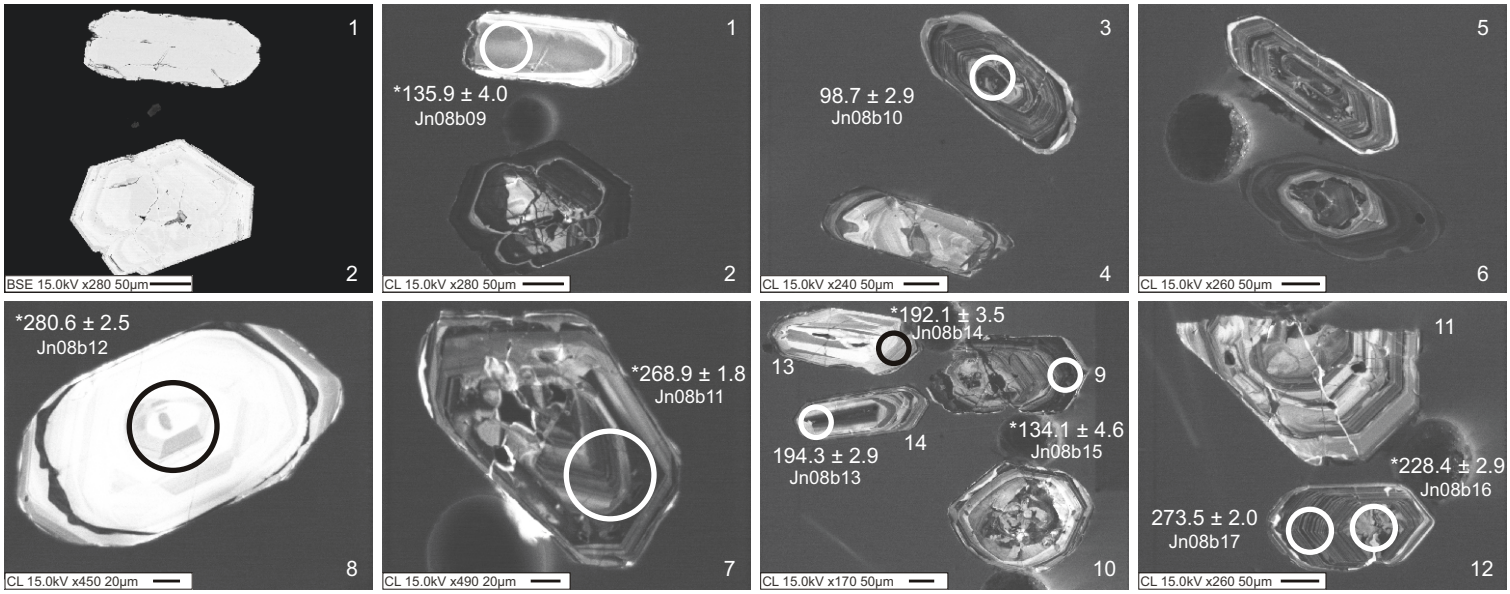

SG 079

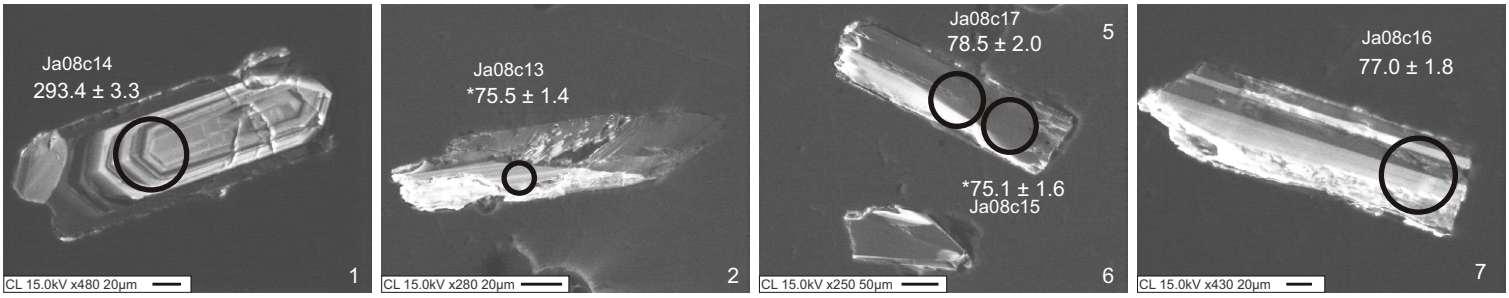

SG 085

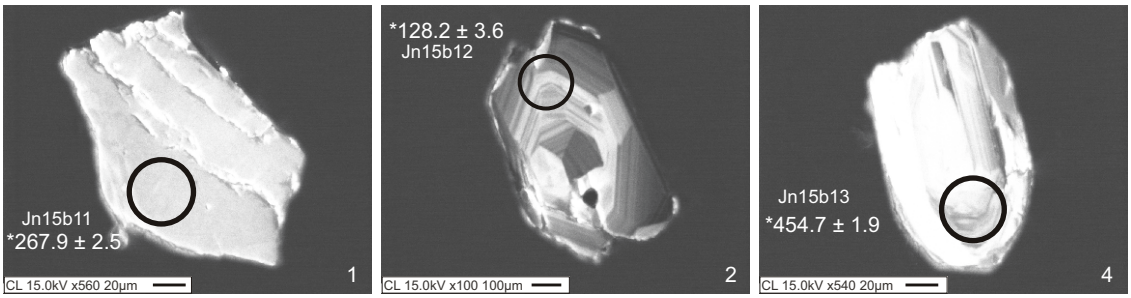

SG 090

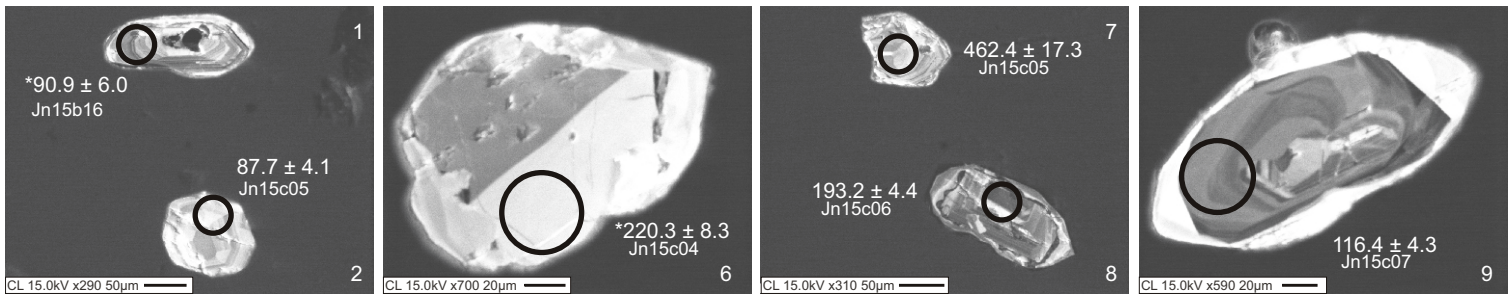

SG 102d

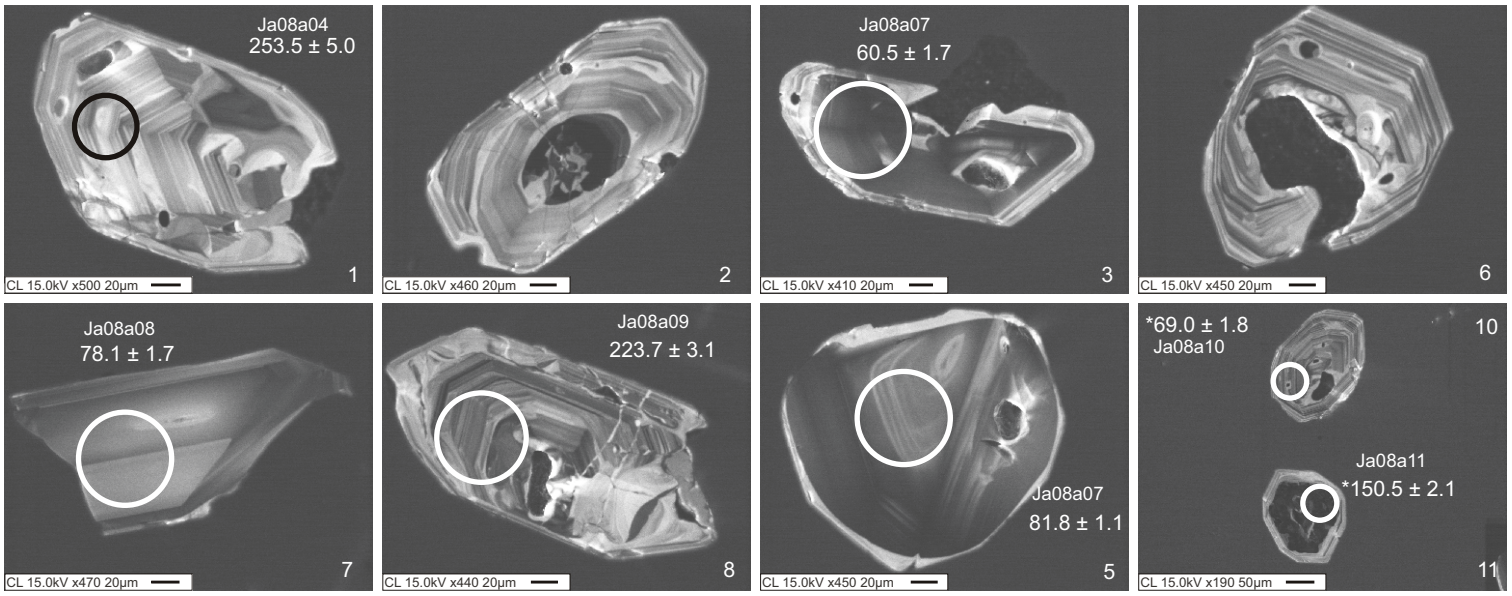

SG 103

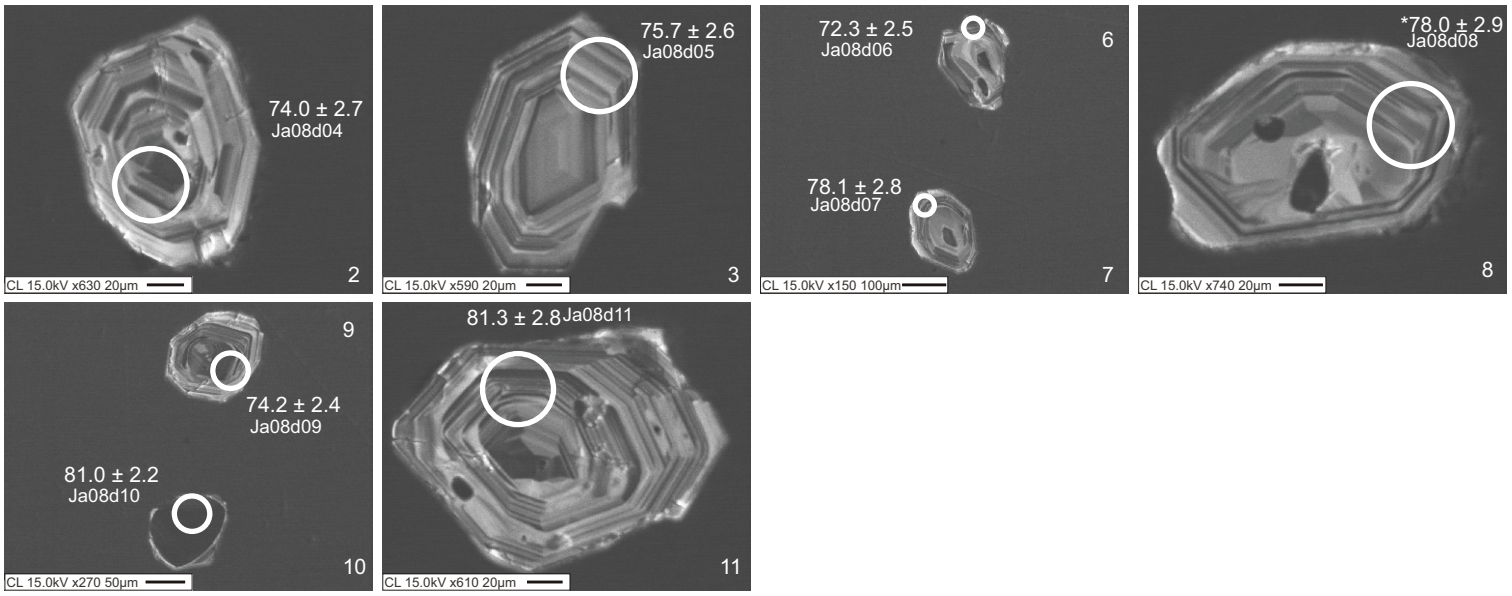

St 25